THÈSE
Pour obtenir le grade de
Docteur

Délivré par

UNIVERSITE DE PERPIGNAN VIA DOMITIA

Préparée au sein de l'école doctorale
Energie et Environnement (ED305)
Et de l'unité de recherche
CEFREM UMR5110

Spécialité : **Océanologie**

Présentée par
Gaël MANY

Impacts of storm and flood events on suspended particulate matter dynamics in the Gulf of Lions

Contributions of gliders to a multi-platform approach

Soutenue le **14/10/2016** devant le jury composé de

P. Le Hir, Directeur de recherche, IFREMER Brest — *Rapporteur*
S. Ouillon, Directeur de recherche, IRD U. Toulouse — *Rapporteur*
S. Ruiz, Directeur de recherche, IMEDEA U. Baléares — *Examinateur*
A. Sottolichio, Maitre de conférences (HDR), U. Bordeaux — *Examinateur*
X. Durrieu de Madron, Directeur de Recherche, CNRS U. Perpignan — *Directeur de Thèse*
F. Bourrin, Maitre de conférences, U. Perpignan — *Co-directeur*

Table of Contents

This PhD is supplemented by additional information that would appear as QR codes. This enable the reader to get more details concerning this work as online video, document and database using a QR Reader available on Mac and Android applications stores. An example of such supplement is shown below and enables to visit the website of the institute where this work was carried out (CEFREM, University of Perpignan).

Video
Document
Database and website

Supplement content

CEFREM website

Supplement information

QR code to scan
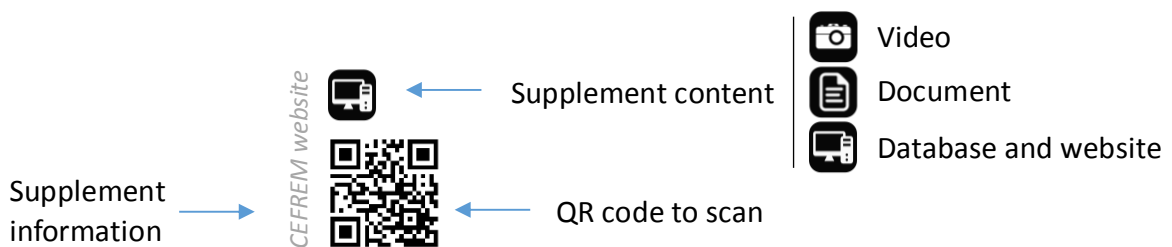
General introduction

The coastal ocean, also called epipelagic zone in oceanography, is considered as the continental shelf waters located between the surface and 200 meters depth. It is generally delimited by the coast in its inner-part and by the shelf break that is the change in inclination marking the boundary between continental shelf and slope. The coastal zone is thus a part of the global ocean, where land, ocean and atmosphere strongly interact (Gattuso et al., 2007).

While the surface of the coastal ocean is small (approx. 7% of the total ocean, i.e. 26 x 10^6 km²), it represents a preferential concentration area for land-derived material (as sediments, dissolved and particulate nutrients), which plays a main role in the sequestration of chemical elements (as carbon), in the sedimentary budget of continental margins as well as in the structuration of benthic habitats. For instance, the coastal ocean represents 15% of the oceanic primary production, 50% of the deposition of calcium carbonate, 90% of sedimentary mineralization, 80% of organic matter burial and 75-90% of the oceanic sink of suspended river load. Economically, the coastal ocean represents 90% of the world fish catch (Smith and Hollibaugh, 1993; Alongi, 1998; Gattuso et al., 1998).

In this context, legislation of the Water Framework Directive (2000) and Marine Strategy Framework Directive (2008) have been set up by European nations. These programs have highlighted several key parameters to monitor in order to evaluate the initial state and evolution of the quality of this compartment. Among those parameters, the turbidity (i.e. the clarity of seawater) appears as a key factor controlling water quality and biogeochemical processes. The response of the scientific community is organized on the basis of LOICZ (Land-Ocean Interaction in the Coastal Zone, see Ramesh et al. (2015)) and IMBER (Integrated Marine Biogeochemistry and Ecosystem Research). These international programs tend to federate national scientific orientations around common objectives concerning fundamental aspects as the actual responses of the coastal ocean to anthropic and climatic forcings.

In past decades the focus on scientific observations have thus been made on the turbidity (from natural and anthropic sources) within shelf seas with, as a main objective, the monitoring of the temporal and spatial variability of suspended particulate matter (SPM) dynamics that contribute to the land-to-sea material continuum. Measurements have permitted to define the diversity of turbid structures, called "nepheloid layers", and have emphasized the role of extreme and moderate events (as storms and floods) as well as particles properties (as nature, size and settling velocity) in the coastal SPM dynamics processes (Nittrouer et al., 2009; Simpson et Sharples, 2012). Authors described the turbidity of the coastal ocean as a key factor involved in the transport of contaminants through the water column, the extent of polluted benthic areas and the negative impact on biological activity by a strong decrease of the light penetration and related photosynthesis. They introduced the need of a multi-platform strategy to follow SPM dynamics over large space and time scales as well as during extreme meteorological events.

The work presented in this PhD is related to French research projects CASCADE (CAscading, Storm, Convection, Advection and Downwelling Events) and TUCPA (Turbidité Côtière et Plateformes

Autonomes", i.e. Coastal Turbidity and Autonomous Platforms). It follows the work carried out during the EUROSTRATAFORM (EUROpean margin STRATAs FORMation) European framework that has highlighted the complex SPM dynamics as well as the variability of suspended particle properties over the shelf of the Gulf of Lions (NW Mediterranean) to assess the fate of land-derived material from source (Rivers) to sink (continental margin, submarine canyons, deep sea) (Syvitski et al., 2004; Weaver et al., 2006; Durrieu de Madron et al., 2008).

The main aims of this PhD, carried out in the "Centre de Formation et de Recherche sur les Environnements Méditerranéens" (CEFREM – UMR5110 CNRS/UPVD) of the University of Perpignan (France) are to improve our understandings of the role of extreme natural events, such as storms and floods, in the land to sea particulate exchanges, i.e. the coastal SPM dynamics, over the shelf of the Gulf of Lions (NW Mediterranean). While storms enhance the particulate resuspension, transport and in some cases export offshelf, floods of coastal rivers are main suppliers of SPM to the shelf and thus play an important role in the suspended particles spread, settling and sedimentation.

Key questions developed forward this work can be resume as follow:

- *What is the spatial variability of the Rhône ROFI particle assemblage during a flood event?*

- *What is the dynamic of the Rhône ROFI nepheloid layers during a flood event?*

- *What are the impacts of a storm on SPM dynamics and properties over the shelf of the GoL?*

This work is based on in situ coastal observations of SPM dynamics within the Gulf of Lions. It has been the opportunity to carry out state-of-the-art measurements to characterize the hydrology, turbidity, currents, as well as particle properties from various platforms (remote sensing, coastal buoys, moorings, gliders, and research vessels).

This PhD is organized around 7 chapters. The first chapter presents the context of this work and is followed by regional settings of the study area. These chapters are constructed around precedent observations carried out over worldwide continental margins and the shelf of the Gulf of Lions. The multi-platform strategy adopted in this PhD is introduced in the Chapter 3.

Three articles compose the next chapters of this thesis (Chapters 4, 5 and 6). Chapter 4 presents the study of the spatial variability of the properties of the particle assemblage (as size, nature and effective density) in the Rhône River ROFI during a flood event. Chapter 5 addresses the dynamic of nepheloid layers within the Rhône ROFI with high temporal and spatial resolutions combining glider, coastal buoy and satellite observations. Chapter 6 describes the impact of a storm on shelf hydrology, hydrodynamism, sediment resuspension and suspended particles transport. Finally, general conclusions and future challenges are presented in Chapter 7.

References

Alongi, D. **1998**. *Coastal ecosystem processes*. Vol. 3.

Durrieu de Madron, X., P.L. Wiberg, P. Puig, **2008**. « Sediment dynamics in the Gulf of Lions: The impact of extreme events. » *Continental Shelf Research* 28, 1867–1876. doi:10.1016/j.csr.2008.08.001

Gattuso, J.P., S.V. Smith, C.M. Hogan, and J.E. Duffy. **2007**. « Coastal zone ». *Encyclopedia of Earth*.

Gattuso, J. P., M. Frankignoulle, and R. Wollast. **1998**. « Carbon and carbonate metabolism in coastal aquatic ecosystems ». *Annual Review of Ecology and Systematics*, 405‑34.

Giorgi, F., **2006**. « Climate change hot-spots. » *Geophysical Research Letters*, 33(8):L08707. doi:10.1029/2006GL025734.

Nittrouer, C., J. Austin, M. Field, J. Kravitz, J. Syvitski, and P. Wiberg. **2009**. *Continental Margin Sedimentation: From Sediment Transport to Sequence Stratigraphy (Special Publication 37 of the IAS)*. John Wiley & Sons. 560 p.

Ramesh, R., Z. Chen, V. Cummins, J. Day, C. D'Elia, B. Dennison, D. L. Forbes, et al., **2015**. « Land–Ocean Interactions in the Coastal Zone: Past, present & future ». *Anthropocene* 12 (décembre): 85‑98. doi:10.1016/j.ancene.2016.01.005.

Simpson, J. H., and J. Sharples. **2012**. *Introduction to the physical and biological oceanography of shelf seas*. Cambridge University Press.

Smith, S. V., and J. T. Hollibaugh. **1993**. « Coastal metabolism and the oceanic organic carbon balance ». *Reviews of Geophysics* 31 (1): 75‑89.

Syvitski, J.P.M., P.P.E. Weaver, S. Berné, C.A. Nittrouer, F. Trincardi, M. Canals, **2004**. « Introduction to this special issue on Strata formation on European Margins. Atribute to EU-NA cooperation in Marine Geology. » *Oceanography* 17, 14–15

Weaver, P.P.E., M. Canals, F.Trincardi, **2006**. « EUROSTRATAFORM Special Issue of Marine Geology. » *Marine Geology* 234, 1–2. doi:10.1016/j.margeo.2006.09.001

Chapter 1.

General background

Chapter 1.   General Background

List of Figures

Figure 1.1 : a) Size spectra of the different components of seawater. Arrows are shown to delimit size classes of each constituent. Suspended particulate matter (SPM) is highlighted by a red rectangle and is further detailed. From Stramski et al. (2004). b) RGB image (LANDSAT/OLI) of the impact of the Mississippi River runoff on coastal turbidity. Note the color of the surface river plume, mainly composed of mineral SPM (sediments as clays and silts). **8**

Figure 1.2 : Schematic representation of the different nepheloid layers that can be found in coastal seas and offshore waters. Mineral and biological sources of SPM are shown in yellow and green, respectively. Nepheloid layers are shown in italic while SPM dynamics are shown in bold. The white rectangle highlights the coastal nepheloid layers and SPM dynamics further detailed. **9**

Figure 1.3 : Conceptual view of the cross-section of a surface-trapped river plume. The various dynamical regions and the mixing processes are shown. The diagram is not to scale, far-field regions are generally larger than estuary and near-field plume regions. From Hetland (2005). **11**

Figure 1.4 : Example of river plumes in different ROFIs around the world (non-exhaustive list) **13**

Figure 1.5 : Conceptual models of the creation of a mid-shelf mud-belt, a) wave cross-shelf diffusion, b) advection in BNL, c) advection in density underflows, d) schematic representation of the horizontal graded bedding observed over continental margins (adapted from Hill et al. 2007) **15**

Figure 1.6 : SPM granulometric classification. Nature of unique sediment are shown (clay, silt and sand). Fine-grained flocs classification is presented. A-D) Examples of Scanning Electron Microscopy images of unique particles of clay and silt, micro-floc, aerated and dense macro-flocs, from Verney (2006). E-F) Transmissiometry and fluorimetry images of a dense macro-floc (∼300µm) (Courtesy, K. Curran). **17**

Figure 1.7 : Conceptual view of the formation of marine flocs within a particle assemblage. Processes and time-scales are shown in italic. From Montgomery (1985). Note the intentionally non-spherical shape of suspended particles. **18**

1.1 The natural turbidity in the ocean

1.1.1 What is the natural turbidity in the ocean?

In the ocean, the turbidity is a proxy of the concentration of suspended matter in the water, i.e. the clarity index of seawater. It translates the quantity of light scattered or attenuated by suspended matter when light passes through a water sample. Matter can be under the dissolved or particulate form and from organic or inorganic sources. The natural turbidity, which is mainly due rivers discharge, suspended matter dynamics and primary production, is generally opposed to the anthropogenic turbidity due to human activities as dredging, trawling or ocean dumping. Nowadays, the level of turbidity is commonly used as a proxy of water quality and is implied in several physical and biogeochemical processes within the ocean as the sediment land-to-sea continuum and the nutrients cycles. Figure 1.1a presents a classification of the different constituents that can contribute to the turbidity in seawater (Stramski et al., 2004). It shows dissolved organic matter (DOM, size < 0.7 μm) and suspended particulate matter (SPM, i.e. size > 0.7 μm). SPM includes mineral particles (i.e. sediments as clay, silt or sand), biological organisms (phyto/zooplankton) as well as organic detritus from organisms maintained in suspension by the turbulence in the water column.

In coastal seas, sediments often represent a major part of the SPM due to river discharge, coastal erosion and bottom resuspension. An example of turbid water mainly composed of sediments in suspension is shown in Fig. 1.1b. It shows the Mississippi River runoff in the Gulf of Mexico visible from satellite and characterized by fine mineral particles composed of silts and clays. These waters present a high opacity and a color from brown to green as captured from satellites optical sensors. In the coastal zone, the monitoring of the variability of this turbidity is key to understand factors impacting coastal ecosystem, light penetration in the ocean, transport of chemicals, and sedimentary budget on continental margins.
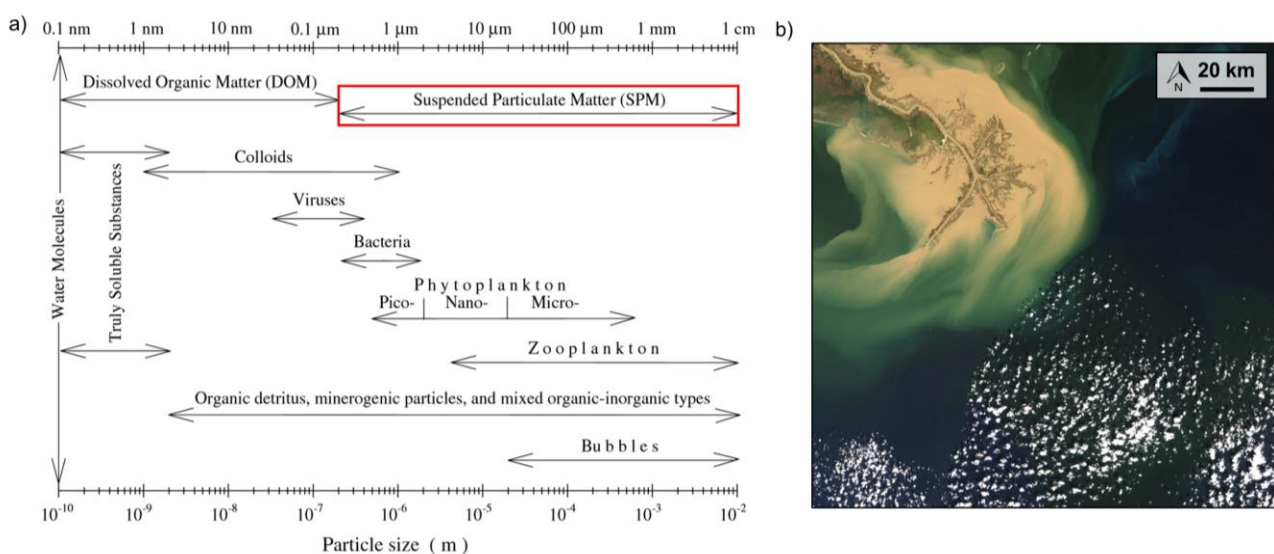

Figure 1.1 : a) Size spectra of the different components of seawater. Arrows are shown to delimit size classes of each constituent. Suspended particulate matter (SPM) is highlighted by a red rectangle and is further detailed. From Stramski et al. (2004). b) RGB image (LANDSAT/OLI) of the impact of the Mississippi River runoff on coastal turbidity. Note the color of the surface river plume, mainly composed of mineral SPM (sediments as clays and silts).

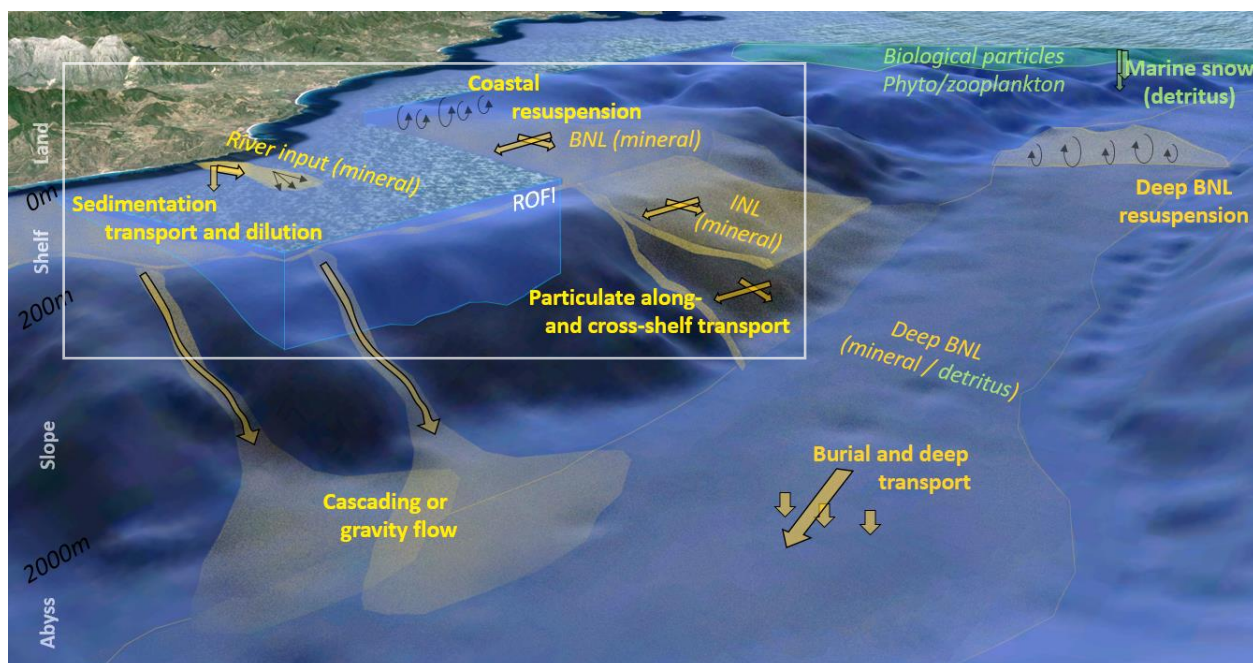## *1.1.2 Spatial distribution within the ocean*

Figure 1.2 : Schematic representation of the different nepheloid layers that can be found in coastal seas and offshore waters. Mineral and biological sources of SPM are shown in yellow and green, respectively. Nepheloid layers are shown in italic while SPM dynamics are shown in bold. The white rectangle highlights the coastal nepheloid layers and SPM dynamics further detailed.

The Figure 1.2 shows the diversity of natural turbid structures, also called "nepheloid layers" that are observed within coastal seas and offshore. Nepheloid layers, mainly composed of fine mineral sediments (clayey and silty fraction) and in some cases of detritus from phyto/zooplankton organisms are observed at several locations in the ocean, extent over hundreds of km² and present variable thickness and concentration depending on ocean conditions. Various turbid structures can be found as Surface, Intermediate and Bottom Nepheloid Layer (SNL, INL, and BNL respectively). SNL from buoyant river plumes are created by solid river discharges, which represent the main sources of SPM to the ocean (Nittrouer et al., 2009; Simpson et Sharples, 2012).

River particulate inputs are then submitted to various processes that enhance the SPM dilution, transport and sedimentation within Regions Of Freshwater Influence (ROFIs) (see 1.2.1). Close to the coast, fresh-particulate deposits can be resuspended by waves and advected toward the shelf by coastal currents (Drake, 1976). The related BNL, adjacent to the seabed, can extent over the whole shelf and is variable in space and time depending on the intensity of waves and currents (Shideler, 1981).

Along the continental slope, the BNL from the continental margin can be detached from the seafloor and can create an intermediate nepheloid layer within the offshore waters. This INL, which is generally located at several hundreds of meters depth, often occurs at the level of the

continental shelf-break and spread along isopycnals in both off- and along-slope direction (Hickey et al., 1986; Thorpe and White, 1988; Durrieu de Madron et al., 1990).

Offshore, the suspended material in the euphotic layer is dominated by biological organisms (as phyto/zooplankton) in the surface layer, which settle under the form of marine detritus, also called "marine snow" (Asper, 1987; Alldredge and Gotschalk, 1988; Alldredge and Silver, 1988).

Close to the seabed, a large but diffuse deep BNL is alimented by the detritus falling from the surface waters as well as from SPM exported from continental margins. This export occurs mainly during meteorological events, as storms, which create instabilities of the water column and enhance the particulate along and cross-shelf transport by advection, cascading or gravity flow (Biscaye and Eittreim, 1977; McCave, 1986). Deep BNL particles can then be advected over large areas by deep bottom currents or can sediment on the seabed. During extreme meteorological (storm) or oceanic (convection and advection) conditions, particulate resuspension can occurred that increases the SPM concentration in the water column (>1000 m high) (Gardner and Sullivan, 1981; Nyffeler and Godet, 1986; Auffret et al., 1994).

1.2 The SPM dynamics over continental margins

The SPM dynamics over continental margins depends on the balance of several processes such as SPM inputs (i.e. ROFIs location and coastal rivers discharge) (see 1.2.1) and particulate deposition, resuspension and transport (i.e. seabed morphology, waves and bottom currents) (see 1.2.2). Properties of suspended particles, as size, nature, density and shape, as well as processes of flocculation / break up of fine and cohesive sediments are factors controlling the particle dynamics as the settling velocity and are thus key factors regulating particulate deposition and transport (see 1.2.3).

1.2.1 Regions Of Freshwater Influence (ROFIs)

Regions Of Freshwater Influence (ROFIs) are considered as distinctive regions of the coastal ocean where the riverine inputs can be very important (Simpson, 1997; Simpson and Sharples, 2012). ROFIs are constrained by several physical processes regulating the mixing of turbid and fresh water from rivers with ambient seawater and are thus key areas in the understanding of the fate of land-derived material.

In micro-tidal areas as most of the Mediterranean, small tides (∼30 cm) generally limit the mixing of river inputs and seawater. The high salinity gradient, which plays the role of a physical barrier, allows the motion of the freshwater and turbid input, called river plume, over the ambient seawater (Fig. 1.3) (Chao and Boicourt, 1986). While the majority of observations carried out in front of worldwide river mouths show the presence of hypopycnal plumes, i.e. surface-trapped, a few example of hyperpycnal, i.e. bottom-trapped river plumes, have been reported (Mulder and Syvitski, 1995; Mulder et al., 2003; Katz et al., 2015). These rare examples of river plumes are generally observed during extreme flooding conditions when the river SPM concentrations are

higher than 5 g L^{-1}. Due to the hypopycnal character of the river plumes further studied in this work, we only considered the behavior of surface-trapped river plumes in terms of SPM dynamics and properties.

In the absence of meteorological forcing, hypopycnal plumes dynamic is controlled by the Coriolis force, tend to deflect to the right in the northern hemisphere and conversely to the left in the southern hemisphere. Due to this deviation, the flow is generally oriented along the coast and is then considered as an along-shelf flow, which is perpendicular to the cross-shelf component. During wind events, river plumes are affected by the Ekman transport (Chao, 1988). In case of continental winds inducing upwelling, river plumes are pushed offshore and detached from river mouths whereas marine winds inducing downwelling favor the spreading of river plumes along the coasts (Fong and Geyer, 2001).

While a low river discharge creates a constant, diffuse and small plume, a flood can carry a lot of SPM and create a large and turbid river plume, which can spread over seawater from tens to hundreds kilometers before settling due to vanishing. Observations of SPM collected near river mouth generally show that sediments as sand and coarse silt, rapidly settle from surface water toward the bottom where they contribute to generate and maintain the local BNL or form ephemeral deposits (Drake, 1976).

River plumes are thus composed of fine silt and clays, which stays in suspension and are progressively advected offshore by currents. River plumes SPM concentration generally presents a seaward logarithmically decrease, due to the dilution within seawater from the near-plume to the far-field plume. In some cases, the removal of suspended particles from the plume can be accentuated by fine sediment flocculation processes (see 1.2.3) that enhance the particles size and related settling velocity. Mixing with seawater generally depends on the level of turbulence induced by waves, tides and winds stress which can create disturbances of the plume stratification and the settling of SPM (Garvine, 1999; Whitney and Garvine, 2005) (Fig. 1.3).
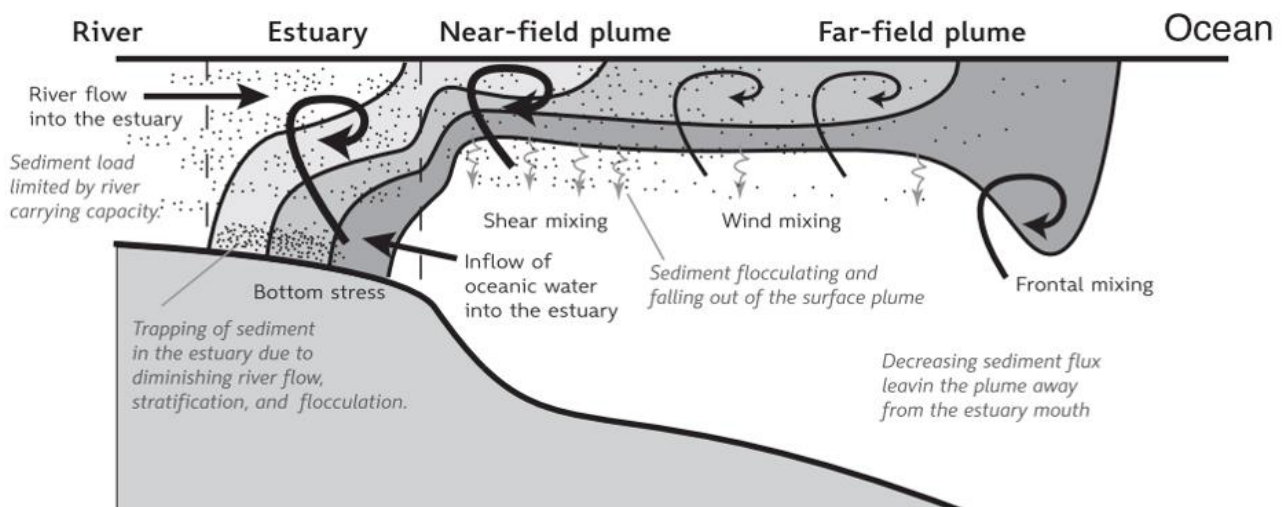

Figure 1.3 : Conceptual view of the cross-section of a surface-trapped river plume. The various dynamical regions and the mixing processes are shown. The diagram is not to scale, far-field regions are generally larger than estuary and near-field plume regions. From Hetland (2005)

To highlight the diversity of surface river plumes, several true color satellite images (MODIS – EOSDIS Worldview) have been assembled in Figure 1.4 (p.15). We present a non-exhaustive list of river inputs to the coastal sea, separated following the river discharge (low < 500 m^3 s^{-1}, medium < 10 000 m^3 s^{-1}, high) and the preferential forcing that permit the SPM sedimentation and/or transport to the local continental margin (winds, waves and tides).
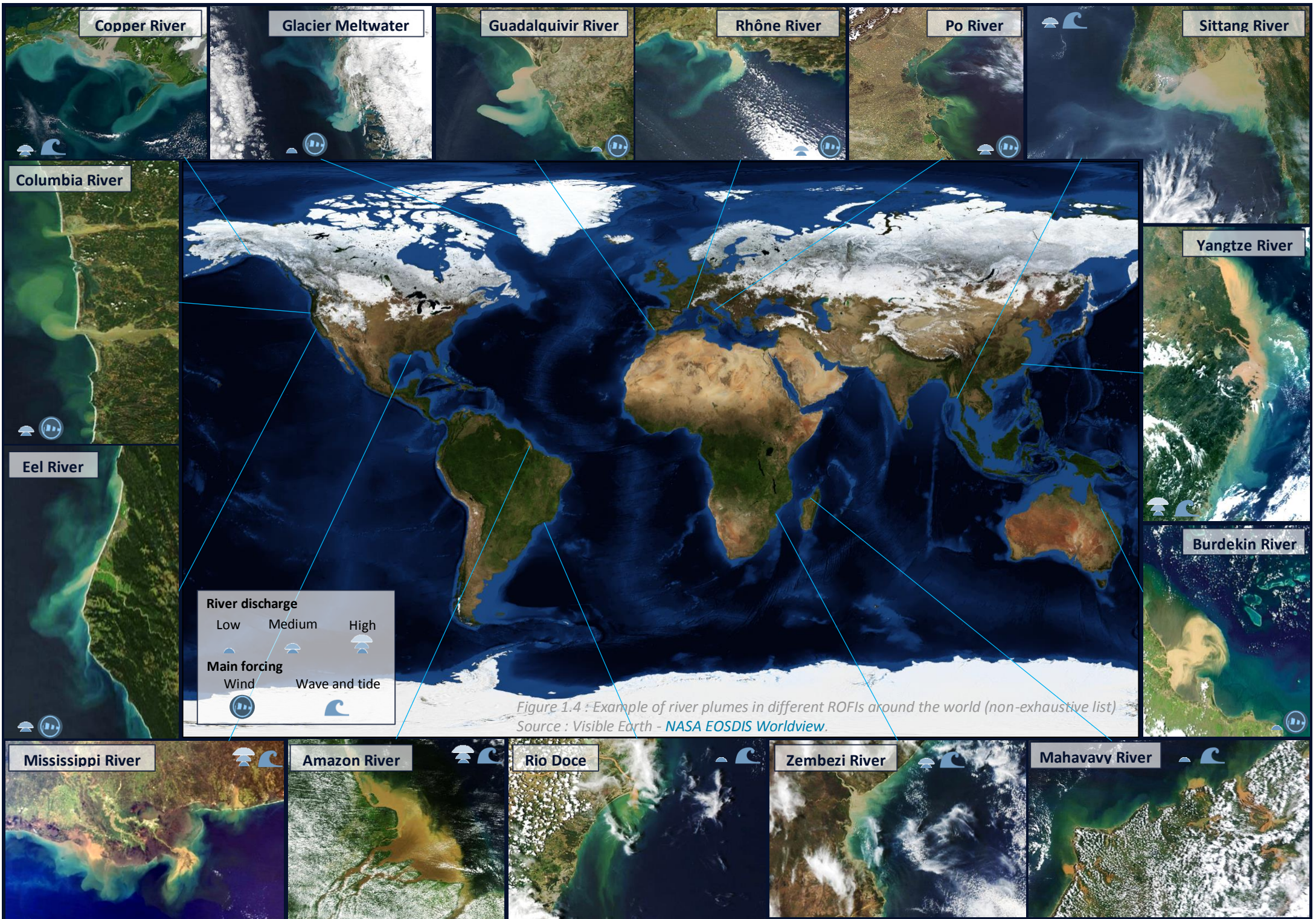
This representation allows the observation of a small part of worldwide ROFIs and emphasizes the role of coastal morphologies, tides, winds, rivers discharge and suspended particles properties in the delivery of SPM within coastal seas (Amazon River: Gibbs and Konwar, 1986 Burdekin River: Bainbridge et al., 2012; Eel River : Hill et al., 2000; Glacier Bay; Hill et al., 1998; Hudson River : Castelao et al., 2008 Po River : Milligan et al., 2007; Fox et al., 2004).

As a matter of fact, Milliman and Meade (1983) and Milliman and Syvitsky (1992) show that the monitoring of large, medium and small rivers are decisive in the worldwide delivery of river SPM, which is estimated to 20 billion tons annually. For instance, these authors estimate that small and medium rivers (i.e. mean annual rivers discharge < 10 000 m^3 s^{-1}) represent for around half the annual suspended sediment load to the sea. While large rivers as Amazon, Yangtze and Mississippi Rivers have been largely described in past decades, a need still exists in the monitoring of both small and medium rivers in order to assess the role of these numerous rivers in the delivery of SPM to coastal seas.

Key Questions

ROFIs appear as key areas in the understanding of the coastal SPM dynamics. While the seasonal variability of river inputs and related nepheloid layers have been studied, a need exists to monitor at **high spatial and temporal-resolution the suspended particles properties and dynamics within ROFIs during large inputs events (floods)**. Sedimentation processes are still seldom quantified, in particular the **in situ particle assemblage properties (nature, size, shape, effective density and settling velocity)**, which are decisive parameters to model the settling of particles from river plumes to the seabed (see modellings of Winterwerp (1998); Khelifa and Hill (2006); Manning et al. (2011); Soulsby et

Hyperpycnal River plume

Hypopycnal River plume

Figure 1.4 : Example of river plumes in different ROFIs around the world (non-exhaustive list)
Source : Visible Earth - NASA EOSDIS Worldview.

Copper River

Glacier Meltwater

Guadalquivir River

Rhône River

Po River

Sittang River

Columbia River

Yangtze River

Eel River

Burdekin River

River discharge

Low   Medium   High

Main forcing

Wind   Wave and tide

Mississippi River

Amazon River

Rio Doce

Zembezi River

Mahavavy River

1.2.2 Deposition, resuspension and transport

The deposition of SPM within ROFIs can subsequently be impacted by erosion (i.e. resuspension by waves) and transport (by currents) that contribute to the particulate redistribution over the entire shelf. The balance between deposition and erosion, called accumulation, is generally estimated on decadal/centennial time scales from geochemical tracers as ^{210}Pb (Nittrouer et al., 2009). In the long term, the study of this accumulation allows the analysis of the succession of storm and flood events, the estimation of sedimentary budgets and the understanding of the formation of sedimentary stratas.

On continental margins a decrease of the influence of wave and current with the increase of depth is generally observed along the cross-shelf transect. The sand, also called "bedload" is generally transported along the shore, where it aliments the local beach. It is generally assumed that the transport of sand is limited for depth greater than 10 m where wave action drastically decreases. The mud, or "suspended load", is commonly transported over depth greater than 10 m within the BNL where it can feed the mid-shelf mud-belt. To explain the formation of the mud-belt in central part of shelves, several processes have been emphasized as the wave-generated diffusion (Swift, 1970), the advection from bottom currents (McCave, 1982) and the transport within gravity-driven flow (Moore, 1969) (see Fig. 1.5 a-c). The seabed over the inner- and mid-shelf generally presents a decreasing sediment particle size with increasing depth, which highlights the seaward graded bedding from the beach (sand) to the mid-shelf (mud-belt) (Fig. 1.5b) (Hill et al., 2007).

The location and thickness of the fine-grained deposits (i.e. the mid-shelf mud-belt) thus depends upon the balance between hydrodynamics and sedimentary inputs. In this balance, storms appear as key processes (McCave, 1972; Harris and Wiberg, 2002; Cattaneo et al., 2007). While episodic, these events can impact large areas over continental margins from the coast to the 40-50 m isobaths. Storm waves (generally > 5 m high) resuspend the recent sediment deposit and strong currents enhance the particulate transport. In some cases, depending on the location over the shelf, suspended particles can then eventually be exported offshelf by gravity flow, downwelling or advection, where it can aliment the deep BNL or extent the mud areas over adjacent continental margins.
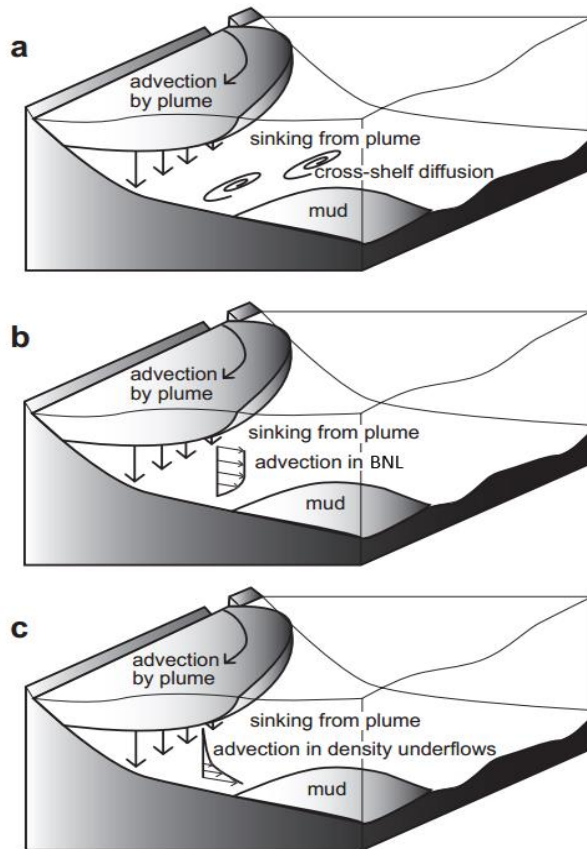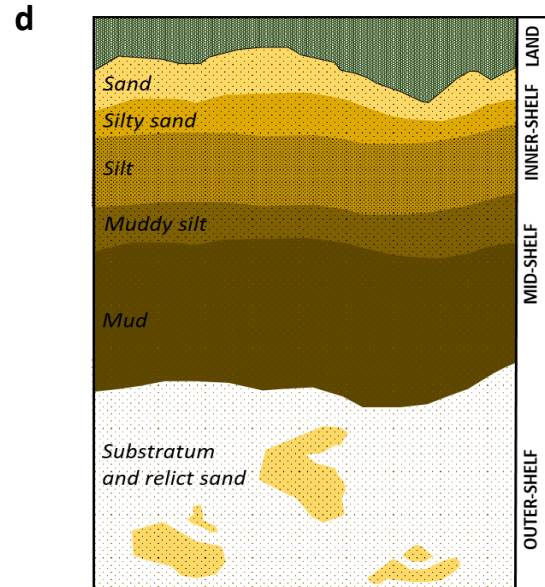
Figure 1.5 : Conceptual models of the creation of a mid-shelf mud-belt, a) wave cross-shelf diffusion, b) advection in BNL, c) advection in density underflows, d) schematic representation of the horizontal graded bedding observed over continental margins (adapted from Hill et al. 2007)

Key Questions

Storms are thus decisive processes in the regulation of SPM dynamics in the coastal zone and are still misunderstood due to the sampling difficulties. A need exists in **the high-resolution description** of the spatial and temporal gradients across continental margins **to evaluate the suspended particles transport** in order to understand the evolution of sedimentary budgets of shelves. **The identification of suspended particles properties** appears as essential in the understanding of the particulate transport across the shelf.

1.2.3 Fine-sediment flocculation

We mentioned that suspended particles properties (as particles nature, shape and size) play a major role in suspended particles spread, settling and sedimentation (Nittrouer et al., 2009; Simpson and Sharples, 2012). The settling velocity of a suspended particle can be basically modeled following Stoke's law (Eq. 1.1) :

$$v = \frac{2 \times r^2 \times g \times \Delta\rho}{9 \times \eta}$$
Eq. 1.1

where *v* is the settling velocity of a spherical particle (m s^{-1}), r its radius (m), g the gravitational acceleration (9.81 m s^{-2}), $\Delta\rho$ the effective density of the particle (kg m^{-3}, i.e. the density of the particle minus the density of ambient seawater) and η the viscosity of seawater (typically 1.07.10^{-3}).

Following Equation 1.1, it is obvious that sand (> 63µm), when present, rapidly settle from the surface to the bottom (*v* ~ cm s^{-1}), whereas unique finest-sediments as fine silts (~10µm) and clays (~1µm) show lower settling velocities (*v* ~ µm-mm s^{-1}) and are thus easily transportable offshore within surface river plumes or bottom nepheloid layers (see Figure 1.2).

To explain the sedimentation of fine sediments, several studies emphasize the role of the aggregation, which increases the particle assemblage size (*v* ~ mm-cm s^{-1}) and decreases the related effective density (Gibbs, 1985; Van Leussen, 1994; Dyer and Manning, 1999). Aggregation mechanisms can be various. For instance, biogenic aggregation is define as the creation of faecal pellets by filter-feeding organisms and is particularly observed offshore, where the "marine snow" feed toward the water column. However, this process cannot explain the settling of finest sediments, especially in river plumes due to the mineral character of the particle assemblage. Due to the low salinities observed in river plumes, aggregation is generally enabled by the van der Walls' forces, which enhance the attraction of cohesive sediments. While this process could occur without the presence of organic compounds (called "coagulation", i.e. glacial-meltwater for instance), it is generally assumed that in low and middle latitudes, organic matter plays a role in the maintain of larger aggregates. In this case, the aggregation process is called flocculation and aggregates are called flocs (see details in Nittrouer et al., 2009).

Global observations carried out over continental margins show the predominant role of SPM concentration variability, turbulence and mixing, induced by sea conditions (wave and current) and river discharge, on the creation / break up of fine cohesive sediment flocs, controlling their size and related settling velocity (Curran et al., 2007; Safak et al., 2013). However, coatings and biological contents are also described as factors controlling flocculation as salinity gradient and its influence on flocs growth (Ayukai and Wolanski, 1997; Dagg et al., 2004). In ROFIs, the flocculation process highly participates to the regulation of the vertical flux of the finest particles from the river input. It is also a factor controlling the expansion of the BNL close to the seabed and mud areas over prodeltas and continental margins (Agrawal and Traykovski, 2001).

We generally separate the marine flocs in 3 groups following their size as follow (Fig. 1.6):

- Unique component particles   < 10 μm

- Micro-flocs   10-125 μm

- Macro-flocs   > 125 μm

Microflocs are described as dense and quasi-spherical, resistant to turbulence whereas macroflocs, which can be aerial or dense (see Fig. 1.6), generally present lower density and can easily be fragmented into microflocs by shear forces. Micro- and macro-flocs are generally in a lower abundance than unique and fine particles but can highly contribute to the total volume concentration (generally expressed in μL L^{-1}) (Manning and Dyer, 1999; Manning et al., 2004).
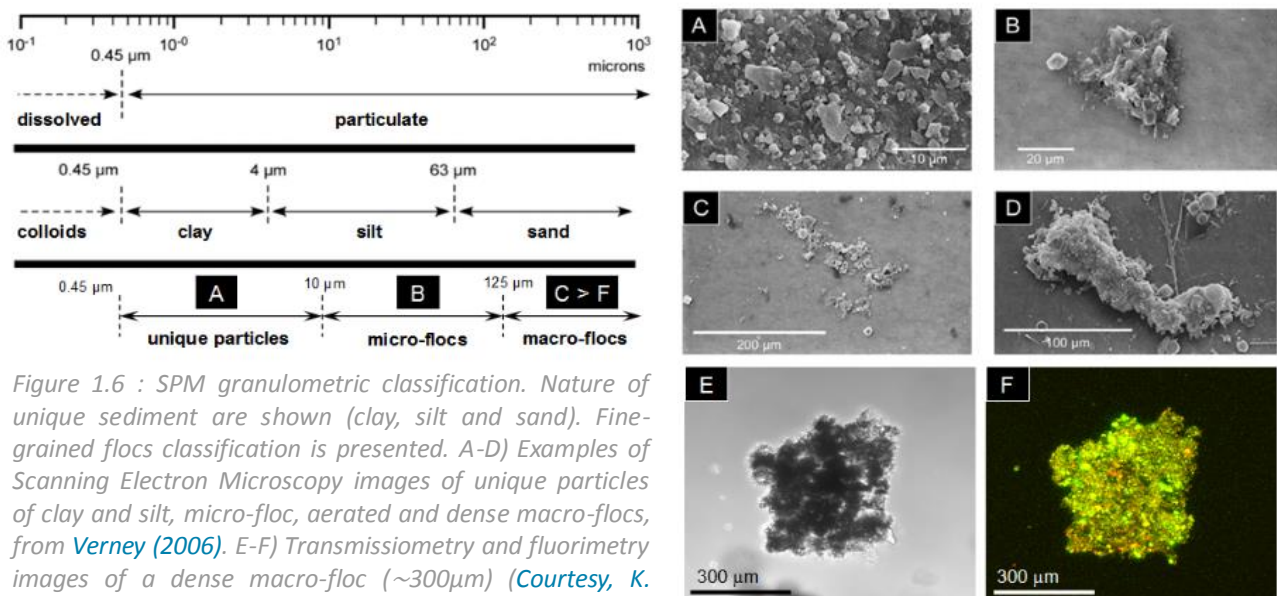
Figure 1.6 : SPM granulometric classification. Nature of unique sediment are shown (clay, silt and sand). Fine-grained flocs classification is presented. A-D) Examples of Scanning Electron Microscopy images of unique particles of clay and silt, micro-floc, aerated and dense macro-flocs, from Verney (2006). E-F) Transmissiometry and fluorimetry images of a dense macro-floc (~300μm) (Courtesy, K. Curran).

The formation of flocs is not constant in space and time (Fig. 1.7). Previous studies highlight the rapid destabilization of a fine-sediment particle assemblage, by an increase of the particle concentration or the setup of strong salinity or biological gradients, which enable the formation of micro-flocs in the particle assemblage in few seconds (Montgomery, 1985; Jarvis et al., 2005). Depending on the particulate transport and the SPM concentration, fragile macro-flocs can then be formed within the particle assemblage. The final particle assemblage observed after the destabilization is composed of unique particles, micro- and macro-flocs whose distribution depends on SPM concentration and turbulence (as waves and currents).
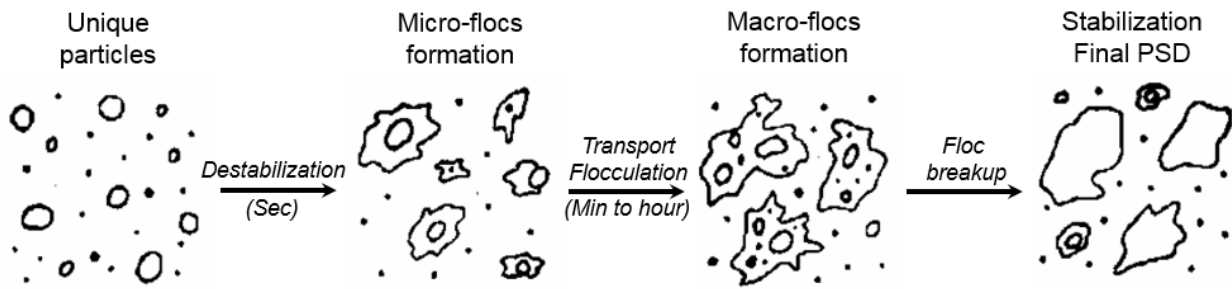
Figure 1.7 : Conceptual view of the formation of marine flocs within a particle assemblage. Processes and time-scales are shown in italic. From Montgomery (1985). Note the intentionally non-spherical shape of suspended particles.

The spread and settling of nepheloid layers thus depends on the variability of the particle assemblage. While the particle size distribution (PSD) is nowadays a common parameter in each SPM dynamics study, the particles shape diversity, however, is still seldom quantified and is often ignored. On Eq. 1.1, the basic settling velocity equation is estimated through the approximation that marine particles are spherical. However, many studies have highlighted the non-spherical shape of suspended particles, in particular of fine-sediments flocs (Jonasz, 1987; Jarvis et al., 2005; 2006; see also the description of Olson (2011)).

On a technical aspect, these observations have highlighted the need to use a "randomly shaped" algorithm process to properly invert the PSD from the light scattering in seawater (see Agrawal et al. (2008) and details in Chapter 3). These observations have introduced the need of an improvement of the estimation of floc settling velocities, considering the flocs shape. Thus, modelling works of Winterwerp (1998), Khelifa and Hill (2006), Manning et al. (2011) or Soulsby et al. (2013) introduce a floc shape parameter. Floc shape parameters can be various (as aspect ratio, convexity, circularity, area, perimeter, see Olson (2011)) and are poorly documented due to the sampling difficulties.

Key Questions

Due to the fragile character of flocs, a need exists in **the in situ monitoring of the size of the particle assemblage**, which avoids turbulences and floc breakup by water sampling and laboratory manipulation. The study of the largest particle size distribution (from 1 to 2000 µm) of the particle assemblage is decisive **to properly estimate the total volume concentration, the proportion of flocs and the effective density** of the particle assemblages. **In situ imagery of flocs shape** remains undocumented and the impact of shape diversity on SPM dynamics is poorly known.

References

Agrawal, Y. C., and P. Traykovski. **2001**. « Particles in the bottom boundary layer: Concentration and size dynamics through events ». *Journal of Geophysical Research* 106: 9533‑42. doi:10.1029/2000JC900160.

Agrawal, Y. C., A. Whitmire, O. A. Mikkelsen, and H. C. Pottsmith. **2008**. « Light scattering by random shaped particles and consequences on measuring suspended sediments by laser diffraction ». *Journal of Geophysical Research* 113 (C4). doi:10.1029/2007JC004403.

Alldredge, A., and C. Gotschalk. **1988**. « In situ settling behavior of marine snow ». *Limnology and Oceanography* 33 (3): 339‑51. doi:10.4319/lo.1988.33.3.0339.

Alldredge, A., and M. Silver. **1988**. « Characteristics, dynamics and significance of marine snow ». *Progress in Oceanography* 20 (1): 41‑82. doi:10.1016/0079-6611(88)90053-5.

Asper, V. L. **1987**. « Measuring the flux and sinking speed of marine snow aggregates ». *Deep Sea Research Part A. Oceanographic Research Papers* 34 (1): 1‑17. doi:10.1016/0198-0149(87)90117-8.

Auffret, G., A. Khripounoff, A. Vangriesheim. **1994**. « Rapid post-bloom resuspension in the northeastern Atlantic. » *Deep Sea Research*, 41, 5, 925-939

Ayukai, T., and E. Wolanski. **1997**. « Importance of Biologically Mediated Removal of Fine Sediments from the Fly River Plume, Papua New Guinea ». *Estuarine, Coastal and Shelf Science* 44 (5): 629‑39. doi:10.1006/ecss.1996.0172.

Bainbridge, Z. T., E. Wolanski, J. G. Álvarez-Romero, S. E. Lewis, and J. E. Brodie. **2012**. « Fine Sediment and Nutrient Dynamics Related to Particle Size and Floc Formation in a Burdekin River Flood Plume, Australia ». *Marine Pollution Bulletin* 65 (4-9): 236‑48. doi:10.1016/j.marpolbul.2012.01.043.

Biscaye, P.E., S.L. Eittreim. **1977** « Suspended particulate loads and transports in the nepheloid layer of the abyssal Atlantic Ocean.» *Marine Geology*, 23, 155—172

Castelao, R., S. Glenn, O. Schofield, R. Chant, J. Wilkin, and J. Kohut. **2008**. « Seasonal Evolution of Hydrographic Fields in the Central Middle Atlantic Bight from Glider Observations ». *Geophysical Research Letters* 35 (3). doi:10.1029/2007GL032335.

Cattaneo, A., F. Trincardi, A. Asioli, and A. Correggiari. **2007**. « The Western Adriatic Shelf Clinoform: Energy-Limited Bottomset ». *Continental Shelf Research* 27 (3-4): 506‑25. doi:10.1016/j.csr.2006.11.013.

Chao, S. **1988**. « Wind-driven motion of estuarine plumes ». *Journal of Physical Oceanography* 18 (8): 1144‑66.

Chao, S., and W. Boicourt. **1986**. « Onset of estuarine plumes ». *Journal of Physical Oceanography* 16 (12): 2137‑49.

Curran, K. J., P. S. Hill, T. G. Milligan, O. A. Mikkelsen, B. A. Law, X. Durrieu de Madron, and F. Bourrin. **2007**. « Settling Velocity, Effective Density, and Mass Composition of Suspended Sediment in a Coastal Bottom Boundary Layer, Gulf of Lions, France ». *Continental Shelf Research* 27 (10-11): 1408‑21. doi:10.1016/j.csr.2007.01.014.

Dagg, M., R. Benner, S. Lohrenz, and D. Lawrence. **2004**. « Transformation of Dissolved and Particulate Materials on Continental Shelves Influenced by Large Rivers: Plume Processes ». *Continental Shelf Research* 24 (7-8): 833‑58. doi:10.1016/j.csr.2004.02.003.

Drake, D. E. **1976**. « Suspended sediment transport and mud deposition on continental shelves ». *Marine sediment transport and environmental management* 40: 127‑58.

Durrieu de Madron, X., F. Nyffeler, and C. H. Godet. **1990**. « Hydrographic structure and nepheloid spatial distribution in the Gulf of Lions continental margin ». *Continental Shelf Research*, France-JGOFS, ECOMARGE Particle Fluxes and Ecosystem Response on a Continental Margin, 10 (9–11): 915‑29. doi:10.1016/0278-4343(90)90067-V.

Dyer, K.R., and A. J. Manning. **1999**. « Observation of the size, settling velocity and effective density of flocs, and their fractal dimensions ». *Journal of Sea Research* 41 (1–2): 87‑95. doi:10.1016/S1385-1101(98)00036-7.

Fong, D. A, and W R. Geyer. **2001**. « Response of a river plume during an upwelling favorable wind event ». *Journal of Geophysical Research: Oceans (1978–2012)* 106 (C1): 1067‑84.

Fox, J. M., P. S. Hill, T. G. Milligan, and A. Boldrin. **2004**. « Flocculation and sedimentation on the Po River Delta ». *Marine Geology* 203 (1–2): 95‑107. doi:10.1016/S0025-3227(03)00332-3.

Gardner, W.D., L.G. Sullivan. **1981** « Benthic storms: temporal variability in a deep-ocean nepheloid layer. » *Science*, 213, 4505, 329-331

Garvine, R. W. **1999**. « Penetration of buoyant coastal discharge onto the continental shelf: A numerical model experiment ». *Journal of Physical Oceanography* 29 (8): 1892‑1909.

Gibbs, R. J. **1985**. « Estuarine Flocs: Their Size, Settling Velocity and Density ». *Journal of Geophysical Research: Oceans* 90 (C2): 3249‑51. doi:10.1029/JC090iC02p03249.

Gibbs, R. J., and L. Konwar. **1986**. « Coagulation and

settling of Amazon River suspended sediment ». *Continental Shelf Research*, Sedimentary Processes on the Amazon Continental Shelf, 6 (1–2): 127‑49. doi:10.1016/0278-4343(86)90057-9.

Harris, C., and P. Wiberg. **2002**. « Across-shelf sediment transport: Interactions between suspended sediment and bed sediment ». *Journal of Geophysical Research: Oceans* 107 (C1).

Hetland, R. **2005**. « Relating river plume structure to vertical mixing ». *Journal of Physical Oceanography* 35 (9): 1667‑88.

Hickey, B., E. Baker, and N. Kachel. **1986**. « Suspended particle movement in and around Quinault submarine canyon ». *Marine Geology* 71 (1): 35‑83. doi:10.1016/0025-3227(86)90032-0.

Hill, P. S., J. M. Fox, J. S. Crockett, K. J. Curran, C. T. Friedrichs, R. W. Geyer, T. G. Milligan, A. S. Ogston, P. Puig, and M. E. Scully. **2007**. « Sediment delivery to the seabed on continental margins ». *Continental-Margin Sedimentation: From Sediment Transport to Sequence Stratigraphy, IAP Special Publication* 37: 49‑100.

Hill, P. S., T. G. Milligan, and W. R. Geyer. **2000**. « Controls on effective settling velocity of suspended sediment in the Eel River flood plume ». *Continental Shelf Research*, Oceanic Flood Sedimentation, 20 (16): 2095‑2111. doi:10.1016/S0278-4343(00)00064-9.

Hill, P. S., J. P. Syvitski, E. A. Cowan, and R. D. Powell. **1998**. « In situ observations of floc settling velocities in Glacier Bay, Alaska ». *Marine Geology* 145 (1–2): 85‑94. doi:10.1016/S0025-3227(97)00109-6.

Jarvis, P., B. Jefferson, and S. A. Parsons. **2005**. « Measuring Floc Structural Characteristics ». *Reviews in Environmental Science and Bio/Technology* 4 (1-2): 1‑18. doi:10.1007/s11157-005-7092-1.

Jarvis, P. **2006**. « Floc structural characteristics using conventional coagulation for a high doc, low alkalinity surface water source ». *Water Research* 40 (14): 2727‑37. doi:10.1016/j.watres.2006.04.024.

Jonasz, M. **1987**. « Nonsphericity of Suspended Marine Particles and Its Influence on Light scattering1 ». *Limnology and Oceanography* 32 (5): 1059‑65. doi:10.4319/lo.1987.32.5.1059.

Katz, T., H. Ginat, G. Eyal, Z. Steiner, Y. Braun, S. Shalev, and B.N. Goodman-Tchernov. **2015**. « Desert flash floods form hyperpycnal flows in the coral-rich Gulf of Aqaba, Red Sea ». *Earth and Planetary Science Letters* 417: 87‑98.

Khelifa, A., and P. S. Hill. **2006**. « Models for effective density and settling velocity of flocs ». *Journal of Hydraulic Research* 44 (3): 390‑401.

Manning, A. J., and K. R. Dyer. **1999**. « A laboratory examination of floc characteristics with regard to turbulent shearing ». *Marine Geology* 160 (1–2):

147‑70. doi:10.1016/S0025-3227(99)00013-4.

Manning, A. J., K. R. Dyer, R. Lafite, and D. Mikes. **2004**. « Flocculation measured by video based instruments in the Gironde Estuary during the European Commission SWAMIEE project ». *Journal of Coastal Research*, 58‑69.

Manning, A. J., J. R. Spearman, J. V. Baugh, R. J. S. Whitehouse, et R. L. Soulsby. **2011**. *Cohesive sediment flocculation and the application to settling flux modelling*. INTECH Open Access Publisher. http://cdn.intechweb.org/pdfs/15517.pdf.

McCave, I. N. **1972**. « Transport and escape of fine-grained sediment from shelf areas. » *Shelf Sediment Transport: Process and Pattern. Dowden, Hutchinson, and Ross, Stroudsburg, Pennsylvania,* 225–248.

McCave, I. N. **1986**. « Local and global aspects of the bottom nepheloid layers in the world ocean. » Netherlands *Journal of Sea Research*, 20, 2, 167-181.

Milligan, T. G., P. S. Hill, and B. A. Law. **2007**. « Flocculation and the loss of sediment from the Po River plume ». *Continental Shelf Research*, Sediment Dynamics in the Western Adriatic Sea, 27 (3–4): 309‑21. doi:10.1016/j.csr.2006.11.008.

Milliman, J.D., and R.H. Meade. **1983**. « World-wide delivery of river sediment to the oceans ». *The Journal of Geology* 91, 1‑21.

Milliman, J.D., and J. Syvitski. **1992**. « Geomorphic/tectonic control of sediment discharge to the ocean: the importance of small mountainous rivers ». *The Journal of Geology* 100, 525‑44.

Moore, D.G. **1969**. « Reflection profiling studies of the California continental borderland: structure and quaternary turbidite basins. » *Geological society of America special papers* 107, 142p.

Montgomery, J. A. **1985**. « Precipitation, Coagulation, Flocculation ». *Water Treatment Principles and Design*, 116‑34.

Mulder, T., and J. P. M. Syvitski. **1995**. « Turbidity currents generated at river mouths during exceptional discharges to the world oceans ». *The Journal of Geology*, 285‑99.

Mulder, T., J. P. M. Syvitski, S. Migeon, J. C. Faugères, and B. Savoye. **2003**. « Marine hyperpycnal flows: initiation, behavior and related deposits. A review ». *Marine and Petroleum Geology* 20 (6-8): 861‑82. doi:10.1016/j.marpetgeo.2003.01.003.

Nittrouer, C. A., James A. Austin, M. E. Field, J. H. Kravitz, J. P. M. Syvitski, and P. L. Wiberg. **2009**. *Continental Margin Sedimentation: From Sediment Transport to Sequence Stratigraphy (Special Publication 37 of the IAS)*. John Wiley & Sons. 560 p.

Nyffeler, F., and C. Godet. **1986**. « The structural

parameters of the benthic nepheloid layer in the northeast Atlantic ». *Deep Sea Research Part A. Oceanographic Research Papers* 33 (2): 195‑207. doi:10.1016/0198-0149(86)90118-4.

Olson, E. **2011**. « Particle Shape Factors and Their Use in Image Analysis-Part 1: Theory ». *Journal of GXP Compliance* 15 (3): 85.

Safak, I., M. A. Allison, and A. Sheremet. **2013**. « Floc variability under changing turbulent stresses and sediment availability on a wave energetic muddy shelf ». *Continental Shelf Research* 53 (février): 1‑10. doi:10.1016/j.csr.2012.11.015.

Shideler, G. L. **1981**. « Development of the benthic nepheloid layer on the south Texas continental shelf, western Gulf of Mexico ». *Marine Geology* 41 (1-2): 25.

Simpson, J. H. **1997**. « Physical processes in the ROFI regime ». *Journal of marine systems* 12 (1): 3‑15.

Simpson, J. H., and J. Sharples. **2012**. *Introduction to the physical and biological oceanography of shelf seas*. Cambridge University Press.

Soulsby, R. L., A. J. Manning, J. Spearman, and R. J. S. Whitehouse. **2013**. « Settling velocity and mass settling flux of flocculated estuarine sediments ». *Marine Geology* 339: 1‑12.

Stramski, D., E. Boss, D. Bogucki, and K. J. Voss. **2004**. « The Role of Seawater Constituents in Light Backscattering in the Ocean ». *Progress in Oceanography* 61 (1): 27‑56. doi:10.1016/j.pocean.2004.07.001.

Swift, D.J.P. **1970**. « Quaterny shelves and the return to grade ». *Marine Geology* 8, 5-30.

Thorpe, S. A., and M. White. **1988**. « A deep intermediate nepheloid layer ». *Deep Sea Research Part A. Oceanographic Research Papers* 35 (9): 1665‑71. doi:10.1016/0198-0149(88)90109-4.

Van Leussen, W. **1994**. *Estuarine Macroflocs and Their Role in Fine-Grained Sediment Transport*. GIP-Gigevens Koninklijke bibliotheek.

Verney, R. **2006**. « Processus de contrôle de la dynamique des sédiments cohésifs: Mesures in situ, mesures expérimentales et modélisation ».

Wheatcroft, R. A., A. W. Stevens, and R. V. Johnson. **2007**. « In Situ Time-Series Measurements of Subseafloor Sediment Properties ». *IEEE Journal of Oceanic Engineering* 32 (4): 862‑71. doi:10.1109/JOE.2007.907927.

Whitney, M. M, and R. W Garvine. **2005**. « Wind influence on a coastal buoyant outflow ». *Journal of Geophysical Research: Oceans* 110 (C3).

Wiberg, P. L., D. A. Cacchione, R. W. Sternberg, and L. D. Wright. **1996**. « Linking sediment transport and stratigraphy on the continental shelf ». *Oceanography-Washington, DC-Oceanography society* ‑ 9: 153‑57.

Winterwerp, J. C. **1998**. « A simple model for turbulence induced flocculation of cohesive sediment ». *Journal of Hydraulic Research* 36 (3): 309‑26.

Wright, L. D. **2012**. « Recent advances in understanding continental shelf sediment transport ». *Sediments, Morphology and Sedimentary Processes on Continental Shelves: Advances in technologies, research and applications (Special Publication 44 of the IAS)* 108: 161.

Chapter 2.

The Gulf of Lions

Chapter 2.   The Gulf of Lions

List of Figures

Figure 2.1 : Morphology of the Gulf of Lions, view is from the south-east. (adapted from Durrieu de Madron et al. (2008)). Vertical exaggeration of 10. Continental and marine winds are shown by orange and red arrows, respectively. Liguro-Provencal current (LPC) is shown by a blue arrow. Mean annual near bottom circulation is shown by a dash-line blue arrow and is detailed on the right panel (Durrieu de Madron et al. (2008)) **26**

Figure 2.2 : a) Significant wave height (m) and b) near-bottom current (cm s^{-1}) fields simulated for the December 4, 2003 storm event. From Ulses et al. (2008b). d) Wave conditions during storm for specific storm return period T (years). Data from Leucate coastal buoy (27 m depth, 2006 − 2015) available on Candhis data center **26**

Figure 2.3 : a) Rhône River water catchment. The yellow star shows the position of Beaucaire-Tarascon gauging station (Code station V7200015) b): Monthly averaged Rhône River discharge from 1920 to 2011(Compagnie Nationale du Rhône) c) Rhône River discharge for specific flood return period T (years).. **27**

Figure 2.4 : a) Volume particle size distribution (PSD) of the Rhône River SPM (gray). Cumulative PSD is shown in orange. b) SPM composition (% of clays, silts and sands in the total volume of SPM). LISST-Streamside measurements (November 2011, SORA station – Arles). **28**

Figure 2.5 : Morphological and bathymetric map of the Gulf of Lions shelf, from Bourrin (2007). a) Map of the Holocene sedimentary deposits (Monaco et Aloisi, 2000). b) Map of the spatial repartition of sedimentary deposits over the shelf (Monaco et Aloisi, 2000). Red dash-line rectangles show the Rhône River ROFI (right) and the Roussillon shelf (left), study areas of Chapter 4 - 5 and 6 respectively. Both maps compiled several sedimentary studies carried out during past decades (Monaco, 1971; Got, 1973; Aloïsi, 1986). These works are integrated in a global GIS available on the OSU OREME (Observatoire de REcherche Méditerranéen de l'Environnement) website. **29**

Figure 2.6 : Conceptual view of the SPM dynamics within the Gulf of Lions during a) stratified and fall conditions, b) unstratified and winter conditions (continental winds), c) unstratified and winter conditions (marine wind). From Palanques et al. (2006). **30**

Figure 2.7 : Conceptual view of the different nepheloid layers found in front of the Rhône River mouth. Surface river plume, intermediate nepheloid layer (INL) and bottom nepheloid layer (BNL) are shown. Filled-arrows show the possible advection of nepheloids, dashed-arrows the possible sedimentation of particles and bold-arrows the burial of sediments. From Aloisi et al. (1982). **32**

This chapter highlights the regional settings of the Gulf of Lions (GoL). First, a general overview of the characteristics of the GoL is presented. Then, the focus is made on the shelf hydrodynamic, the rivers influence and related suspended particle dynamics.

2.1 Overview

2.1.1 General description

The Gulf of Lions, located in the northwestern Mediterranean, is a wide continental shelf surrounded by the Alps, the Massif Central, and the Pyrenees. It has crescent-shape form and extends over 6700 km² from Cap Croisette at the eastern end to Cap de Creus at its southwestern end. The Gulf presents mean and maximal depths of 90 and 170 m, respectively. It has a maximum shelf width of 70 km and represents a privileged area for rivers deposits from the Rhône and small coastal rivers. The continental slope (between 130 and 2000 m depth with an average seabed inclination of 5-10%) is incised by several submarine canyons (Figure 2.1), which play an important role in the hydrodynamic of the Gulf, particularly in the export of water and particulate matter between the shelf and the basin (Durrieu de Madron et al., 1990, 1999; Bonnin et al., 2008; Flexas et al., 2002; Palanques et al., 2006, 2008).

2.1.2 Regional hydrodynamical conditions

The Gulf of Lions is considered as a very dynamical system where wind-induced current and wave actions are important for particulate transport. Due to the micro-tidal character of the Mediterranean (maximum tidal amplitude of 30 cm (Makaske and Augustinus, 1998)), coastal hydrodynamical conditions are mainly influenced by the general circulation along the continental slope (i.e. the northern Liguro-Provencal Current (LPC), see Petrenko (2003)), the freshwater inputs from the Rhône River (Broche et al., 1998; Marsaleix et al., 1998; Estournel et al., 2001; Lorthiois et al., 2012) and the wind-driven circulations (Millot, 1990; Estournel, 2003; Duffau-Julliand et al., 2004; Petrenko et al., 2005; Palanques et al., 2006; Ulses et al., 2008a; Dufois et al., 2014) (Fig. 2.1).

Marine storms are a consequence of winds coming from east and south-east and are generally observed during fall and winter. These winds are higher than 10 m s^{-1}, generally brief (3 days) and rare (6% of the time) (Ulses et al. 2008a). The long fetch leads to a large swell and strong currents that enable particulate resuspension and transport over most of the shelf (see 2.2.2). Besides, marine storms often precede river floods as the transport of humidity over coastal relief induces high precipitation.

During these events, the general circulation is cyclonic and the convergence at the southwestern end of the Gulf induces a strong downwelling on the upper slope and canyon heads (see Fig. 2.2b). During winter, the export toward the basin can be enhanced by the combination of storm–induced downwelling with the presence of cold dense water on the shelf and the weak stratification of the water column on the slope (Palanques et al., 2006; Ulses et al. 2008a).
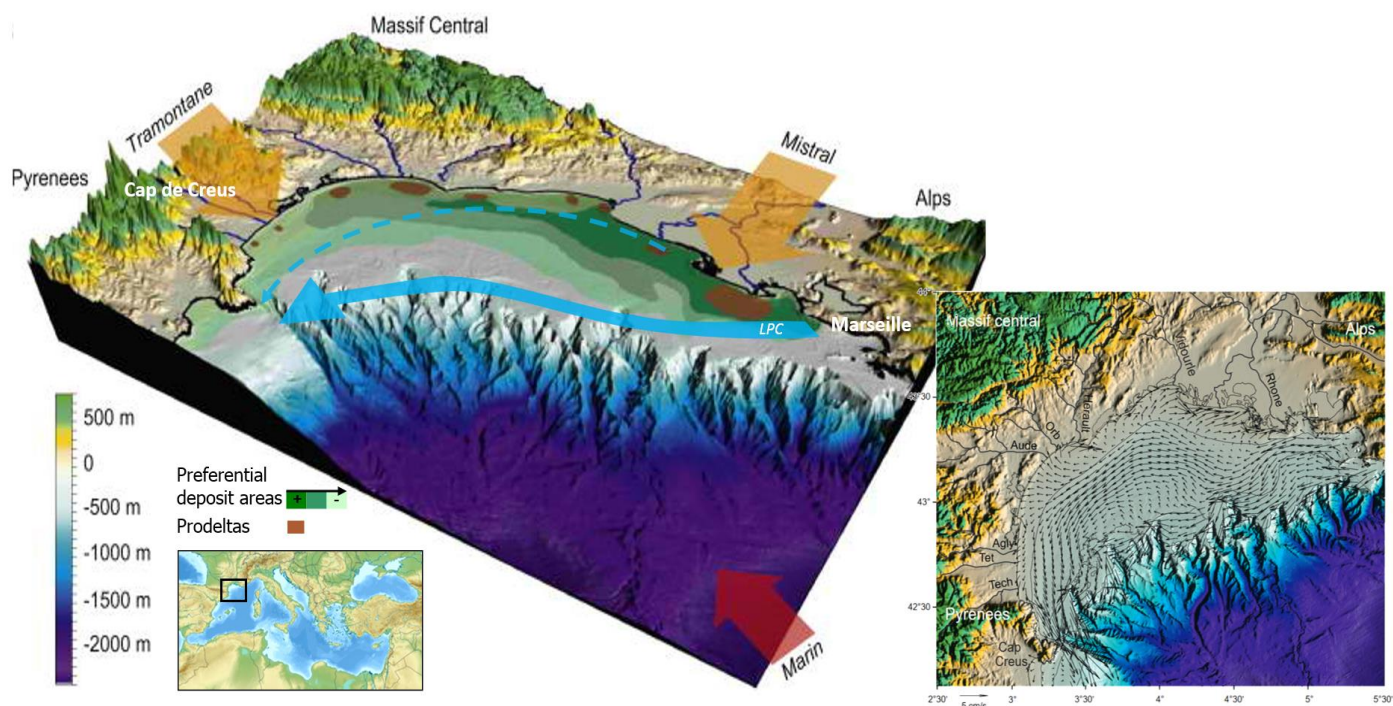
Figure 2.1 : Morphology of the Gulf of Lions, view is from the south-east. (adapted from *Durrieu de Madron et al. (2008)*). Vertical exaggeration of 10. Continental and marine winds are shown by orange and red arrows, respectively. Liguro-Provencal current (LPC) is shown by a blue arrow. Mean annual near bottom circulation is shown by a dash-line blue arrow and is detailed on the right panel (*Durrieu de Madron et al. (2008)*).
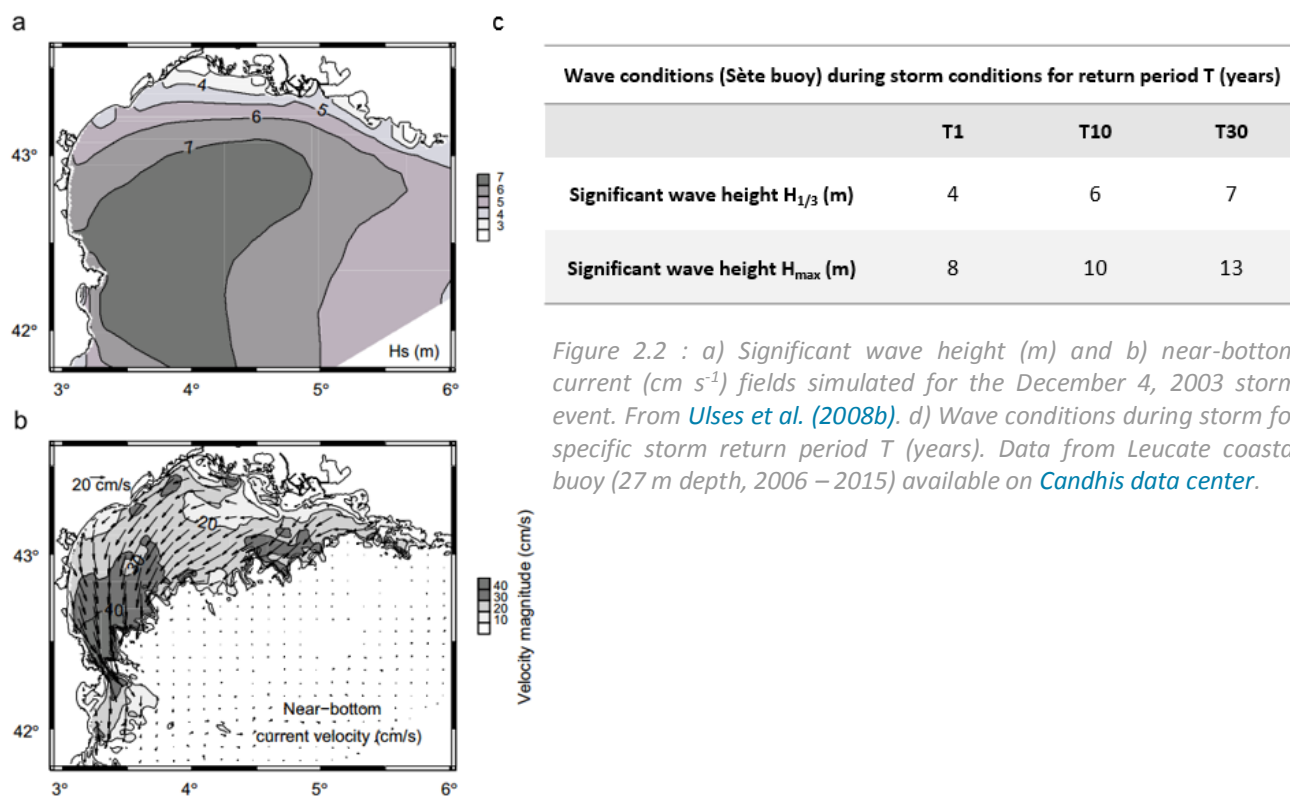

Wave conditions (Sète buoy) during storm conditions for return period T (years)

	T1	T10	T30
Significant wave height $H_{1/3}$ (m)	4	6	7
Significant wave height H_{max} (m)	8	10	13

Figure 2.2 : a) Significant wave height (m) and b) near-bottom current (cm s^{-1}) fields simulated for the December 4, 2003 storm event. From *Ulses et al. (2008b)*. d) Wave conditions during storm for specific storm return period T (years). Data from Leucate coastal buoy (27 m depth, 2006 – 2015) available on *Candhis data center*.

2.1.3 Rivers influence

Rhône River - Since the dramatic decrease of the Nil river discharge (Assouan dam, 1970), the Rhône is the largest Mediterranean river in term of particulate and freshwater inputs (Copin-Montégut, 1993; Pont et al., 2002). The Rhone River drains a water catchment of 97 800 km² (Fig. 2.3a). Sixty kilometers upstream the sea, the river is divided in the Grand Rhône and Petit Rhône Rivers that represent respectively 90 and 10% of the total water and solid discharges.

The Rhône presents a high seasonal variability (mean annual discharge of 1700 m^3 s^{-1}) with maximum discharges observed during autumn and winter, during which the largest floods generally occur, or during the melting snow period in spring (see Fig. 2.3b, Compagnie Nationale du Rhône, 1920-2011 database). The river supplies 80% of the sedimentary input to the Gulf of Lions (Courp and Monaco, 1990; Bourrin and Durrieu de Madron, 2006).

Typical flood events of 5000 m^3 s^{-1} (annual) and 8000 m^3 s^{-1} (decennial) have been investigated by Maillet et al. (2006) (see Fig. 2.3c). These authors estimate average annual particle flux about 7.10^6 tons per year with a high interannual variability of 1.2 to 19.7 .10^6 t y^{-1}. This estimation is complemented with the work of Sadaoui et al. (2016), who estimate an average annual particle flux to 8.10^6 t y^{-1} ± 4.5 t y^{-1} (1977-2013 period). Pont (1996) estimates the contribution of flood events at 70% of the total particle flux, highlighting the role of these episodic events in the SPM delivery to the shelf.
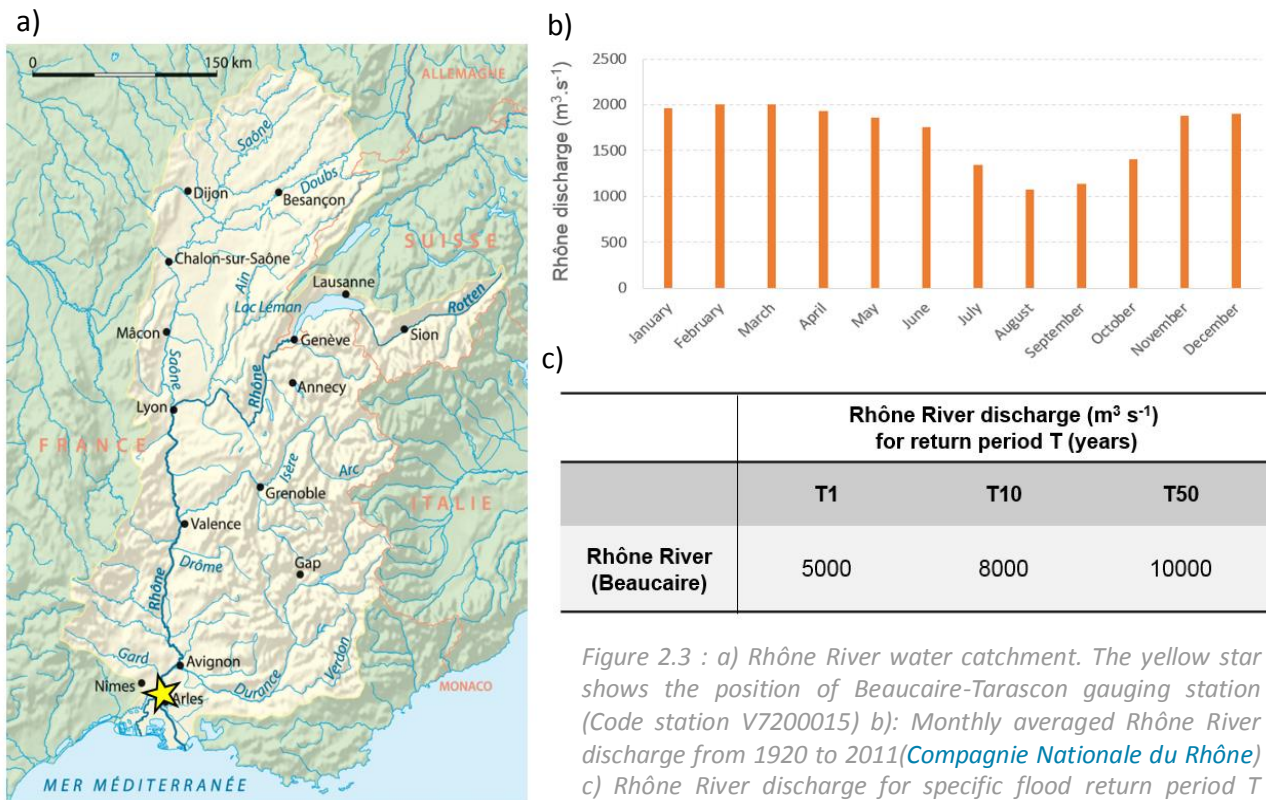
a)

b)

c)

	Rhône River discharge (m^3 s^{-1}) for return period T (years)		
	T1	**T10**	**T50**
Rhône River (Beaucaire)	5000	8000	10000

Figure 2.3 : a) Rhône River water catchment. The yellow star shows the position of Beaucaire-Tarascon gauging station (Code station V7200015) b): Monthly averaged Rhône River discharge from 1920 to 2011(Compagnie Nationale du Rhône) c) Rhône River discharge for specific flood return period T (years).

A few studies highlight the composition of the solid discharge of the Rhône River. For instance, Antonelli (2002) and Antonelli et al. (2008) show the importance of clays, silts and sands in the SPM inputs to the shelf with average values of 18 and 80 and 2%, respectively. These proportions are not constant over time and can significantly change during flooding conditions. For instance, during the 2003 flood event (Rhône discharge of 11 000 m^3 s^{-1}), Antonelli et al. (2008) estimate that sand and clays/silts fractions represented respectively 15 and 85%. These estimations are complemented with the work of Adell (2013) (Fig. 2.4), who estimate to 12, 79 and 9% the proportions of clays, silts and sands in the SPM load of the Rhône River during a 1-month monitoring (November 2011, SORA station, Arles).
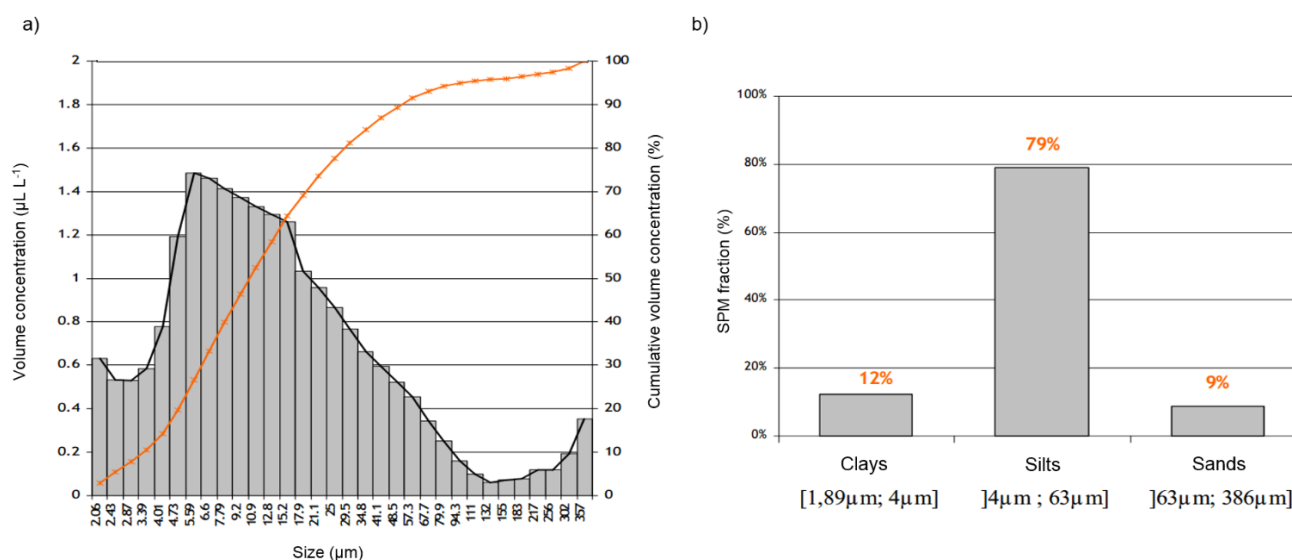
Figure 2.4 : a) Volume particle size distribution (PSD) of the Rhône River SPM (gray). Cumulative PSD is shown in orange. b) SPM composition (% of clays, silts and sands in the total volume of SPM). LISST-Streamside measurements (November 2011, SORA station – Arles).

Coastal rivers - Coastal rivers of the Gulf of Lions (i.e. from south to north: Tech, Têt, Agly, Aude, Orb, Herault, Lez and Vidourle, see Fig. 2.5) present a different character than the Rhône River with a higher seasonal variability. These small mountainous rivers present small discharges during summer and large flood events during winter conditions (Serrat et al., 2001). They generally present water catchment areas that are generally steeper and smaller than large water catchments as for the Rhône River (see Milliman and Syvitski, 1992). Due to their orientations facing the sea and their "auditorium" forms, they present a receptacle for clouds and related precipitations bring by marine winds. Thus, during episodic east-southeast (E-SE) wind that yield to large precipitation, these rivers can reach dramatic discharges in a short timeframe, called "flash-flood" or "oceanic-flood" events (Wheatcroft, 2000). For instance, Bourrin et al. (2008b) highlighted the role of the Têt River in the SPM delivery to the shelf during a 5 year flood in April 2004. During this flood event, these authors estimated to ~25% and ~75% the fraction of sands and clays/silts in the total SPM delivered by small rivers to the Gulf of Lions shelf.

2.1.4 Morpho-bathymetry and sedimentary properties

The Gulf of Lions appears as a preferential region of particle deposit mostly influenced by Rhône Rivers inputs. The morpho-bathymetry and sediment properties of the shelf is presented on the Figure 2.4.

In Fig. 2.5a, Holocene mud thickness deposits clearly highlight the role of the Rhône River in the fine-sediment supply to the shelf over the last 10 ky (approx. Holocene period). Maximum mud thickness (~50 m) are located close to the Rhône mouth whereas thickness of less than 5 m are located on the Roussillon shelf (SW of the GoL) where the Rhône influence is minimal and where strong current take place during stormy events (see 2.1.2). Deposit thickness highlights the role of the cyclonic circulation over the shelf in the sediment-deposition and minimum values are observed in front of Cap de Creus, where Quaternary rocky formations outcrop.

Sedimentary units of the Gulf of Lions form a seaward graded bedding from the beach to the mid-shelf mud belt (Fig. 2.5b). In the inner-part of the shelf (~20 m), the fine silt-belt is connected to the coastal sand-belt. The silt-to-clay transition is located at 30 m depth and corresponds to the limit of waves action. The mid-shelf mud-belt is located between 40 and 90 m. These clayey deposits are connected to the Rhône River mouth but detached from others coastal rivers. Relic sands mix with fine and modern sediments appears on the outer shelf and next to the heads of central and western canyons.

Figure 2.5 : Morphological and bathymetric map of the Gulf of Lions shelf, from Bourrin (2007). a) Map of the Holocene sedimentary deposits (Monaco et Aloisi, 2000). b) Map of the spatial repartition of sedimentary deposits over the shelf (Monaco et Aloisi, 2000). Red dash-line rectangles show the Rhône River ROFI (right) and the Roussillon shelf (left), study areas of Chapter 4 - 5 and 6 respectively. Both maps compiled several sedimentary studies carried out during past decades (Monaco, 1971; Got, 1973; Aloïsi, 1986). These works are integrated in a global GIS available on the OSU OREME (Observatoire de REcherche Méditerranéen de l'Environnement) website.

2.2 Suspended particle dynamics

We focus here on the importance of the Rhône River ROFI and its prodelta, where the suspended particle properties and dynamics can be highly variable in space and time. We then focus on the southwest (SW) part of the GoL, where particulate resuspension and transport are enhanced during marine storms. Both regions are highlighted by red-squares in Fig. 2.5.

SPM dynamics and properties have been largely described in both regions during the two past decades. Observations have been regularly made to characterize the spatial and temporal variability of SPM dynamics and properties within both the surface and bottom nepheloid layers. Past studies concerning the Rhône River plume (i.e. the dynamic / properties of the Rhône River particles delivered to the shelf) as well as past observations of the bottom particulate transport over the shelf are further detailed. These observations are resumed in the infographic p.33 as a function of the programmatic context and the evolution of measurement platforms (see Chapter 3).

The Figure 2.6, adapted from Millot (1990) and Palanques et al. (2006), summarizes the different wind regimes prevailing in the Gulf of Lions and the related hydrological processes contributing to the particulate delivery, resuspension and transport over the shelf.
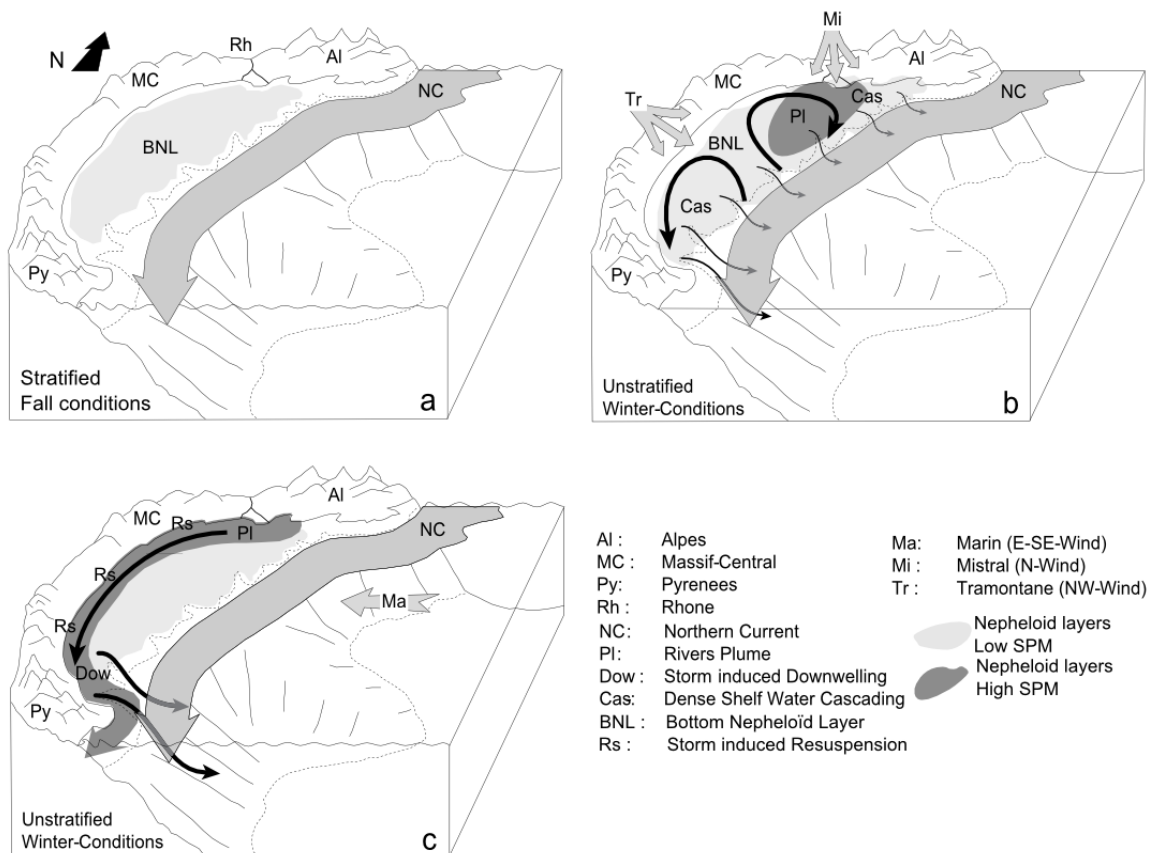
Figure 2.6 : Conceptual view of the SPM dynamics within the Gulf of Lions during a) stratified and fall conditions, b) unstratified and winter conditions (continental winds), c) unstratified and winter conditions (marine wind). From Palanques et al. (2006).

Historical studies of the SPM dynamics and transport over the shelf of the Gulf of Lions
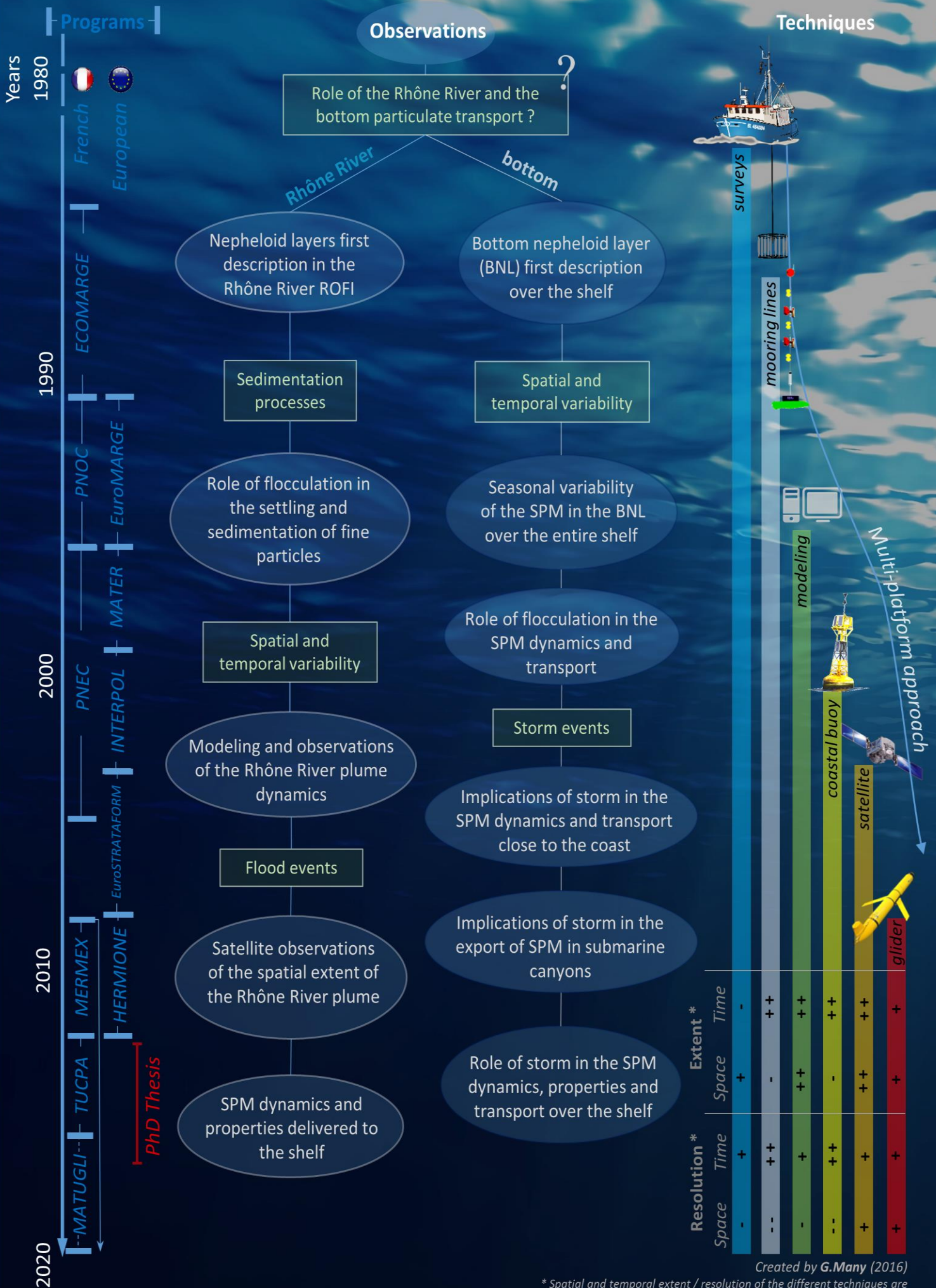
Created by G.Many (2016)
* Spatial and temporal extent / resolution of the different techniques are shown here as a relative information and are further detailed in Chapter 3

2.2.1 The nepheloid layers within the Rhône ROFI and over the shelf

The Rhône River ROFI is characterized by the presence of a prodelta. This shallow area represents the receptacle of coarse sediments as sands and silts. The prodelta presents a seaward graded bedding from the beach (sand and silt, 20 m) to an abrupt slope (fine-silt and clays, 60 m) and a mid-shelf mud-belt (mud, more than 60 m) (Monaco and Aloisi, 2000). In front of the River mouth the sedimentation rates are estimated to 20-50 cm y^{-1} and rapidly decrease to ~0.5 cm y^{-1} over the mid-shelf mud-belt (Miralles et al., 2005; Drexler and Nittrouer, 2008).

In micro-tidal ROFI, as in the Rhône River ROFI, the particle export through the coastal sea is complex. The SPM is distributed in different nepheloid layers, whose characteristics (concentration, extent, thickness) depend on the river discharge and the environmental conditions (stratification, wind, currents and waves). In front of the Rhône River mouth, Aloisi et al. (1982) look into this complexity and show the various type of nepheloid layers that can be found (Fig. 2.7).

For instance, the spreading of the turbid and fresh Rhône River plume forms a surface nepheloid layer, which can feed local intermediate and bottom nepheloid layers (INL and BNL respectively). While the INL is poorly documented due to sampling difficulties (i.e. low extent in space and time), the BNL has been characterized in several studies, which highlight the role of the particle settling from the surface river plume, as well as the waves-induced particulate resuspension and advection by bottom currents (Aloisi et al., 1982; Naudin et al., 1992; Dufois et al., 2014).
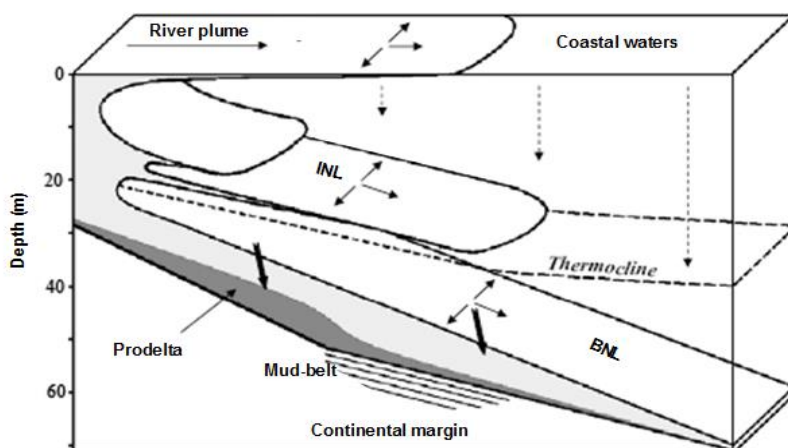
Figure 2.7 : Conceptual view of the different nepheloid layers found in front of the Rhône River mouth. Surface river plume, intermediate nepheloid layer (INL) and bottom nepheloid layer (BNL) are shown. Filled-arrows show the possible advection of nepheloids, dashed-arrows the possible sedimentation of particles and bold-arrows the burial of sediments. From Aloisi et al. (1982).

During flood events of the Rhône River, the delivery of particles to the shelf is strongly enhanced. The surface river plume can spread over several kilometers off the mouth (Aloisi et al., 1979; Naudin et al., 1997; Thill et al., 2001).

The Rhône River plume rapidly responds to the wind forcings (~5-10h according to Demarcq and Wald (1984)) and is advected through the shelf by surface currents enhanced by continental (i.e. north-northwesterly) wind or fostered along the coast during marine (i.e. east-southeasterly) wind (Naudin et al., 1997; Broche et al., 1998; Forget and Ouillon, 1998; Estournel et al., 2001; Arnau et al., 2004; Lorthiois et al., 2012; Ody et al., 2016) (Fig. 2.8). These observations, mainly based on coastal drifters, satellite and radar measurements have been completed with modeling works of Marsaleix et al. (1998), Thill et al. (2001), Arnoux-Chiavassa et al. (2003), Ulses et al. (2005) and Dufois (2008).

Marine wind   **Continental wind**

Figure 2.8 : RGB images (MODIS-Aqua) of the Petit (left) and Grand (right) Rhône River plumes during the annual flood event of January 2014. Left: under a marine prevailing wind. Right: under continental prevailing winds (i.e. Mistral & Tramontane). The red dash lines show the SPM concentration threshold of 10 mg L^{-1}.

Rhône River plume

Over the shelf, deposited surface sediments are resuspended by waves and currents and dispersed by bottom currents. Several studies highlight the presence of a BNL (1 - 5 mg L^{-1}) up to 15 m thick over the shelf (Aloisi et al., 1979, 1982; Durrieu de Madron et al., 1990; Durrieu de Madron and Panouse, 1996). This nepheloid layer highly participates to the particulate transport over the shelf during all year round during both fall and extreme conditions.

Durrieu de Madron and Panouse (1996) highlight the spatial extent of this BNL over the shelf during fall conditions. This observation can be reinforced with recent glider observations over the SW part of the shelf (April 2013 – unpublished data) during similar conditions (Fig. 2.9). These results highlight the large area impacted by the BNL, which tends to spread over the entire shelf, as well as the seaward gradient of its thickness (10-30 m) and SPM concentration (1-3 mg L^{-1}) during fall conditions (see conceptual view in Fig. 2.6a).
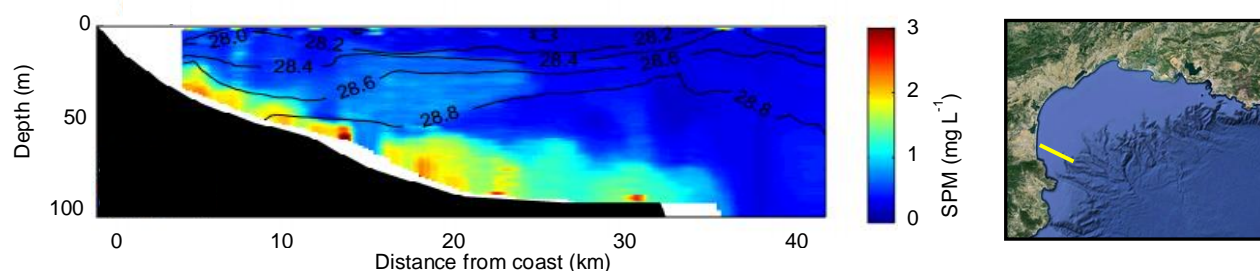
Figure 2.9 : Glider cross-shelf section (see yellow bar on map) of SPM concentration carried out during fall and stratified conditions (April 2013). Density contour lines are shown in black (unpublished data).

Close to the shelf break (~120 m depth), mechanisms responsible of SPM shelf-slope exchanges (i.e. between the BNL and offshore waters) are generally more vigorous during winter. Various processes are identified as the cascading of dense water formed by cold and dry continental winds over the shelf (Durrieu de Madron and Panouse, 1996; Durrieu de Madron et al., 2005), bottom Ekman transport induced by the cyclonic along-shelf currents (Durrieu de Madron et Panouse, 1996) and instabilities of the northern Liguro-Provencal Current (Durrieu de Madron et al., 1999) (see Fig. 2.5b).

2.2.2 Impacts of storms on sediment dynamics and particulate transport over the shelf

Marine storm events have been described as a principal factor producing sediment resuspension and redistribution over the shelf (see modelling works of Dufois, 2008; Ferré et al., 2008; Ulses et al., 2008a,b; Dufois et al., 2014). The sediment erosion induced by waves and strong currents, which can reach several centimeters, enhances the SPM concentration (> 30 mg L^{-1}) in the water column down to 40-50 m depth (Ferré et al., 2005; Guillén et al., 2006; Bourrin al., 2008b) (Fig. 2.10). Besides, the particulate transport is accentuated by the cyclonic circulation ($\sim$ 50-70 cm s^{-1} close to the coast, see Fig. 2.2b), which favors the suspended particle transport along the shelf (see blue arrow on the map in Fig. 2.10).
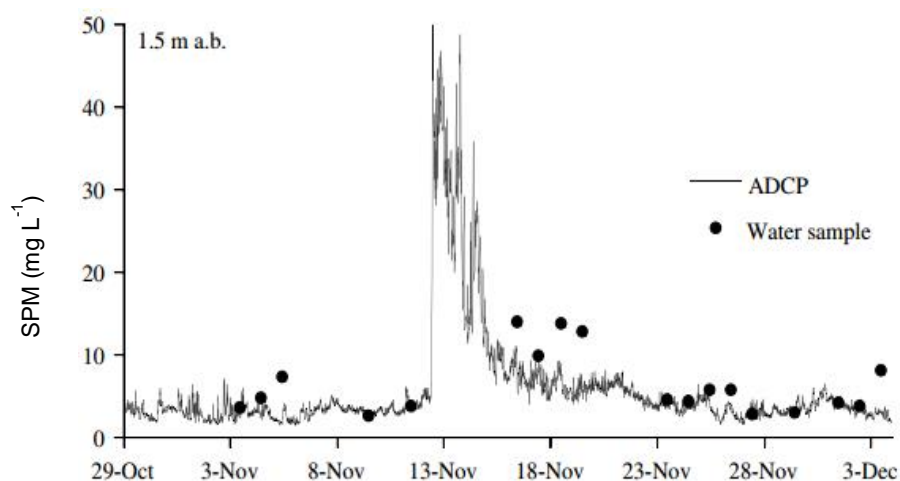
Figure 2.10 : Time-series of SPM concentrations close to the seabed (1.5 mab) in the Banyuls bay (27 m, see yellow dot on map) during a storm event (Autumn 1999). From Ferré et al. (2005).

Over the SW part of the shelf, the export of suspended particles offshelf occurs by downwelling through the Cap de Creus and Lacaze-Duthier submarine canyons as well as by bypassing the Cap de Creus to the Catalan shelf (Palanques et al., 2006, 2008; Bonnin et al., 2008; Martín et al., 2013) (Fig. 2.11).
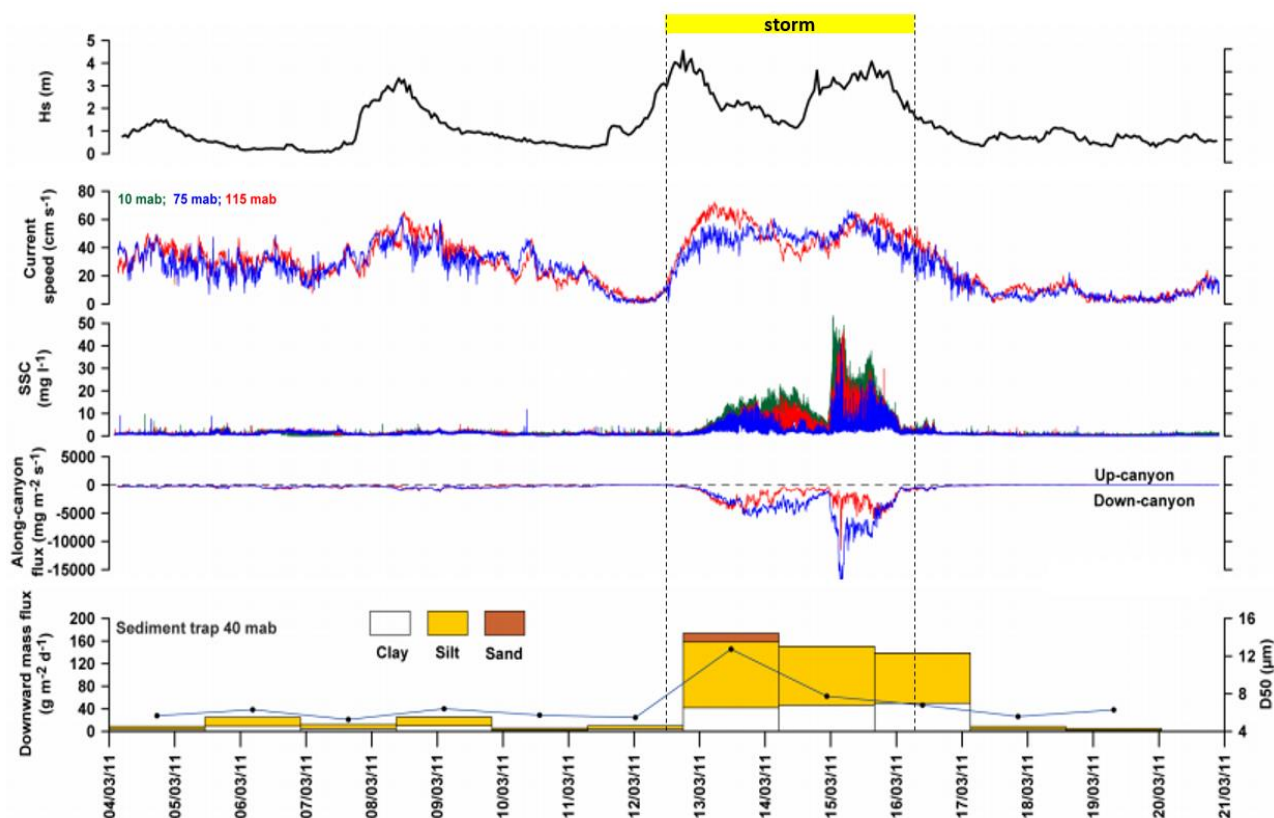
Figure 2.11 : Time-series of sea conditions and SPM fluxes in the south flank of the Cap de Creus canyon during marine storms conditions (see red dot on map in Fig. 2.10). From top to bottom : Wave significant height measured at the POEM coastal site (Têt River), current speed measured at 75 and 115 mab in the canyon, SPM concentration measured at 10, 75 and 115 mab, along-canyon SPM fluxes at 75 and 115 mab (negative values down-canyon) and downward mass flux measured by a sediment trap at 40 mab. Trap fluxes are divided in three components according to the major grain-size classes. The d50 in sediment trap samples is also shown (blue line) (see Martin et al., 2013).

While these fixed observations emphasize the role of marine storms in the sediment dynamics and particulate transport close to the coast and in submarine canyons, a need still exists in the monitoring of the along- and cross-shelf particle fluxes over the entire shelf to assess the role of storms in the redistribution of resuspended particles from the coast to the mid-shelf mud-belt.

Besides, there is still a lack of knowledge about the fraction of the particulate transport that downwells within submarine canyons and the one that bypass the Cap de Creus towards the northern Catalan shelf.

2.2.3 Suspended particles characteristics

Within the Rhône ROFI, previous in situ observations highlight the fast vertical transfer of both silt and sand from the River plume to the seabed (Aloisi et al., 1982; Naudin et al., 1992). The settling of finest particles (fine-silt and clays), which compose the surface river plume as well as the INL and BNL, is reinforced by the flocculation phenomena. Thill et al. (2001) highlight the possible role of salt-induced flocculation along the dilution gradient of the river plume, whereas Naudin et al. (1997) emphasize the role of the electro-chemical action of the organic matter in the maintain of flocs. These latter authors also show the correlation between the increase of the SPM concentration and the growth of flocs (>150 μm) in the particle assemblage.

Besides, several studies highlight that the BNL is mainly composed of fine particles over the shelf, which tend to form micro- (~50 μm) and macro-flocs (~150 μm) (Ferré et al., 2005; Durrieu de Madron et al., 2005; Curran et al., 2007; Bourrin et al., 2008b) (Fig. 2.12). Martin et al. (2013) also emphasize the export of silt and clays offshelf during energetic conditions induced by marine storms (see bottom panel in Fig. 2.11). All these measurements do not enable to determine the variability of the particle assemblage over the entire shelf with high temporal and spatial resolutions, which remains decisive to assess the fate of suspended particles.
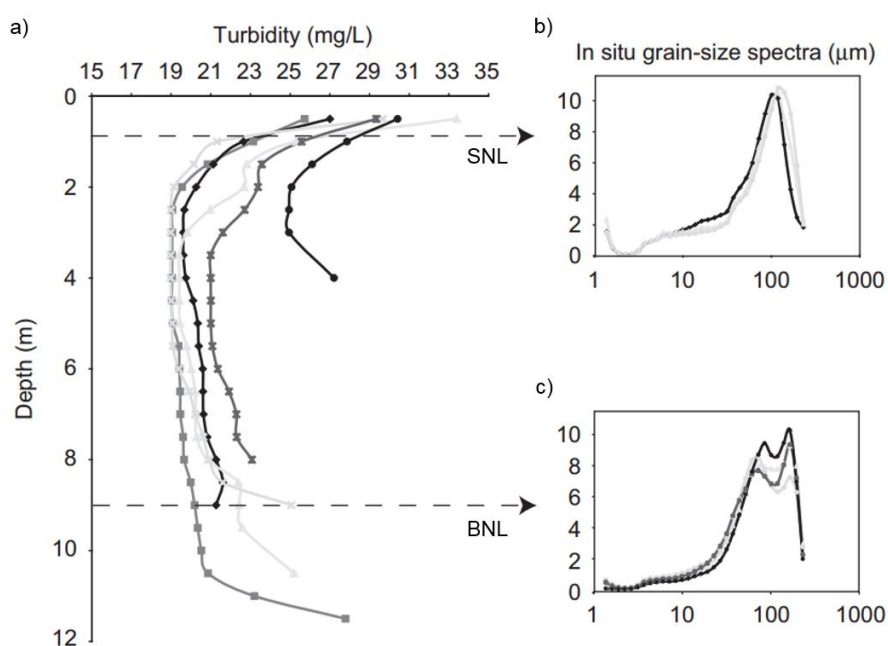
Figure 2.12 : a) Typical turbidity profiles (six stations - April 2004) observed in the vicinity of the Têt River during winter conditions. b-c) In situ grain-size spectra (% of the total volume particle concentration) measured in the SNL (b) and the BNL (c), LISST measurements from Bourrin et al. (2008b). Note the high proportion of large particles (100 μm) probably highlighting the presence of fine sediments flocs.

2.3 Objectives

The main objectives of this work are to improve knowledges on the role of a Rhône River flood event in the delivery of SPM to the shelf and the importance of a marine storm event on the sediment dynamics and the particulate transport over the shelf.

Issues of this work can be resumed as follow:

- What is the spatial variability of the Rhône ROFI particle assemblage during a flood event?

- What is the dynamic of the Rhône ROFI nepheloid layers during a flood event?

- What are the impacts of a storm on the particulate transport over the shelf of the GoL?

To answer these issues, this work was the opportunity to test an ensemble of observations collected from different platforms. As described in Chapter 3, we adopted a multi-platform approach using simultaneously research vessel, satellite, glider, coastal buoy and mooring to get a comprehensive view of the particulate matter characteristics off the Rhône river mouth during a flood and of the along- and cross-shelf particulate matter transport during a storm.

We experimented an instrumental package combining two technologies (LASER diffraction and holography) to determine the full in situ particle properties (size, shape, nature and effective density) in the Rhône ROFI, and assess the role of fine-sediment flocculation in the vertical transfer of particles from the Rhône River plume to the seabed (Chapter 4).

We tested the capabilities of a glider equipped with optical sensors to assess the high-resolution temporal and spatial variability of the Rhône River ROFI nepheloid layers structure and properties during a flood (Chapter 5).

We described the hydrological and nepheloid layers structure as well as to quantify the particle transport and properties in the southwest part of the Gulf of Lions during a marine storm. These observations were compared against measurements collected in the nearby Cap de Creus canyon, and allowed to assess the fraction of particle transport exported off the shelf (Chapter 6).

This work was carried out in collaboration with specialists from various institutes. The following page highlights the different role of each of them.

References

Adell, W. **2013** « Caractérisation de la distribution granulométrique des particules en transit dans le Rhône aval au cours du temps et des conditions hydrologiques ». Institut de radioprotection et de sûreté nucléaire. *Rapport de stage de Master Sciences de l'eau et de l'environnement 2ème année*. Encadré par M. Zebracki et F. Eyrolle-Boyer.

Aloisi, J. C., C. Millot, A. Monaco, and H. Pauc. **1979**. « Dynamique des suspensions et mécanismes sédimentogénétiques sur le plateau continental du Golfe du Lion ». *CR Acad. Sc* 289 (13): 879‑82.

Aloisi, J. C., J. P. Cambon, J. Carbonne, G. Cauwet, C. Millot, A. Monaco, and H. Pauc. **1982**. « Origine et rôle du néphéloïde profond dans le transfert des particules au milieu marin. Application au Golfe du Lion ». *Oceanologica Acta* 5 (4): 481‑91.

Aloisi, J. C. **1986**. « Sur un modele de sédimentation deltaıque: contribution ala connaissance des marges passives ». *Thèse de Doctorat d'Etat, Université de Perpignan*. 195 p.

Antonelli, C. **2002**. « Flux sédimentaires et morphogenèse récente dans le chenal du Rhône aval ». *Thèse de Doctorat, Université de Provence.* 291 p.

Antonelli, C., F. Eyrolle, B. Rolland, M. Provansal, and F. Sabatier. **2008**. « Suspended sediment and 137 Cs fluxes during the exceptional December 2003 flood in the Rhône River, southeast France ». *Geomorphology* 95 (3): 350‑60.

Arnau, P., C. Liquete, and M. Canals. **2004**. « River mouth plume events and their dispersal in the Northwestern Mediterranean Sea ». *Oceanography-Washington DC-Oceanography Society-* 17: 22‑31.

Arnoux-Chiavassa, S., V. Rey, and Philippe Fraunié. **2003**. « Modeling 3D Rhône river plume using a higher order advection scheme ». *Oceanologica acta* 26 (4): 299‑309.

Bonnin, J., S. Heussner, A. Calafat, J. Fabres, A. Palanques, X. Durrieu de Madron, M. Canals, P. Puig, J. Avril, et N. Delsaut. **2008**. « Comparison of horizontal and downward particle fluxes across canyons of the Gulf of Lions (NW Mediterranean): Meteorological and hydrodynamical forcing ». *Continental Shelf Research* 28 (15): 1957‑70. doi:10.1016/j.csr.2008.06.004.

Bourrin, F., and X. Durrieu de Madron. **2006**. « Contribution to the study of coastal rivers and associated prodeltas to sediment supply in the Gulf of Lions (NW Mediterranean Sea) ». *Vie et Milieu* 56 (4): 307‑14.

Bourrin, F. **2007**. « Variabilité des apports sédimentaires par les fleuves côtiers: Cas du systeme Têt: Littoral Roussillonnais dans les Golfe du Lion ». *Thèse de Doctorat. Université de Perpignan*. 305 p.

Bourrin, F., X. Durrieu de Madron, S. Heussner, and C. Estournel. **2008a**. « Impact of Winter Dense Water Formation on Shelf Sediment Erosion (evidence from the Gulf of Lions, NW Mediterranean) ». *Continental Shelf Research* 28 (15): 1984‑99. doi:10.1016/j.csr.2008.06.006.

Bourrin, F., P. Friend, C. Amos, E. Manca, C. Ulses, A. Palanques, X. Durrieu de Madron, et C. Thompson. **2008b**. « Sediment dispersal from a typical Mediterranean flood: the Têt River, Gulf of Lions ». *Continental Shelf Research* 28 (15): 1895‑1910.

Broche, P., J. L. Devenon, P. Forget, J. C. de Maistre, J. J. Naudin, et G. Cauwet. **1998**. « Experimental study of the Rhone plume. Part I: physics and dynamics ». *Oceanologica Acta* 21 (6): 725‑38.

Copin-Montégut, C. **1993**. « Alkalinity and carbon budgets in the Mediterranean Sea ». *Global Biogeochemical Cycles* 7 (4): 915‑25.

Courp, T., and A. Monaco. **1990**. « Sediment dispersal and accumulation on the continental margin of the Gulf of Lions: sedimentary budget ». *Continental Shelf Research* 10 (9): 1063‑87.

Curran, K.J., P.S. Hill, T.G. Milligan, O.A. Mikkelsen, B.A. Law, X. Durrieu de Madron, et F. Bourrin. **2007**. « Settling Velocity, Effective Density, and Mass Composition of Suspended Sediment in a Coastal Bottom Boundary Layer, Gulf of Lions, France ». *Continental Shelf Research* 27 (10-11): 1408‑21. doi:10.1016/j.csr.2007.01.014.

Demarcq, H., and L. Wald. **1984**. « La dynamique superficielle du panache du Rhône d'après l'imagerie infrarouge satellitaire ». *Oceanologica Acta* 7 (2): 159‑62.

Drexler, T.M., and C.A. Nittrouer. **2008**. « Stratigraphic signatures due to flood deposition near the Rhône River: Gulf of Lions, northwest Mediterranean Sea ». *Continental Shelf Research* 28 (15): 1877‑94. doi:10.1016/j.csr.2007.11.012.

Dufau-Julliand C., P. Marsaleix, A. Petrenko, and I. Dekeyser. **2004**. « Three-dimensional modeling of the Gulf of Lion's hydrodynamics (northwest Mediterranean) during January 1999 (MOOGLI3 Experiment) and late winter 1999: Western Mediterranean Intermediate Water's (WIW's) formation and its cascading over the shelf break ». *Journal of Geophysical Research*, 109, C11002, doi:10.1029/2003JC002019.

Dufois, F. 2008. « Modélisation du transport particulaire dans le Golfe du Lion en vue d'une application au devenir des traceurs radioactifs issus du Rhône ». *Thèse de Doctorat. Institut de Radioprotection et de Sûreté Nucléaire.* 414 p.

Dufois, F., R. Verney, P. Le Hir, F. Dumas, and S. Charmasson. **2014**. « Impact of winter storms on sediment erosion in the Rhone River prodelta and fate of sediment in the Gulf of Lions (North Western Mediterranean Sea) ». *Continental Shelf Research* 72: 57‑72. doi:10.1016/j.csr.2013.11.004.

Durrieu de Madron, X., F. Nyffeler, and C. H. Godet. **1990**. « Hydrographic structure and nepheloid spatial distribution in the Gulf of Lions continental margin ». *Continental Shelf Research*, France-JGOFS, ECOMARGE Particle Fluxes and Ecosystem Response on a Continental Margin, 10 (9–11): 915‑29. doi:10.1016/0278-4343(90)90067-V.

Durrieu de Madron, X., and M. Panouse. **1996**. « Transport de matiere particulaire en suspension sur le plateau continental du Golfe du Lion. Situation estivale et hivernale ». *Comptes rendus de l'Académie des sciences. Série 2. Sciences de la terre et des planètes* 322 (12): 1061‑70.

Durrieu de Madron, X., O. Radakovitch, S Heussner, M.D. Loye-Pilot, and A. Monaco. **1999**. « Role of the climatological and current variability on shelf-slope exchanges of particulate matter: evidence from the Rhone continental margin (NW Mediterranean) ». *Deep Sea Research Part I: Oceanographic Research Papers* 46 (9): 1513‑38.

Durrieu de Madron, X., B. Ferré, G. Le Corre, C. Grenz, P. Conan, M. Pujo-Pay, R. Buscail, and O. Bodiot. **2005**. « Trawling-Induced Resuspension and Dispersal of Muddy Sediments and Dissolved Elements in the Gulf of Lion (NW Mediterranean) ». *Continental Shelf Research* 25 (19‑20): 2387‑2409. doi:10.1016/j.csr.2005.08.002.

Durrieu de Madron, X., P. L. Wiberg, and P. Puig. **2008**. « Sediment Dynamics in the Gulf of Lions: The Impact of Extreme Events ». *Continental Shelf Research* 28 (15): 1867‑76. doi:10.1016/j.csr.2008.08.001.

Estournel, C., P. Broche, P. Marsaleix, J. L. Devenon, F. Auclair, and R. Vehil. **2001**. « The Rhone River Plume in Unsteady Conditions: Numerical and Experimental Results ». *Estuarine, Coastal and Shelf Science* 53 (1): 25‑38. doi:10.1006/ecss.2000.0685.

Estournel, C. **2003**. « Observation and modeling of the winter coastal oceanic circulation in the Gulf of Lion under wind conditions influenced by the continental orography (FETCH experiment) ». *Journal of Geophysical Research* 108 (C3). doi:10.1029/2001JC000825.

Ferré, B., K. Guizien, X. Durrieu de Madron, A. Palanques, J. Guillén, and A. Grémare. **2005**. « Fine-Grained Sediment Dynamics during a Strong Storm Event in the Inner-Shelf of the Gulf of Lion (NW Mediterranean) ». *Continental Shelf Research* 25 (19-20): 2410‑27. doi:10.1016/j.csr.2005.08.017.

Ferré, B., X. Durrieu de Madron, C. Estournel, C. Ulses, and G. Le Corre. **2008**. « Impact of Natural (waves and Currents) and Anthropogenic (trawl) Resuspension on the Export of Particulate Matter to the Open Ocean ». *Continental Shelf Research* 28 (15): 2071‑91. doi:10.1016/j.csr.2008.02.002.

Flexas, M.M., X. Durrieu De Madron, M.A. Garcia, M. Canals, and P. Arnau. **2002**. « Flow variability in the Gulf of Lions during the MATER HFF experiment (March–May 1997) ». *Journal of Marine Systems* 33: 197‑214.

Forget, P., and S. Ouillon. **1998**. « Surface suspended matter off the Rhone river mouth from visible satellite imagery ». *Oceanologica acta* 21 (6): 739‑49.

Got, H. **1973**. « Etude des corrélations tectonique-sédimentation au cours de l'histoire quaternaire du précontinent pyrénéo-catalan ». *Thèse de Doctorat d'Etat. Université de Perpignan*. 294 p.

Guillén, J., F. Bourrin, A. Palanques, X. Durrieu de Madron, P. Puig, and R. Buscail. **2006**. « Sediment dynamics during wet and dry storm events on the Têt inner shelf (SW Gulf of Lions) ». *Marine Geology* 234 (1-4): 129‑42. doi:10.1016/j.margeo.2006.09.018.

Lorthiois, T., D. Doxaran, and M. Chami. **2012**. « Daily and seasonal dynamics of suspended particles in the Rhône River plume based on remote sensing and field optical measurements ». *Geo-Marine Letters* 32 (2): 89‑101. doi:10.1007/s00367-012-0274-2.

Maillet, G. M., C. Vella, S. Berné, P. L. Friend, C. L. Amos, T. J. Fleury, and A. Normand. **2006**. « Morphological changes and sedimentary processes induced by the December 2003 flood event at the present mouth of the Grand Rhône River (southern France) ». *Marine Geology* 234 (1-4): 159‑77. doi:10.1016/j.margeo.2006.09.025.

Makaske, B., and P. Augustinus. **1998**. « Morphologic changes of a micro-tidal, low wave energy beach face during a spring-neap tide cycle, Rhone-Delta, France ». *Journal of Coastal Research*, 632‑45.

Marsaleix, P., C. Estournel, V. Kondrachoff, et R. Vehil. **1998**. « A numerical study of the formation of the Rhône River plume ». *Journal of Marine Systems* 14 (1–2): 99‑115. doi:10.1016/S0924-7963(97)00011-0.

Martín, J., X. Durrieu de Madron, P. Puig, F. Bourrin, A. Palanques, L. Houpert, M. Higueras, et al., **2013**. « Sediment Transport along the Cap de Creus Canyon Flank during a Mild, Wet Winter ». *Biogeosciences* 10 (5): 3221‑39. doi:10.5194/bg-10-3221-2013.

Milliman, J.D., and J. Syvitski. **1992**. « Geomorphic/tectonic control of sediment discharge to the ocean: the importance of small mountainous rivers ». *The Journal of Geology* 100, 525‑44.

Millot, C. **1990**. « The gulf of Lions' hydrodynamics ».

Continental Shelf Research 10 (9): 885‑94.

Miralles, J., O. Radakovitch, and J.C. Aloisi. **2005**. « 210Pb sedimentation rates from the Northwestern Mediterranean margin ». *Marine Geology* 216 (3): 155‑67. doi:10.1016/j.margeo.2005.02.020.

Monaco, A. **1971**. « Contribution à l'étude géologique et sédimentologique du plateau continental du Roussillon (Golfe du Lion) ». *Thèse de Doctorat d'Etat, Université de Perpignan.* 295 p.

Monaco, A., and J.C. Aloisi. **2000**. « Carte de la nature des fonds du Golfe du Lion. » Perpignan. site OSU OREME : http://www.oreme.org/.

Naudin, J. J., G. Cauwet, M. Leveau, F. Lochet, H. Pauc, J. C. Romano, and R. Sempere. **1992**. « Le néphéloïde benthique au large du Rhône. Transferts particulaires à l'interface continent-océan ». *Oceanologica Acta* 15 (6): 621‑38.

Naudin, J.J., G. Cauwet, M.J. Chrétiennot-Dinet, B. Deniaux, J.L. Devenon, and H. Pauc. **1997**. « River Discharge and Wind Influence Upon Particulate Transfer at the Land–Ocean Interaction: Case Study of the Rhone River Plume ». *Estuarine, Coastal and Shelf Science* 45 (3): 303‑16. doi:10.1006/ecss.1996.0190.

Ody, A., D. Doxaran, Q. Vanhellemont, B. Nechad, S. Novoa, G. Many, F. Bourrin, R. Verney, I. Pairaud, and B. Gentili. **2016**. « Potential of High Spatial and Temporal Ocean Color Satellite Data to Study the Dynamics of Suspended Particles in a Micro-Tidal River Plume ». *Remote Sensing* 8 (3): 245.

Palanques, A., X. Durrieu de Madron, P. Puig, J. Fabres, J. Guillén, A. Calafat, M. Canals, S. Heussner, and J Bonnin. **2006**. « Suspended sediment fluxes and transport processes in the Gulf of Lions submarine canyons. The role of storms and dense water cascading ». *Marine Geology* 234 (1): 43‑61.

Palanques, A., J. Guillén, P. Puig, and X. Durrieu de Madron. **2008**. « Storm-driven shelf-to-canyon suspended sediment transport at the southwestern Gulf of Lions ». *Continental Shelf Research* 28 (15): 1947‑56.

Petrenko, A. **2003**. « Variability of circulation features in the Gulf of Lion NW Mediterranean Sea. Importance of inertial currents ». *Oceanologica Acta* 26 (4): 323‑38.

Petrenko A., Y. Leredde, P. Marsaleix. **2005**. « Circulation in a stratified and wind-forced Gulf of Lions, NW Mediterranean Sea: In situ and modeling data ». *Continental Shelf Research*, 25, 1, 7-27.

Pont, D. **1996**. « Evaluation of water fluxes and sediment supply. » *Oral Communication, MEDDELT, Final Meeting*, Venezia, October 2–5.

Pont, D., J. P. Simonnet, and A. V. Walter. **2002**. « Medium-Term Changes in Suspended Sediment Delivery to the Ocean: Consequences of Catchment Heterogeneity and River Management (Rhône River, France) ». *Estuarine, Coastal and Shelf Science* 54 (1): 1‑18. doi:10.1006/ecss.2001.0829.

Sadaoui, M., W. Ludwig, F. Bourrin, and P. Raimbault. **2016**. « Controls, budgets and variability of riverine sediment fluxes to the Gulf of Lions (NW Mediterranean Sea). » Journal of Hydrology, in press.

Serrat, P., W. Ludwig, B. Navarro, and J.L. Blazi. **2001**. « Variabilité spatio-temporelle des flux de matières en suspension d'un fleuve côtier méditerranéen: la Têt (France) ». *Comptes Rendus de l'Académie des Sciences-Series IIA-Earth and Planetary Science* 333 (7): 389‑97.

Thill, A., S. Moustier, J. M. Garnier, C. Estournel, J. J. Naudin, and J. Y. Bottero. **2001**. « Evolution of particle size and concentration in the Rhône river mixing zone:: influence of salt flocculation ». *Continental Shelf Research* 21 (18): 2127‑40.

Ulses, C. **2005**. « Dynamique océanique et transport de la matière particulaire dans le Golfe du Lion: crue, tempête et période hivernale. » *Thèse de Doctorat. Université de Toulouse*. 262 p.

Ulses, C., C. Grenz, P. Marsaleix, E. Schaaff, C. Estournel, S. Meulé, and C. Pinazo. **2005**. « Circulation in a semi-enclosed bay under influence of strong freshwater input ». *Journal of Marine Systems* 56 (1-2): 113‑32. doi:10.1016/j.jmarsys.2005.02.001.

Ulses, C., C. Estournel, J. Bonnin, X. Durrieu de Madron and P. Marsaleix. **2008a**. « Impact of storms and dense water cascading on shelf-slope exchanges in the Gulf of Lion (NW Mediterranean). » Journal of Geophysical Research, 113, C02010. doi:10.1029/2006JC003795.

Ulses, C., C. Estournel, X. Durrieu de Madron, and A. Palanques. **2008b**. « Suspended Sediment Transport in the Gulf of Lions (NW Mediterranean): Impact of Extreme Storms and Floods ». *Continental Shelf Research* 28 (15): 2048‑70. doi:10.1016/j.csr.2008.01.015.

Wheatcroft, R. A. **2000**. « Oceanic flood sedimentation: a new perspective ». *Continental Shelf Research* 20 (16): 2059‑66.

Chapter 3.

The general strategy :

a multi-platform approach

Chapter 3.   The general strategy: a multi-platform approach

List of Figures

List of Tables

3.1 Overview

Dickey et al. (2006) have emphasized the need of a multi-platform approach, i.e. the combination of existing observation platforms as surveys (UNESCO, 1996), fixed platforms such as buoys and moorings (Allison et al., 1994; Weller et al., 2000; Stenberg, 2005), autonomous vehicles such as gliders (Glenn et al., 2000; Davis et al., 2002; Dickey et al., 2002; Testor et al., 2010) and remote sensing from satellites (Robinson, 1985; IOC, 1998; Lindstrom et al., 2000), to characterize coastal processes regulating SPM dynamics and transport, which can take place over large time- (i.e. hours to years) and space-scales (meters to kilometers). This have been largely described in the integrated, strategic design plan for the coastal ocean observations module of the global ocean observing system (UNESCO, 2003).

The Figure 3.1 resumes the platforms used in this work. It presents the general complementarity between spatial and temporal extents of each platform that permits the investigation of processes impacting the SPM dynamics over the Gulf of Lions during both flooding and storm conditions (adapted from Dickey et al., 2006).
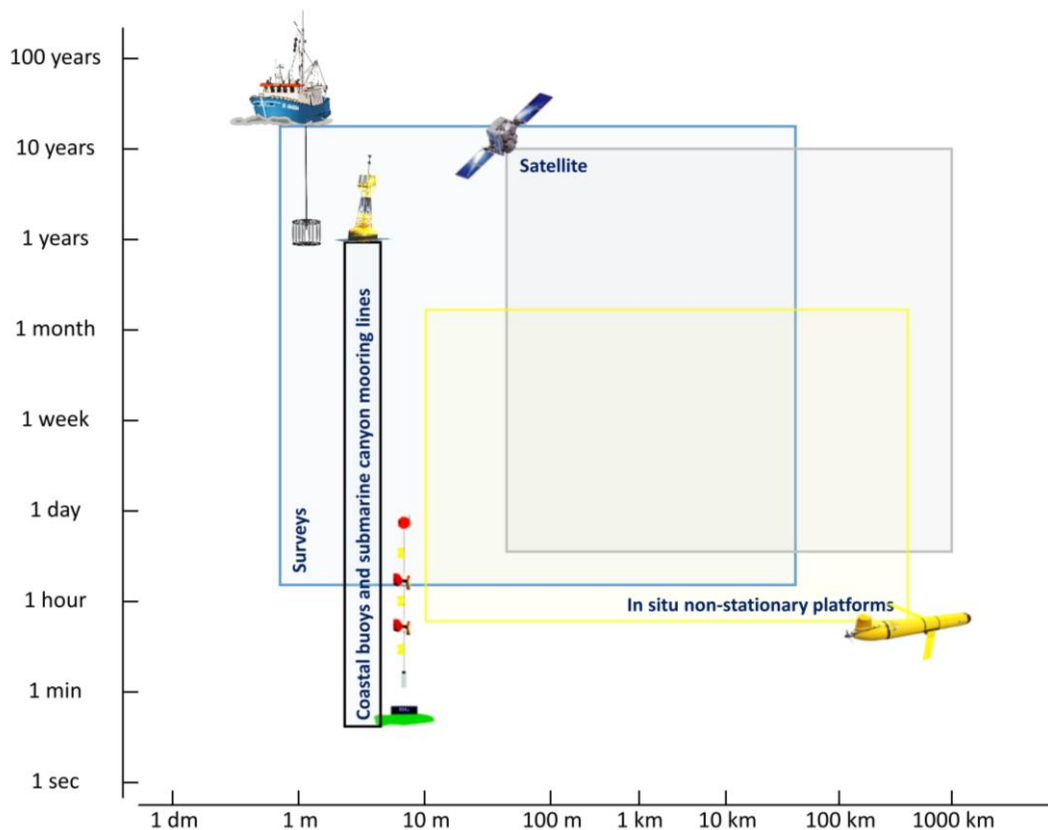

Figure 3.1 : Time-space diagram showing measurement platforms used during this work. Adapted from Dickey et al. (2006).

The combination of these platforms (see Table 3.1) was used to determine hydrological and hydrodynamical conditions as well as suspended particle dynamics, properties and transport along cross-shelf transects within the Rhône River ROFI and over the southwest part of the shelf (see Fig. 3.2).

Fixed platforms as rivers gauging stations (Rhône and Têt), coastal buoys (POEM and MESURHO), canyon mooring lines (Cap de Creus) enabled to follow the variability of meteorological (wind, precipitation), hydrodynamical (waves, current) and SPM dynamics (river discharge, SPM concentration) condition with a high-temporal resolution (~ hour). We used satellite and glider observations to determine large-scale SPM concentrations and properties variability between fixed platforms. The combination of both satellite and glider permitted to get a 3 dimensional view of the Gulf of Lions during flooding and storm conditions with high-temporal (1 day) and spatial (~200 m) resolutions.

This strategy was completed with surveys (generally 1-week on board on small coastal research vessel) that enabled to carry out punctual measurements during flooding and fall conditions. While weather-limited, surveys still remained decisive in the following of parameters as the particle assemblage properties (i.e. the in situ determination of the size, nature and shape of suspended particles) as well as in the calibration of the different sensors on board of each platform (as CTD, current, SPM concentration, index of particle size).

	Location	Sampling depth	Spatial resolution	Temporal resolution	Spatial extent	Temporal extent
River and meteorological stations	Continent	0 m	-	1 h	-	∞
Coastal buoys	Inner-shelf	0 and ~25 m	-	15 – 60 min	-	6 – 12 months
Ship-board observations	Shelf	0 – 200 m	1 profile / 3 km	10 profile / day	40 km	1 – 7 day(s)
Marine glider	Shelf	0 – 200 m	1 profile / 200 m	100 profile / day	40 km	2 – 8 weeks
Mooring lines	Submarine canyon	150 and 300m	-	1 h	-	6 – 12 months
Satellite observations	Shelf	0 m	30 – 250 m	1 day	> 50 km	∞

Table 3.1 : Measurement platforms used in this work. General properties are shown to highlight the complementarity of each platform in the general strategy.
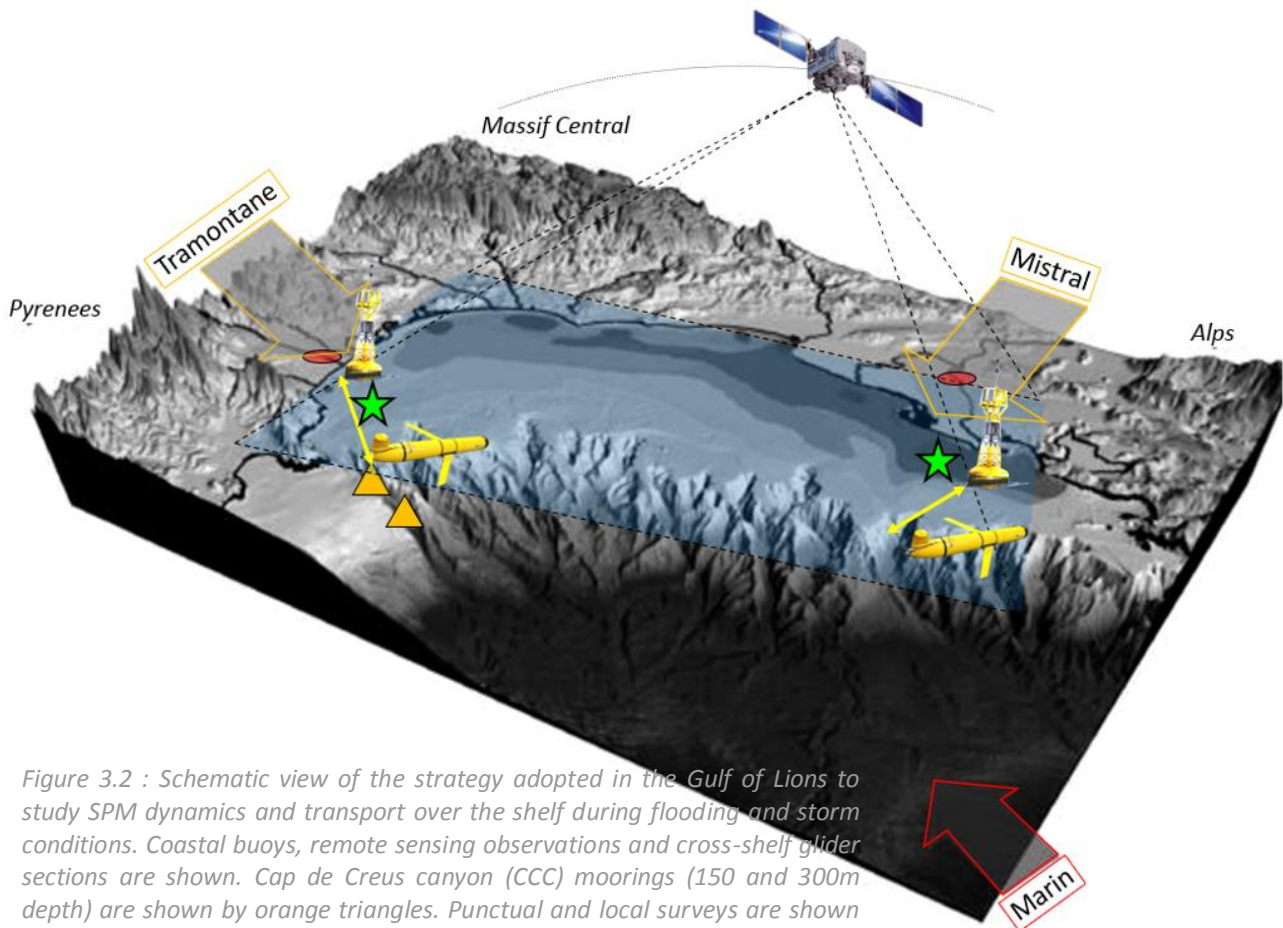
Figure 3.2 : Schematic view of the strategy adopted in the Gulf of Lions to study SPM dynamics and transport over the shelf during flooding and storm conditions. Coastal buoys, remote sensing observations and cross-shelf glider sections are shown. Cap de Creus canyon (CCC) moorings (150 and 300m depth) are shown by orange triangles. Punctual and local surveys are shown by green stars. Rivers and meteorological stations are shown in red. Principal wind forcings are shown in orange (continental) and red (marine).

3.2 The platforms

3.2.1 Shipboard observations

Surveys - During my work I participated to three surveys, for a total of 27 days at sea. Table 3.2 details the work at sea effectuated during these surveys (only data acquired during CASCADE and TUCPA 2 are further discussed).

The CASCADE (CAscading, Storm, Convection, Advection and Downwelling Events) survey (March, 1st-23rd, 2011) was carried out on board of the *R/V Atalante* in the southwest part of the Gulf of Lions to assess the spatial and temporal variability of SPM dynamics and transport during a "back-to-back" storm and flood event of small coastal rivers (as Agly, Aude, Hérault and Têt) (see Chapter 6). This survey complemented a larger observational effort composed of cross-shelf glider deployments, remote sensing observations, coastal surface buoys and submarine canyons moorings on the shelf slope.

Date (yyyy-mm)	Name	Ship	Days	Area	Main observations	Annex objectives
2011-03*	CASCADE	Atalante	22	GoL shelf	SPM dynamics during storm and flood events over the entire shelf	Canyon moorings deployment Glider deployment and recovery
2014-01	TUCPA 1	Antédon II	7	Rhône ROFI	SPM dynamics and properties during flooding conditions	Glider deployment
2014-02*	TUCPA 2	Tethys II	7	Rhône ROFI	SPM dynamics and properties during flooding conditions	Glider recovery
2015-02	PLUMRHO	Tethys II	14	Rhône ROFI	SPM dynamics and properties during flooding conditions	Glider calibration LISST variability Glider deployment and recovery
2016-02	MATUGLI	Tethys-II	7	Rhône ROFI	SPM dynamics and properties during flooding conditions	-

Table 3.2 : List of surveys carried out before and during this thesis. Only data from CASCADE and TUCPA 2 experiments are further used. Surveys marked with * show the surveys where I did not participate.

As a part of the TUCPA framework ("TUrbidité Côtière et Plateformes Autonomes" - Coastal Turbidity and Autonomous Platforms), two 1-week surveys were carried out on board of the *R/V*

Antédon II, in January and February 2014, to assess the variability of SPM dynamics and properties within the Rhône ROFI during flooding conditions (Chapter 4). TUCPA 1 survey also permitted the deployment of a glider from the Rhône river mouth to the shelf edge. Glider observations were calibrated and compared against in situ, remote sensing, and coastal buoy observations. Results permitted to describe the SPM properties and dynamics with high temporal and spatial resolution during a flood event and various wind forcings (Chapter 5).

An additional 1-week survey (PLUMRHO - "PLUMe of RHOne") was carried out during the MATUGLI project ("Mesures Autonomes de la TUrbidité par GLIder " – Autonomous turbidity measurements by marine gliders) on board of the *R/V Tethys II* in the Rhône River ROFI during January 2015. This survey permitted the calibration of the turbidity sensor of the glider as well as the determination of long-term LISST instruments variability (see 3.4.2).

Sampling strategy – During these surveys, observational efforts were made to focus on the SPM dynamics and properties within turbid structures as river plume and bottom nepheloid layer. Thus, we generally effectuated steps (~1-2 min) with optical instruments (backscatter sensors, LISST instruments) and sampled waters with "Niskin" bottles in surface (~1-2 m) and close to the seabed (1-2 meters above bottom (mab)). Sampling stations were generally oriented along a cross-shelf transect and were spaced by 10 m depth of bathymetry from the near-shore (20 m) to the shelf break (120 m). We determine ex situ the gravimetric SPM concentration, the particulate organic carbon (POC) content and the deflocculated particle size distribution.

3.2.2 Coastal buoys

During this work we used data provided by two coastal buoys. The POEM buoy located in front of the Têt River (southwest of the GoL) and the MESURHO buoy located in front of the Rhône River (north of the GoL). A brief presentation of the operating system of both buoys is detailed and the various instruments used to study hydrological and particle properties close to the coast are listed.

POEM buoy - The POEM (Plateforme d'Observation de l'Environnement Méditerranéen) coastal buoy is located at 28 m water depth, 2.5 km off the Têt river mouth (Bourrin, 2007). This buoy has a three-point helicoidal anchoring tightly linked to mid-water depth flotation to prevent any particulate resuspension (Fig. 3.3). At the surface the POEM buoy is equipped with a wind station and solar panels, providing energy to the surface instruments.

The surface probe is generally a YSI 6600 multi-parametric probe measuring the temperature, salinity, turbidity (700nm - NTU) and chlorophyll a (fluorimeter, $\mu g_{Chla}.L^{-1}$, factory calibrated) ($\sim$1m depth). Close the seabed, different benthic instruments are used as ALTUS altimeters (seabed level), YSI probe and an upward-looking ADCP (generally a 600 kHz, RDInstrument).
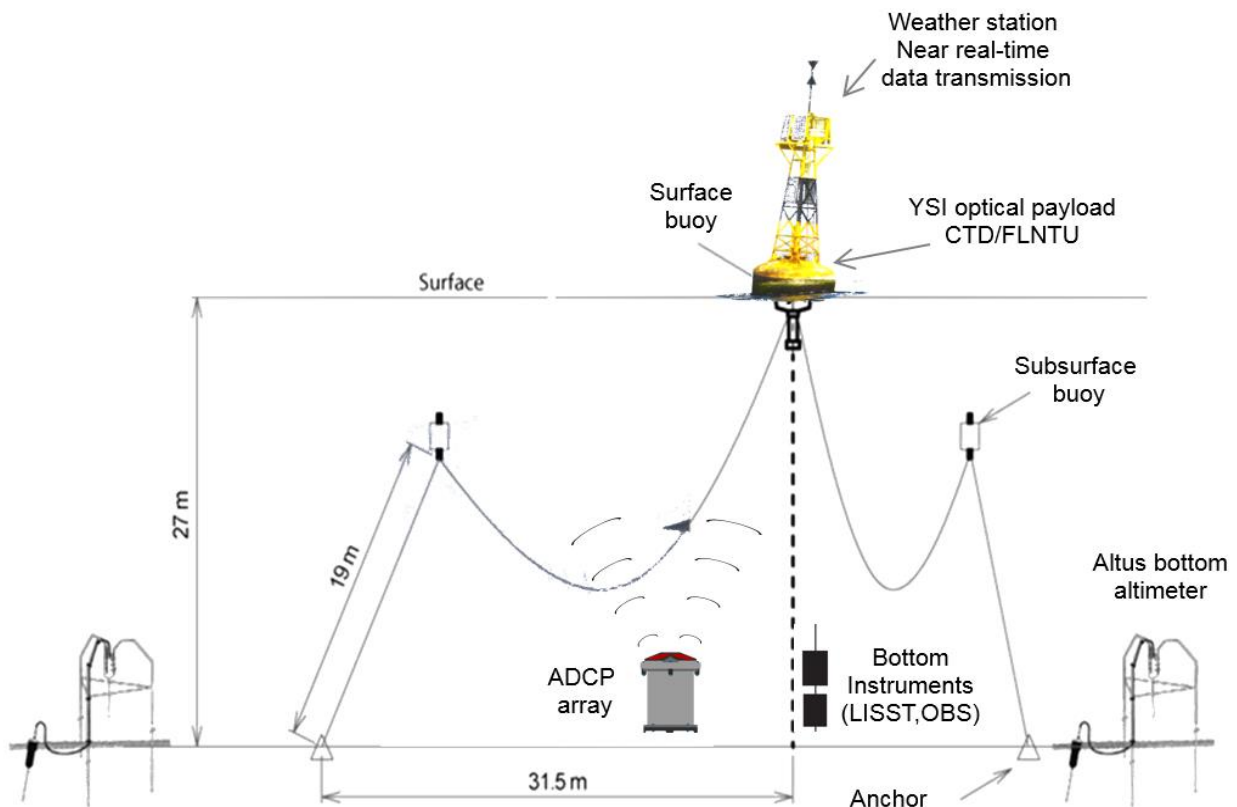
Figure 3.3 : Schematic view of the POEM coastal buoy system. Not to scale.
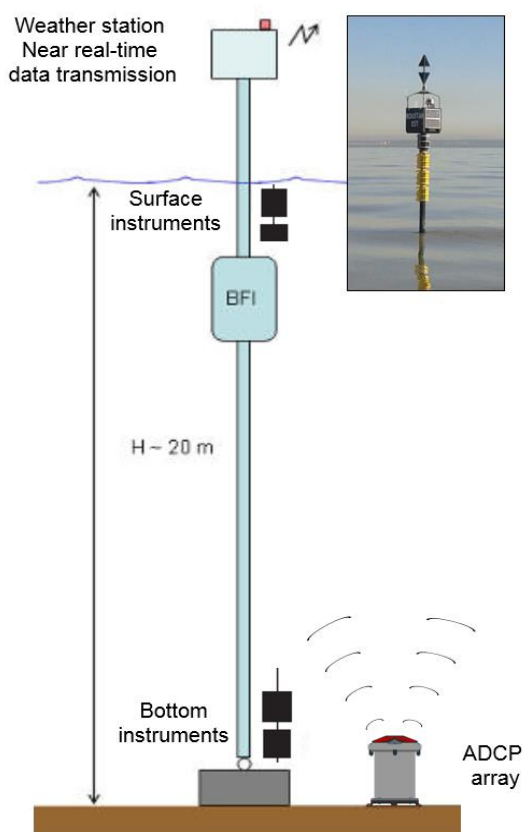
Figure 3.4 : Schematic view of the MESURHO coastal buoy system. Adapted from Pairaud et al. (2015). Not to scale.

MESURHO buoy - The MESURHO buoy (Fig. 3.4) (Pairaud et al., 2015) is located on the East limit of the Rhône prodelta at 20 m depth, 2.6 km of the river mouth. The platform consists of a buoyancy beacon, which permits the cable communication between the surface and bottom instruments. The top of the buoy is composed of a solar panel providing energy to surface instruments.

As for the POEM buoy, observational efforts are made to study the surface and near bottom waters with various instruments as YSI and SMTPS multi-parametric sensors (temperature, salinity, turbidity and chlorophyll). Bottom mooring enables to equip the buoy with an upward-looking ADCP (generally a 600 kHz, RDInstrument).

Periodic data are transmitted in real-time by a GSM network and are directly integrated to the Coriolis data center and Previmer analysis system.

MESURHO system

3.2.3 Marine glider

Marine gliders are increasingly used in ocean observations (Testor et al., 2010). These Autonomous Underwater Vehicles (AUVs) are self-propelled by a control of their buoyancy, which made them able to move to a specific location and depth. They are equipped with physical and optical sensors and permit the description of the variability of hydrological and biogeochemical processes operating within coastal waters with a high spatial and temporal resolution (Fig. 3.5a).

The coastal (30 - 200 m depth) *slocum* electric glider (Davis et al., 2002 - Webb Research Corporation) used in this work is a small torpedo-shaped AUV displacing 52 L and measuring 1.8 m in length with a diameter of 20 cm (Fig. 3.5b). It uses a variable buoyancy to sink or to rise through the water column. This motion is converted to a sawtooth-shaped trajectory (pitch angle of approx. 25°) by the presence of rigid wings near the center of the vehicle (Fig. 3.5a) (see technical description in Niewiadomska (2008)).

Gliders are typically equipped with a CTD sensor (Conductivity, Temperature, Depth) as well as miniaturized optical sensors. The glider used in this work, called *Tenuse*, was equipped with an external un-pumped CTD (Fig. 3.5e; see 3.3.1) and optical fluorimeter and backscatter sensors at several wavelengths from WETLAB Technologies (Fig 3.5d; see 3.4).
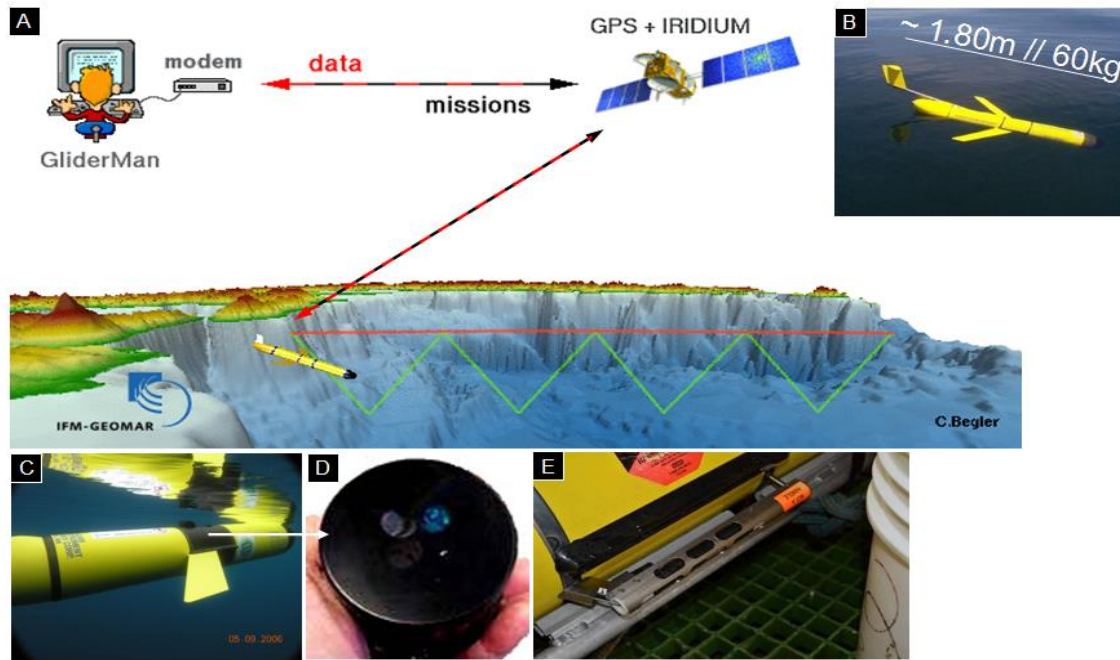
Figure 3.5 : General description of the glider operating system. A) Schematic view of mission orders (black) and data transmission (red) between the operator and the glider. The sawtooth-shaped trajectory of the glider is shown in green. B) Photo of a Slocum electric glider. C) Position of science payload on glider. D) Example of optical ECO Puck used to measure turbidity and fluorescence of Chlorophyll a. E) External un-pumped CTD used to measure conductivity, temperature and depth.

Gliders can be deployed during long periods (> 1 month), long distances (> 50 km) and during energetic events (as storms). They provide a high density of in situ information illustrated in Figure 3.6. It shows a comparison between observations made during a one-day cruise and a one-day glider deployment in the Rhône River ROFI (~40 km from the coast to the shelf edge). The glider can monitored coastal waters with a cast every 100 m (depending of bottom depth, ~150 casts per day) whereas ship observations (limited by whether and sea conditions) are limited at ~10 casts per day. The related cost-efficiency of glider observations is very low (~10€/cast) compared to ship observations (~100€/cast) and shows the *"middle-cost for a high efficiency"* character of gliders.
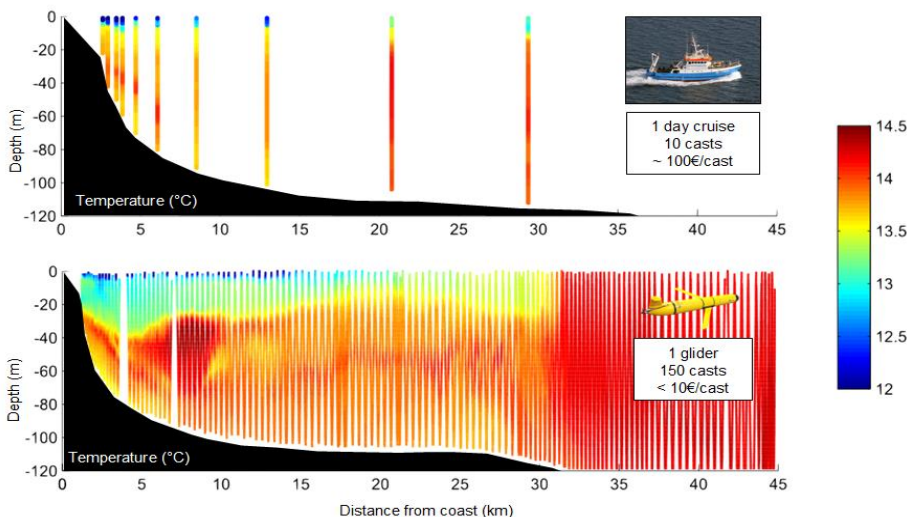
Figure 3.6 : Comparison of one-day ship-based observations (top) with one-day glider cross-shelf deployment (bottom). We choose an arbitrary cross-shelf section of temperature conditions within the Rhône River ROFI carried out during the TUCPA experiment (February 2014). Glider data are only averaged within 1m vertical bins.

Two glider deployments carried out over the shelf of the Gulf of Lions were used in this work (see Fig. 3.7).

A first feasibility study of a coastal deployment during winter conditions over a European continental margin was carried out in March-April 2011 over the Roussillon shelf (SW GoL). This deployment permitted the monitoring of the impact of a storm and a subsequent flood events on the shelf suspended particle dynamics and transport (see Chapter 6). The glider carried out 26 sections (corresponding to approx. 1300 km linear) between the Têt River mouth (~30 m depth) and the entry of the Lacaze-Duthier submarine canyon (~130 m).

A glider was then deployed in the Rhône River ROFI in February 2014 to assess the spatial and temporal high-frequency variability of nepheloid layers and suspended particles properties during flooding conditions (see Chapter 5). This deployment also permitted to verify the ability of gliders to provide an index of the suspended particles size through the spectral slope of backscattering coefficients (see 3.4.2.2 and Chapter 4).
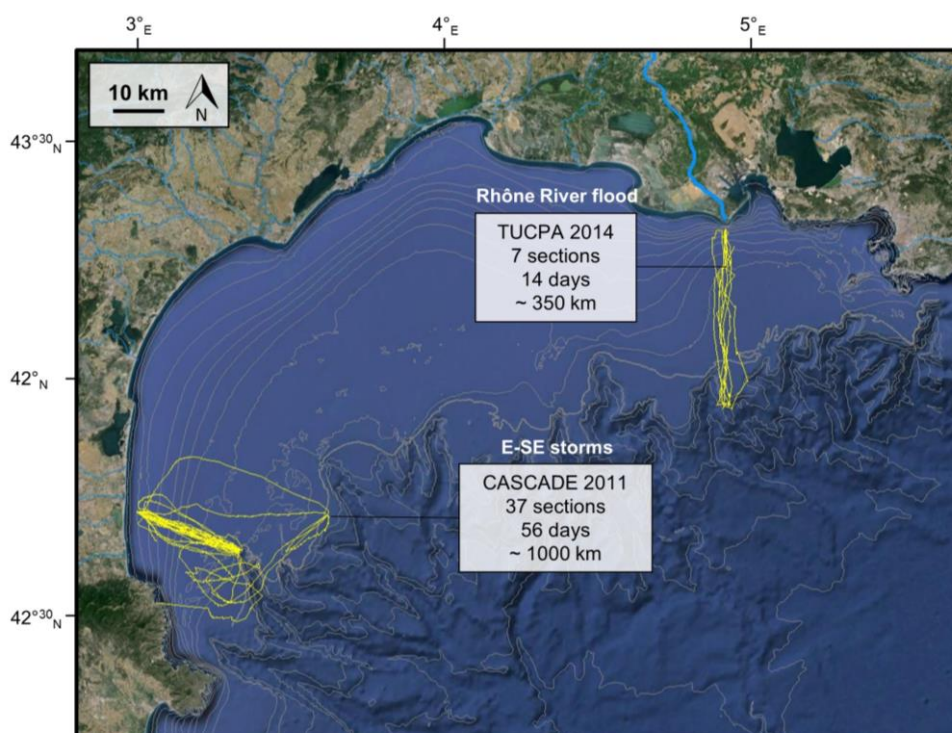
Figure 3.7 : Map of glider deployments carried out during this work. TUCPA (2014) and CASCADE (2011) deployments are shown in yellow and are detailed in Chapter 4, 5 (TUCPA) and 6 (CASCADE). Depth contours are shown in gray and represent the 10 m isobaths from the coast to the shelf edge (120m – thick gray line) and the 200 m isobaths from the shelf break to the abyss. Coastal Rivers are shown in blue. Grand Rhône River is shown by a thick blue line.

Glider system

3.2.4 Canyon mooring lines

As further detailed in Chapter 6, the southwest part of the GoL and particularly the Cap de Creus submarine canyon (Fig. 3.8a) represent preferential areas of SPM and water export offshelf during marine storm events (see also Martín et al. (2013)).

Two instrumented mooring lines were deployed during the CASCADE experiment (2011) along the southern flank of the canyon (290 m and 365 m respectively – Fig. 3.8b). Both lines were equipped with current meters, CTD, and turbidity sensors and sediment traps (Fig. 3.8c). Only results from downward-looking ADCP (155 meters above bottom (mab)), Seapoint backscattering sensors (OBS at 800 nm – 9, 62, 102 mab) and SeaBird SBE 37-SMP CTD (8 mab) are used in this work.
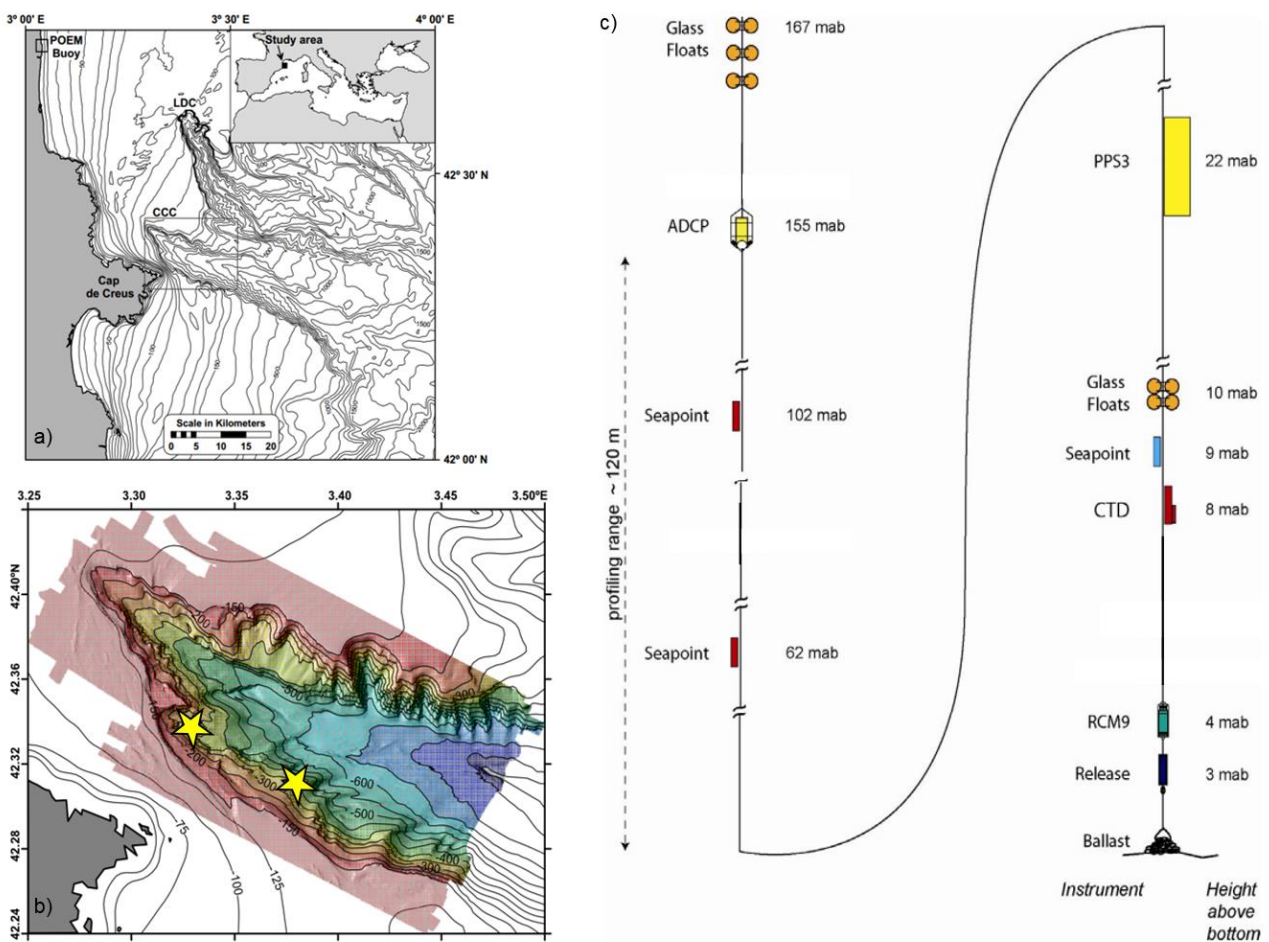
Figure 3.8 : a) Bathymetric chart of the SW part of the GoL. The position of the POEM buoy is shown by a black square. Gray square shows the area of b). b) Multibeam bathymetry of the Cap de Creus canyon. Stars show the position of the two instrumented mooring lines maintained in the southern canyon flank from the 3rd to 21st march 2011 (from Martín et al. (2013)). c) Design of the twin mooring lines. ADCP: RDI WH 300 kHz Acoustic Doppler Current Profiler; PPS3: Technicap Sequential Sediment Trap; CTD: SBE37 SMP; SeaPoint: SeaPoint Turbidity meter + AQUAlogger 210TY; RCM9: Aanderaa Recording Current Meter.

3.2.5 Satellite observations

Ocean color images are commonly used to measure the geophysical quantities at the sea surface, as the SPM concentration. These measurements enable to describe with a high spatial resolution and over regional scales the SPM dynamics, particularly the river inputs that tend to create surface river plumes.

During this work, the Moderate-Resolution Imaging Spectroradiometer (MODIS) on board on Aqua/Terra satellites, was used to describe large scale SPM dynamics at the sea surface of the Gulf of Lions. The surface SPM concentration and properties (see 3.4) were obtained using MODIS products from the NASA Ocean Color website. Different processing processes, based on algorithms of Gohin (2011) and Ody et al. (2016) – Annex 1) have been used. Details are presented within following articles (i.e. Chapter 5 and 6).

Example of RGB image of Landsat-8/OLI (30 m resolution – available on LIBRA website) is shown to illustrate the visible aspect of the surface reflectance of SPM in front of the Rhône River mouth during the 2014 flood (see Fig. 3.9).
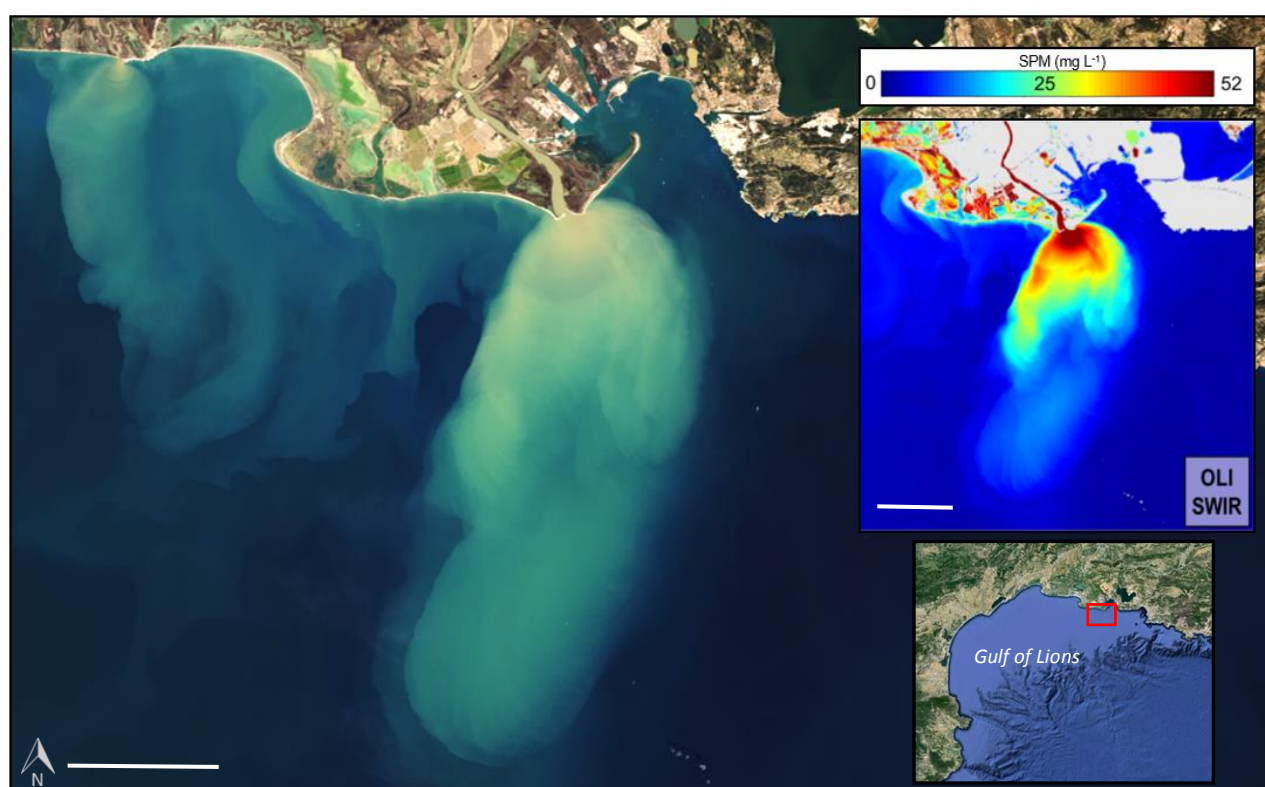
Figure 3.9 : Example of a Landsat-8/OLI image (30m resolution) of the Rhône River plume during an annual flood event (February 23, 2014) downloaded from the LIBRA website. The retrieval of SPM concentrations (mg L^{-1}) from the surface reflectance at 645 nm following algorithm of Ody et al. (2016) is shown (see Annex 1). The white scale bar represents 10 km. The location of the Rhône River plume is shown by a red square on the map of the Gulf of Lions (bottom-right corner)

LIBRA database

3.3 The hydrological measurements

3.3.1 The CTD measurements

The conductivity, temperature and depth (CTD) parameters are commonly used in oceanography. From decades, these parameters are measured from ship through a profiling instrument package (called "CTD"), which allows the determination of the vertical structure of thermo-haline parameters. In some cases, measurements from sensors are transmitted to the surface via a communication cable. The CTDs (deployed from ship or fixed on glider) used in this work were composed of a conductivity cell coupled with seawater through electrodes, a high-quality platinum resistance thermometer, and a strain gauge sensor that allowed the measurements of the pressure and the related depth. The CTD package used during surveys was a Seabird 19+ CTD while the glider was equipped with an un-pumped SeaBird 41cp CTD. For both platforms, basics derived parameters were then derived as salinity and density following general UNESCO polynomial relationships (UNESCO, 1983).

3.3.2 Sea conditions measured from fixed platforms and gliders

Currents and waves measured from fixed platforms – Currents and waves were measured with Acoustic Doppler Current Profilers (ADCP) from Teledyne RD Instruments deployed on fixed platforms. Coastal buoys and submarine canyon mooring lines (160 mab) were respectively equipped with upward- and downward-looking ADCPs at 600 and 300 kHz. ADCPs transmit high frequency acoustic signals that are backscattered from seawater constituents (as suspended sediment, phyto/zooplankton and bubbles). It is assumed that these constituents travel with the speed of the water. The estimation of the horizontal and vertical current velocity and direction as a function of depth (generally 1 m bin) is possible through the Doppler effect, which allows the measurement of the radial velocity between the instrument and the seawater constituents.

Currents were generally measured at 1 Hz and were averaged every 3 h. We used thereafter the following convention for current values: positive northward and negative southward, and positive westward and negative eastward. High-frequency measurements of near-surface wave orbital velocities, surface track, and pressure were used to compute significant wave height, peak period and direction according to the technical manual of Teledyne RD Instruments (2007). Waves were generally measured during 20 min bursts every 3 h.

Currents magnitude and direction from the glider drift and the geostrophic balance – The glider "drift", i.e. the difference between the glider's expected surfacing location and the actual new GPS position (Fig. 3.10a), was used as an estimation of horizontally depth-averaged current between two surfacings (Webb Research Slocum manual, 2005). To further characterize the current we estimated geostrophic velocities to determine how much the flow perpendicular to the section was affected by the density field (Fig. 3.10b). The glider's interpolated density field was used to

estimate the baroclinic component of the geostrophic velocities. Then, we derived the along-shelf velocity field by adjusting the depth-averaged geostrophic velocities to the corresponding glider's drift (Fig. 3.10c). This correction includes the barotropic geostrophic and ageostrophic terms, such as currents induced by surface wind stress and bottom friction.
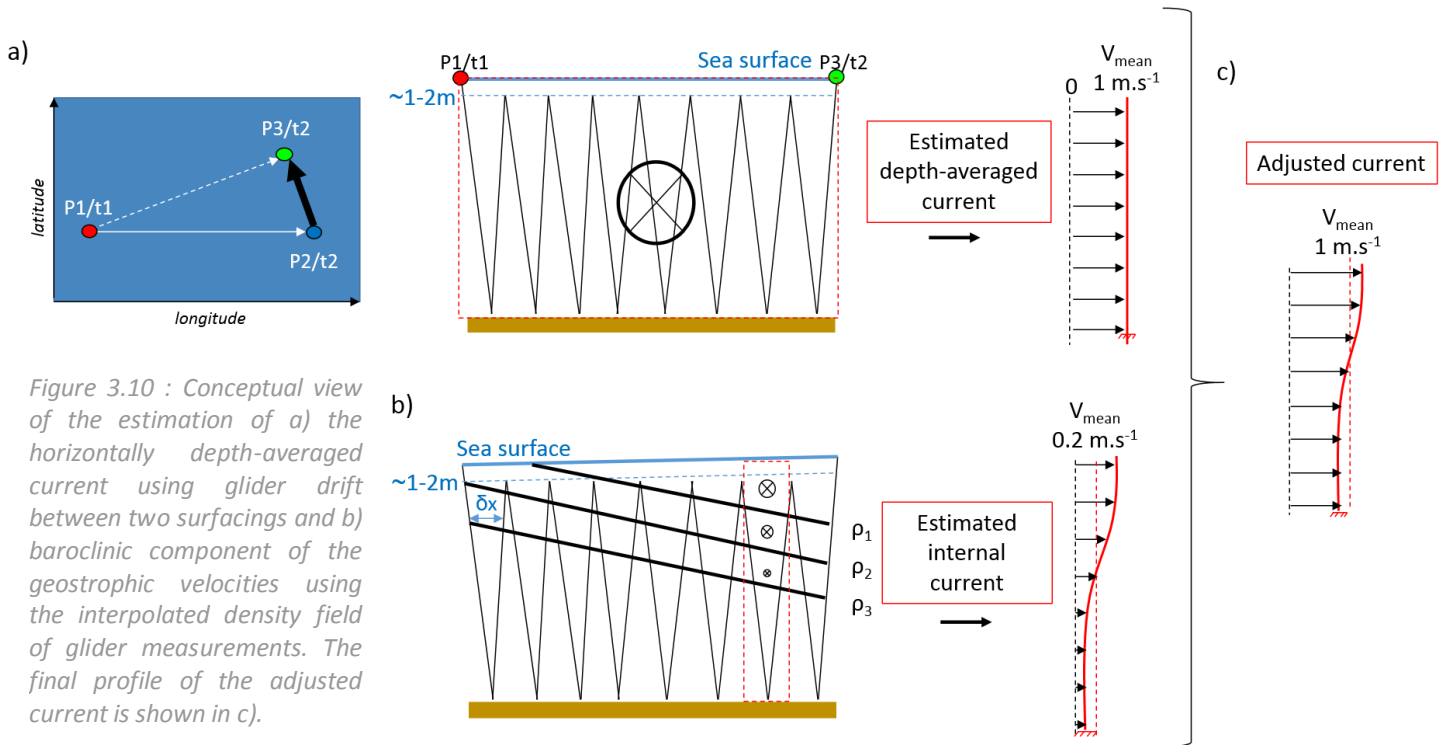
Figure 3.10 : Conceptual view of the estimation of a) the horizontally depth-averaged current using glider drift between two surfacings and b) baroclinic component of the geostrophic velocities using the interpolated density field of glider measurements. The final profile of the adjusted current is shown in c).

3.3.3 Derived parameters from glider drift and CTD measurements

The Brunt-Väisälä frequency (N - Eq. 3.1), also known as the buoyancy frequency, was derived from the glider CTD measurements and used as an indicator of the Rhône River plume stratification (see Chapter 5). Then, we used the dimensionless number of Richardson (Ri – Eq. 3.2), which allowed the estimation of the mixing intensity by comparing the Brunt-Väisälä frequency to the vertical gradient of the horizontal current velocity (see 3.3.2) (Pacanowski et Philander, 1981).

$$N = \sqrt{(-g/\rho)}\; \delta\rho/\delta z \qquad\qquad\qquad \text{Eq. 3.1}$$

$$Ri = N^2 / (\delta u/\delta z)^2 \qquad\qquad\qquad \text{Eq. 3.2}$$

where g is the acceleration of gravity (m² s⁻¹), ρ the water density (kg m⁻³) and u the current velocity vector (m s⁻¹). Generally, we considered a stable stratification for N > 0, while if N ~ 0 the stratification is unstable (Turner, 1973). The Richardson number, which defines the mixing intensity, is equal to 0.25 in a stable flow and Ri < 0.25 if the turbulence overcomes the density stratification and generates vertical mixing (Miranda et al., 2002; Kirinus et al., 2012).

3.4 The particle properties measurements

3.4.1 SPM concentration

Optical backscattering - The SPM concentration is commonly measured through the turbidity parameter. In this work, the turbidity was measured through backscattering sensors. Backscattering sensors can be various, with different backscatter angles or reference wavelengths (see Fig. 3.11). For instance, during ship-board measurements made during the CASCADE and TUCPA experiments, a Seapoint OBS 3+ (880 nm) was used in a profiling frame to determine the vertical structure of the SPM concentration. During both experiments, the sensor output (in Nephelometric Turbidity Units – NTU) was calibrated against gravimetric SPM concentrations, sampled with Niskin bottles and measured following the process described in Aminot and Kérouel (2004).

During the same experiment, the glider *Tenuse* was equipped of a Wetlabs FLNTU miniaturized sensor (ECO Puck), which measured the turbidity (expressed in NTU) based on backscattering measurements at 700 nm (140°). The measurements of turbidity were calibrated with gravimetric measurements (see details in articles, i.e. Chapter 4 and 6). Besides, a Wetlabs BB2FLS was used and provided backscattering measurements at 532 and 660 nm (TUCPA) and 532 and 880 nm (CASCADE). These measurements are factory calibrated in m^{-1} and are made at 124° in the backward direction. They were used to estimate the spectral slope of backscattering measurements (see 3.4.2.2)
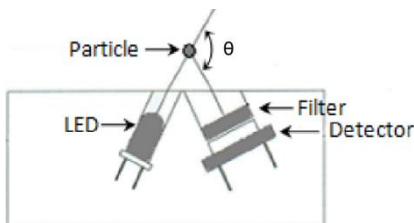
Figure 3.11 : Schematic view of the principle of optical backscattering. The light from the source is scattered by the particle. The light scattered is then measured by the detector in the backward direction. The angle of backscattering measurements (ϑ) is dependent of the instrument

Acoustic backscattering - Acoustic backscattered intensities from ADCP signal are commonly used to estimate a proxy of SPM concentrations in the water column. The acoustic pulse emitted from a single beam has a certain initial intensity, which progressively diminishes as it travels through the water column and is reflected by suspended particles. During the CASCADE experiment (2011), the Sediview software (HR Wallingford) was used, based on an iterative method to solve a simplified version of the sonar equation derived from Thorne et Campbell (1992) and Hay (1991) (Eq. 3.3):

$Log_{10}(M_r)$ = 1/S × {dB + 2r (α_w + α_s) – Ks} **Eq. 3.3**

where M_r is the gravimetric concentration per unit volume of range r, S is the relative backscatter coefficient , α_w is the water attenuation coefficient (Francois-Garrison model) and α_s is the

sediment attenuation coefficient, Ks is the site and instrument constant and dB is the measured relative backscatter intensity corrected for spherical spreading. The signals measured from the four beams were averaged and forced against in-situ gravimetric SPM concentration measurements. Sediment attenuation was estimated using relative effective particle size of 25 μm measured prior to the experiment with an in-situ Sequoia LISST-100 type B (see 3.4.2).

Due to the limited number of SPM concentration measurements and the multimodal particle size distribution observed in the Rhône ROFI during the TUCPA experiment (2014), ADCP backscatter index was derived from the echo intensity and was simply used as a relative information concerning the SPM concentration over the Rhône River prodelta (see details in Chapters 4 and 5).

3.4.2 Particles size, nature and shape

3.4.2.1 Ship-board particle properties measurements

As described in 1.2.3, the particle size distribution (PSD) in nepheloid layers plays a main role in the SPM dynamics. A need exists in the in situ determination of the particle assemblage size to avoid any turbulence and related break up of aggregates that can occur during water sampling, transport and laboratory analyses. In situ optical instruments have been developed to fill in this gap, with various technologies as LASER diffraction or imagery (holography, visual camera, microscope observations).

In this work, we used several instruments of SEQUOIA Inc. to characterize the suspended particle properties (nature, size, effective density and shape) within the Rhône River ROFI described in Chapter 4. We used the LISST-100 TYPE B and the LISST-100X TYPE C (LASER diffraction) to determine the in situ particle size from 1.25 to 250 μm and the on board deflocculated PSD from 2.5 to 500 μm respectively. These observations were completed with measurements from a LISST-HOLO (holographic camera), which permitted the in situ determination of the PSD from 20 to 2000 μm as well as the determination of several shape parameters and visual observations of largest particles (> 50 μm). A synthetic view of both systems is presented thereafter. The focus is made on their operating systems and the basis of the data processing. Then, the temporal in situ variability of both LASER and holographic systems is presented to determine the relative uncertainties of the measurements of both techniques.

 LASER diffraction - The LISST-100 was used to estimate the PSD from 1.25 to 250 μm by laser diffraction (Type B) (Fig. 3.12). The LISST-100 separates the size range in 32 logarithmic classes and uses a red LASER (670 nm) through a path of 5 cm. The instrument was deployed in situ to measure the PSD of the surface river plume and bottom nepheloid layer.

With similar optical specifications, a LISST-100X (Type C, 2.5–500 μm, 1 Hz) was used onboard to estimate the PSD of primary particles composing the particle assemblage in water sampled from surface river plume and BNL. Samples were deflocculated by ultrasonification for 5 min. PSD was then estimated from 1 min average LISST-100X measurements.
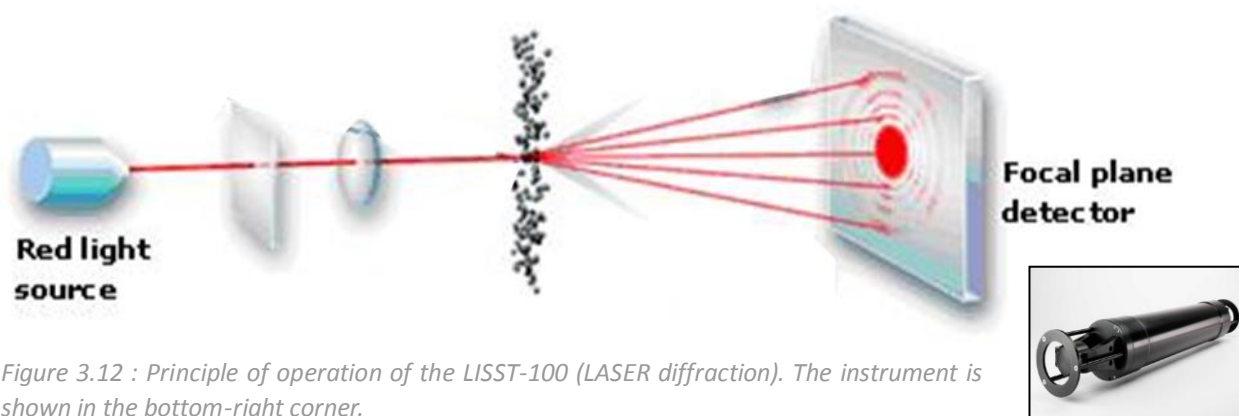
Figure 3.12 : Principle of operation of the LISST-100 (LASER diffraction). The instrument is shown in the bottom-right corner.

PSD was derived from the laser diffraction spectrum using the "randomly shaped" Mie's theory (Traykovski et al., 1999; Agrawal and Pottsmith, 2000; Agrawal et al., 2008). The raw spectrum was converted in particulate volume concentration (expressed in µL L^{-1}) using the factory volume calibration constant. Extreme size classes (1.25–2.5 and 250–500 µm) showed typical "rising tails" explained by the presence of smal particles (for the first class) and large particles (for the last class) outside the measurement range (Mikkelsen et al., 2005). Except for the LISST-100X data processing (primary particle characterization), we excluded the extreme size classes of the PSD before calculating the derived parameters used in Chapter 4 (total volume concentration (VC$_{tot}$), effective density).

Holography - The LISST-HOLO is a digital holographic camera (0.2 Hz) used to study the volume, number and shape of large particles as complex aggregates and biological organisms within the range of 20-2000 µm (Graham and Smith, 2010). It is different from the LISST-100 in that it uses holography instead of LASER diffraction to measure particles size (Fig. 3.13). The other main difference is the capacity of the LISST-HOLO to provide images of suspended particles that permit the determination of the nature of particles (as biological organisms, fine-grained aggregates, sands) as well as individual particle shape analysis.

When the collimated red LASER reference beam (659 mm) is scattered by suspended particles along the 5 cm optical path, the resultant scattered light create an hologram on the 7*4 mm CCD array. The holographic method permits the elimination of the typical depth of field issues encountered with others imagery systems as camera and microscope. Thus, the LISST-HOLO is able to bring all particles seen through the path onto the same image plan and allows the analysis of a 50*7*4 mm volume. The large path of the LISST-HOLO permits to sample the suspended particles without disturbance and therefore capture their real size and shape.

To emphasize the ability of the LISST-HOLO in the characterization of mineral (sand is excluded, the focus is made on fine-grained flocs) and organic (i.e. phyto/zooplankton) particles, example of images taken during this thesis and various frameworks (2013-2016 period) are shown .

Figure 3.13 : Principle of operation of the LISST-HOLO (holographic camera). The instrument is shown in the bottom-right corner.
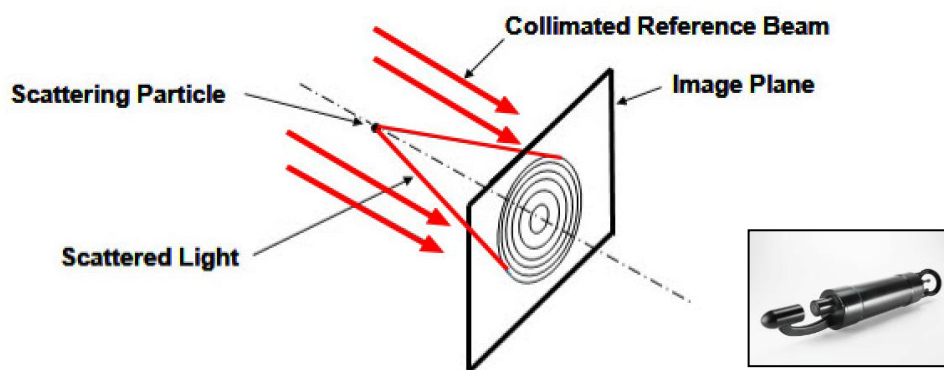
The Figure 3.14 presents the different steps of the process of LISST-HOLO measurements. First, the raw hologram (Fig. 3.14a) is converted using the latest version of HOLO-Batch (v3.0, SEQUOIA Inc.). The resultant processed image (.tiff) shows the size and shape of particles (Fig. 3.14b). At the same time, the process generates a file per image (.mat), which includes all the statistics (as diameter, volume, eccentricity, solidity, eccentricity) of each particle within the image (Fig. 3.14c) and a general particle size file (.mat, .cnv) which includes the PSD of all images analyzed (Fig. 3.14e). Based on processed images, it is possible to create a random montage ("montagemaker.m" on MATLAB) to get a visual representation of the in situ particulate assemblage (Fig. 3.14d).
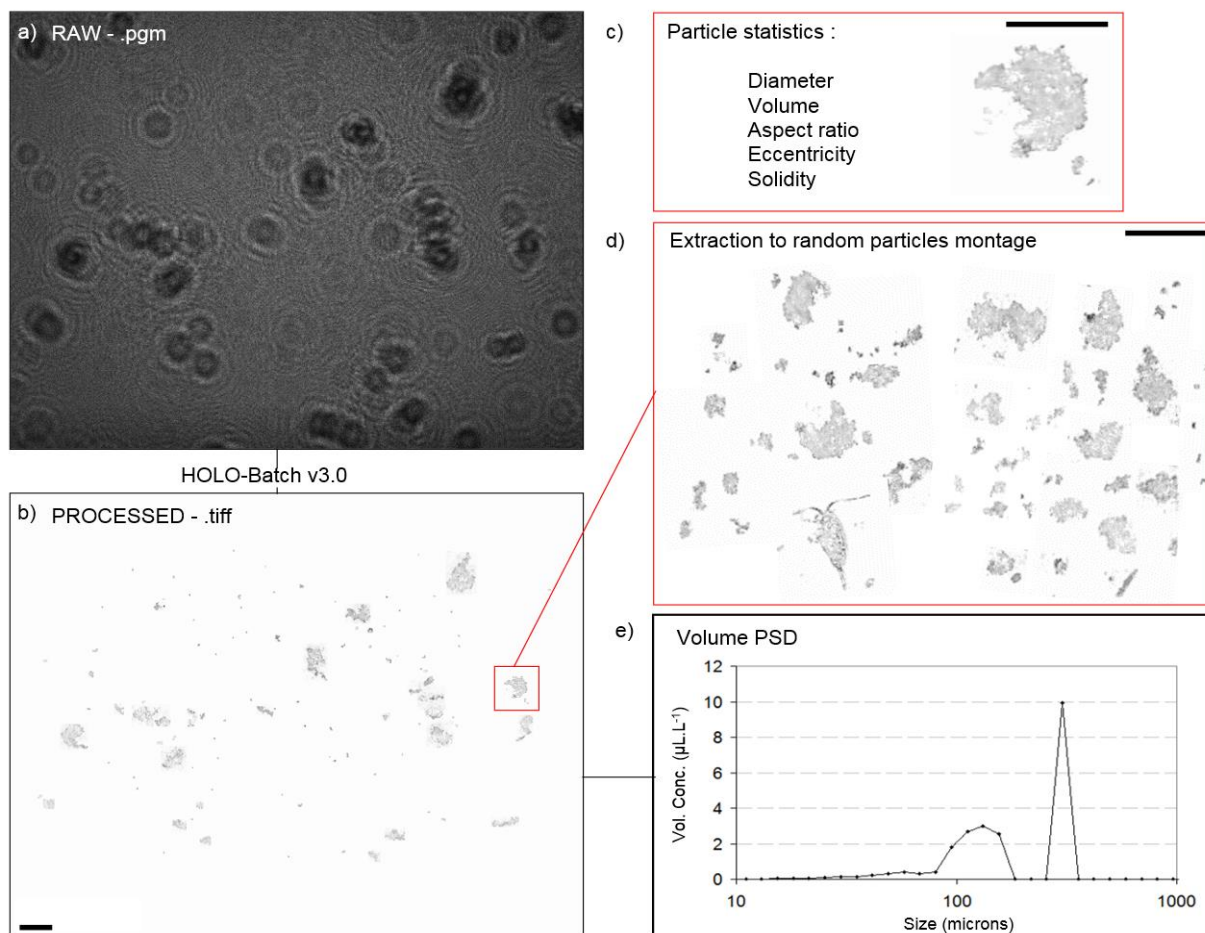
Figure 3.14 : Processing of LISST-HOLO measurements. a) Raw hologram (.pgm) b) Processed image (.tiff) with HOLO-Batch v3.0 c) Particle statistics extracted from each particle d) Extraction of particles for the random particles montage, e) Volume PSD extracted from (b). Black bars represent the 300µm scale.

Mineral

Organic

Fine particles (50μm)

Large particles (1000μm)

The LISST-HOLO provides several shape parameters for each particle analyzed.

Among them, we chose to focus on the aspect ratio (AR) (Fig. 3.15, Eq. 3.4), which underlines the spherical aspect of suspended particles. It is estimated through the equation:

AR = Ax$_{min}$ / Ax$_{maj}$ **Eq. 3.4**

where Ax$_{min}$ and Ax$_{maj}$ represents, respectively, the minor and major axes of the particle. An aspect ratio of 1 indicates a spherical shape, whereas an aspect ratio of 0 indicates a straight shape (see Clavano et al. (2007)).

Figure 3.15 : Example of particle images provided by the LISST-HOLO. The estimation of the aspect ratio is shown. Major axis length is shown in green while minor axis length is in orange.
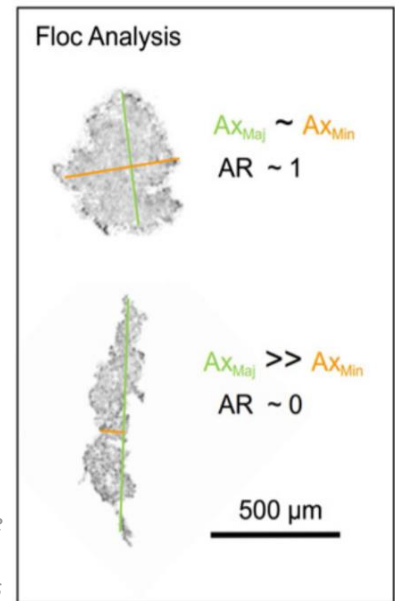
LISST instruments relative uncertainties - During the PLUMRHO campaign (February 2015 - see 3.2.1) a specific 1-h-long sampling procedure was carried out to test the variability of both LASER and holographic measurements in the Rhône River plume (5 m depth, 5 km off the river mouth).

This experiment enabled the collection of 700 holograms for the LISST-HOLO and 3500 scans for the LISST-100. A multiple random permutations of an increasing number of samples (i.e. scans/holograms) was then tested to assess the uncertainties associated to the measurements of the total volume concentration (Fig. 3.16).

Main objectives of this experiment were 1) the determination of an optimal number of measurements to minimize both the uncertainty and the collection time, and 2) the determination of the relative uncertainties related to the LISST measurements of the TUCPA experiment (February 2014 – see 3.2.1).
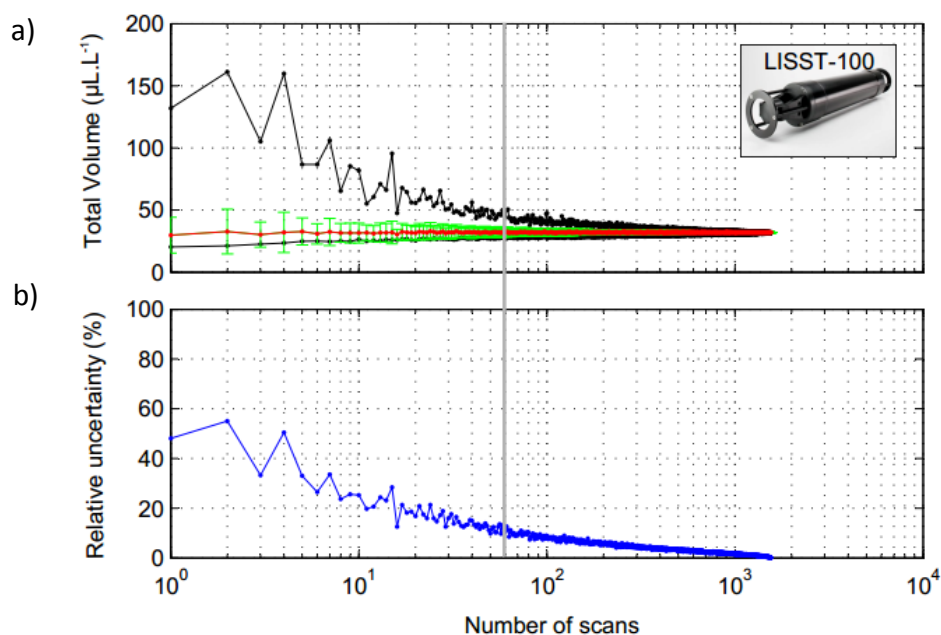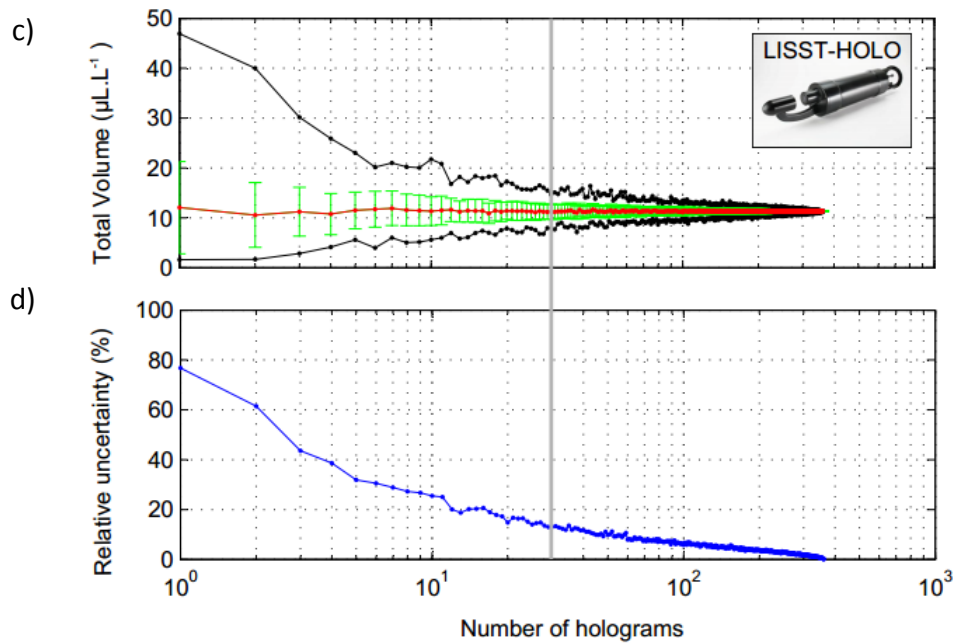
Figure 3.16 : LISST-100 and LISST-HOLO measurements statistical variability. a-c) SPM total volume concentration as a function of number of measurements made during the 5 m depth level (black : minimum and maximum; red : mean of measurements; green : standard deviation). b-d) Relative uncertainties of SPM total volume concentration as a function of number of measurements made during the experiment. Numbers of measurements made during the TUCPA experiment for both LISSTs are shown by vertical gray lines.

The relative uncertainty related to the measurements of the total volume concentration of the 60-70 LISST-100 scans acquired during the TUCPA experiment was estimated to ~4% (Fig. 3.16b). The 20-30 LISST-HOLO images generally taken during a step in the Rhône River plume presented a relative uncertainty of ~15% (Fig. 3.16d).

While this experiment was carried out after the TUCPA experiment, in different conditions of wind and river discharge, it clearly emphasized the need of long acquisition time within nepheloid layers to properly estimate the total volume concentration and the related PSD with the lowest relative uncertainty as possible. At last, it shows that the threshold used during the TUCPA experiment was satisfactory, i.e. a good compromise between the duration of the step (limited by sea conditions) and results provided by both instruments.
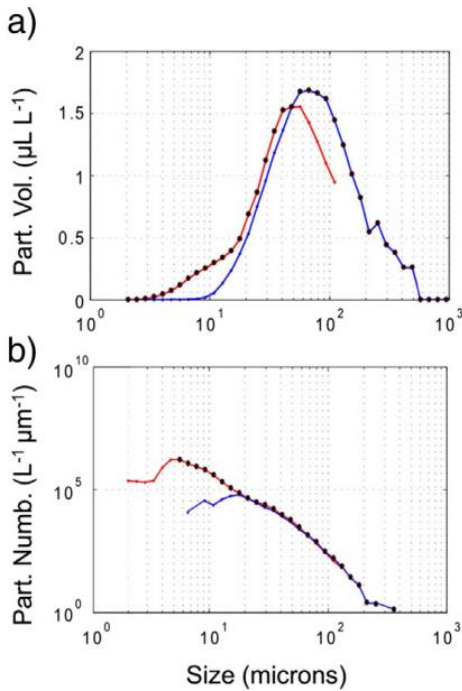
Figure 3.17 : Combination of LISST-100 type B (red line) and LISST-HOLO (blue line) particle size/number distribution. Example of the Rhône River plume (5m depth; 5km offshore). a) The volumetric representation of the combined distribution from 1.25 to 2000 is shown by black circles and is used to calculate the total particle volume concentration and associate effective density. b) Particle number distribution of the combined distribution used to estimate the Junge parameter j.

LISSTs combination and derived parameters – In order to compare and merge the PSD from the LISST-100 and the LISST-HOLO, only measurements made near the surface and the bottom were considered. Data at these two measurement levels were collected during 60-90 s period (depending on sea conditions), which allowed to gather between 60 and 70 scans for the LISST-100, and 20 and 30 images for the LISST-HOLO (see above). These data were averaged for each level. The LISST-100 and LISST-HOLO PSDs were finally merged. The maximum particle volume concentration of each common size class was selected to constitute the final PSD ranging between 1.25 and 1000 µm (Fig. 3.17a). The normalized PSD was then converted to the number of particle per size class by dividing by an elementary spherical volume (Fig. 3.17b). For mineral particle assemblage, which was mainly the case in this work, it is assumed that the resultant relation between the number of particle (n, expressed in L^{-1} μm^{-1}) and the particle size (D) follows a power law (Eq. 3.5) (Jonasz, 1983; Stramski and Kiefer, 1991; Buonassissi and Dierssen, 2010).

n(D) ∼ D^{-j} **Eq. 3.5**

Due to the rare presence of large particles, particle number less than 1 per liter, are often exclude of the power law calculation. Due to the sensitivity to the finest particles of the LISST-100 (i.e. 1.25-6µm) (Agrawal and Traykovski, 2001; Agrawal et al., 2008), the "tail" for small size classes (i.e. < 6µm) is also filtered. This tail is generally due to an uncertain refractive index for the finest particle and can be interpreted as a contamination of our power law approximation (Graham and Smith, 2010; Xi et al., 2014). The slope, *j*, extracted from the power law approximation, or Junge parameter (dimensionless), is used to estimate the relative number of small to large particle for the 6-500 µm size range (Junge, 1963). High *j* (∼4) implies a higher proportion of small particles and, reciprocally, low *j* (∼2.4) implies higher proportion of large particles, with respect to the "normal" distribution for which *j* = 3.

Finally the particle assemblage effective density was derived, Δρ (kg m^{-3}), using simultaneous measurements of SPM concentrations (mg L^{-1}) from the calibrated backscatter sensor (OBS 3+) (see 3.4.1) and the total volume concentration, VC$_{tot}$ (µL L^{-1}) from the LISSTs, following Eq. 3.6:

Δρ = SPM$_{OBS}$ / VC$_{tot}$ **Eq. 3.6**

3.4.2.2 The measurements of particle size from glider and satellite

Spectral slope of glider backscattering measurements – The spectral slope of glider particulate backscattering coefficients [$b_{bp}(\lambda)$] at 532 nm, 660 nm (TUPCA) – 880 nm (CASCADE) and 700 nm, called γ_{Glider}, was used as an index of the spatial and temporal variability of the particle assemblage (i.e. the lower the γ_{Glider}, the higher the contribution of large particles to the total particle assemblage, and reciprocally) (Boss et al., 2001).

FLNTU (λ = 700 nm) and BB2FLS (λ = 532 and 660/880 nm) sensors provided respectively the volume scattering function [$\beta(\theta,\lambda)$] at θ = 140° and θ =124° in the backward direction (Sullivan et al., 2010). BB2FLS sensor directly give output in $m^{-1}\ sr^{-1}$ while measurements of the FLNTU, factory calibrated in NTU, were converted to extract the volume scattering function thanks to the Beta Scale Factor provided by the manufacturer (i.e. the NTU Scale Factor multiply by a coefficient of 2.5×10^{-3}).

Due to the negligible absorption effects (a few % of the total signal measured) we did not correct values of [$\beta(\theta,\lambda)$]. For each sensor, we then estimated the volume scattering of particles [$\beta_p(\lambda)$], by subtracting the molecular scattering of pure water (Morel, 1974). The particulate backscattering coefficients [$b_{bp}(\lambda)$] (m^{-1}) were finally derived following [$b_{bp}(\lambda)$] = $2\pi.X.[\beta_p(\theta,\lambda)]$ where X is an adjustment factor according to water type (1.077 for the BB2FLS and 1.132 for the FLNTU).

From Morel (1973) and Babin et al. (2003), the light scattered by suspended marine particles depends of the particle size distribution and the wavelength of detection. Authors describe this variation as a power law approximation in the case of non-absorbing particles, which follows: $b_{bp}(\lambda)=b_{bp}(\lambda_0).(\lambda/\lambda_0)^{-\gamma}$ where λ_0 is the reference wavelength and γ the spectral slope. γ was thus calculated as the slope of the linear relationship between $\log_e(b_{bp}(\lambda))$ and $\log_e(\lambda)$, using λ = 532, 660 and 700 nm during the TUCPA experiment (January / February 2014 – Chapter 4-5) and using λ = 532, 700 and 880 nm during the CASCADE experiment (March 2011 – Chapter 6). Morel (1973) reported a relationship between the spectral slope and the Junge parameter (see 3.4.2.1) ($\gamma = j - 3$), but more recently, Boss et al. (2001) proposed a new relation, valid for particle > 10 μm and non-spherical particles: $\gamma = j - 3 - 0.5e^{-6j}$.

Spectral slope of satellite backscattering measurements – We derived the particulate backscattering coefficient bbp(λ) at 10 MODIS wavebands between 412 and 678 nm applying the QAA (Quasi-Analytical Algorithm) (Lee et al. 2002, 2013). QAA derives the absorption and backscattering coefficients by analytically inverting the spectral remote-sensing reflectance. The spectral bbp(λ) is modeled assuming that both pure water and particles contribute to the total backscattering coefficient, and assuming that the spectral variations of bbp(λ) follow a power-law function. The spectral slope of the particulate backscattering coefficient, γ_{MODIS}, was therefore obtained by fitting a power-law function to the spectral bbp coefficients. γ_{MODIS} is further used as a relative information of the surface spatial variability of the particle assemblage (i.e. the lowest the spectral slope the highest the abundance of large particles).

References

Agrawal, Y. C., and H. C. Pottsmith. **2000**. « Instruments for particle size and settling velocity observations in sediment transport ». *Marine Geology* 168 (1–4): 89‑114. doi:10.1016/S0025-3227(00)00044-X.

Agrawal, Y. C., and P. Traykovski. **2001**. « Particles in the bottom boundary layer: Concentration and size dynamics through events ». *Journal of Geophysical Research* 106: 9533‑42. doi:10.1029/2000JC900160.

Agrawal, Y. C., A. Whitmire, O. A. Mikkelsen, and H. C. Pottsmith. **2008**. « Light scattering by random shaped particles and consequences on measuring suspended sediments by laser diffraction ». *Journal of Geophysical Research* 113 (C4). doi:10.1029/2007JC004403.

Allison, M., C. A. Nittrouer, G. C. Kineke and R. W. Sternberg. **1994**. « Use of an instrumented tripod system to examine sediment dynamics and fine-scale strata formation in muddy surfzone and nearshore environments ». *Journal of coastal research*, 488-496.

Aminot, A., and R. Kérouel. **2004**. *Hydrologie des écosystèmes marins: paramètres et analyses*. Editions Quae.

Babin, M., A. Morel, V. Fournier-Sicre, F. Fell, and D. Stramski. **2003**. « Light scattering properties of marine particles in coastal and open ocean waters as related to the particle mass concentration ». *Limnology and Oceanography*, 843‑59.

Boss, E., M. S. Twardowski, and S. Herring. **2001**. « Shape of the particulate beam attenuation spectrum and its inversion to obtain the shape of the particulate size distribution ». *Applied Optics* 40 (27): 4885‑93.

Bourrin, F. **2007**. « Variabilité des apports sédimentaires par les fleuves côtiers: Cas du systeme Têt: Littoral Roussillonnais dans les Golfe du Lion ». *Thèse de Doctorat, Université de Perpignan.* 305 p.

Buonassissi, C. J., and H. M. Dierssen. **2010**. « A Regional Comparison of Particle Size Distributions and the Power Law Approximation in Oceanic and Estuarine Surface Waters ». *Journal of Geophysical Research* 115 (C10). doi:10.1029/2010JC006256.

Clavano, W.., E. Boss, and L. Karp-Boss. **2007**. « Inherent Optical Properties of Non-Spherical Marine-like Particles : From Theory to Observation ». *Oceanography and Marine Biology* 45: 1‑38.

Davis, R. E., C. C. Eriksen, and C. P. Jones. **2002**. « Autonomous buoyancy-driven underwater gliders ». *The technology and applications of autonomous underwater vehicles*, 37‑58.

Dickey, T., **2002**. « Emerging instrumentation and new technologies in the early 21st century. » *In: J.G. Field, G. Hempel and C.P. Summerhayes (eds.): Oceans 2020: Science for Future Need*, p.213-256.Washington, DC Island Press.

Dickey, T, M. Lewis, and G. Chang. **2006**. « Optical oceanography: recent advances and future directions using global remote sensing and in situ observations ». *Reviews of Geophysics* 44 (1).

Glenn, S., W. Boicourt, B. Parker, and T. Dickey. **2000**. « Long-term, real-time coastal ocean obeservation networks ». *Oceanography,* 13, 12-23.

Gohin, F. **2011**. « Annual cycles of chlorophyll-a, non-algal suspended particulate matter, and turbidity observed from space and in-situ in coastal waters ». *Ocean Science* 7 (5): 705.

Graham, G. W., and W. a. M. Smith. **2010**. « The application of holography to the analysis of size and settling velocity of suspended cohesive sediments ». *Limnology and Oceanography: Methods* 8: 1‑15.

Hay, A. E. **1991**. « Sound scattering from a particle-laden, turbulent jet ». *The Journal of the Acoustical Society of America* 90 (4): 2055‑74.

IOC, **1998**. « The Global Ocean Observing System Prospectus ». *GOOS Publication* 42. Paris, UNESCO, 168 pp.

Jonasz, M. **1983**. « Particle-Size Distributions in the Baltic ». *Tellus B* 35 (5). doi:10.3402/tellusb.v35i5.14624.

Junge, C. E. **1963**. « Air chemistry and radioactivity », 382.

Kirinus, E. W. Correa, J. C. da Costa, and E. H. Leão Fernandes. **2012**. « The contribution of waves in mixing processes of the Patos Lagoon plume ». *International Journal of Geosciences* 3: 1019.

Lee, Z., K.L. Carder., and R.A. Arnone. **2002**. « Deriving inherent optical properties from water color: a multiband quasi-analytical algorithm for optically deep waters. » *Applied Optics*, 41(27), 5755-5772.

Lee, Z., B. Lubac, J. Werdell, and R.A. Arnone. **2013**. http://www.ioccg.org/groups/Software_OCA/QAA_v5.pdf.

Lindstrom, E., J. Fellous, M. Drinkwater, R. Navalgund, J. Marra, T. Tanaka, J. Johannessen, C. Summerhayes and L. Charles. **2000**. « An Ocean Theme for the IGOS Partnership: Final report from the Ocean Theme Team ».

Martín, J., X. Durrieu de Madron, P. Puig, F. Bourrin, A. Palanques, L. Houpert, M. Higueras, et al., **2013**. « Sediment Transport along the Cap de Creus Canyon Flank during a Mild, Wet Winter ». *Biogeosciences* 10 (5): 3221‑39. doi:10.5194/bg-10-3221-2013.

Mikkelsen, O. A., P. S. Hill, T. G. Milligan, and R. J.

Chant. **2005**. « In situ particle size distributions and volume concentrations from a LISST-100 laser particle sizer and a digital floc camera ». *Continental Shelf Research* 25 (16): 1959‑78. doi:10.1016/j.csr.2005.07.001.

Miranda, L. B. de, B. M. de Castro, and B. Kjerfve. **2002**. « Princípios de oceanografia física de estuários ». *São Paulo: EDUSP* 414.

Morel, A. **1973**. « The scattering of light by sea water: Experimental results and theoretical approach (Diffusion de la lumière par les eaux de mer; résultats expérimentaux et approche théorique; in French) ». *Optics of the sea, interface and in-water transmission and imaging* AGARD Lecture Series (61): 3.1.1‑3.1.76.

Morel, A. **1974**. « Optical properties of pure water and pure sea water ». *Optical aspects of oceanography*, Acadamic Press, London*, , 1‑24.

Niewiadomska, K. **2008** « Couplage physique-biogéochimique à différentes échelles spatiales et temporelles : le cas du courant Ligure étudié par un planeur sous-marin bio-optique ». *Thèse de Doctorat*. Laboratoire d'océanographie de Villefranche-sur-mer. 272 p.

Ody, A., D. Doxaran, Q. Vanhellemont, B. Nechad, S. Novoa, G. Many, F. Bourrin, R. Verney, I. Pairaud, and B. Gentili. **2016**. « Potential of High Spatial and Temporal Ocean Color Satellite Data to Study the Dynamics of Suspended Particles in a Micro-Tidal River Plume ». *Remote Sensing* 8 (3): 245.

Pacanowski, R. C., and S. G. H. Philander. **1981**. « Parameterization of vertical mixing in numerical models of tropical oceans ». *Journal of Physical Oceanography* 11 (11): 1443‑51.

Pairaud, I., Répécaud, C., Ravel, M., Fuchs, R., Arnaud, M., Champelovier, A., Rabouille, C., Bombled, B., Toussaint, F., Garcia, F., Raimbault, P., Verney, R., Meulé, S., Gaufrès, P., Bonnat, A., Cadiou, J.F., **2015**. MesuRho: plateforme instrumentée de suivi des paramètres environnementaux à l'embouchure du Rhône. In: Schmitt, F.G., Lefebvre, A. (Eds.), Mesures haute résolution dans l'environnement marin côtier. Presses du CNRS sous presse.

Robinson, I. S. **1985**. « Satellite oceanography; an introduction for oceanographers and remote-sensing scientists ».

Simpson, J. H., and J. Sharples. **2012**. « Introduction to the physical and biological oceanography of shelf seas ». *Cambridge University Press.*

Stramski, D., and D. A. Kiefer. **1991**. « Light scattering by microorganisms in the open ocean ». *Progress in Oceanography* 28 (4): 343‑83.

Sullivan, J.M., P.L. Donaghay, and J. Rines. **2010**. « Coastal thin layer dynamics: consequences to biology and optics ». *Continental Shelf Research* 30 (1): 50‑65.

Teledyne RD Instruments, **2007**. WAVES PRIMER: Wave Measurements and the RDI ADCP Waves Array technique. Available from RDInstruments.com.

Testor, P., G. Meyers, C. Pattiaratchi, R. B., D. Hayes, S. Pouliquen, L. Petit de la Villeon, T. Carval, A. Ganachaud, and L. Gourdeau. **2010**. « Gliders as a component of future observing systems ».

Thorne, P. D, and S. C Campbell. **1992**. « Backscattering by a suspension of spheres ». *The Journal of the Acoustical Society of America* 92 (2): 978‑86.

Traykovski, P., R. J. Latter, and J. D. Irish. **1999**. « A laboratory evaluation of the laser in situ scattering and transmissometery instrument using natural sediments ». *Marine Geology* 159 (1–4): 355‑67. doi:10.1016/S0025-3227(98)00196-0.

Turner, J. S. **1973**. « Buoyancy effects in uids ». *Cambridge University*.

UNESCO. **1983**. « Algorithms for computation of fundamental properties of seawater ». *Technical papers in marine science* 44: 53.

UNESCO. **1996**. « Oceanographic survey techniques and living resources assessment methods ». *IOC Manuals and guides* 32.

UNESCO. **2003**. « The integrated, strategic design plan for the Coastal Ocean Observations Module of the Global Ocean Observing System ». *GOOS Report* 125. IOC Information Documents Series n°1183.

Webb Research. **2005**. Operations Manual Slocum Shallow Battery Glider Ver 1.6 1/11/2005.

Weller, R., J. Toole, M. McCartney and N. Hogg, **2000**. « Outposts in the Ocean ». *Oceanus*, *42*(1), 20.

Xi, H., P. Larouche, S. Tang, and C. Michel. **2014**. « Characterization and Variability of Particle Size Distributions in Hudson Bay, Canada ». *Journal of Geophysical Research: Oceans* 119 (6): 3392‑3406. doi:10.1002/2013JC009542.

Chapter 4.

Particle assemblage characterization

in the Rhône River ROFI

Chapter 4. Particle assemblage characterization in the Rhône River ROFI

Gaël Many[1], François Bourrin[1], Xavier Durrieu de Madron[1], Ivane Pairaud[2], Aurélien Gangloff[3], David Doxaran[4], Anouck Ody[4], Romaric Verney[3], Christophe Menniti[1], David Le Berre[3], Matthias Jacquet[3]

[1] CEFREM, UMR 5110 CNRS - UPVD, 52 Avenue Paul Alduy, 66860 Perpignan Cedex, France
[2] LERPAC, IFREMER, ZP de Brégaillon, 83507, La Seyne-sur-Mer, France

[3] PHYSED, IFREMER, ZI Pointe du Diable, 29280, Plouzané, France

[4] LOV, UMR 7093 CNRS - UPMC, 181 Chemin du Lazaret, 06230, Villefranche-sur-mer, France

Online version

List of Figures

wavelengths (γ$_{Glider}$), and the Boss et al (2001) relationship based on the Junge parameter estimated from the LISST particle number distribution (γ$_{LISST}$). River plume samples are in grey dots and BNL samples are in white squares. The grey line represents the 1:1 relationship. **88**

List of Tables

Abstract

An innovative experiment was carried out in the vicinity of the Rhône River mouth in February 2014. An instrumental package, composed of a CTD, a LISST-100 type B (1.25-250 μm) and a LISST-HOLO (20-2000 μm), was used to characterize the hydrological parameters and suspended particles properties (concentration, size, composition, shape and effective density) in the region of freshwater influence (ROFI) of the Rhône River. Besides, a coastal SLOCUM glider, equipped with a CTD and optical backscattering sensors at several wavelengths, was deployed to detail the spatial description of the hydrological parameters and some particle properties. Large river discharge (annual flood ~5000 m^3 s^{-1}) and strong wind conditions favored the dispersal of the river plume on the shelf. Surface suspended particulate matter concentrations decreased rapidly seaward from 20 mg L^{-1} next to the river mouth to 1.5 mg L^{-1} at the shelf break. A persistent bottom nepheloid layer was observed across the shelf with concentrations decreasing from 8 mg L^{-1} at the coast to 1 mg L^{-1} at the shelf break. Observations showed that most of suspended particles were mainly flocculated in micro and macro-flocs (30-400 μm) in inner shelf waters. The particle assemblage in the Rhône River plume and in the bottom nepheloid layer became progressively finer seaward and the associated effective density increased from 370 to 1600 kg m^{-3}. Outside the plume, planktonic organisms increasingly contributed to the total volume concentration. Finally, we demonstrated the ability of gliders, equipped with optical backscattering sensors at several wavelengths, to describe the fine scale distributions of suspended particles, and provide an index of their size distribution.

Keywords:

Gulf of Lions, Rhône River, ROFI, turbid structures, particle properties, glider

Highlights:

- Description of the suspended particles size distribution in the Rhône River ROFI

- Evidence of fine-grained flocculation in the surface and bottom nepheloid layers

- Evidence of seaward gradient of particle concentration, size, and effective density

- Verification of the ability to measure an index of particle size from a glider

4.1 Introduction

In the source-to-sink approach, regions of freshwater influence (ROFI) are critical transition zones between the continent and the ocean, but still concentrate many knowledge gaps regarding the dynamics of suspended particles. In particular, particles size and effective density, which play a main role in settling velocity and dispersal of suspended sediment over the shelf (Nittrouer et al., 2009; Simpson and Sharples, 2012), are still insufficiently documented. Observations of suspended particulate matter (SPM) near river mouths generally show that sandy sediment and part of finer silty and clayey particles rapidly settle from surface water toward the bottom where they contribute to generate and maintain a bottom nepheloid layer (BNL) or form ephemeral mud deposits (Drake, 1976).

In many ROFIs, river inputs form hypopycnal turbid plume which spread over several kilometers on continental shelves (McCave, 1972). At the freshwater/seawater interface, riverine suspended particles can form flocs of variable abundance and characteristics which are responsible for a large part of the total vertical particle flux from the river plume to the BNL. Previous studies on fine cohesive sediment flocs have identified that, SPM concentration variability in one hand, and turbulence on the other, are the main factors controlling floc aggregation and break up (Curran et al., 2007; Safak et al., 2013; Manning and Schoellhamer, 2013). Flocculation processes have an effect on clayey and silty fine particles (< 10 μm) and form "microflocs" (size < 125 μm) or "macroflocs" (size > 125 μm, principally composed of microflocs) (Gibbs, 1985; Van Leussen, 1994). Microflocs are described as dense and quasi-spherical, resistant to turbulence, whereas macroflocs generally present lower density and can easily be fragmented into microflocs by shear forces (Manning and Dyer, 1999; Manning et al., 2004). Coatings and biological contents, as well as salinity gradient are also described as factors controlling the flocculation of particles (Ayukai and Wolanski, 1997; Dagg et al., 2004). Close to the seabed, flocculation of resuspended fine sediments appears as a key factor in the fate of the BNL (Agrawal and Traykovski, 2001). Hence particle properties (composition, flocs size, shape, effective density and settling velocity) are determining parameters to understand and model particle dynamics, but are still seldom quantified (Winterwerp, 1998; Khelifa and Hill, 2006; Manning et al., 2011; Soulsby et al., 2013).

4.2 Regional settings

The Gulf of Lions (GoL) in the NW Mediterranean is a wide continental shelf mostly influenced by freshwater and particulate matter inputs from the Rhône River. The Rhône River (catchment area = 97 800 km^2) supplies 80% of the sedimentary input to the Gulf of Lions (Courp and Monaco, 1990; Bourrin et al., 2006). The Rhône River discharge is characterized by a strong annual variability with a mean annual discharge of 1700 m^3 s^{-1} and typical annual flood with discharge >5000 m^3 s^{-1} (Maillet et al., 2006). These authors estimated a total suspended solid flux around 7×10^6 tons per year with a high annual variability from 1.2 to 19.7 ×10^6 t y^{-1}. Pont (1996) estimated that flood events contributed to 70% of the total particulate flux. During floods, freshwater and sediment inputs form a surface plume that can spread over several kilometers off the mouth (Aloisi et al., 1979; Naudin et al., 1997; Thill et al., 2001). Sediment delivery from the Rhône River can also be transported as intermediate and bottom nepheloid layer as described in Aloisi et al. (1982). Previous studies emphasized the diversity of physical processes (river discharge, oceanic conditions, behavior of the thermocline) in regulating the transport of particles within turbid structures.

The Rhône prodelta is a shallow area of high sedimentation rates (typically ranging from 20 to 50 cm y^{-1}) (Marion et al., 2010; Miralles et al., 2005). It is subjected to wave energy that induces particle resuspension and contributes to maintain a permanent bottom nepheloid layer (BNL), whose thickness, concentration, and composition vary with the Rhône River inputs and episodic storms (Aloisi et al., 1982; Naudin et al., 1992; Dufois et al., 2014). This BNL extends over the whole shelf, where it feeds the mid-shelf muddy belt and is eventually exported off the shelf (Durrieu de Madron and Panouse, 1996).

Previous in situ observations suggested the fast vertical transfer of both fine (silts) and coarse (sand) particles from the Rhône river plume to the seabed (Aloisi et al., 1982; Naudin et al., 1992). To explain the spread and settling of fine particles, previous studies suggested the role of aggregation phenomena by salt flocculation along the dilution gradient of the river plume (Thill et al., 2001), and by the electro-chemical action of the organic matter (Naudin et al., 1997). These latter authors also highlighted the correlation between the increase of particulate concentration and the growth of flocs. They showed the predominant role of wind on the mixing time of the plume, which appears to enhance the settling of suspended matter, particularly, the largest organo-mineral aggregates. Babin et al. (2003) used in situ optical light scattering measurements at different wavelengths to characterize the particle properties of the Rhône ROFI. More recently, Slade and Boss (2015) derived the spectral slope of backscattering measurements, γ, and emphasized the link between the spectral slope and the Junge parameter, *j*, exponent of the power law approximation of the particle number distribution (PND). These observations highlighted the link existing between optical in situ measurements and spatio-temporal variability of particle assemblage (i.e. the more or less large proportion of flocs).

The current study presents a comprehensive set of hydrological, hydrodynamical, and optical measurements collected with different platforms (mooring, ship and glider) in the Rhône River

ROFI. It aims at: 1) characterizing the spatial variability of turbid structures in the ROFI during an annual flood event, 2) assessing the link between the in situ estimate of spectral slope, γ, and the particle size distribution (PSD), 3) determining the particle assemblage properties (size, shape, composition) and 4) determining the cross-shore spatial variability of particle properties in the surface and bottom layers.

4.3 Material & Methods

4.3.1 Presentation of the experiment

We used a multi-platform strategy to characterize the Rhône ROFI suspended particles during flood events. We coupled coastal buoy time-series observations of oceanic and meteorological conditions with cross-shelf hydrological observations. High spatial resolution of turbid and hydrological structures was characterized with a coastal glider, and was completed with local but detailed shipboard measurements.

A SLOCUM glider was deployed from January 30, 2014 to February 12, 2014 off the Rhône River mouth. Glider's sections consisted of N-S lines of 40 km long running across the GoL shelf from the MESURHO buoy (20 m depth) to the shelf break (150 m depth) (Fig. 4.1). Each section was generally performed in 2 days.
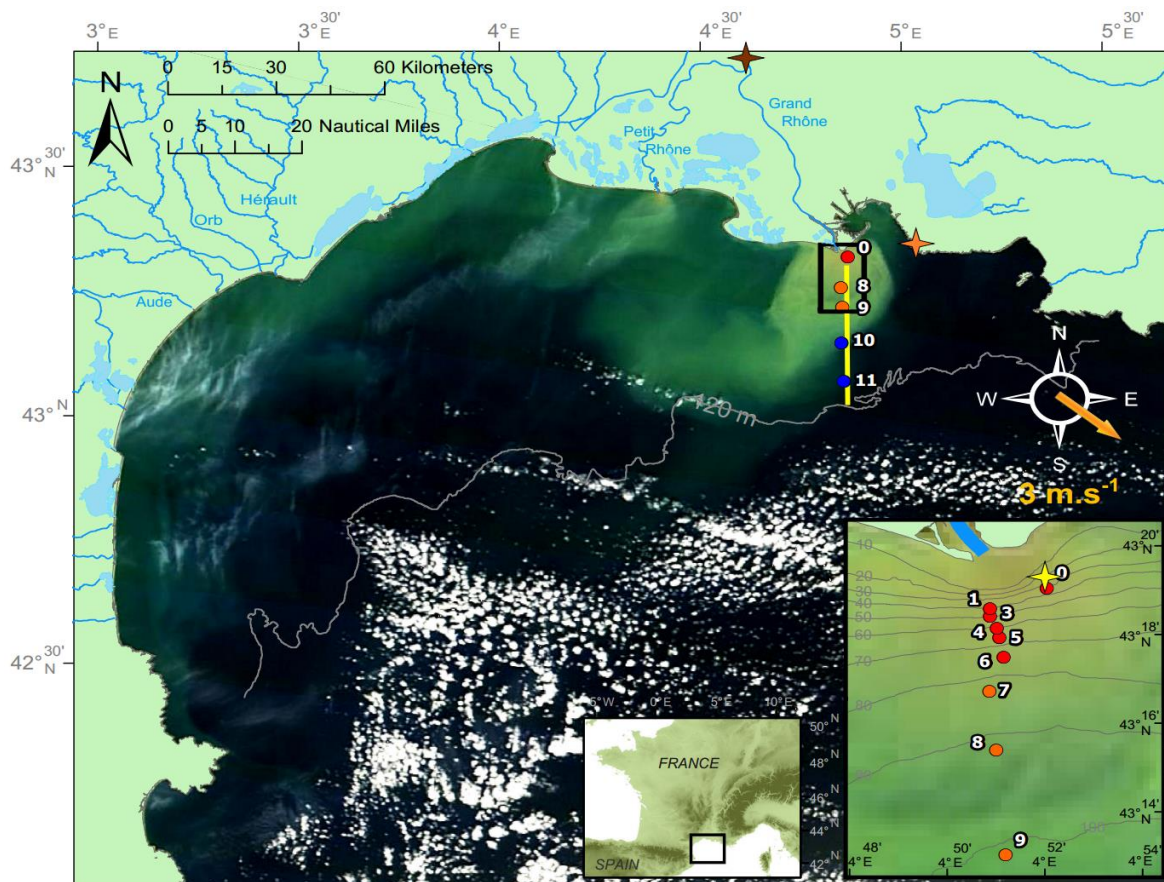
Figure 4.1 : MODIS Aqua visible image of the February 17, 2014. Rhône plume stations are shown by red (inner-shelf), orange (mid-shelf), and blue (outer-shelf) circles. Beaucaire gauging station, Cap-Couronne wind station, and MESURHO buoy are shown by brown, orange and yellow star, respectively. The shelf edge (120 m depth) is shown by a gray line.

A cruise was carried out on board of the research vessel *Antédon II*, in front of the Rhône River mouth between the 17 and 21 February 2014. The first day took place immediately after an annual flood of the Rhône River and 11 stations were sampled along a 30 km cross-shelf transect corresponding to the glider section. We used an original instrumental package (Fig. 4.2c) composed of two in situ particle size analyzers manufactured by Sequoia Scientific Inc (laser scattering sensor and holographic camera), and a CTD package (Fig. 4.2a-b). Due to the low acquisition frequency of the holographic camera (0.2 Hz), two levels of sampling were selected in order to collect statistically significant measurements to precisely determine the particle properties of the main turbid structures. The first level was at ~3-5 m depth within the surface nepheloid layer (SNL) and the second at ~1 meter above bottom (mab) in the BNL. Water samples were collected at these two depths from Niskin bottles. The stations were located every 10 m of depth from the near-shore (20 m) up to the shelf break (120 m). We divided the transect into three domains: the inner shelf (0 - 5 km from the river mouth, maximum 80 m water depth), the mid-shelf (5 - 20 km, maximum 100 m water depth) and the outer-shelf (> 20 km, maximum 200 m water depth) (see Fig. 4.1). These 3 domains correspond to the Rhône River submarine delta, to the mid-shelf mud-belt and to the outer-shelf relict sand outcrops respectively.
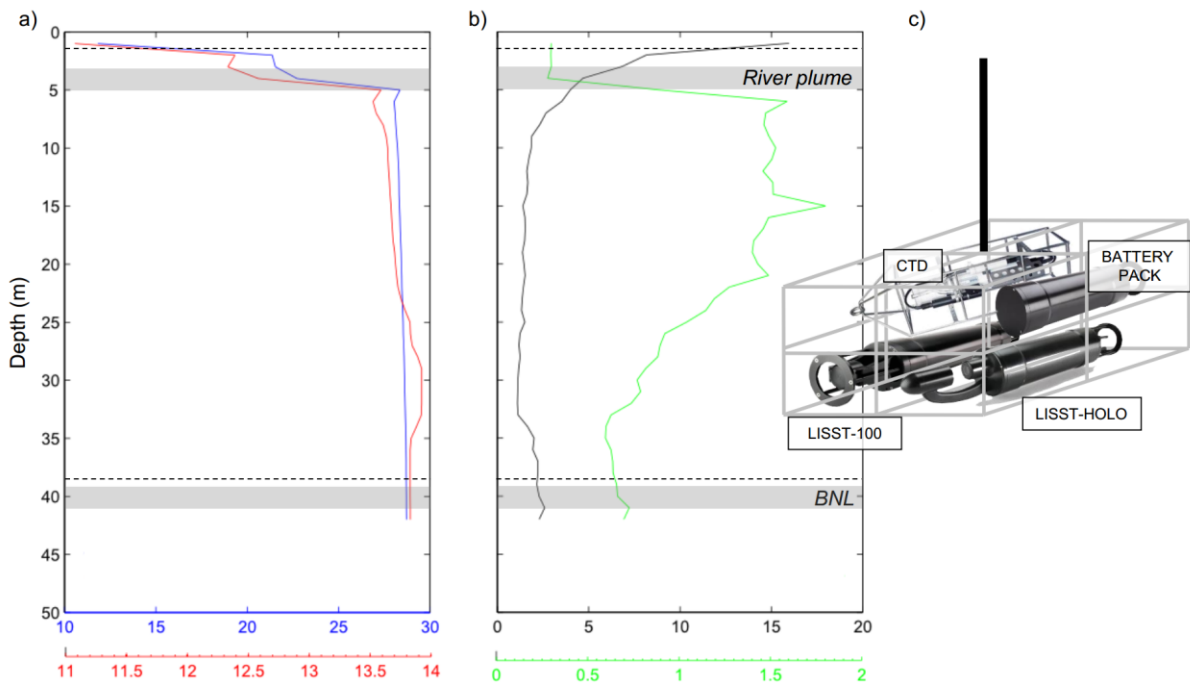
Figure 4.2 : Typical CTD cast (st.3 - Inner-shelf) showing profiles of a) temperature (°C - red) and density anomaly (kg m^{-3} - blue) and b) SPM concentrations (mg L^{-1} - black) and Chlorophyll-a fluorescence (µg L^{-1} - green). Water sample depths are indicated by the dashed lines. Depth ranges of in situ measurements of suspended particle optical properties are indicated by the grey bands. c) Illustration of the instrumental package used to characterize the BNL and the SNL particles.

4.3.2 Nearshore hydrological, hydrodynamical and meteorological observations

Meteorological time-series – Hourly (10 minute burst average) wind speed and direction were measured at the Météo-France station of Cap-Couronne (43°20.23'N ; 5°01.38'E). Data were provided by the Publithèque database.

Rhône River discharge time-series - Daily Rhône discharge was measured at Beaucaire-Tarascon gauging station (Compagnie National du Rhône - code V7200015), 50 km upstream of the river mouth. Data were provided by the Banque Hydro database.

MESURHO buoy time-series – Currents, waves and echo intensity were monitored using a 600 kHz RDI upward looking ADCP fixed at the bottom of the MESURHO buoy (Pairaud et al., 2015) off the Rhône River mouth (43°19.13'N ; 4°51.98'E, 20 m depth). Depth-averaged hourly-mean currents were estimated from the high frequency current profiles. Wave directions were estimated using wave orbital velocities, pressure and sea surface track (Teledyne RD Instruments, 2007). High-frequency wave measurements were then averaged every 3 h.

ADCP echo intensity is a measure of the signal strength of the echo returning from the ADCP's transmit pulse. Echo intensity depends on sound absorption, beam spreading, transmitted power and backscatter coefficient. Backscatter measurements were used here as a relative information on suspended sediment concentration.

4.3.3 Cross-shelf hydrological observations

Ship CTD/optical data and water sampling - Water pressure, temperature and conductivity were measured by profiling a Seabird 19+ CTD. Practical scale salinity and anomaly density were derived using the EOS-80 algorithms (UNESCO, 1983). Turbidity and Chlorophyll-a fluorescence were simultaneously measured with an OBS 3+ turbidimeter (at 850 nm) and a Chelsea fluorimeter respectively.

Water samples were collected with Niskin bottles triggered by a messenger that is sent down the cable from the surface. A horizontal bottle was used separately to sample the SNL (0.5 - 1 m). Besides, a vertical bottle mounted 1 m above the instrument package was used to sample the BNL (2 mab). SPM concentrations were determined by filtering seawater on GF/F filters (0.7 μm nominal pore size) following the method described in Aminot and Kérouel (2004). Filters were then used to determine particulate organic carbon (POC) content. Firstly, dry samples were decarbonated with repeated additions of H_3PO_4 (1M) and HCl (2M) until the end of effervescence. Then, POC contents were measured using a VarioMAX CN, Elementar Instrument. Close to the seabed, Nuclepore polycarbonate filters (0.4 μm pore size) were preferred against GF/F due to their lower mass that enabled to measure low SPM concentrations with better accuracy. Nevertheless GF/F filters were used in parallel to determine POC contents.

Glider CTD/optical data - The autonomous underwater coastal glider (30-200 m) used for the experiment was a Teledyne Webb Research Slocum (Davis et al., 2002). The glider was carefully ballasted in order to enter and measure both in the low-density river plume and in the denser outer-shelf waters. The glider was equipped of an un-pumped Seabird 41-CP CTD providing temperature, depth and conductivity data. Derived parameters such as salinity and density anomaly were derived following the equation of EOS-80 (UNESCO, 1983). A Wetlabs FLNTU sensor provided chlorophyll a concentrations measurements (expressed in $\mu g\ L^{-1}$), and turbidity (expressed in nephelometric turbidity units - NTU) based on backscattering measurements at 700 nm. A Wetlabs BB2FLS provided light backscattering measurements (expressed in m^{-1}) at 532 and 660 nm. The glider moved in a sawtooth-shaped trajectory between 1 m below the surface and 2 mab at an average horizontal speed of $0.2\ m\ s^{-1}$. When the glider reached the surface (every 6 dives), data are transferred through iridium communication protocol and the glider received new GPS positions to correct its future trajectory. Data were projected along a N-S segment from the Rhône River mouth to the shelf edge. A final 2D linear interpolation was then applied to our data, within a grid of 1 m vertical and 100 m horizontal resolution.

Turbidity sensors calibration – During a subsequent experiment in February 2015, a direct comparison between the turbidity measured with the shipboard CTD's OBS 3+ sensor and the glider's FLNTU sensor used during both experiments, was made by performing a profile where the glider was coupled to a SeaBird 911 CTD equipped with a rosette.
Backscattering measurements from both experiments were then calibrated against SPM concentrations derived from gravimetric measurements. We used a single Pearson's major axis regression (Model II) and found the following relationship between SPM concentrations and turbidity: [SPM] $_{(mg\ L^{-1})}$ = 2.29 (±0.18) × Turbidity $_{(NTU)}$ (R^2=0.90) for turbidity between 0 and 2.05 NTU, and [SPM] $_{(mg\ L^{-1})}$ = 3.08 (±4.03) + 0.79 (±0.11) × Turbidity $_{(NTU)}$ (R^2=0.73) for turbidity between 2.05 and 70 NTU ranges (Fig. 4.3).
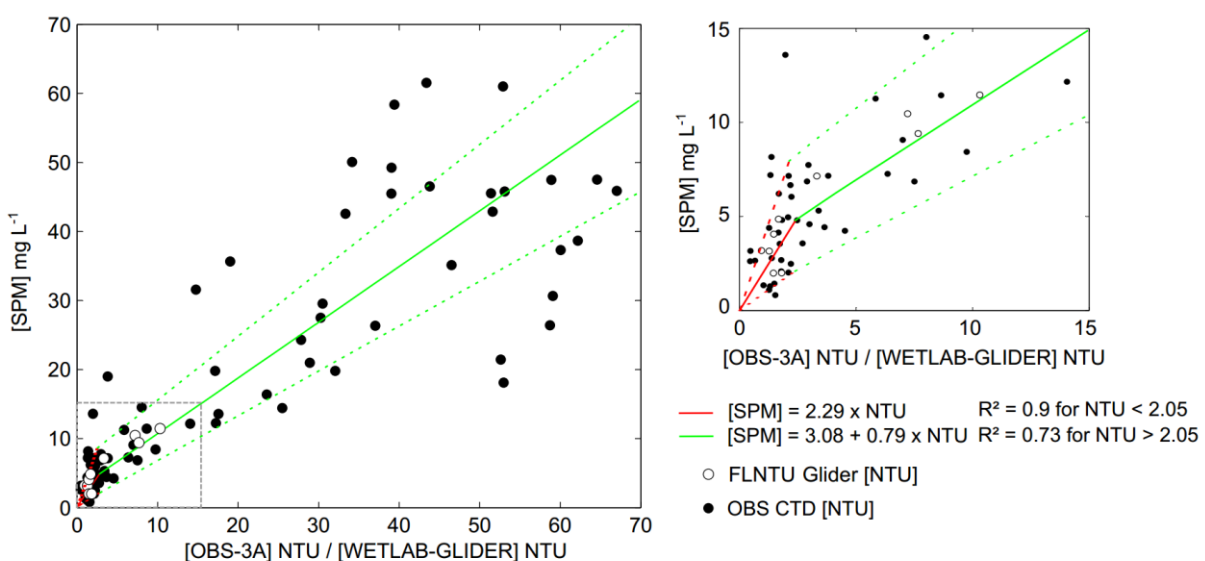
Figure 4.3 : Turbidity sensors (OBS-3+ on the CTD and FLNTU on the glider) calibration with gravimetric measurements. Dash-lines represent the error bounds of the regressions estimated. The right plot is a zoom of the left plot for low turbidities and SPM concentrations.

4.3.4 SPM properties

Laser diffraction - A LISST-100 (Type B, 1.25 - 250 µm range, 1 Hz) was used to estimate the in situ PSD in the SNL and the BNL. A LISST-100X (Type C, 2.5 - 500 µm, 1 Hz) was used onboard to estimate the PSD of primary particles composing the particle assemblage in water samples from the SNL and BNL. Water samples were deflocculated by ultrasonification for 5 minutes. PSD was then estimated from 1 minute average LISST-100X measurements.

PSD was derived from the laser diffraction spectrum using the "randomly shaped" Mie's theory (Agrawal and Pottsmith, 2000; Agrawal et al., 2008; Traykovski et al., 1999). The raw spectrum was converted in volume concentration (expressed in µL L^{-1}) using the factory volume calibration constant. Extreme size classes (1.25 - 2.5 and 250 - 500 µm) showed typical "rising tails" explained by the presence of smaller particles (for the first class) and bigger particles (for the last class) outside the measurement range (Mikkelsen et al., 2005). Except for the LISST-100X data processing (primary particle characterization), we excluded the extreme size classes of the PSD before calculating the derived parameters (total volume concentration (VC$_{tot}$), effective density, see section 4.3.5).

Holography - A digital holographic camera (LISST-HOLO, 0.2 Hz) was used to study the volume, number and shape of large particles, complex aggregates and biological organisms within the range 20 - 2000 µm (Graham and Smith, 2010). Reconstructed images were combined to obtain a representative estimation of particle composition in the SNL and the BNL. PSD was estimated using an image analysis processing (based on the estimate of the spherical equivalent diameter) and the size spectrum was expressed in µL L^{-1}. The LISST-HOLO also measured several particle shape parameters. The aspect ratio (AR) (Fig. 4.4c, Eq. 1), which underlines their spherical aspect was of particular interest. It is estimated by the equation:

AR = Ax$_{min}$/Ax$_{maj}$ **(Eq. 1)**

where Ax$_{min}$ and Ax$_{maj}$ represents respectively the minor and major axes of the particle. An aspect ratio of 1 indicates a spherical shape, whereas an aspect ratio of 0 indicates a straight shape (see Clavano et al., 2007). All particles measured by the LISST-HOLO during the experiment were used to characterize the particles aspect ratios as a function of their size, regardless of their location along the transect.

LISST-100 and HOLO PSD combination – In order to compare and merge the PSD derived from the LISST-100 and LISST-HOLO, only the measurements made near the surface and the bottom were considered (see 4.3.1). Data at these two measurement levels were collected for 60 - 90 seconds, which allowed to gather between 60 and 70 scans for the LISST-100, and 20 and 30 images for the LISST-HOLO. These data were averaged for each level and each station. A specific 1-hour long sampling procedure enabled the collection of 700 LISST-HOLO images and 3500 LISST-100 scans, and the assessment of the measurement uncertainty by multiple random permutations of an

increasing number of samples. The relative uncertainty associated to the measurements of the total volume concentration of the 20 - 30 LIST-HOLO images was then estimated to 15 %, and that associated to the 60 - 70 LISST-100 scans was estimated to 4%. The LISST-100 and LISST-HOLO PSD were finally merged within a 1.25 - 1000 µm size range to fit within the same 50 logarithmically spaced classes and the maximum volume PSD of each median size class was selected to constitute the final PSD (Fig. 4.4a).

Figure 4.4 : Combination of LISST-100 type B (red line between 1.25 and 250 µm) and LISST-HOLO (blue line between 20 to 2000 µm) particle size/number distribution in the river plume (St. 3). a) The volumetric representation of the combined distribution from 1.25 to 2000 µm is characterized by black circles and is used to calculate total particle volumetric concentration and associated effective density. b) Particle number distribution of the combined distribution used to estimate the Junge parameter j is characterized by black circles. c) Examples of large aggregates (> 300 µm) and associated aspect ratios (AR) calculated as the ratio between the minor axis length (Axmin, in orange) and the major axis length (Axmaj, in green).

4.3.5 Derived SPM properties

Effective density estimation - We estimated the effective density, $\Delta\rho$ (kg m^{-3}), of the particle assemblage using simultaneous measurements of SPM concentrations (mg L^{-1}) from the OBS 3+, and total volume concentration, VC_{tot} (µL L^{-1}) from the LISSTs - following equation 2.

$\Delta\rho = SPM_{OBS} / VC_{tot}$ (Eq. 2)

Power law approximation - The volume normalized PSD was converted to the number of particle per size class by dividing by an elementary spherical volume (Fig. 4.4b). For mineral particle assemblage, it is assumed that the resultant equation between the number of particles (n, expressed in L^{-1} µm^{-1}) and the particles size (D) follow a power law (Eq. 3) (Jonasz, 1983; Stramski and Kiefer, 1991; Buonassissi and Dierssen, 2010).

$n(D) \sim D^{-j}$ (Eq. 3)

Due to the rare presence of large particles, particle number less than 1 per litter (i.e. flocs and planktonic organisms > 500 μm), were excluded of the power law calculation. Due to the sensitivity to the finest particles of the LISST-100 (i.e. 1.25 - 6 μm) (Agrawal and Traykovski, 2001; Agrawal et al., 2008), the "tail" in small size classes (i.e. < 6 μm) were also filtered (Fig. 4.4b). This tail is generally due to an uncertain refractive index for the finest particles and can be interpreted as a contamination of our power law approximation (Graham et al., 2012; Xi et al., 2014). The slope, *j*, extracted from the power law approximation, or Junge parameter (dimensionless), is used to estimate the relative number of small to large particle for the 6 - 500 μm size range (Junge, 1963). High *j* (*j* ∼ 4) implies a higher proportion of small particles, and, reciprocally, low *j* (j ∼ 2.4) implies a higher proportion of large particles (Bader, 1970).

Spectral slope estimation – Measurements from the FLNTU (λ = 700 nm) and BB2FLS (λ = 532 and 660 nm) optical sensors of the glider were used to estimate the particulate backscattering coefficients [$b_{bp}(\lambda)$]. The BB2FLS sensors provided the volume scattering function [$\beta(\theta,\lambda)$] in m^{-1} sr^{-1}, at θ = 124°. The FLNTU optical backscattering sensor (θ = 140° in the backward direction (Sullivan et al., 2010)) was factory calibrated in NTU out of which the volume scattering function was computed, using the Beta Scale Factor (i.e. the NTU Scale Factor multiplied by a coefficient of 0.0025) provided by the manufacturer. Values of [$\beta(\theta,\lambda)$] were not corrected by absorption effects, which were negligible (a few % of the total signal detected). For each wavelength, we then estimated [$\beta_p(\theta,\lambda)$], the volume scattering of particles, by subtracting the molecular scattering of pure water as described in Morel (1974). The particulate backscattering coefficient [$b_{bp}(\lambda)$] with units of m^{-1}, was then determined through estimation from the single measurement of [$\beta_p(\theta,\lambda)$] using an X factor : [$b_{bp}(\lambda)$] = 2π . X . [$\beta_p(\theta,\lambda)$], where X is an adjustment factor according to water type (X=1.077 for the BB2FLS and X=1.132 for the FLNTU).

From Morel (1973) (see also Babin et al., 2003), the light scattered by marine particles depends of the particle size distribution, concentration, refractive index and the detection wavelength. This variation is considered as a power law approximation following: $b_{bp}(\lambda)=b_{bp}(\lambda_0).(\lambda/\lambda_0)^{-\gamma}$ where λ_0 is the reference wavelength and γ the spectral slope (dimensionless) in the case of non-absorbing spherical particles with a Junge-like size distribution. Morel (1973) reported a relationship between the spectral slope and the Junge parameter (γ = *j* - 3), but more recently Boss et al. (2001) proposed a new relation, valid for particle > 10 μm and non-spherical particles: γ = *j* - 3 - 0.5e^{-6j}.

4.4 Results

4.4.1 Meteorological and oceanic conditions at the MESURHO station

During the glider deployment, two south-east (SE) wind ("Marin") events on February 5 and 10, 2014 induced precipitations over the Rhône water catchment (Fig. 4.5a). The Rhône River discharge increased shortly after (3500 m^3 s^{-1} on February 5, and 5500 m^3 s^{-1} on February 11, 2014,

Fig. 4.5b). This flood affected directly the hydrology of the Rhône River ROFI. During that period, depth-averaged currents at the MESURHO buoy varied from 0.1 to 1 m s^{-1} and were generally oriented to the south / south-west (Fig. 4.5c). During these events, the currents were stronger and homogenous throughout the water column (from 2 to 20 mab), and the significant wave height ranged between 2 and 3.5 m (Fig. 4.5d). The BNL followed the increasing/decreasing pattern of the Rhône River discharge, interrupted by short incursions of clearer water. The BNL reached 15 m thick with echo intensity of 180 counts at the peak of the flood.

During the day of measurements at sea (February 17, 2014), a weak north-westerly wind of 3 m s^{-1} was measured at the Cap-Couronne station (Fig. 4.5a), which allowed to get a cloud-free MODIS satellite picture (see Fig. 4.1). The Rhône discharge was still high, about 4000 m^3 s^{-1} (Fig. 4.5b). During the previous two days, strong south-southwesterly wind-driven currents swept the plume away toward the shelf edge (Fig. 4.5c). Sea conditions were calm with small waves (<1 m height) (Fig. 4.5d). MESURHO bottom SPM concentrations in front of the Rhône River mouth showed a BNL of 5 m thick with echo intensity of 150 – 160 counts (Fig. 4.5e).
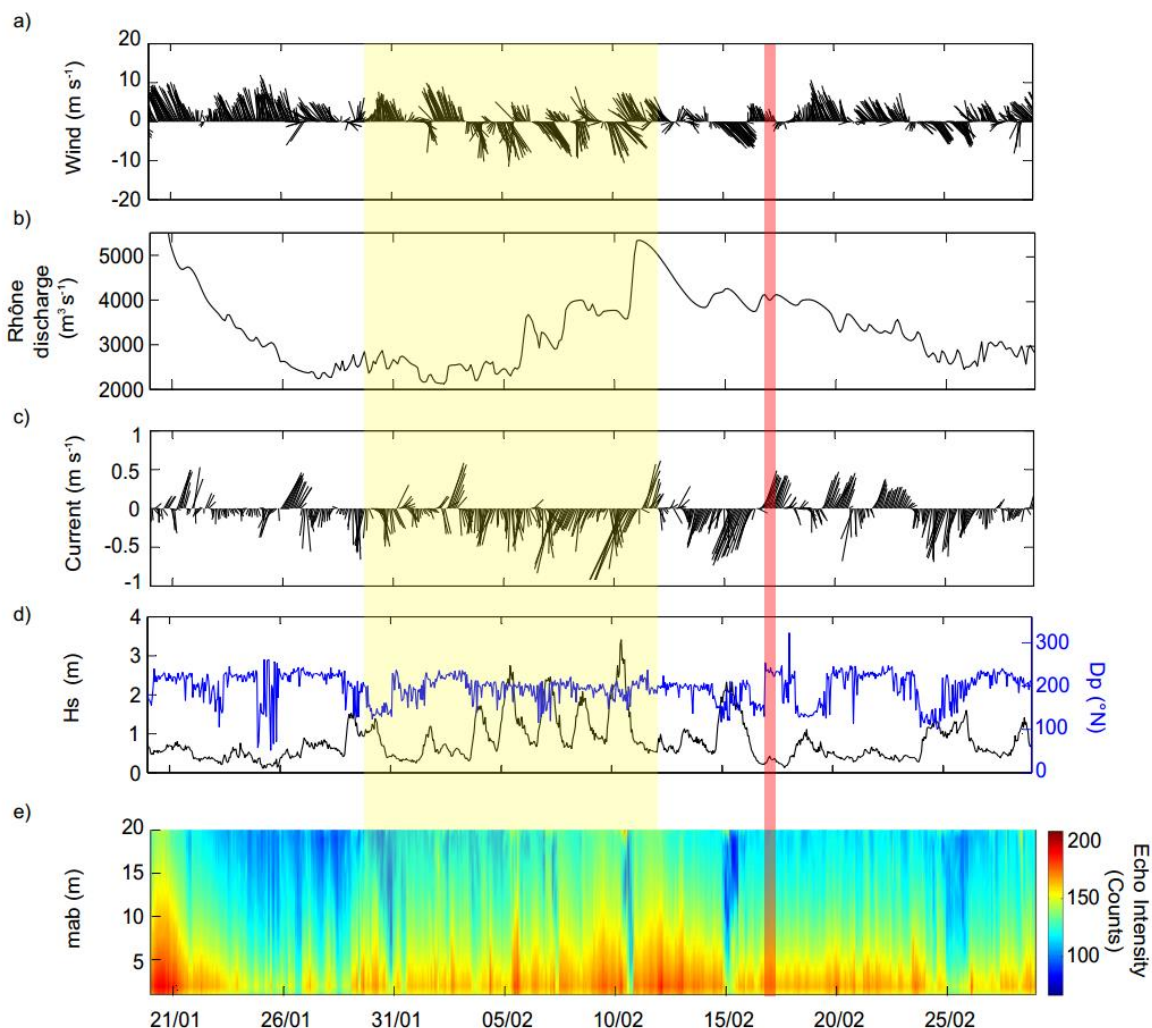
Figure 4.5 : Time-series from January 20 to March 1, 2014 of: (a) hourly-mean wind speed and direction, (b) Rhône River daily-mean discharge, (c) hourly-mean depth-averaged currents speed and direction, (d) significant wave height and direction, and (e) acoustic echo intensity. The yellow box shows the duration of the glider deployment and the red bar, the cruise measurements.

4.4.2 Cross-shelf hydrological structures

Glider cross-shelf sections - Glider's cross-shelf section (Fig. 4.6a) represented the median of the 7 sections carried out during the 30 January – 12 February 2014 period. The 7 sections highlighted the persistence of surface and bottom nepheloid layers in the Rhône ROFI (data not shown). It is well characterized by the median situation that smoothed the small-scale variability of the measured parameters. The Rhône River plume and the BNL were clearly identified, with their thickness and SPM concentration decreasing seaward. The glider observations enabled to describe the offshore limit of the plume on the outer shelf. The dilution of the plume with ambient water was clearly visible with an increase of the average temperature and salinity from 13 to 14.5 °C and from 32 to 38, respectively. Meanwhile SPM concentration in the plume decreased from 20 mg L^{-1} to 1.5 mg L^{-1}. Chlorophyll-a concentrations were higher (1 to 3 µg L^{-1}) and limited to the surface layer in the plume, but showed a large dilution throughout the water column outside the plume. SPM concentrations in the BNL varied from ~8 mg L^{-1} close to the river mouth to less than 1 mg L^{-1} at its outer edge.

Ship CTD/optical observations - The hydrographical structures observed from shipborne measurements on the 17 February 2014 (Fig 4.6b) showed rather similar characteristics to those obtained from glider observations. CTD observations showed the presence of the Rhône River plume with colder, fresher, and lighter water. The pycnocline, defined by the 28 kg m^{-3} isopycnal, delimited the vertical extension of the plume those thickness decreased seaward (from 20 to 5 m). SPM concentrations in the plume progressively decreased seaward from 15 to 5 mg L^{-1}. Chlorophyll-a concentrations were higher around the pycnocline and maximum (~ 3 µg L^{-1}) on the mid- and outer shelf. A BNL of 5 to 20 m thick was present along the entire section with SPM concentrations decreasing seaward from 5 mg L^{-1} on the inner shelf to 2 mg L^{-1} at the end of the section (30 km off the coast).

4.4.3 Cross-shelf SPM properties

Particle concentration, size and composition measured by optical instruments on the 17 February 2014 are presented in Figures 4.7 and 4.8.

Primary particles size distribution - LISST-100X was used on board in laboratory mode to determine the primary particle composition of the particle assemblage sampled with Niskin bottles (see green curves on top panel of Figures 4.7 and 4.8). In the SNL, the inner (station 3), mid (station 8) and outer-shelf (station 11) samples (Fig. 4.7) showed a similar primary PSD with a mode centered around 10-20 µm (typical of fine silts), and a significant contribution of the finest particles (<2.5 µm, typical of fine clays). Conversely to the fraction of fine silts that decreased seaward, the fraction of the finest primary particles increased. Maximum primary particle size decreased from 80 µm close on the inner-shelf to 35 µm on the outer-shelf (Fig. 4.7a – left to right panel).
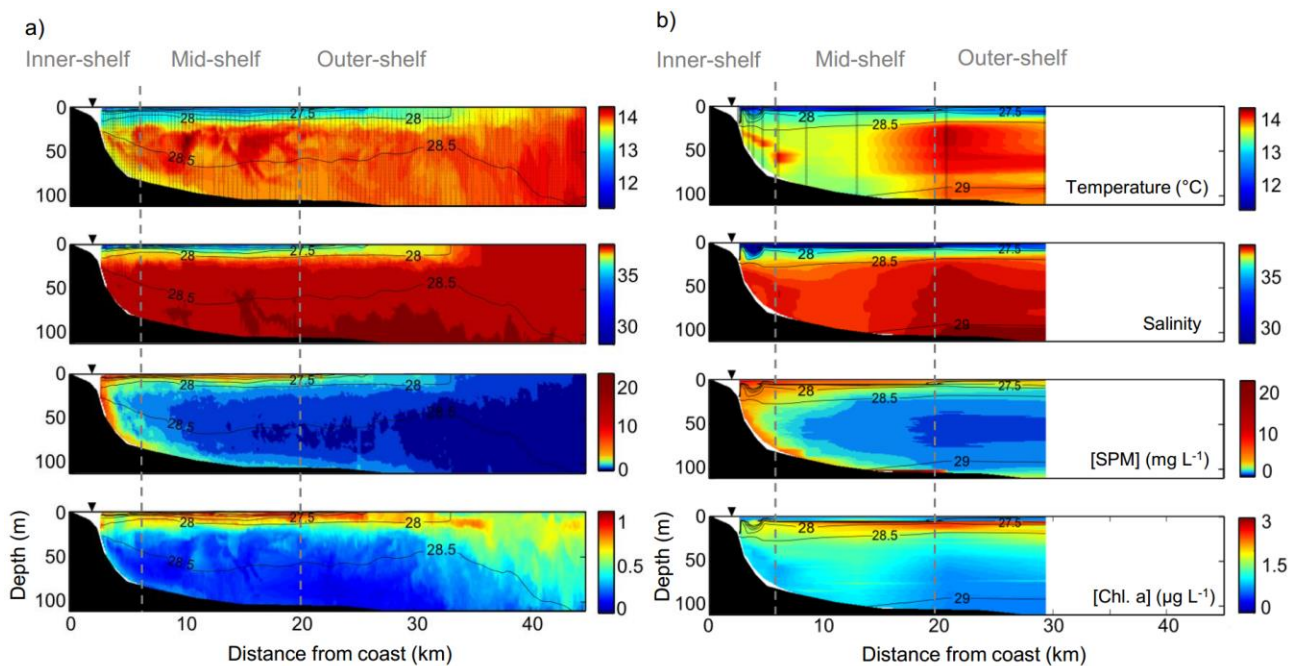
Figure 4.6 : Cross-shelf hydrological section based on (a) glider observations averaged during the 12-day long deployment (Jan. 30 – Feb 12, 2014) and (b) ship observations on Feb 17, 2014. From top to bottom: temperature (°C), salinity, suspended sediment concentration (mg L^{-1}), Chlorophyll-a fluorescence (μg L^{-1}). Potential density anomaly contour lines (kg m^{-3}) are superimposed. The location of the CTD casts or the glider trajectory are shown on the top plots. Inner, mid and outer-shelf areas are delimited by thick grey dashed lines. The black triangle indicates the position of the coastal MESURHO buoy.

Close to the seabed (Fig. 4.8), the primary particle PSD at the different station also showed a large mode centered around 10-20 μm, but with a larger spread towards the coarser sizes than for the SNL, and a lesser contribution of the finest particles (<2.5 μm). Maximum primary particle size increased from 110 μm close on the inner-shelf to 70 μm on the outer-shelf.

In situ particle size and number distributions in the plume - In situ PSD showed a good complementarity between the LISST-100 and LISST-HOLO measurements (see red and blue dots on top panel of Figure 4.7 and 4.8). In situ PSD, which differed significantly from primary particles PSD, showed modes of larger sizes, corresponding to flocs.

On the inner-shelf (3 - 5 km, see Table 4.1 for hydrological characteristics), VC$_{tot}$ was about 23.4 μL L^{-1} and in situ particle size ranged from 3 to 400 μm. PSD was centered on micro-flocs of 30-100 μm (>5 % VC$_{tot}$ for both instruments). LISST-100 showed a low volume (<2 %) of fine-sedimentary particles (5 - 10 μm). Holography permitted to complete the particle spectrum with the detection of larger flocs of 200 - 400 μm (~2 % per class size). An effective density of the entire particle assemblage was estimated to 372 ± 80 kg m^{-3}. The PND clearly followed a negative power law that underlined the low abundance of the largest flocs (<10 particles per liter), which contrast with their volumetric significance. A Junge parameter *j* (PND slope) for 6 to 300 μm size range was estimated to 3.6 (R² = 0.978).

On the mid-shelf (Fig. 4.7 – middle panel) (5 - 20 km), VC$_{tot}$ decreased at 5.9 μL L^{-1}, but particle assemblage was similar to the inner-shelf station. In situ PSD showed the presence of a small proportion of fines (<2 % for size class of 3 - 10 μm) and a mode centered on 30 - 70 μm (>5 % for

each size class). Largest particles appeared between 120 and 200 µm (6 and 7 % of VC$_{tot}$). We estimated a *j* of 3.53 (R² = 0.989) and an effective density of 859 ± 223 kg m^{-3}.

On the outer-shelf (Fig. 4.7 – right panel) (20 - 30 km), we measured a VC$_{tot}$ of 4.2 µL L^{-1}. Although the PSD from both instruments were more fluctuating, we observed 3 modes centered around 10 µm (3 - 30 µm), 100 µm (30 - 200 µm) and 400 µm.

A representative sample of LISST-HOLO images in the surface layer shown in Figure 4.7c, enables to characterize the composition of the particle assemblage. Micro- (20 - 250 µm) and macro-flocs (>250 µm) present on the inner and mid-part of the plume are easily identified. A large contribution of planktonic organisms (diatoms, pteropods, copepods) appeared on the outer shelf, outside the plume (Fig. 4.7c – right panel). These planktonic organisms contributed to a significant fraction of VC$_{tot}$ (40%, peak at 400 µm Fig. 4.7a – right panel). Due to their non-mineral composition we did not include them in the calculation of the Junge parameter and the particulate assemblage effective density. Hence, we estimated a *j* of 3.96 (R² = 0.991) and an effective density of 1547 ± 510 kg m^{-3} (VC$_{tot}$ = 2.5 µL L^{-1}).

Hydrological parameters and the derived particulate parameters for the different stations are summarized in Table 4.1.

In situ particle size and number distributions in the BNL - On the inner-shelf (1 mab - Fig. 4.8a and 4.8b) (see Table 4.2 for hydrological characteristics), in situ PSD showed a main mode centered on particle size of 30 - 100 µm (>5 % of VC$_{tot}$ for each size classes) and a secondary mode between 250 and 450 µm (~10 % of VC$_{tot}$). We measured a VC$_{tot}$ of 10.47 µL L^{-1}. From the PND, *j* was estimated to 3.76 (R² = 0.986) and the global effective density to 537 ± 80 kg m^{-3}.

On the mid-shelf (Fig. 4.8 – middle panel), VC$_{tot}$ decreased to 2.38 µL L^{-1}. The particle assemblage was globally finer than on the inner-shelf and 2 modes were observed centered between 10 - 30 µm and 60 - 150 µm (>5 %) respectively. We determined a Junge parameter of 3.98 (R² = 0.986) and an effective density of 1626 ± 243 kg m^{-3}.

On the outer-shelf (Fig. 4.8 – right panel), measurements were more fluctuating and the VC$_{tot}$ was estimated to 2.4 µL L^{-1}. In situ PSD showed a mode for fine particles of 7 - 10 µm, and two others modes for particles of 20 and 100 µm (7 and 25 % of VC$_{tot}$, respectively). We estimated a value of *j* of 4.01 (R² = 0.961) and an effective density of 1180 ± 400 kg m^{-3}.

As for the plume, particle images emphasized the mineral composition of aggregates and clearly showed the complex and diverse aspects of micro- and macro-flocs (Fig. 4.8c). Hydrological parameters and the derived particulate parameters for the different stations are summarized in Table 4.2.
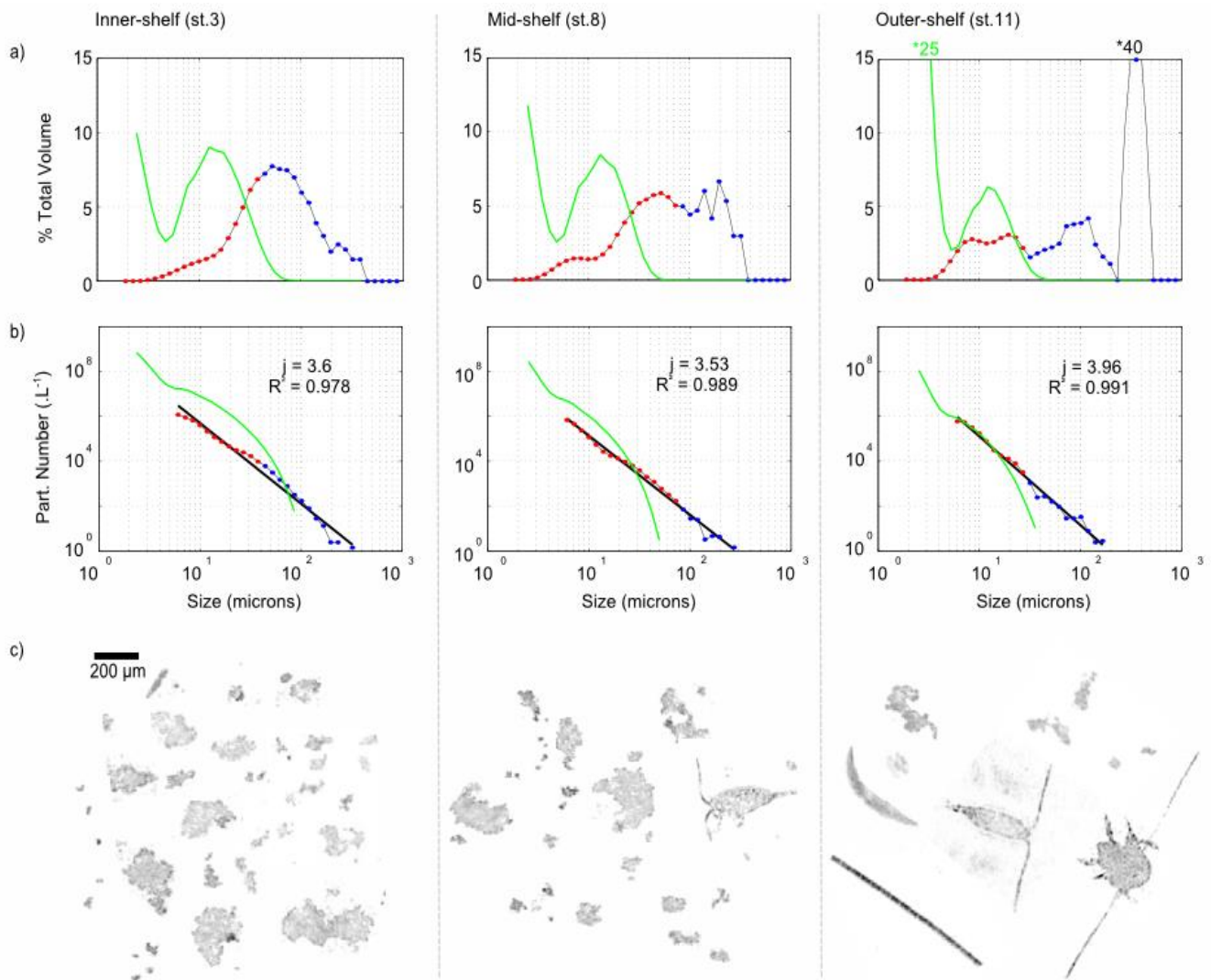
Figure 4.7 : Figure 7: Particle properties in the surface layer (around 5 m depth) at station 3 (inner shelf), station 8 (mid-shelf) and station 11 (outer shelf). See Fig. 4.1 for stations position. (a) Particle size distribution. (b) Particle number distribution with power law regression (black line) and Junge parameter estimation. In situ measurements are shown by the combined particle size (or number) distribution from the LISST-100 (red) and LISST-HOLO (blue) measurements, whereas on-board deflocculated primary particles distribution are shown in green. (c) Examples of particle assemblage from the LISST-HOLO images.

	Inner-Shelf (station 3)	Mid-Shelf (station 8)	Outer-Shelf (station 11)
Depth (m)	5	5	5
Water Temperature (°C)	12.84	12.91	13.14
Water Salinity	30.06	33.41	35.94
Water Potential Density Anomaly (kg m^{-3})	22.62	25.20	27.11
Chlorophyll a (µg L^{-1})	1.71	2.23	2.53
POC (%)	2.3	2.9	5.4
SSC (mg L^{-1})	8.70	4.37	3.90
Volume Total (µL L^{-1})	23.40	5.10	2.52
Effective density (kg m^{-3})	372±86	859±223	1547±510

Table 4.1 : SNL hydrological characteristics and particle assemblage properties
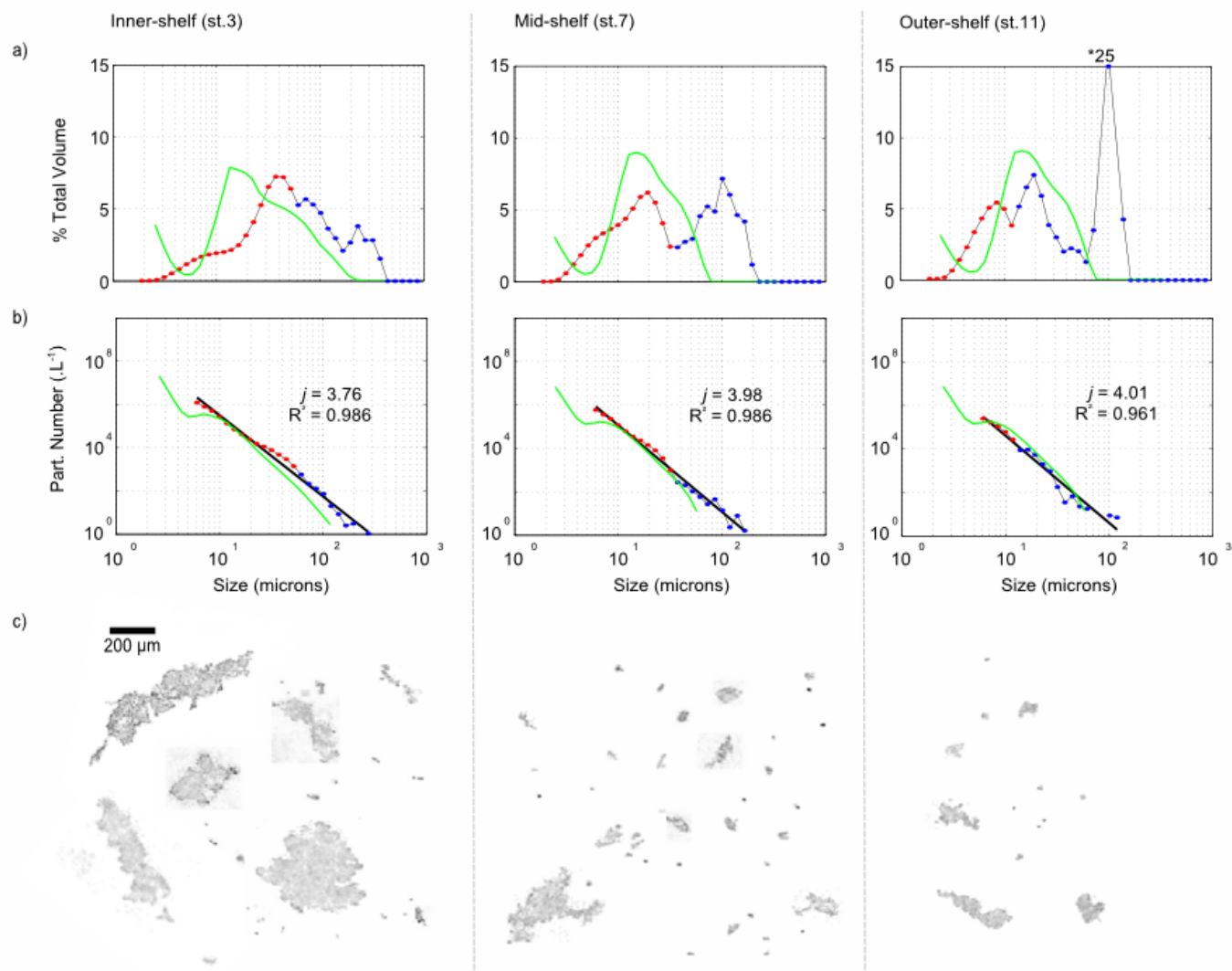
Figure 4.8 : Particle properties in the bottom layer (around 1 - 2 mab) at station 3 (inner shelf), station 7 (mid-shelf) and station 11 (outer shelf). See Fig. 4.1 for stations position. (a) Particle size distribution. (b) Particle number distribution with power law regression (black line) and Junge parameter estimation. In situ measurements are shown by the combined particle size (or number) distribution from the LISST-100 (red) and LISST-HOLO (blue) measurements, whereas on-board deflocculated primary particles distribution are shown in green. (c) Examples of particle assemblage from the LISST-HOLO images.

	Inner-Shelf (station 3)	Mid-Shelf (station 7)	Outer-Shelf (station 11)
Depth (m)	50	80	110
Water Temperature (°C)	13.76	13.68	13.96
Water Salinity	37.93	37.96	38.2
Water Potential Density Anomaly (kg m^{-3})	28.70	28.95	29.2
Chlorophyll a (µg L^{-1})	1.10	0.98	0.74
POC (%)	2.5	1.9	1.8
SSC (mg L^{-1})	5.63	3.9	2.8
Volume Total (µL L^{-1})	10.47	2.38	2.4
Effective density (kg m^{-3})	538±80	1639±243	1167±401

Table 4.2 : BNL hydrological characteristics and particle assemblage properties

4.4.4 Derived SPM properties

The change of the aspect ratio parameter with size for all particles observed on the 17 February 2014 is shown in Figure 4.9. We observed aspect ratios of 0.61 to 0.49 for particles of 20 to 150 μm with a standard deviation of ~0.15. Large flocs (150 - 500 μm) were characterized by higher aspect ratios of 0.50 to 0.77 (i.e. a more spherical aspect) with a standard deviation of ~0.1.
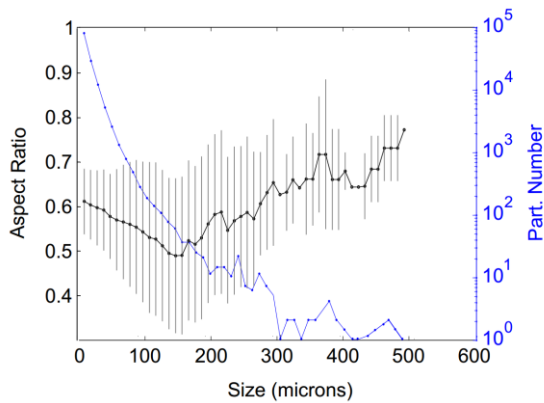
Figure 4.9 : Particles averaged aspect ratio as a function of particles size (black line). Standard deviations per size class are shown by gray bars. Number of particle analyzed per size class is shown by a blue line.

4.4.5 Light backscattering spectral slope and Junge parameter estimations

We estimated the spectral slope, γ, from glider backscattering measurements at 532, 660, and 700 nm (Fig. 4.10a). Both in the SNL and the BNL, γ showed a progressive increase seawards (i.e. a higher proportion of smaller particles along the transect). Minimum γ of 0.3 was observed on the inner-shelf, and γ increased seawards with values of 0.7 at 30 km offshore.

The values of γ within the SNL clearly increased with increasing salinity and decreasing SPM concentrations (Fig. 4.10b, 4.10c). Besides, γ values within the BNL were not linked to salinity (Fig. 4.10e), yet they clearly increased with decreasing SPM concentrations (Fig. 4.10d).

Based on the relation of Boss et al. (2001), we estimated the spectral slope, γ_{LISST}, from the Junge parameter, *j*, derived from the power law approximation of the in situ PND (Fig. 4.7 and 4.8). The values of γ_{glider} and γ_{LISST} for similar locations (inner-, mid- and outer-shelf) and turbidities ($SPM_{Glider} = SPM_{OBS} \pm 0.1$ mg L^{-1}) along the transect are shown in Figure 4.11 and indicated that both estimates are close though estimates were not made at the same time (30 January - 12 February 2014 for the glider measurements, 17 February 2014 for the LISST measurements).
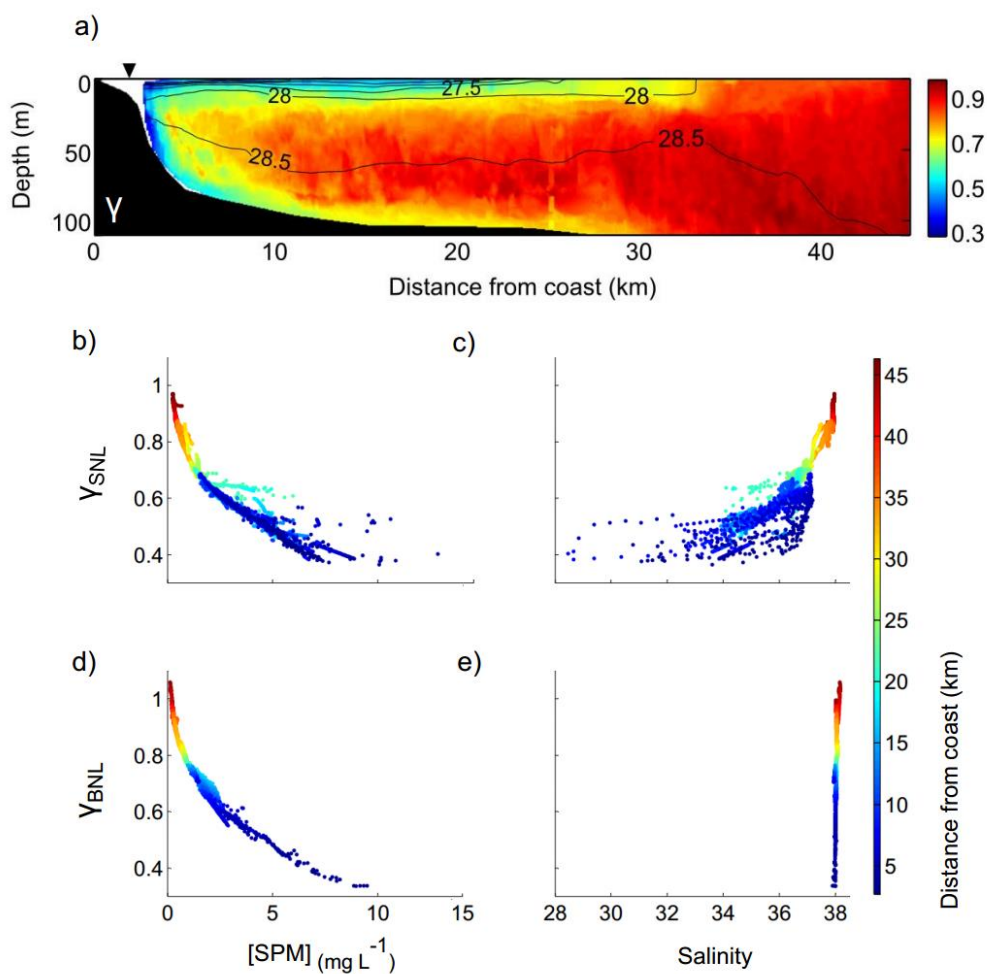
Figure 4.10 : a) Section of the mean spectral slope measured during the glider deployment (January 30 – February 12, 2014). The black triangle indicates the position of the MESURHO buoy, density contour lines are superimposed. Variation of the spectral slope of the SNL with SPM concentration (b) and salinity (c). Variation of the spectral slope of the BNL with SPM concentration (d) and salinity (e).
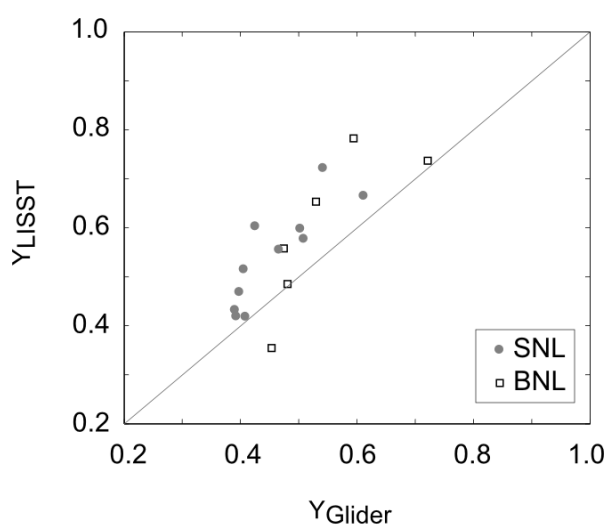
Figure 4.11 : Scatterplot of spectral slopes derived from the glider backscattering measurements at 3 wavelengths (γ_{Glider}), and the Boss et al (2001) relationship based on the Junge parameter estimated from the LISST particle number distribution (γ_{LISST}). River plume samples are in grey dots and BNL samples are in white squares. The grey line represents the 1:1 relationship.

4.5 Discussion

4.5.1 Spatial variability of nepheloid layers in the Rhône River ROFI

We sampled the Rhône River ROFI after an annual flood in February 2014 (Maillet et al., 2006) while a Northern wind was blowing. CTD measurements emphasized the development of a coastal hypopycnal plume and optical measurements highlighted the presence of large SNL and BNL spreading out across most of the shelf and weakening seaward (Figs. 1 and 6). Next to the shelf edge, the plume was deflected over the continental shelf by along-slope cyclonic circulation. These turbid structures are consistent with those already observed by previous studies next to the Rhône river mouth (Aloisi et al., 1982; Naudin et al., 1992) and across the shelf (Durrieu de Madron and Panouse, 1996).

On the inner shelf, the whole water column water down to depths of 80 m showed the highest SPM concentration, and the SNL and BNL merged for depths less than 20 m (Fig 4.6). Based on bottom ADCP measurements next to the Rhône River mouth (Fig 4.4), the BNL thickness and SPM concentration increased with river discharge, and also with the wave- and current-induced activity. This suggests that the BNL is fed both by river plume particles that settle rapidly through the water column, and sedimentary particles probably resuspended on the shallow part of the prodelta.

On the mid- and outer-shelf, the SNL and BNL were clearly separated (Fig. 4.6). The Rhône River SNL, confined by a strong density gradient, presented a strong seaward decrease of SPM concentrations (from 20 to 1 mg L^{-1}). The linear decrease of SPM concentration with increasing salinity (data not shown) indicated that the dilution of the plume was the main factor of the SPM concentration decline.

4.5.2 On the use of an ad-hoc strategy to study the Rhône River ROFI

Several previous studies emphasized the necessity to combine various measurement methods to characterize the whole size distribution of marine particles and thus determine the link between the scattering detection and the composition/shape of marine particles (Cartwright et al., 2011; Davies et al., 2011; Reynolds et al., 2010; Smith and Friedrichs, 2011). During the TUCPA experiment, the combination of LISST-100/LISST-HOLO instruments was determinant to follow the spatial variability of the particle assemblage (Fig. 4.7 – 4.8). Holographic measurements highlighted the high part of dense and inorganic micro- and macro-flocs in the particle assemblage (Fig. 4.7c and 4.8c) (Wolanski, 2007).

The determination of the spectral slope of the particulate backscattering coefficient (532, 660, 700 nm) using the glider was in line with past studies of Babin et al. (2003), Loisel et al. (2006), Niewiadomska et al. (2008), Slade and Boss (2015) and Bourrin et al. (2015), where authors

showed a range of γ from 0.3 to 1.2, typical values found in coastal seas influenced by different particle assemblages. The present study is one of the first study describing and comparing the spatial variability of particle properties based on gliders measurements and LISSTs measurements (PND slope). The comparison of $γ_{glider}$ and $γ_{LISST}$, following Boss et al. (2001), indicated a good agreement between both variables within the BNL and the SNL. Thus, $γ_{glider}$ seemed to be an adequate proxy of the proportion of fine particles vs large flocs but the comparison with in situ LISSTs measurements still needs more investigations (Fig. 4.11).

4.5.3 Particle assemblage properties

Flocculation - LISST measurements of both disaggregated and in situ suspended particles (Fig 4.7 – 4.8) clearly showed the importance of fine-grained flocs in the SNL and the BNL. Single particles composing flocs were characterized by 2 size groups: one fraction which size < 1.25 µm probably illite and chlorite clays (Garnier et al., 1991), and the other fraction ranged from 10 to 20 µm composed of fine silts particles. This terrestrial fine sediment fraction has a mean effective density assumed to be ~1650 kg m^{-3} (Boss et al., 2009).

Ayukai and Wolanski (1997) and Naudin et al. (1997) showed the possible role of organic contents as a factor enhancing the flocculation. The spectral slope, γ, estimated from glider backscattering measurements and the Junge parameter, *j*, were neither correlated with the POC contents (< 2 %) nor to the Chlorophyll a concentrations (1 - 3 µg L^{-1}). While weak, this organic fraction could nevertheless play a role in the maintenance of flocculated particles in the form of transparent exopolymer particles (Wolanski, 2007). The increase of macro-floc proportion in the SNL (i.e. a decrease of γ and *j*) was nevertheless correlated with an increase of SPM concentration and a decrease of salinity (Fig 10b-10c). These observations are in line with studies of Naudin et al. (1997) and Thill et al. (2001) which emphasized the role of SPM and salinity gradient in the flocculation occurring within the Rhône River plume. Close to the seabed, γ solely varied with SPM concentrations (Fig. 4.10d). This observation is consistent with results of Slade and Boss (2015) and underlined the role of SPM concentration in the control of the flocculation within the BNL.

Flocs properties - In our study, flocs size was mainly centered around 30 - 200 µm. Similar observations have been done on the Gulf of Lions shelf both in the SNL by Curran et al. (2007) and Bourrin et al. (2008) in the Têt River plume, and in the BNL by Durrieu de Madron et al. (2005) in a trawl-induced turbid plume. We observed maximum macro-floc sizes of 600 µm, consistent with observations carried out in other ROFI. Eisma et al. (1991) found flocs of 600 - 800 µm in the Ems, Rhine, and Gironde estuaries. Kineke and Sternberg (1989) found flocs of 450 µm in the San Pablo bay. Manning and Schoellhamer (2013) found flocs of 600 µm in the San Francisco bay. All these studies highlighted the general low abundance of macro-flocs, their low densities and their importance in the total volume concentration.

We did not find any significant change of the flocs shape with their location on the shelf. The aspect ratio parameter shows the large diversity of flocs shape (Fig. 4.9). The aspect ratios of fine-grained (< 150 µm) presented a mean value of 0.55, underlying their non-spherical aspect. The

largest and rare flocs (> 300 µm) presented higher aspect ratios (0.65-0.75) evidencing a more spherical shape. These observations highlighted the importance to characterize the shape of the flocs (Clavano et al., 2007), in order to properly estimate their settling velocity using models derived by Winterwerp (1998), Khelifa and Hill (2006), or Boss et al. (2009). All these models used a particle shape-related factor, and in the absence of measurements used the spherical approximation when applying them. This also implies the need to use a "randomly shaped" algorithm process to invert particle size from in-situ measurements of light scattering (Agrawal et al., 2008).

4.5.4 Spatial variability of particle assemblage

On the inner-shelf, particulate assemblage was rather similar in the SNL and the BNL (5/65/30 % for primary particles/microflocs/macroflocs), and the largest macro-flocs (400 - 600 µm) were concentrated in the proximity of the River mouth. Particulate assemblage densities were the lowest with values of ~370 ± 80 and ~530 ± 100 kg m^{-3} for the SNL and the BNL respectively. These estimations were comparable to the effective densities estimated by Soulsby et al. (2013) and highlighted that the particle assemblage was dominated by micro- and macro-flocs. Within the SNL, the settling velocities of micro- and macro-flocs were estimated to 2 mm s^{-1} (~7 m h^{-1}) and 17 mm s^{-1} (~60 m h^{-1}) following Stokes law. These estimations were in line with measurements of Manning and Schoellhamer (2013) in the San Francisco Bay and showed that due to their larger size macro-flocs settled more rapidly than micro-flocs and probably left the river plume and settled to the BNL. This rapid settling of flocs was shown by other studies on various rivers (Fly River: Ayukai and Wolanski, 1997 and Dagg et al., 2004; Po River: Milligan et al., 2007; Eel River: Hill et al., 2000; Amazon River: Gibbs and Konwar, 1986; Burdekin River: Bainbridge et al., 2012). However, during the present study, wave- and current-induced resuspension also likely contributed to the high particle volume concentration observed close to the seabed (~10 µL L^{-1}) and the formation of large flocs in the BNL.

Mid-shelf observations of the SNL (5 - 20 km off the mouth) showed that the particle assemblage (10/30/60 %) was rather similar to inner-shelf particulate assemblage, with maximum floc size of 300 µm. Observations highlighted the settling of biggest flocs (>300µm) which increased the particulate assemblage effective density (850 kg m^{-3}). Yet, the high part of macro-flocs (125 - 300 µm) could be explained by a flocculation still active in the River plume due to the absence of turbulence. Particle assemblage on the outer-shelf was the finest (10/85/5 %, planktonic organisms excluded) and presented maximum density of 1550±500 kg.m^{-3}. The resultant effective density increased as a result of the higher proportion of primary particles and micro-flocs (i.e. the settling of large flocs leaving the small one behind). A similar trend occurred in the BNL for mid and outer shelf stations. The progressive sedimentation of macro-flocs on the inner- shelf, enhanced the proportion of micro-flocs and fine-grained in the rest of the BNL (30/70/0 %). The resultant effective density increased, and reached maximum values of 1600±400 kg.m^{-3} above the mid-shelf mud-belt.

The increase of the floc proportion and the decrease of the associated effective density of the particle assemblage have been also observed in the Gulf of Lions by Curran et al. (2007), and in

others ROFI such as in the Glacier Bay (Hill et al., 1998), the Po (Fox et al., 2004) and Pearl estuaries (Xia et al., 2004).

4.6 Conclusion

This experiment provided a unique view of the impact of a Rhône River flood on the distribution and properties of suspended particles. The combination of a coastal buoy monitoring, glider transects, and ship observations enabled to describe in details the temporal variability of the forcings and SPM near the river mouth, and the spatial variability of the turbid structures across the whole shelf.

Our results emphasized the high proportion of flocs (30 - 400 µm) of fine-grained (∼10 µm) in the Rhône River ROFI and their general non-spherical shape. We highlighted the role of the SPM concentrations and the salinity in the control of flocculation. Close to the river mouth, a link between the river plume and the BNL, induced by the Rhône River discharge and episodic sediment resuspension was shown. Both turbid layers presented similar particle assemblage with minimal effective density of 370 kg m^{-3}. At mid-shelf, both SNL and BNL showed a decrease of the proportion of macro-flocs by settling and dilution, and an increase of the effective density due to the higher proportion of finest particles. It is noteworthy that the maximum effective density in the BNL, with maximum values of 1600 kg m^{-3}, is taking place above the mid-shelf mud-belt. On the outer-shelf, the finest particles were observed within the SNL, and holographic measurements helped us to determine the part of biological organisms in the particulate assemblage.

Finally we demonstrated the good correlation between the spectral slope of glider light backscattering measurements at different wavelengths and the power law approximation of LISSTs particle number distribution. This result shows the possibility to get some useful information on the particle size distribution from autonomous underwater glider when shipboard measurements are not possible.

Acknowledgements

References

Agrawal, Y. C., and H. C. Pottsmith. **2000**. « Instruments for particle size and settling velocity observations in sediment transport. » *Marine Geology* 168 (1–4): 89‑114. doi:10.1016/S0025-3227(00)00044-X.

Agrawal, Y. C., and P. Traykovski. **2001**. « Particles in the bottom boundary layer: Concentration and size dynamics through events. » *Journal of Geophysical Research* 106: 9533‑42. doi:10.1029/2000JC900160.

Agrawal, Y. C., A. Whitmire, O. A. Mikkelsen, and H. C. Pottsmith. **2008**. « Light scattering by random shaped particles and consequences on measuring suspended sediments by laser diffraction. » *Journal of Geophysical Research* 113 (C4). doi:10.1029/2007JC004403.

Aloisi, J. C., C. Millot, A. Monaco, and H. Pauc. **1979**. « Dynamique des suspensions et mécanismes sédimentogénétiques sur le plateau continental du Golfe du Lion. » *CR Acad. Sc* 289 (13): 879‑82.

Aloisi, J. C., J. P. Cambon, J. Carbonne, G. Cauwet, C. Millot, A. Monaco, and H. Pauc. **1982**. « Origine et rôle du néphéloïde profond dans le transfert des particules au milieu marin. Application au Golfe du Lion. » *Oceanologica Acta* 5 (4): 481‑91.

Aminot, A., and R. Kérouel. **2004**. « Hydrologie des écosystèmes marins: paramètres et analyses. » *Editions Quae.*

Ayukai, T., and E. Wolanski. **1997**. « Importance of biologically mediated removal of fine sediments from the Fly River plume, Papua New Guinea. » *Estuarine, Coastal and Shelf Science* 44 (5): 629‑39. doi:10.1006/ecss.1996.0172.

Babin, M., A. Morel, V. Fournier-Sicre, F. Fell, and D. Stramski. **2003**. « Light scattering properties of marine particles in coastal and open ocean waters as related to the particle mass concentration. » *Limnology and Oceanography*, 843‑59.

Bader, H. **1970**. « The hyperbolic distribution of particle sizes. » *Journal of Geophysical Research* 75 (15): 2822‑30. doi:10.1029/JC075i015p02822.

Bainbridge, Z. T., E. Wolanski, J. G. Álvarez-Romero, S. E. Lewis, and J. E. Brodie. **2012**. « Fine sediment and nutrient dynamics related to particle size and floc formation in a Burdekin River flood plume, Australia. » *Marine Pollution Bulletin* 65 (4-9): 236‑48. doi:10.1016/j.marpolbul.2012.01.043.

Boss, E., M. S. Twardowski, and S. Herring. **2001**. « Shape of the particulate beam attenuation spectrum and its inversion to obtain the shape of the particulate size distribution ». *Applied Optics* 40 (27): 4885‑93.

Boss, E., W. Slade, and P. Hill. **2009**. « Effect of particulate aggregation in aquatic environments on the beam attenuation and its utility as a proxy for particulate mass ». *Optics Express* 17 (11): 9408‑20.

Bourrin, F., and X. Durrieu de Madron. **2006**. « Contribution to the study of coastal rivers and associated prodeltas to sediment supply in the Gulf of Lions (NW Mediterranean Sea). » *Vie et Milieu* 56 (4): 307‑14.

Bourrin, F., P. Friend, C. Amos, E. Manca, C. Ulses, A. Palanques, X. Durrieu de Madron, and C. Thompson. **2008**. « Sediment dispersal from a typical Mediterranean flood: the Têt River, Gulf of Lions. » *Continental Shelf Research* 28 (15): 1895‑1910.

Bourrin, F., G. Many, X. Durrieu de Madron, J. Martín, P. Puig, L. Houpert, P. Testor, S. Kunesch, K. Mahiouz, and L. Béguery. **2015**. « Glider monitoring of shelf suspended particle dynamics and transport during storm and flooding conditions ». *Continental Shelf Research* 109 (10): 135‑49. doi:10.1016/j.csr.2015.08.031.

Buonassissi, C. J., and H. M. Dierssen. **2010**. « A regional comparison of particle size distributions and the power law approximation in oceanic and estuarine surface waters. » *Journal of Geophysical Research* 115 (C10). doi:10.1029/2010JC006256.

Cartwright, G. M., C. T. Friedrichs, and L. P. Sanford. **2011**. « In situ characterization of estuarine suspended sediment in the presence of muddy flocs and pellets. » *Proceedings of Coastal Sediments,* 2-6.

Clavano, W. R., E. Boss, and L. Karp-Boss. **2007**. « Inherent optical properties of non-spherical marine-like particles—from theory to observation ». *Oceanography and marine biology: an annual review* 45: 1‑38.

Courp, T., and A. Monaco. **1990**. « Sediment dispersal and accumulation on the continental margin of the Gulf of Lions: sedimentary budget. » *Continental Shelf Research* 10 (9): 1063‑87.

Curran, K. J., P. S. Hill, T. G. Milligan, O. A. Mikkelsen, B. A. Law, X. Durrieu de Madron, and F. Bourrin. **2007**. « Settling velocity, effective density, and mass composition of suspended sediment in a coastal bottom boundary layer, Gulf of Lions, France. » *Continental Shelf Research* 27 (10-11): 1408‑21. doi:10.1016/j.csr.2007.01.014.

Dagg, M., R. Benner, S. Lohrenz, and D. Lawrence. **2004**. « Transformation of dissolved and particulate materials on continental shelves influenced by large rivers: plume processes. » *Continental Shelf Research* 24 (7-8): 833‑58. doi:10.1016/j.csr.2004.02.003.

Davies, E. J., W. a. M. Nimmo-Smith, Y. C. Agrawal, and A. J. Souza. **2011**. « Scattering signatures of suspended particles: an integrated system for combining digital

holography and laser diffraction. » *Optics express* 19 (25): 25488‑99.

Davis, R. E., C. C. Eriksen, and C. P. Jones. **2002**. « Autonomous buoyancy-driven underwater gliders. » *The technology and applications of autonomous underwater vehicles*, 37‑58.

Drake, D. E. **1976**. « Suspended sediment transport and mud deposition on continental shelves. » *Marine sediment transport and environmental management* 40: 127‑58.

Dufois, F., R. Verney, P. Le Hir, F. Dumas, and S. Charmasson. **2014**. « Impact of winter storms on sediment erosion in the Rhone River prodelta and fate of sediment in the Gulf of Lions (North Western Mediterranean Sea). » *Continental Shelf Research* 72 (1): 57‑72. doi:10.1016/j.csr.2013.11.004.

Durrieu de Madron, X., B. Ferré, G. Le Corre, C. Grenz, P. Conan, M. Pujo-Pay, R. Buscail, and O. Bodiot. **2005**. « Trawling-induced resuspension and dispersal of muddy sediments and dissolved elements in the Gulf of Lion (NW Mediterranean). » *Continental Shelf Research* 25 (19-20): 2387‑2409. doi:10.1016/j.csr.2005.08.002.

Durrieu de Madron, X., and M. Panouse. **1996**. « Transport de matière particulaire en suspension sur le plateau continental du Golfe du Lion. Situation estivale et hivernale. » *Comptes rendus de l'Académie des sciences. Série 2. Sciences de la terre et des planètes* 322 (12): 1061‑70.

Eisma, D. **1991**. « Particle size of suspended matter in estuaries. » *Geo-Marine Letters* 11 (3-4): 147‑53.

Fox, J. M., P. S. Hill, T. G. Milligan, A. S. Ogston, and A. Boldrin. **2004**. « Floc fraction in the waters of the Po River prodelta. » *Continental Shelf Research* 24 (15): 1699‑1715. doi:10.1016/j.csr.2004.05.009.

Garnier, J. M., J. M. Martin, J. M. Mouchel, and A. J. Thomas. **1991**. « Surface reactivity of the Rhône suspended matter and relation with trace element sorption. » *Marine Chemistry*, 36 (1–4): 267‑89. doi:10.1016/S0304-4203(09)90066-4.

Gibbs, R. J. **1985**. « Estuarine flocs: their size, settling velocity and density. » *Journal of Geophysical Research: Oceans* 90 (C2): 3249‑51. doi:10.1029/JC090iC02p03249.

Gibbs, R. J., and L. Konwar. **1986**. « Coagulation and settling of Amazon River suspended sediment. » *Continental Shelf Research*, Sedimentary Processes on the Amazon Continental Shelf, 6 (1–2): 127‑49. doi:10.1016/0278-4343(86)90057-9.

Graham, G. W., and W. a. M. Smith. **2010**. « The application of holography to the analysis of size and settling velocity of suspended cohesive sediments. » *Limnology and Oceanography: Methods* 8: 1‑15.

Graham, G. W., E. J. Davies, W. a. M. Nimmo-Smith, D. G. Bowers, and K. M. Braithwaite. **2012**. « Interpreting LISST-100X measurements of particles with complex shape using digital in-line holography. » *Journal of Geophysical Research: Oceans* 117 (C5): C05034. doi:10.1029/2011JC007613.

Hill, P. S., J. P. Syvitski, E. A. Cowan, and R. D. Powell. **1998**. « In situ observations of floc settling velocities in Glacier Bay, Alaska. » *Marine Geology* 145 (1–2): 85‑94. doi:10.1016/S0025-3227(97)00109-6.

Hill, P. S., T. G. Milligan, and W. R. Geyer. **2000**. « Controls on effective settling velocity of suspended sediment in the Eel River flood plume. » *Continental Shelf Research*, Oceanic Flood Sedimentation, 20 (16): 2095‑2111. doi:10.1016/S0278-4343(00)00064-9.

Jonasz, M. **1983**. « Particle-size distributions in the Baltic. » *Tellus B* 35 (5). doi:10.3402/tellusb.v35i5.14624.

Junge, C. E. **1963**. « Air chemistry and radioactivity », 382.

Khelifa, A., and P. S. Hill. **2006**. « Models for effective density and settling velocity of flocs. » *Journal of Hydraulic Research* 44 (3): 390‑401.

Kineke, G. C, and R. W Sternberg. **1989**. « The effect of particle settling velocity on computed suspended sediment concentration profiles. » *Marine Geology* 90 (3): 159‑74. doi:10.1016/0025-3227(89)90039-X.

Loisel, H., J. M., Nicolas, A., Sciandra, D., Stramski, and A. Poteau, **2006**. « Spectral dependency of optical backscattering by marine particles from satellite remote sensing of the global ocean. » *Journal of Geophysical Research* 111, C09024. doi:10.1029/2005JC003367.

Maillet, G. M., C. Vella, S. Berné, P. L. Friend, C. L. Amos, T. J. Fleury, and A. Normand. **2006**. « Morphological changes and sedimentary processes induced by the December 2003 flood event at the present mouth of the Grand Rhône River (southern France). » *Marine Geology* 234 (1-4): 159‑77. doi:10.1016/j.margeo.2006.09.025.

Manning, A. J., and K. R. Dyer. **1999**. « A laboratory examination of floc characteristics with regard to turbulent shearing. » *Marine Geology* 160 (1–2): 147‑70. doi:10.1016/S0025-3227(99)00013-4.

Manning, A. J., K. R. Dyer, R. Lafite, and D. Mikes. **2004**. « Flocculation measured by video based instruments in the Gironde Estuary during the European Commission SWAMIEE project. » *Journal of Coastal Research*, 58‑69.

Manning, A. J., J. R. Spearman, J. V. Baugh, R. J. S. Whitehouse, and R. L. Soulsby. **2011**. « Cohesive sediment flocculation and the application to settling flux modelling. » *INTECH Open Access Publisher*.

http://cdn.intechweb.org/pdfs/15517.pdf.

Manning, A. J., and D. H. Schoellhamer. **2013**. « Factors controlling floc settling velocity along a longitudinal estuarine transect. » *Marine Geology* 345 (10): 266‑80. doi:10.1016/j.margeo.2013.06.018.

Marion, C., F. Dufois, M. Arnaud, and C. Vella. **2010**. « In situ record of sedimentary processes near the Rhône River mouth during winter events (Gulf of Lions, Mediterranean Sea). » *Continental Shelf Research* 30 (9): 1095‑1107. doi:10.1016/j.csr.2010.02.015.

McCave, I. N., **1972**. « Transport and escape of fine-grained sediment from shelf areas. » *Shelf Sediment Transport: Process and Pattern. Dowden, Hutchinson, and Ross, Stroudsburg, Pennsylvania,* 225–248.

Mikkelsen, O. A., P. S. Hill, T. G. Milligan, and R. J. Chant. **2005**. « In situ particle size distributions and volume concentrations from a LISST-100 laser particle sizer and a digital floc camera ». *Continental Shelf Research* 25 (16): 1959‑78. doi:10.1016/j.csr.2005.07.001.

Milligan, T. G., P. S. Hill, and B. A. Law. **2007**. « Flocculation and the loss of sediment from the Po River plume. » *Continental Shelf Research*, Sediment Dynamics in the Western Adriatic Sea, 27 (3–4): 309‑21. doi:10.1016/j.csr.2006.11.008.

Miralles, J., O. Radakovitch, and J. C. Aloisi. **2005**. « 210Pb sedimentation rates from the Northwestern Mediterranean margin. » *Marine Geology* 216 (3): 155‑67. doi:10.1016/j.margeo.2005.02.020.

Morel, A. **1973**. « The scattering of light by sea water: Experimental results and theoretical approach. » *Optics of the sea, interface and in-water transmission and imaging* AGARD Lecture Series (61): 3.1.1‑3.1.76.

Morel, A. **1974**. « Optical properties of pure water and pure sea water. » *Optical aspects of oceanography*, Acadamic Press, London, 1‑24.

Naudin, J. J., G. Cauwet, M. Leveau, F. Lochet, H. Pauc, J. C. Romano, and R. Sempere. **1992**. « Le néphéloïde benthique au large du Rhône. Transferts particulaires à l'interface continent-océan. » *Oceanologica Acta* 15 (6): 621‑38.

Naudin, J. J., G. Cauwet, M. J. Chrétiennot-Dinet, B. Deniaux, J. L. Devenon, and H. Pauc. **1997**. « River Discharge and Wind Influence Upon Particulate Transfer at the Land–Ocean Interaction: Case Study of the Rhone River Plume ». *Estuarine, Coastal and Shelf Science* 45 (3): 303‑16. doi:10.1006/ecss.1996.0190.

Niewiadomska, K., H. Claustre, L. Prieur, and F. d'Ortenzio. **2008**. « Submesoscale physical-biogeochemical coupling across the Ligurian current (northwestern Mediterranean) using a bio-optical glider. » *Limnology and Oceanography* 53 (5): 2210.

Nittrouer, C., J. Austin, M. Field, J. Kravitz, J. Syvitski, and P. Wiberg. **2009**. « Continental margin sedimentation: From sediment transport to sequence stratigraphy » *Special publication 37 of the IAS*. Vol. 25. John Wiley & Sons.

Pairaud I., C. Répécaud, M. Ravel, R. Fuchs, M. Arnaud, A. Champelovier, C. Rabouille, B. Bombled., F. Toussaint, F. Garcia, P. Raimbault, R. Verney, S. Meulé, P. Gaufrès, A. Bonnat, and J. F. Cadiou **2015**. « MesuRho : plateforme instrumentée de suivi des paramètres environnementaux à l'embouchure du Rhône. » *Schmitt, F.G. et Lefebvre A. (Eds.). Mesures haute résolution dans l'environnement marin côtier, Presses du CNRS*.

Pont, D. **1996**. « Evaluation of water fluxes and sediment supply. » *Oral Communication, MEDDELT, Final Meeting*, Venezia, October 2–5.

Reynolds, R. A., D. Stramski, V. M. Wright, and S. B. Woźniak. **2010**. « Measurements and characterization of particle size distributions in coastal waters. » *Journal of Geophysical Research: Oceans (1978–2012)* 115 (C8).

Safak, I., M. A. Allison, and A. Sheremet. **2013**. « Floc variability under changing turbulent stresses and sediment availability on a wave energetic muddy shelf. » *Continental Shelf Research* 53 (2): 1‑10. doi:10.1016/j.csr.2012.11.015.

Simpson, J. H., and J. Sharples. **2012**. « Introduction to the physical and biological oceanography of shelf seas. » *Cambridge University Press*.

Slade, W. H. and E., Boss. **2015**. « Spectral attenuation and backscattering as indicators of average particle size. » *Applied Optics* 54, 7264-7277.

Smith, S. J., and C. T. Friedrichs. **2011**. « Size and settling velocities of cohesive flocs and suspended sediment aggregates in a trailing suction hopper dredge plume. » *Continental Shelf Research* 31 (10): S50‑63. doi:10.1016/j.csr.2010.04.002.

Soulsby, R. L., A. J. Manning, J. Spearman, and R. J. S. Whitehouse. **2013**. « Settling velocity and mass settling flux of flocculated estuarine sediments. » *Marine Geology* 339: 1‑12.

Stramski, D., and D. A. Kiefer. **1991**. « Light scattering by microorganisms in the open ocean. » *Progress in Oceanography* 28 (4): 343‑83.

Sullivan, J. M., P. L. Donaghay, and J. E. B. Rines, **2010**. « Coastal thin layer dynamics: consequences to biology and optics. » *Continental Shelf Research* 30, 50–65. doi:10.1016/j.csr.2009.07.009.

Teledyne RD Instruments. **2007**. « Waves primer: Wave measurements and the RDI ADCP waves array technique. available from RDInstruments.com. » http://www.rdinstruments.com/pdfs/waves_primer.pdf.

Thill, A., S. Moustier, J. M. Garnier, C. Estournel, J. J. Naudin, and J. Y. Bottero. **2001**. « Evolution of particle size and concentration in the Rhône river mixing zone: influence of salt flocculation. » *Continental Shelf Research* 21 (18): 2127‑40.

Traykovski, P., R. J. Latter, and J. D. Irish. **1999**. « A laboratory evaluation of the laser in situ scattering and transmissometery instrument using natural sediments. » *Marine Geology* 159 (1–4): 355‑67. doi:10.1016/S0025-3227(98)00196-0.

UNESCO. **1983**. « Algorithms for computation of fundamental properties of seawater. » *Technical papers in marine science* 44: 53.Van Leussen, W. 1994. « Estuarine Macroflocs and Their Role in Fine-Grained Sediment Transport. » *GIP-Gigevens Koninklijke bibliotheek.*

Van Leussen, W. **1994**. « Estuarine macroflocs and their role in fine-grained sediment transport. » *Koninklijke bibliotheek, GIP-Gigevens*.

Verney, R., R. Lafite, and J. C. Brun-Cottan. **2009**. « Flocculation potential of sstuarine particles: the importance of environmental factors and of the spatial and seasonal variability of suspended particulate matter. » *Estuaries and Coasts* 32 (4): 678‑93. doi:10.1007/s12237-009-9160-1.

Winterwerp, J. C. **1998**. « A simple model for turbulence induced flocculation of cohesive sediment. » *Journal of Hydraulic Research* 36 (3): 309‑26.

Wolanski, E. 2007. « Estuarine ecohydrology. » *Elsevier*.Xia, X. M., Y. Li, H. Yang, C. Y. Wu, T. H. Sing, et H. K. Pong. **2004**. « Observations on the size and settling velocity distributions of suspended sediment in the Pearl River Estuary, China. » *Continental Shelf Research* 24 (16): 1809‑26. doi:10.1016/j.csr.2004.06.009.

Xi, H., P. Larouche, S. Tang, and C. Michel. **2014**. « Characterization and variability of particle size distributions in Hudson Bay, Canada. » *Journal of Geophysical Research: Oceans* 119 (6): 3392‑3406. doi:10.1002/2013JC009542.

Chapter 5.

Glider and satellite monitoring of the variability of the suspended particle distribution and size in the Rhône ROFI

Chapter 5. *Glider and satellite monitoring of the variability of the suspended particle distribution and size in the Rhône ROFI*

Gaël Many[1], François Bourrin[1], Xavier Durrieu de Madron[1], Anouck Ody[2], David Doxaran[2], Pierre Cauchy[1].

[1]CEFREM, UMR 5110 CNRS, UPVD, 52 Avenue Paul Alduy, 66860 Perpignan Cedex, France

[2]LOV, UMR 7093 CNRS, UPMC, 181 Chemin du Lazaret, 06230 Villefranche-sur-mer, France

List of Figures

List of Tables

Abstract

An experiment was carried out in the Gulf of Lions (NW Mediterranean) in February 2014 to assess the temporal and spatial variability of the distribution and size of suspended particulate matter (SPM) in the Rhône Region Of Freshwater Influence (ROFI). A set of observations from an autonomous underwater glider, satellite ocean color data, meteorological and hydrological time-series highlighted the high variability of the Rhône River surface turbid plume and the presence of a bottom nepheloid layer (BNL), depending on wind and river discharge conditions. While continental winds pushed the surface plume offshore, marine winds that pressed the plume at the coast favored the sedimentation of particles and the nourishment of the BNL. Moderate storm event favored the break of the plume stratification and the along-shelf transport of Rhône River particles. The spectral slopes of glider and satellite-derived light backscattering coefficients, γ, were used as a proxy of the SPM size distribution. Results clearly showed the change of the SPM size in nepheloid layers, induced by the flocculation of fine sediments, which became finer seaward throughout the ROFI and the effect of rough weather in the breakup of flocs.

Keywords:

Nepheloid layers, ROFI, Gulf of Lions, Rhône River, flood, glider

Highlights:

- High-resolution description of the variability of nepheloid layers in the Rhône ROFI

- Evidence of the Rhône River as a major supplier of the bottom nepheloid layer

- Evidence of storm induced nearshore break of the plume stratification

- Combination of glider and satellite to characterize the particle size variability

5.1 Introduction

River plumes, which are primary signature of continental inputs of freshwater as well as dissolved and particulate materials, remain poorly documented regarding the in-situ monitoring of their spatio-temporal variability (Dagg et al., 2004). The structures and position of river plumes are highly variable as their dynamics is strongly affected by the intensity of the river discharge and the wind conditions (Garvine, 1995). This forcings also strongly affect the transport of suspended particulate matter (SPM), the specific dynamics (aggregation/disaggregation, settling velocity) of which primarily depends on their concentration, size, and density (Curran et al, 2007; Manning and Schoellamer, 2013).

Over the past decade, different works on river plume dynamics have been conducted with ocean color imagery of surface SPM (Thomas and Weatherbee, 2006; Lihan et al., 2008; Saldías et al., 2012; Fernández-Nóvoa et al., 2015; Ody et al., 2016). These authors described the benefits of such observations in the description of the large-scale spatial and temporal variability of river plumes. Satellite data nevertheless do neither provide information about the vertical structure of river plumes (as water stratification, plume thickness, SPM vertical gradient) nor about bottom nepheloid layers (BNL) characteristics. In-situ monitoring throughout the water column is thus essential to assess the link existing between surface plumes and BNL that plays a major role in sedimentary transport and deposition.

The recent use of coastal glider has made it possible to reduce this lack of knowledge in the water column. Castelao et al. (2008a, 2008b) first used a coastal glider to describe the dynamic of a river plume in response to upwelling winds. More recently, Saldías et al. (2016) used glider and satellite observations of salinity to characterize the seasonal variability of the Columbia River plume. However, to our knowledge, there are no studies that characterized the structure and variability of nepheloid layers in ROFI using SPM measurements from both glider and satellite. A need exists in the high frequency observations of the 3-D temporal variability of SPM concentrations and size in ROFIs during flood events (Nittrouer et al., 2009; Simpson and Sharples, 2012).

This work brings together a comprehensive set of hydrological, hydrodynamical, and optical measurements collected from a coastal buoy, a satellite and a glider in the Rhône River ROFI. It aims at: 1) assessing the temporal variability of the Rhône River ROFI nepheloid layers during a flood event and different wind conditions, and 2) determining the temporal variability of the SPM size.

5.2 Regional setting

In the semi-enclosed Mediterranean Sea, the inputs of freshwater and sediment are of paramount importance for the sedimentary budgets at both the local and Mediterranean scales. The Po and Rhône rivers alone account for about 30% of the freshwater discharge to the Mediterranean (Ludwig et al., 2009; Sadaoui et al., this issue). Because the importance of their freshwater inputs and the large extent of their ROFIs, these rivers are key control factors of the particle dynamics for the Gulf of Lions and the Adriatic shelves, respectively.

The Gulf of Lions (NW Mediterranean) is a wide continental shelf mostly influenced by the inputs of particulate matter from the Rhône River, which represents on average between 80 and 95% to the total inputs to the gulf (Bourrin et al., 2006; Sadaoui et al., 2016). The Rhône River has a mean annual discharge of 1700 m^3 s^{-1} and typical annual floods with discharge larger than 5000 m^3 s^{-1} (Maillet et al., 2006). According to Pont (1996), floods deliver 70% of the annual sediment load, highlighting the pivotal role of these events in the delivery of SPM to the coastal area. During floods, freshwater and sediment delivered by the Rhône River form a surface plume and a BNL that can spread over the shelf (Aloisi et al., 1982).

Previous works focused on the remote sensing of the plume extent (Arnau et al., 2004; Lorthois et al., 2012; Ody et al., 2016) or used shipborne in situ measurements to characterize the suspended particles in the water column (Naudin et al., 1997; Thill et al., 2001; Many et al., 2016). The plume is generally advected seaward across the shelf by surface currents driven by continental (i.e. northerly) wind or restricted to the coast during marine (i.e. southeasterly) wind events (Broche et al., 1998; see also modelling works of Marsaleix et al., 1998; Estournel et al., 2001; Ulses et al., 2008).

The coastal area generally presents a strong seaward decrease of surface SPM concentrations due to the dilution of the plume and the settling of large particles (as sand and silt) on the prodelta off the river mouth. This settling is enhanced by the flocculation of fine sediments that enables the settling of "flocs" closer to the coast (Naudin et al., 1997; Many et al., 2016). Near the seabed, the BNL extents over the inner shelf off the river mouth and presents a seaward decrease of the SPM concentration and size (Durrieu de Madron and Panouse, 1996; Many et al., 2016). On the Rhône prodelta, the BNL is fueled by the settling of large particles from the river plume (Many et al., 2016). Resuspension induced by waves, especially during storm events, also contributes to the supply of the BNL (Durrieu de Madron et al., 2008; Dufois et al., 2014).

5.3 Material & Methods

5.3.1 Presentation of the experiment

Time-series measurements of the coastal MESURHO buoy (43°19.130'N; 4°51.980'E, 20 m depth, 2.6 km off the Rhône River mouth) were used to describe the meteorological and oceanic conditions in front of the Rhône River mouth. Besides, a SLOCUM glider was deployed within the Rhône ROFI during a 14-day period (January, 30 to February, 12 2014). Seven complete cross-shelf sections (Fig. 5.1) were carried out from the coast to the shelf edge (40 km offshore – 120 m depth).
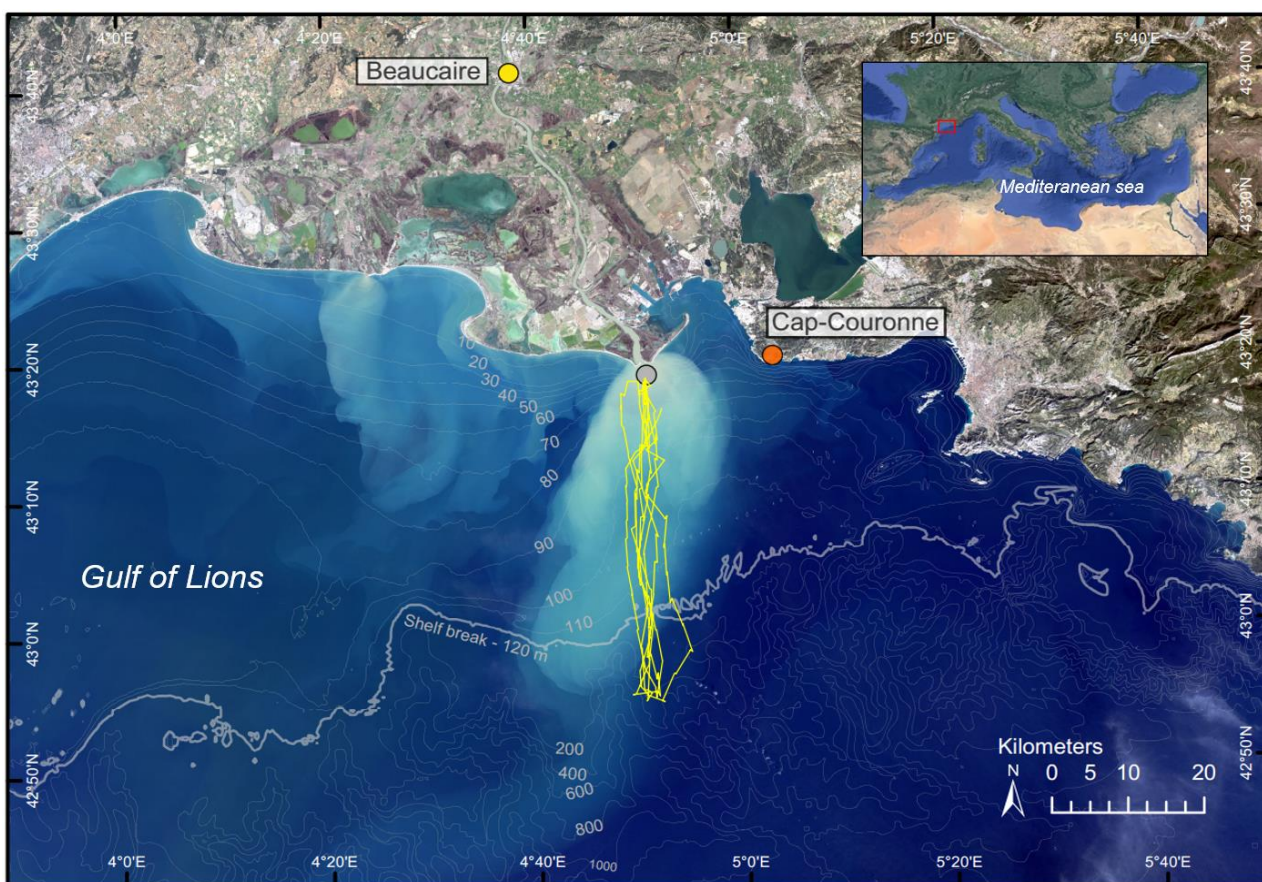
Figure 5.1 : RGB geo-referenced OLI image (Landsat-8) of the Rhone River plume (23 February 2014). Glider cross-shelf deployment (30 January – 12 February, 2014 – 7 sections) is shown in yellow. The position of the coastal MESURHO buoy is shown by a gray dot, 2.6 km of the Rhône river mouth. The Cap-Couronne wind station and Beaucaire gauging station are shown by orange and yellow dots, respectively. Depth contour lines are shown in gray.

5.3.2 Nearshore hydrological, hydrodynamical and meteorological observations

Meteorological time-series - Hourly (10 minutes burst average) wind speed and direction were measured at the Cap-Couronne Météo-France Station (43°20'.230'N; 5°01.380'E). We derived the wind stress at the sea surface, τ, expressed in N m^{-2}, following Equation 5.1:

τ = W$_f$ ^{2} × ρ$_{air}$ × C$_D$ **Eq. 5.1**

where W$_f$ is the wind speed (m s^{-1}), ρ$_{air}$ the air density (assumed to be 1,22 kg m^{-3}) and C$_D$ the drag coefficient of 1.3 × 10^{-3} (see Large et Pond, 1981).

Rhône river time-series – The daily Rhône discharge was measured at the Beaucaire gauging station, 50 km upstream from the river mouth (Compagnie Nationale du Rhône - code V7200015).

MESURHO buoy time-series - Currents and waves were measured using a 600 kHz RDI upward looking ADCP fixed at the bottom (27 m) of the MESURHO buoy off the Rhône River mouth (Pairaud et al., 2016). Hourly-mean horizontal currents (1 m bin) were estimated from the high frequency horizontal current profiles. Waves direction were estimated by computing near-surface waves orbital, pressure and surface track (Teledyne RD Instruments, 2007). High-frequency waves measurements were then averaged over 20 min period every 3 h.

ADCP's backscatter index (BI in dB) was derived from the sonar equation (Eq. 5.2) and used as a relative information concerning the SPM concentration. It can be calculated by adding the echo intensity (EI) received by the instrument, the transmission loss by the sound absorption in seawater (Tl$_w$), the beam spherical spreading (Tl$_g$) and the constant A, which incorporates the emitted intensity and the time- and distance-independent coefficients (Gartner, 2004; Gostiaux and Van Haren, 2010).

BI = EI + Tl$_w$ + Tl$_g$ + A **Eq. 5.2**

Tl$_w$ and Tl$_g$ depend on the temperature (13°C) and salinity (38) of seawater, the beam angle (20°), the distance to the ensonified SPM volume and the absorption coefficient. We assumed these parameters constant in space and time.

5.3.3 Glider CTD and optical observations

The autonomous underwater glider (30 – 200 m) used for this work is a Teledyne Webb Research Slocum G1 (Davis et al., 2002). Conductivity, temperature and pressure measurements were made by an un-pumped SeaBird 41cp CTD. Salinity and density were derived following the equation of EOS-80 (UNESCO, 1983). A Wetlabs FLNTU provided turbidity (expressed in nephelometric turbidity units – NTU) based on light backscattering measurements at 700 nm. We used the

calibration of Many et al. (2016), established during the same deployment and based on in situ SPM gravimetric measurements, to convert NTU in mg L^{-1}. A Wetlabs BB2FLS provided light backscattering measurements (m^{-1} sr^{-1}) at 532 and 660 nm.

The glider moved in a sawtooth-shaped trajectory (generally with a pitch angle of 25°) between the surface (1 m depth) and the seabed (2 meters above bottom (mab)). We generally observed an average horizontal speed of 0.4 m s^{-1} with an average vertical speed of 0.2 m s^{-1}. When surfacing every 6 dives, the glider takes GPS fixes and corrected its navigation toward the next waypoint. Data were first projected along a N-S transect and then interpolated within a 1 m vertical and 100 m horizontal resolution grid.

5.3.4   *Optical, hydrodynamical and hydrological derived parameters*

Spectral slope estimate – We computed the spectral slope (γ_{Glider}) of glider particulate light backscattering coefficients ($b_{bp}(\lambda)$) at 532, 660 and 700 nm to describe the spatial and temporal variability of the particulate assemblage within the Rhône ROFI (Boss et al., 2001). FLNTU (λ = 700 nm) and BB2FLS (λ = 532 and 660 nm) sensors provided light scattering measurements ($\beta(\theta,\lambda)$) at specific angles θ = 142° and θ =124° in the backward direction (Sullivan et al., 2010). The BB2FLS sensor directly gives output in m^{-1} sr^{-1}, while measurements of the FLNTU (factory calibrated in NTU) were converted to extract the volume scattering function thanks to the Beta Scale Factor provided by the manufacturer (i.e. the NTU Scale Factor multiplied by a coefficient of 2.5×10^{-3}). We did not correct values of ($\beta(\theta,\lambda)$) for loss by absorption due to negligible effects (a few % of the total signal measured). For each sensor, we estimated the volume scattering function of particles ($\beta_p(\theta, \lambda)$), by subtracting the molecular scattering of pure water (Morel, 1974). The particulate backscattering coefficients ($b_{bp}(\lambda)$) (m^{-1}) were finally derived following ($b_{bp}(\lambda)$) = $2\pi.X.(\beta_p(\theta,\lambda)$) where X is an adjustment factor provided by the manufacturer according to particles type (1.077 for the BB2FLS and 1.132 for the FLNTU).

From Morel (1973) and Babin et al. (2003), the light scattered by suspended marine particles depends of the particle size distribution and is wavelength-dependent. Authors described this variation as a power law approximation in the case of spherical, homogeneous and non-absorbing particles: $b_{bp}(\lambda)=b_{bp}(\lambda_0).(\lambda/ \lambda_0)^{-\gamma_{Glider}}$ where λ_0 is the reference wavelength and γ_{Glider} the spectral slope. γ_{Glider} was thus calculated as the slope of the linear relationship between $\log_e(b_{bp}(\lambda))$ and $\log_e(\lambda)$, using λ = 532, 660 and 700 nm (i.e. the lower the γ_{Glider}, the higher the proportion of large particles to the total particle assemblage, and reciprocally).

Coastal along-shelf current estimate – The glider "drift", i.e. the difference between the glider's expected surfacing location and the actual new GPS position, was used as an estimate of horizontally depth-averaged current between two surfacings (Webb Research Slocum manual, 2005). To further characterize the current we estimated geostrophic velocities to determine how

much the flow perpendicular to the section was affected by the density field. The glider's interpolated density field was used to estimate the baroclinic component of the geostrophic velocities. Then, we derived the E-W velocity field (i.e. normal to the gliders' section) by adjusting the depth-averaged geostrophic velocities to the corresponding glider's drift. This correction includes the barotropic geostrophic and ageostrophic terms, such as currents induced by surface wind stress and bottom friction.

Hydrological derived parameters - The Brunt-Väisälä frequency (N - Eq. 5.3) was used as an indicator of the stratification. One maximum, indicative of the pycnocline between the colder and fresher plume and the shelf water appeared on the different sections (Fig. 5.2). A threshold of N = 0.01 s^{-1} was used to delimit the pycnocline and defined the lower limit of the plume, which corresponded to the 28.3 $\pm$ 0.1 kg m^{-3} isopycnal (Fig. 5.2).

N = √ (-g/ρ) δρ/δz   **Eq. 5.3**
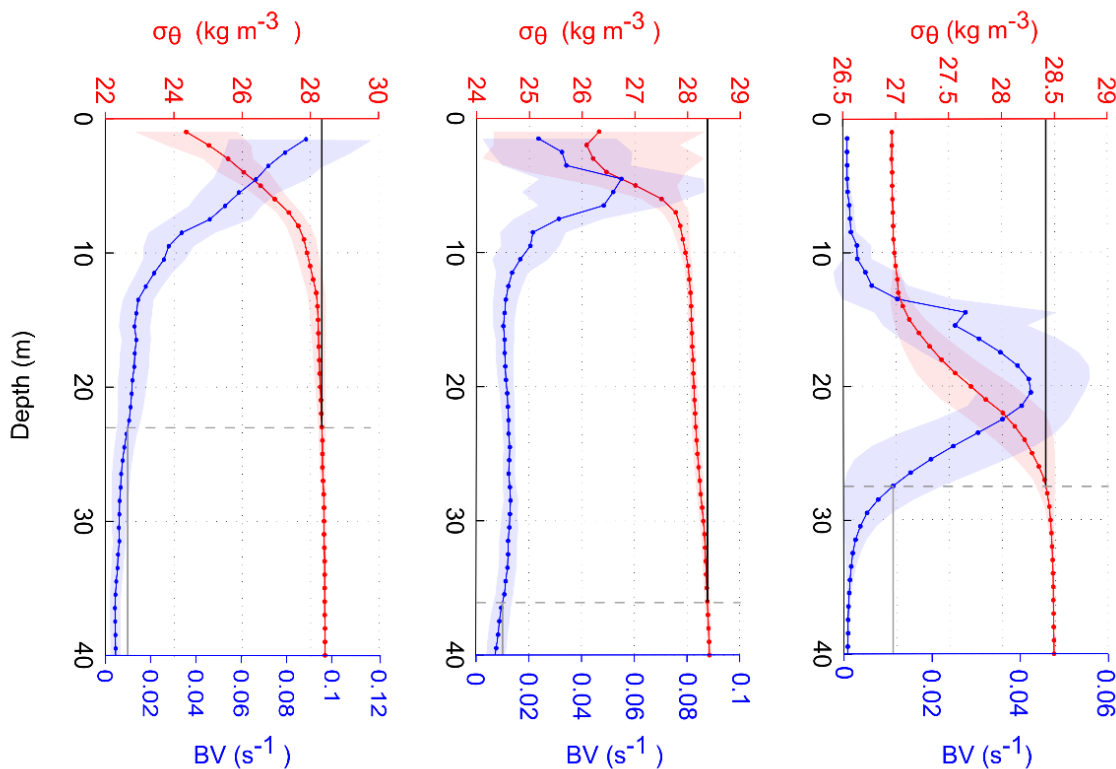
Figure 5.2 : Example of vertical profiles (average: solid line; standard deviation : shaded region) of potential density anomaly (red) and Brunt-Väisälä frequency (blue) for different glider sections performed in the Rhône River plume in February 2014. A threshold of 0.01 s^{-1} is used to define the lower limit of the pycnocline.

We used the dimensionless Richardson number (Ri – Eq. 5.4) to estimate the mixing intensity by comparing the Brunt-Väisälä frequency to the vertical gradient of the horizontal current velocity (Pacanowski and Philander, 1981).

$$Ri = N^2 / (\delta u/\delta z)^2 \qquad\qquad \text{Eq. 5.4}$$

where g is the acceleration of gravity (m² s^{-1}), ρ the water density (kg m^{-3}) and u the E-W (i.e. along-shelf) current velocity component (m s^{-1}). The stratification is stable for N > 0 and vice-versa. The Richardson number, which defines the mixing intensity, is equal to 0.25 in a stable flow and Ri < 0.25 if the turbulence overcomes the density stratification and generates vertical mixing (Turner, 1973).

5.3.5 Satellite data

Spatial maps of SPM concentrations (250 m resolution) were generated from Moderate Resolution Imaging Spectroradiometer (MODIS) data recorded onboard the Aqua satellite platform. Intermediate Level 1-A (L1A) products were downloaded from the Nasa Ocean Color website (http://oceancolor.gsfc.nasa.gov/cms/). Processing was made using the SeaDAS (version 7.0) software to generate geo-referenced and radiometrically calibrated Level 1-B (L1B) files. L2 remote sensing reflectance products at 645 nm (Rrs(645)) were generated using the l2gen function. The MUMM atmospheric correction (Ruddick et al., 2000) was used as it is the most appropriate to correct MODIS data from aerosols effects in the moderately turbid waters of the Rhône River plume (Ody et al., 2016). Rrs(645) was converted to SPM$_{mg\ L}$$^{-1}$ applying the regional equation established by Ody et al. (2016). The same authors studied the surface plume dynamics and fixed a threshold of 10 mg L^{-1} to characterize the plume boundary when using this regional equation. Thus, we used a similar value to determine the extent of the surface plume. We derived the particulate backscattering coefficient bbp(λ) at 10 MODIS wavebands between 412 and 678 nm applying the QAA (Quasi-Analytical Algorithm) (Lee et al., 2002, 2013). QAA derives the absorption and backscattering coefficients by analytically inverting the spectral remote-sensing reflectance. The spectral bbp(λ) is modeled assuming that both pure water and particles contribute to the total backscattering coefficient, and assuming that the spectral variations of bbp(λ) follow a power-law function. The spectral slope of the particulate backscattering coefficient, γ$_{MODIS}$, was therefore obtained by fitting a power-law function to the spectral bbp coefficients.

A filter was applied on γ$_{MODIS}$ to exclude slope values obtained from power-law functions fitted with a R² coefficient lower than 0.9. Excluded values generally corresponded to SPM$_{MODIS}$ > 35 mg L^{-1} and were located close to the river mouth during peak discharges. γ$_{MODIS}$ is further used as relative information of the surface spatial variability of the particulate assemblage (i.e. the lowest the spectral slope the highest the abundance of large particles, see 5.3.4).

5.4 Results

5.4.1 Meteorological and oceanic conditions

During the experiment, different wind conditions were observed. North-westerly (i.e. continental) winds were measured on January 30, February 2 (Situation 1) and 11 (Situation 3), 2014 with maximum wind speed of 12 m s^{-1}. Several south-east (i.e. marine) wind events of ~10 m s^{-1} occurred on February, 5-7 (Situation 2), 8 and 10, 2014, which led to precipitation over the Rhône water catchment (Fig. 5.3a) and resulted in a rapid increase of the Rhône discharge from 3500 m^3 s^{-1} (February 5) to 5500 m^3 s^{-1} (February 11) (Fig. 5.3b). During these SE wind events, waves mainly came from the south with significant height ranging from 2 to 3.5 m (Fig. 5.3c). Currents were stronger and generally oriented toward the north (maximum current speed was observed during such an event on February 10). Conversely, currents were weaker and oriented toward the south for NW winds. ADCP echo intensity showed that SPM concentrations in the water column followed the increase of the Rhône River discharge and wave height conditions with a maximum acoustic intensity at the peak of the flood. During episodic high waves and strong northward currents (February, 10), a drastic decrease of SPM concentrations was observed throughout the water column (Fig. 5.3f). Dash-line boxes on Figure 3 represent the three situations describe hereafter. Meteorological and hydrodynamical conditions during these situations are summarized in Table 5.1. The third situation (February, 10-11) is further qualified as a "back-to-back" storm and flood event due to the marine storm occurring on February, 10 (i.e. marine winds > 10 m s^{-1} and waves > 3 m) and the subsequent flood event on February, 11.

5.4.2 Glider cross-shelf CTD measurements

Temperature and salinity sections measured by the glider between January 30 and February 12, 2014 are presented in Figure 5.4. Results showed the cross-shelf extension of the Rhône River surface plume with fresher (<37.6), colder (<13.5°C) and lighter water (< 28.3 kg m^{-3}). During the first two sections (Fig. 5.4a-b), the plume was pushed offshore by continental winds. During the following three sections, under a prevailing S-SE wind (Fig. 5.4c-e), the plume was pressed against the coast and its thickness increased. The sixth section (Fig. 5.4f) showed a larger plume, which extended offshore due to continental wind and an increase of the Rhône discharge. Due to the glider direction, we monitored twice the structure of the plume close to the coast within a small time interval (i.e. a few hours during the 10 February 2014). During this period, the plume separated from the river mouth and deepened to 50 m deep. The seventh section (Fig. 5.4g) showed the largest plume, which extended up to 45 km offshore, associated to the large discharge of the Rhône River. Finally a notable decrease of temperature was observed near the bottom, forming a distinct layer extending southward with a thickness of 15 m.
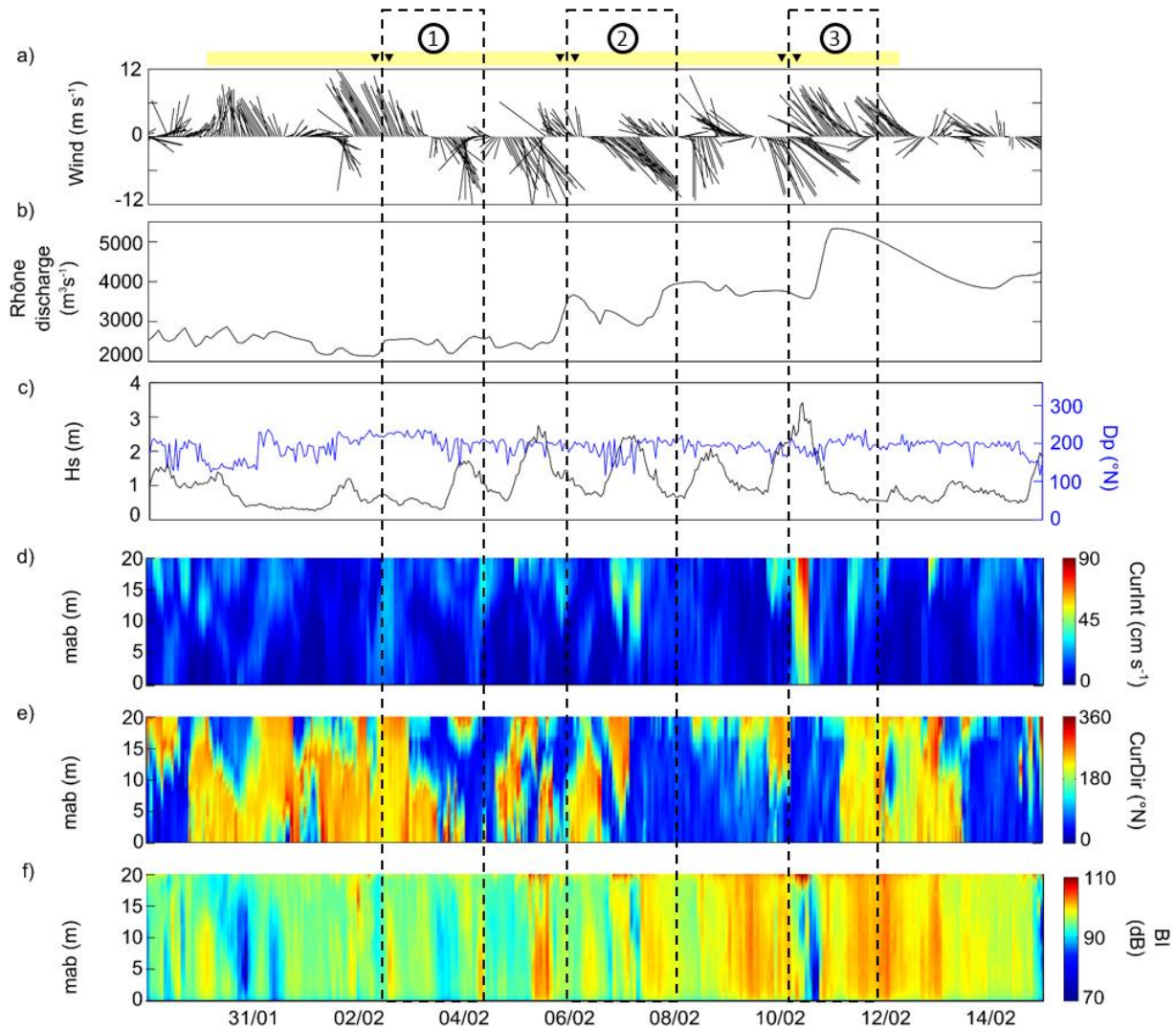
Figure 5.3 : Time-series from January 30 to February 15, 2014 of: (a) the hourly-mean wind speed and direction, (b) the Rhône River daily-mean discharge, (c) the significant wave height and direction, (d) the hourly-mean currents speed and (e) direction and (f) the backscatter index. The duration of the glider deployment is shown in yellow above (a). Black triangles show when the glider was close to the MESURHO buoy. The dash-line boxes show the 3 situations discussed. Wind and waves directions indicate the direction from which the wind and waves are coming.

Table 5.1 : Meteorological and hydrodynamical conditions at the MESURHO buoy station for the 3 situations discussed.

	Situation 1	Situation 2	Situation 3*
Date	2-3 Feb 2014	6-7 Feb 2014	10-11 Feb 2014
Rhône River discharge (m³ s⁻¹)	2440	3500	3600 - 5340
Prevalent wind speed (m s⁻¹)	10.1	6.7	8.1 – 11.9
Prevalent wind direction (°N)	165	352	170 - 340
Maximum wave significant height (m)	< 1	2	<1 – 3.5
Maximum current speed (m s⁻¹)	0.1	0.4	0.1 – 0.9
Prevalent current direction (°N)	185	0	0 – 190

*Due to the "back-to-back" storm and flood events of the third situation both marine and continental wind events are detailed.

Figure 5.4 : Cross-shelf hydrological sections of temperature (left panel) and salinity (right panel) measured by the glider. Density contour lines are shown in black and white on temperature and salinity sections, respectively. White arrows in bottom-left corner of each temperature section represent the direction of the glider trajectory. The position of the MESURHO buoy station is shown by a black triangle over the first section. From top to bottom, the seven sections carried out by the glider. The three situations discussed hereafter are numbered from 1 to 3.
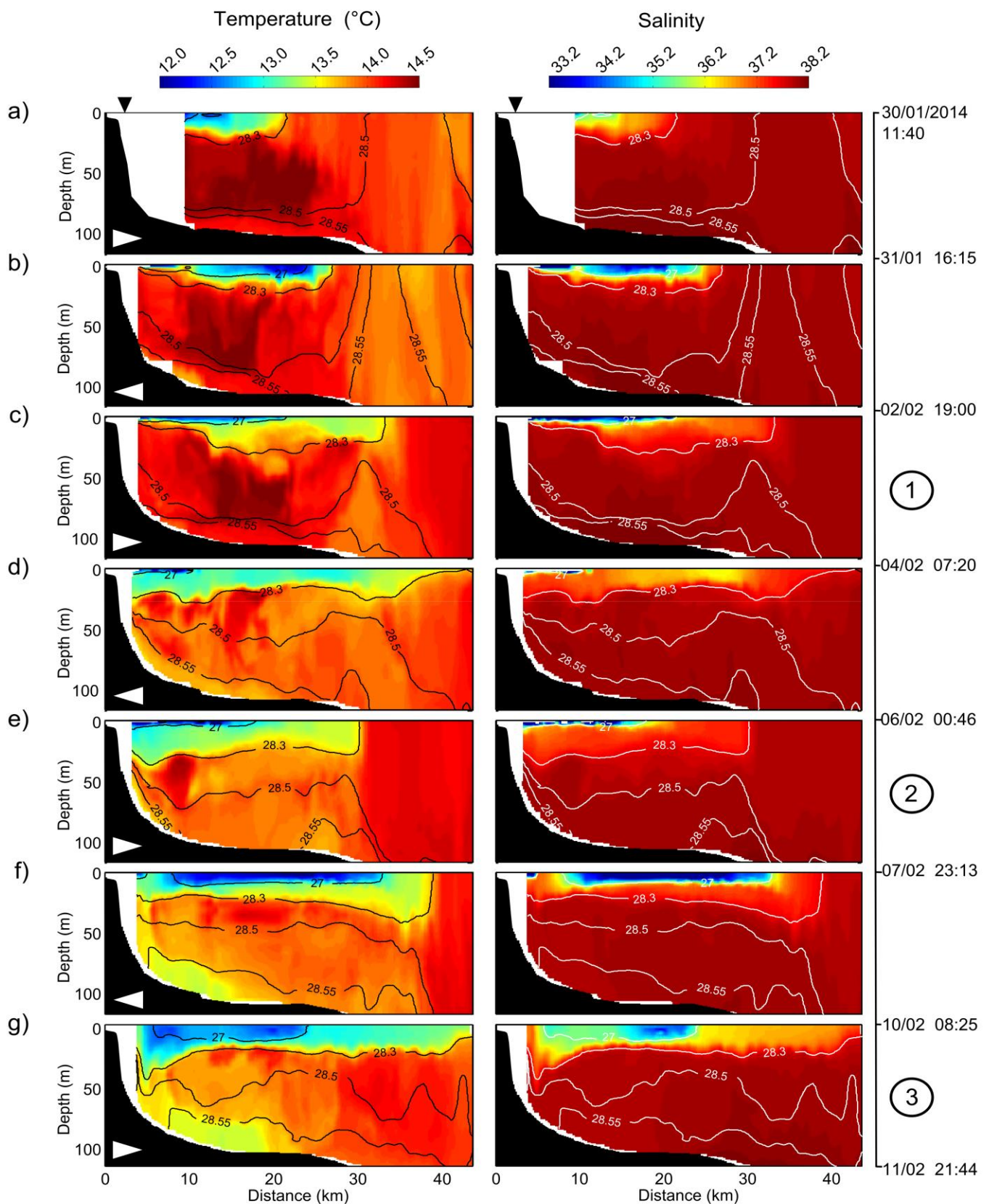
5.4.3 SPM concentrations and properties from glider and satellite

Comparison of glider and satellite surface SPM measurements– The comparison between glider and satellite-derived γ (dimensionless) and $(SPM)_{mg\ L^{-1}}$ is presented Figure 5.5. Both for glider and satellite data, γ rapidly decreased with increasing SPM concentration, indicating an increase of the abundance of flocs with SPM concentration. Moreover the shift between the two populations suggested contrasted particle assemblages between thin surface layer (<1 m) sensed by the satellite and the underlying layer (1-2 m depth) sampled by the glider.

a) $SPM_{MODIS} = 2.45 \times SPM_{Glider}$
$R^2 = 0.83$

b) $\gamma_{MODIS} = 1.41 \times \gamma_{Glider}$
$R^2 = 0.75$

c)
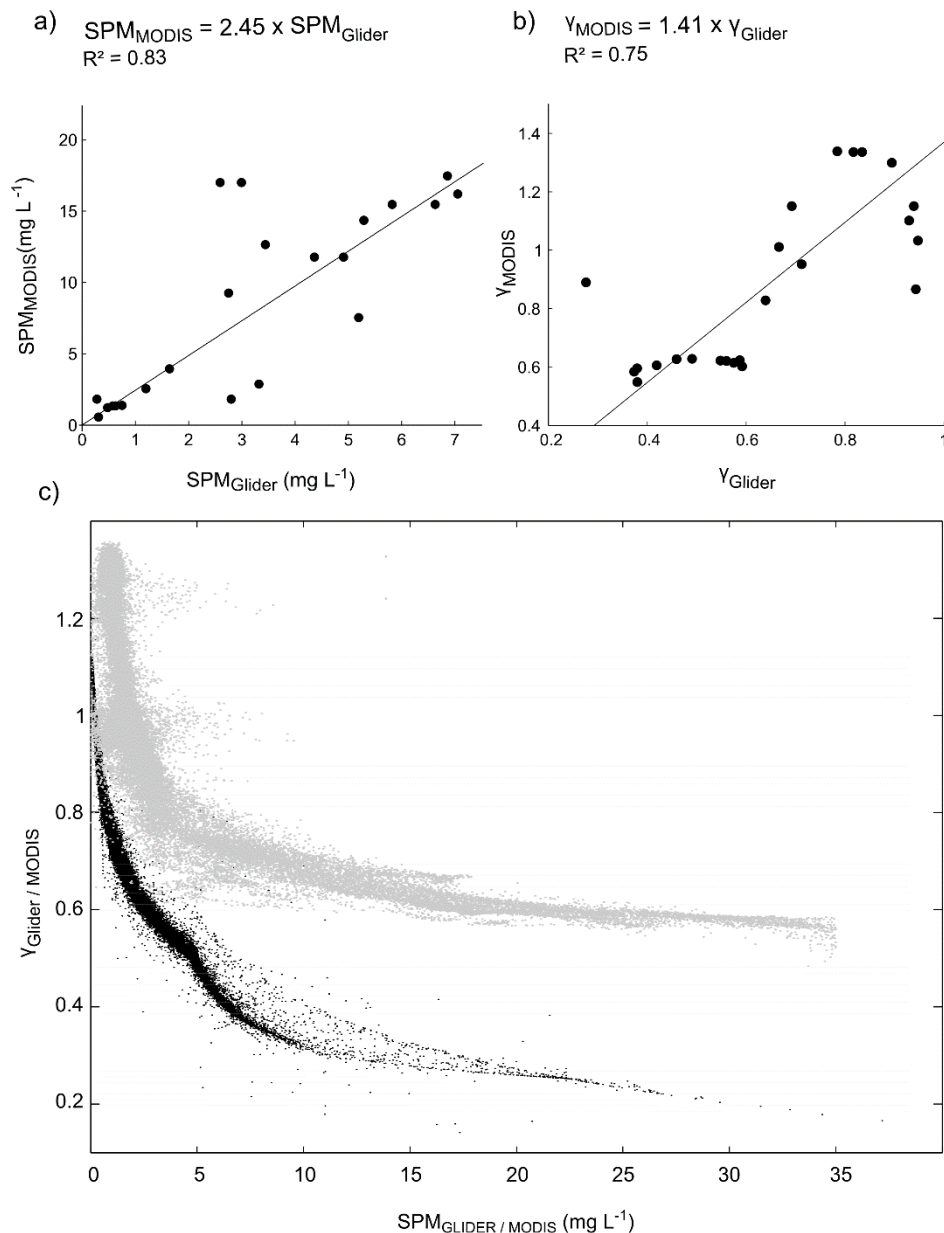
Figure 5.5 : Relationship between glider and satellite-derived a) $(SPM)_{mg\ L^{-1}}$ and b) γ (dimensionless). Relationship between $\gamma_{Glider/MODIS}$ and $(SPM)_{Glider/MODIS\ mg\ L^{-1}}$ for the 0-35 mg L^{-1} range. Satellite (February 11, 2014) Satellite measurements are in gray. Glider measurements are in black.

Nepheloid layers dynamics – Three situations were selected to characterize the SPM dynamics in the ROFI for different river discharges, wind and sea conditions (Fig. 5.6). Dimensions of the surface plume are derived from both satellite measurements using a threshold of 10 mg L^{-1} (Ody et al., 2016), and glider measurements using a density threshold of 28.3 kg m^{-3} (defining the base of the pycnocline).

Under a continental prevailing wind and a moderate river discharge (Situation 1 in February 4, Fig. 5.6a) the vertical distribution of surface SPM concentrations closely corresponded to the thermo-haline structure of the surface plume. Satellite observations showed that the plume presented a seaward gradient of SPM concentrations from 28 to 10 mg L^{-1} from the river mouth to 22 km offshore. Glider surface observations showed a similar decrease from 13 to 2 mg L^{-1} with the largest SPM concentrations (> 5 mg L^{-1}) restricted by the 27 kg m^{-3} isopycnal. A thin BNL was observed over the shelf and presented SPM concentration of 1-2 mg L^{-1}.

During a marine prevailing wind (Situation 2 on February 7, Fig. 5.6b), the plume remained over the shelf and thickened down to 30 m depth. The whole water column showed a SPM concentration of 2 mg L^{-1}. The most turbid part of the plume restricted by the 27 kg m^{-3} isopycnal was pressed against the coast. Satellite observations showed a similar trend and were completed with glider measurements that showed a more turbid BNL (2.5-5 mg L^{-1}) 10 km off the river mouth. During the storm event (Situation 3 on February 10, Fig. 5.6c), glider measurements showed the thickening of the plume down to 50 m depth. At the same time, the BNL presented higher SPM concentrations close to the coast. During the subsequent flood event (Situation 3 on February 11), the plume extended up to 45 km offshore and showed highest SPM concentrations between 10 and 20 km off the river mouth.
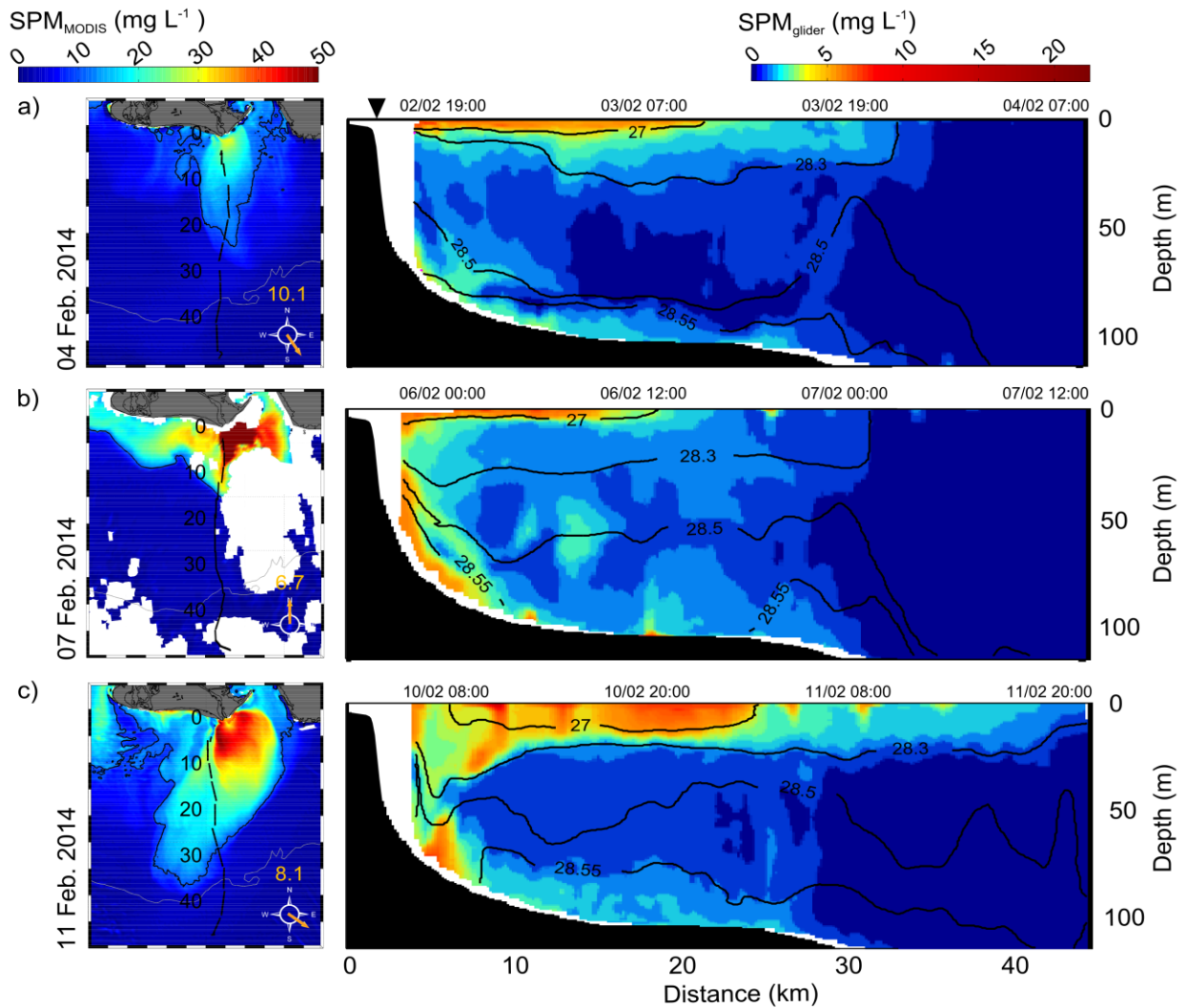
Figure 5.6 : Left panels: Surface SPM concentrations retrieved from satellite data. The distance from the coast (km) and along the glider track is shown in black. Dat and wind speed and direction are specified. The threshold of 10 mg L⁻¹ used for comparison with glider measurements is shown in black. Clouds are shown in white. Right panels: Corresponding glider sections of SPM concentrations. Density contour lines are shown in black. MESURHO buoy is shown by a black triangle above the first section. From top to bottom, the three situations discussed. Note the different colorbars used for satellite and glider observations.

SPM properties variability – We used the spectral slopes of glider and satellite-derived backscattering measurements, γ_{Glider} and γ_{MODIS}, as indexes of the particle assemblage properties (Fig. 5.7). Both indexes ranged from 0.3 to 1.4 and highlighted variable particulate assemblages in nepheloid layers depending on meteorological and sea conditions. From our results, both indexes were clearly linked with the SPM concentration: the higher the SPM concentration, the higher the proportion of large flocs in the particulate assemblage (i.e. low γ). The lower γ values were generally observed in the most turbid of the plume restricted by the 27 kg m⁻³ isopycnal.

Under a continental prevailing wind and a moderate river discharge (Situation 1 in February 4, Fig. 5.7a) both γ indexes showed that the plume close to the river mouth was characterized by increasing values with distance from the river mouth. Larger γ values were also observed in the BNL. During a marine prevailing wind (Situation 2 on February 7, Fig. 5.7b), when the plume was

pressed against the coast, γ indexes decreased both in the inner parts of the plume and the BNL. During the storm and subsequent flood event (Situation 3 on February 11, Fig. 5.7c), γ generally decreased in the plume that significantly thickened and widened. Close to the seabed, the BNL showed lower γ values close to the coast.
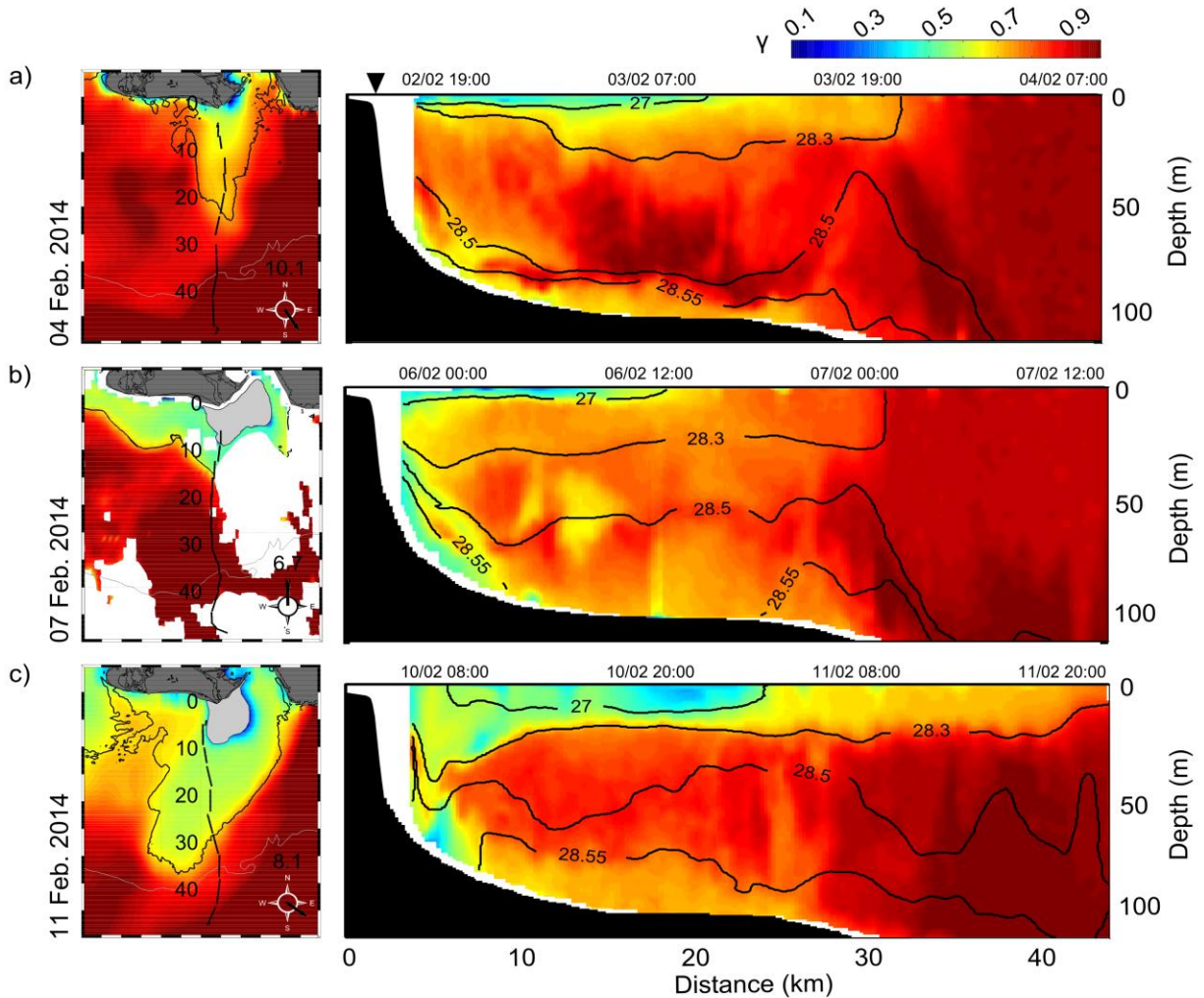
Figure 5.7 : Left panels: Surface estimated γ~MODIS~ from satellite data. The distance from the coast (km) and along the glider track is shown in black. Dat and wind speed and direction are specified. SPM concentration threshold of 10 mg L⁻¹ used for river plume description is shown in black. Right panels: Corresponding sections of γ~glider~ . Density contour lines are shown in black. MESURHO buoy is shown by a black triangle above the first section. From top to bottom, the three situations discussed.

5.4.4 Hydrodynamical and hydrological derived parameters

Along-shelf (E-W) current component, Brunt-Väisälä frequency (N), and Richardson number (Ri) derived from glider measurements are presented in Figure 5.8. We presented these observations together with wind and wind stress (τ) measurements for the three situations (Fig. 5.8a).

During the two first situations (left and middle panel in Fig. 5.8), results showed the high subsurface (1-5 m) stratification of the plume. The Richardson number highlighted a probable mixing offshore (i.e. Ri < 0.25) between the frontal zone of the plume and outer shelf waters.

During the third situation (Fig. 5.8c – right panel), wind stress showed maximum value of 0.38 N m^{-2} under a marine prevailing wind (February 10, 2014 at 9:00 AM). At that time, the currents close to the coast were the strongest ($\pm$50 cm s^{-1}) and in opposite direction between the surface and the bottom layers. Besides, N values were low throughout the water column and Ri values were lower than 0.25. During the subsequent flood and under a continental prevailing wind, high N between 10 and 40 km offshore highlighted the plume thickening (Fig. 5.8c).
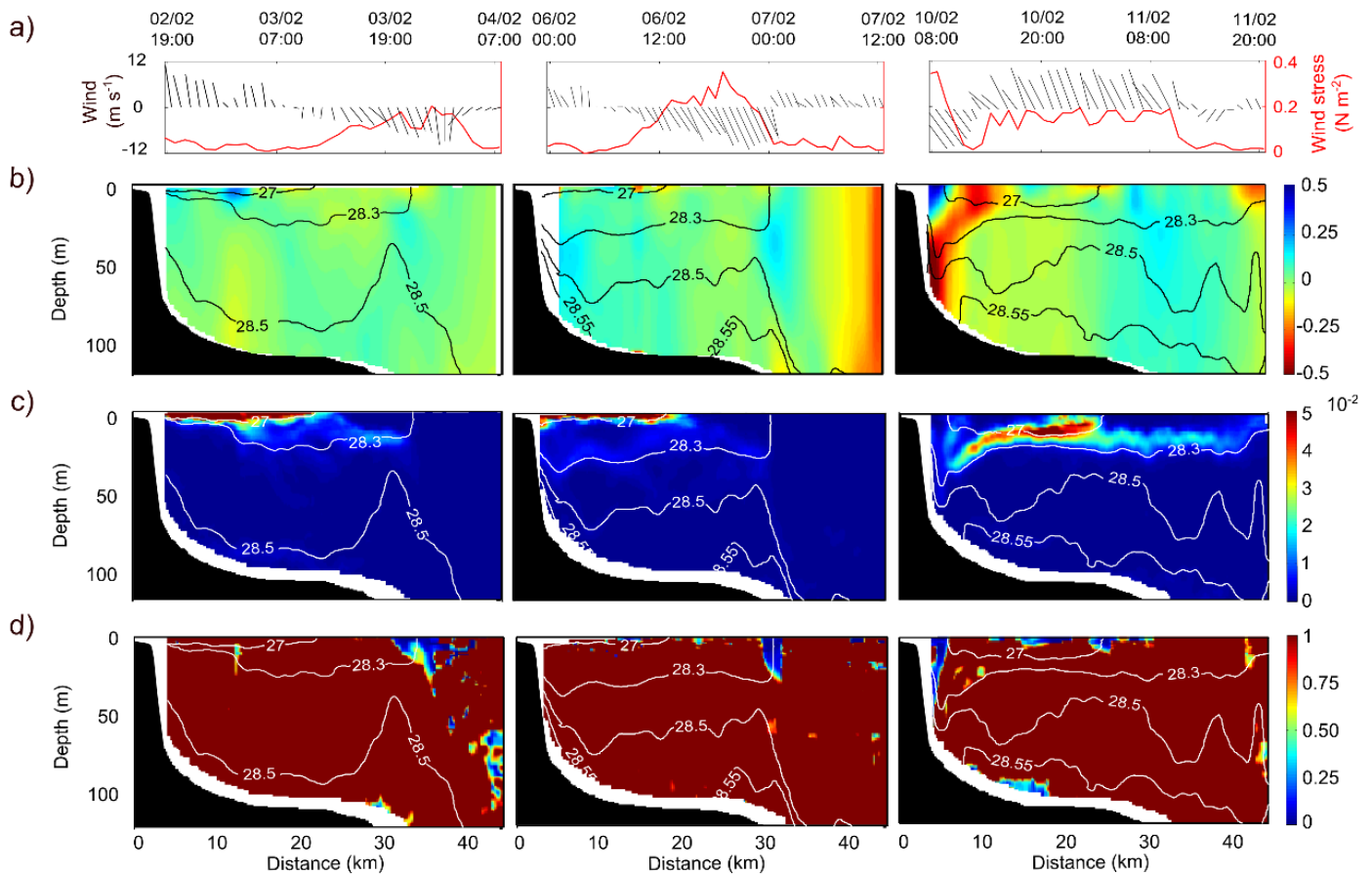
Figure 5.8 : a) Time-series of wind speed and direction (m s^{-1}). The wind stress is shown in red (N m^{-2}). Cross-shelf section of b) the along-shelf current (m s^{-1}), c) the derived Brunt-Väisälä frequency (s^{-1}) and d) the Richardson Number (dimensionless). Density contour lines are shown in black on the upper panel and in white on middle and lower panels.

5.5 Discussion

Several studies emphasized the necessity to combine satellite and glider platforms and perform high spatial and temporal resolution measurements to properly characterize SPM dynamics in the coastal area, especially during energetic events (Castelao et al., 2008b; Bourrin et al., 2015; Miles et al., 2015; Saldías et al., 2016). Based on simultaneous use of satellite and glider observations, we intend here to better understand the variability of the dynamics of nepheloid layers and of particle characteristics in the Rhône River ROFI.

5.5.1 Nepheloid layers dynamics

The extent of the surface plume was derived both from satellite and glider data. We examine here the consistency of the estimates based on these two data sets. The estimate of the plume extent from satellite data was solely infer from turbidity using a threshold value of 10 mg L^{-1} defined by Ody et al. (2016). It appears that this threshold delimited in fact the core of the plume when compared to the extent of the plume as defined by the glider data. The glider data allowed to define the buoyant plume both in terms of turbidity and density, the latter being a more physically relevant parameter. Consequently, the plume dimension inferred from the satellite derived turbidity threshold rather matched the core of the plume delimited by the 27 kg m^{-3} isopycnal, as observed by the glider. This implies that a turbidity limit lower than 10 mg L^{-1} should have been considered using satellite data to define the actual size of the plume delineated by the 28.3 kg m^{-3} isopycnal. Hence, care must be taken when using only a turbidity criterion from satellite images to define the plume size.

Previous studies based on models (Marsaleix et al., 1998; Estournel et al., 2001) and observations from radars and drifters (Broche et al., 1998; Naudin et al., 2001) highlighted the variability of the thermo-haline structure of the surface plume for different wind conditions and river discharges. Remote sensing of the surface SPM completed these observations and showed the role of the wind-driven circulation on the SPM transport, especially during flood events (Arnau et al., 2004; Lorthiois et al., 2012; Ody et al., 2016). Our observations are in line with these previous works, evidencing the agreement between the turbid and freshwater plumes, and their rapid temporal variability.

Under continental prevailing wind and moderate river discharge (Situation 1), the plume was deflected and rapidly diluted offshore over the continental shelf, and a BNL developed beneath it. This result suggest a persistent character of the vertical transfer of SPM in the ROFI towards the BNL during continental wind periods, probably because of the large particles sinking from the plume as shown by Many et al. (2016).

Under a marine prevailing wind (Situation 2) the plume was pressed against the coast, increasing the turbidity both in the surface plume and in the BNL close to the river mouth (Fig. 5.6b). These observations suggest an increasing transfer of the Rhône River SPM to the BNL. Such a direct

supply, which was poorly documented due to sampling difficulties (Aloisi et al., 1982; Lorthois et al., 2012), emphasizes the role of marine wind in the increase of the vertical transfer of particles from the plume toward the BNL. This transfer is believed to contribute to the sedimentation over the inner-part of the shelf where high sedimentation rates (20-40 cm y^{-1}) were estimated (Maillet et al., 2006; Drexler and Nittrouer, 2008; Marion et al., 2010). Similar observations were made in others micro-tidal areas as in the Po River ROFI (Palinkas et al., 2005; Milligan et al., 2007).

During the storm event (Situation 3), the occurrence of large waves and a strong westward coastal jet probably enhanced the particle resuspension over the prodelta down to 70 m deep, and at the same time transport river and resuspended material along the coast. We estimated a bottom shear stress induced by waves and currents of 0.2 Pa, which can resuspend non-cohesive sediment up to 25µm in grain size according to the Sedtrans05 model (Neumeier et al., 2005). It stress the role of storm events on the sediment redistribution from the prodelta to the shelf, and are in agreement with previous studies on the stratigraphy off the Rhône prodelta by Drexler and Nittrouer (2008) and Marion et al. (2010) and on the modelling of sediment transport by Ulses et al. (2008) and Dufois et al. (2014). Besides, the low Brunt-Väisälä frequency and Richardson number (see Fig. 5.8 – right panel) in this area indicated a breaking of the plume and mixing throughout the water column close to the coast. Several studies (Kirinus et al., 2012; Rogowski et al., 2014; Rong et al., 2014) described such a mixing of a buoyant plume induced by current-wave interactions.

5.5.2 Spatio-temporal variability of SPM properties

We compared the spectral slopes of glider (γ_{Glider}) and satellite-derived (γ_{MODIS}) backscattering measurements, as indexes of the SPM size. Both indexes ranged from 0.3 to 1.4, consistent with the estimates of Niewiadomska et al. (2008), Bourrin et al. (2015) and Many et al. (2016) in the northwestern Mediterranean Sea, and showed similar decreasing trends with regards to SPM concentration (Fig. 5.5). These observations are consistent with previous studies of Boss et al. (2001) and Slade and Boss (2015) where the authors inferred a similar decreasing trend. It is noteworthy that γ_{Glider} followed the same tendency whatever the depth. γ_{MODIS} was significantly larger than γ_{Glider} implying that satellite measurements systematically saw finer particle assemblage, especially for large SPM concentrations, than glider measurements. The high stratification of the plume could be the main factor involved in differences observed between satellite, which primarily sensed the top first meter, and the glider, which sampled below 1 m depth. Higher SPM concentration might be found in the very superficial plume water due to the strong stratification within the plume (see Fig. 5.9). The density gradient in the top meters of the plume could also limit the mixing with underlying waters and thus limit the action of flocculation. The transition between both surface and subsurface layers within the plume appeared as decisive in the variability of the SPM concentration and size and needs further investigations using an appropriate strategy.
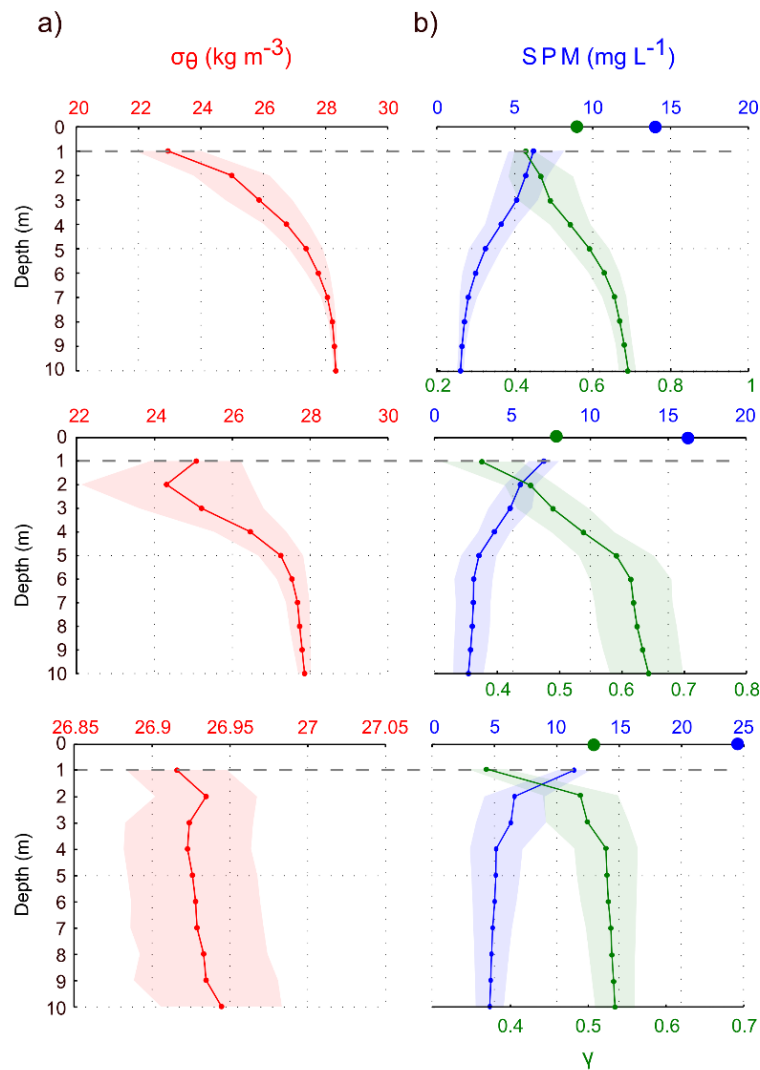
Figure 5.9 : Mean surface profiles of a) density anomaly (red) and b) SPM concentration (blue) and γ (green) estimated from glider measurements in the Rhône River ROFI. The standard deviation of each measurement is shown by shaded areas. Blue and green circles on b) show satellite-based estimates of the SPM concentration and γ. From top to bottom the three situations discussed.

Besides, whereas Many et al. (2016) proved in the same region for similar conditions that γ_{Glider} is representative of the SPM size spectra, γ_{MODIS} has not been calibrated against direct measurements of the SPM size spectra. As a matter of fact, Sahay et al. (2011) showed that the derivation of the particulate backscattering coefficients (bbp(λ)), derived from remote sensing through the QAA approach (see 5.3.5), could present an overestimate of 20% and 43% for 470 nm and 700 nm wavelengths, respectively. They based these estimates on in situ measurements and emphasized the variability existing between study areas and water types. This implies the need of an empirical relationship to improve the estimate of bbp through the QAA approach in the Rhône ROFI using in-situ calibrations of the SPM size, especially close to the river mouth where highest SPM concentrations (i.e. > 35 mg L^{-1}) were measured and corresponded to saturated bbp and non-representative γ_{MODIS}.

Since the spatial and temporal distributions of γ_{MODIS} at the level of the surface plume showed the same trends with that of γ_{Glider}, it can be considered that, apart from the offset, the results are complementary. For marine wind conditions, when the Rhône River plume was pressed against

the coast (Fig. 5.7b), γ_{MODIS} showed lower values that coincide with minimum γ_{Glider} values in the whole water column. It likely results from a higher proportion of large flocs that formed due to increasing SPM concentrations. Such flocs, which have a larger settling velocity, can rapidly reach the bottom layer and contribute to sustain the BNL. This observation supports the hypothesis made by Naudin et al. (1997), Thill et al. (2001) and Lorthiois et al. (2012), who identified the role of the flocculation in the rapid settling of particles close to the coast during flood events. Fox et al. (2004) and Milligan et al. (2007) also stressed the role of the flocculation in the fate and settling of SPM from the surface plume close to the Po river mouth in the Adriatic.

During the storm event (Fig. 5.7c), γ_{Glider} showed that the particle assemblage near the river mouth was finer throughout water column. This diminution of the particle size is believed to result both from the breakup of flocs by turbulent motions induced by the large waves and strong along-shore current. Moreover, wave-induced resuspension of sediment down to 70 m depth could enhance the flocculation close to the seabed and accentuate the SPM transport off the Rhône River ROFI in the BNL (see similar results in Curran et al. (2007) and Bourrin et al. (2015)).

5.6 Conclusion

The TUCPA experiment offered a unique set of observations on the high-frequency spatial and temporal variability of the Rhône River ROFI for different wind conditions and river discharge, including a flood event. The combination of coastal buoy monitoring, glider transects and satellite observations provided a detailed description of the hydrology, the hydrodynamics and SPM characteristics in the ROFI. Results emphasized the high variability of the Rhône River plume extent as well as the persistence of a bottom nepheloid layer. Three typical meteorological situations involved in the general transport and sedimentation of Rhône River particles have been detailed. The continental wind enhanced the offshore export of SPM within the surface river plume, the thickness and concentration of which vary with the river discharge. Conversely marine wind, which leads wavy and flood conditions, limited the offshore dispersion of the river plume. This situation thus increased the surface SPM concentration and favored the formation of large particles by flocculation and their settling toward the BNL. Moreover, the BNL was also fed by the resuspension of sediment due to the wave action. During a storm event, results emphasized the role of waves and current on the break of the plume stratification and the resuspension of sediments down to 70 m depth that favored the export of SPM off the ROFI. The combination of both satellite and glider SPM measurements was determinant to monitor both surface (< 1m depth, satellite data) and subsurface (> 1m depth, glider data) parts of the river plume. Results from both platforms showed a similar pattern (i.e., increasing abundance of large particles – typically flocs – with increasing SPM concentrations) but different ranges, probably due to the strong stratification of the plume. The estimates of the index of the particle size distribution, γ, highlighted the larger proportion of flocs within the plume as well as the change of the particle assemblage, which became finer seaward in both river plume and BNL due to the settling of flocculated particles. At last, the use of this index permitted to identify the role of rough weather on the breakup of flocculated particles during the storm event that favored the transport of finest sediments off the ROFI.

Acknowledgments

References

Aloisi, J.C., J.P. Cambon, J. Carbonne, G. Cauwet, C. Millot, A. Monaco and H. Pauc. **1982**. « Origine et rôle du néphéloïde profond dans le transfert des particules au milieu marin. Application au Golfe du Lion. » *Oceanologica Acta* 5 (4): 481‑91.

Arnau, P., C. Liquete and M. Canals. **2004**. « River mouth plume events and their dispersal in the Northwestern Mediterranean Sea ». *Oceanography* 17: 22‑31.

Babin, M., A. Morel, V. Fournier-Sicre, F. Fell and D. Stramski. **2003**. « Light scattering properties of marine particles in coastal and open ocean waters as related to the particle mass concentration. » *Limnology and Oceanography*, 843‑59.

Boss, E., M.S. Twardowski and S. Herring. **2001**. « Shape of the particulate beam attenuation spectrum and its inversion to obtain the shape of the particulate size distribution ». *Applied Optics* 40 (27): 4885‑93.

Bourrin, F., X. Durrieu de Madron and W. Ludwig. **2006**. « Contribution to the study of coastal rivers and associated prodeltas to sediment supply in the Gulf of Lions (NW Mediterranean Sea) ». *Vie et Milieu* 56 (4): 307‑14.

Bourrin, F., G. Many, X. Durrieu de Madron, J. Martín, P. Puig, L. Houpert, P. Testor, S. Kunesch, K. Mahiouz and L. Béguery. **2015**. « Glider monitoring of shelf suspended particle dynamics and transport during storm and flooding conditions ». *Continental Shelf Research* 109 (10): 135‑49. doi:10.1016/j.csr.2015.08.031.

Broche, P., J.L. Devenon, P. Forget, J.C. de Maistre, J.J. Naudin and G. Cauwet. **1998**. « Experimental study of the Rhone plume. Part I: physics and dynamics ».

Oceanologica Acta 21 (6): 725‑38.

Castelao, R., S. Glenn, O. Schofield, R. Chant, J. Wilkin and J. Kohut. **2008a**. « Seasonal evolution of hydrographic fields in the central Middle Atlantic Bight from glider observations ». *Geophysical Research Letters* 35 (3). doi:10.1029/2007GL032335.

Castelao, R., O. Schofield, S. Glenn, R. Chant and J. Kohut. **2008b**. « Cross-shelf transport of freshwater on the New Jersey shelf ». *Journal of Geophysical Research* 113 (C7). doi:10.1029/2007JC004241.

Curran, K., P. Hill, T. Milligan, O. Mikkelsen, B. Law, X. Durrieu de Madron, F. Bourrin, **2007**. « Settling velocity, effective density, and mass composition of suspended sediment in a coastal bottom boundary layer, Gulf of Lions, France ». Continental Shelf Research 27, 1408–1421

Dagg, M., R. Benner, S. Lohrenz and D. Lawrence. **2004**. « Transformation of dissolved and particulate materials on continental shelves influenced by large rivers: plume processes. » *Continental Shelf Research* 24 (7-8): 833‑58. doi:10.1016/j.csr.2004.02.003.

Davis, R.E., C.C. Eriksen and C.P. Jones. **2002**. « Autonomous buoyancy-driven underwater gliders ». *The technology and applications of autonomous underwater vehicles*, 37‑58.

Drexler, T. M., and C. A. Nittrouer. **2008**. « Stratigraphic signatures due to flood deposition near the Rhône River: Gulf of Lions, northwest Mediterranean Sea ». *Continental Shelf Research* 28 (15): 1877‑94. doi:10.1016/j.csr.2007.11.012.

Dufois, F., R. Verney, P. Le Hir, F. Dumas and S. Charmasson. **2014**. « Impact of winter storms on

sediment erosion in the Rhone River prodelta and fate of sediment in the Gulf of Lions (North Western Mediterranean Sea) ». *Continental Shelf Research* 72: 57‑72. doi:10.1016/j.csr.2013.11.004.

Durrieu de Madron, X., and M. Panouse. **1996**. « Transport de matière particulaire en suspension sur le plateau continental du Golfe du Lion. Situation estivale et hivernale ». *Comptes rendus de l'Académie des sciences. Série 2. Sciences de la terre et des planètes* 322 (12): 1061‑70.

Durrieu de Madron, X., P.L. Wiberg and P. Puig. **2008**. « Sediment dynamics in the Gulf of Lions: The impact of extreme events ». *Continental Shelf Research* 28 (15): 1867‑76. doi:10.1016/j.csr.2008.08.001.

Estournel, C., P. Broche, P. Marsaleix, J.L. Devenon, F. Auclair and R. Vehil. **2001**. « The Rhone River plume in unsteady conditions: numerical and experimental results ». *Estuarine, Coastal and Shelf Science* 53 (1): 25‑38. doi:10.1006/ecss.2000.0685.

Fernández-Nóvoa, D., R. Mendes, J.M. Dias, A. Sánchez-Arcilla and M. Gómez-Gesteira. **2015**. « Analysis of the influence of river discharge and wind on the Ebro turbid plume using MODIS-Aqua and MODIS-Terra data ». *Journal of Marine Systems* 142: 40‑46.

Fox, J. M., P. S. Hill, T. G. Milligan and A. Boldrin. **2004**. « Flocculation and sedimentation on the Po River Delta ». *Marine Geology* 203 (1–2): 95-107. doi:10.1016/S0025-3227(03)00332-3.

Gartner, J. W. **2004**. « Estimating suspended solids concentrations from backscatter intensity measured by acoustic Doppler current profiler in San Francisco Bay, California ». *Marine Geology* 211 (3): 169‑87.

Garvine, R.W. **1995**. « A dynamical system for classifying buoyant coastal discharges ». *Continental Shelf Research* 15 (13): 1585‑96.

Gostiaux, L., and H. Van Haren. **2010**. « Extracting meaningful information from uncalibrated backscattered echo intensity data ». *Journal of Atmospheric and Oceanic Technology* 27 (5): 943‑49.

Kirinus P., E. Marques, J. Correa da Costa and E. Fernandes. **2012**. « The contribution of waves in mixing processes of the Patos Lagoon plume ». *International Journal of Geosciences* 3: 1019.

Large, W.G., and S Pond. **1981**. « Open ocean momentum flux measurements in moderate to strong winds ». *Journal of physical oceanography* 11 (3): 324‑36.

Lee, Z., K.L. Carder., and R.A. Arnone. **2002**. « Deriving inherent optical properties from water color: a multiband quasi-analytical algorithm for optically deep waters. » *Applied Optics*, 41(27), 5755-5772.

Lee, Z., B. Lubac, J. Werdell, and R.A. Arnone. **2013**. http://www.ioccg.org/groups/Software_OCA/QAA_v5.pdf.

Lihan, T., S. Saitoh, T. Iida, T. Hirawake and K. Iida. **2008**. « Satellite-measured temporal and spatial variability of the Tokachi River plume ». *Estuarine, Coastal and Shelf Science* 78 (2): 237‑49. doi:10.1016/j.ecss.2007.12.001.

Lorthiois, T., D. Doxaran and M. Chami. **2012**. « Daily and seasonal dynamics of suspended particles in the Rhône River plume based on remote sensing and field optical measurements. » *Geo-Marine Letters* 32 (2): 89‑101. doi:10.1007/s00367-012-0274-2.

Ludwig, W., E. Dumont, M. Meybeck and Heussner, S. **2009**. «River discharges of water and nutrients to the Mediterranean and Black Sea: Major drivers for ecosystem changes during past and future decades? » *Progress in Oceanography*, 80, 199-217.

Maillet, G., C. Vella, S. Berné, P.L. Friend, C.L. Amos, T.J. Fleury and A. Normand. **2006**. « Morphological changes and sedimentary processes induced by the December 2003 flood event at the present mouth of the Grand Rhône River (southern France) ». *Marine Geology* 234 (1-4): 159‑77. doi:10.1016/j.margeo.2006.09.025.

Manning, A.J, and D.H. Schoellhamer. **2013**. « Factors controlling floc settling velocity along a longitudinal estuarine transect ». *Marine Geology* 345 (11): 266-80.

Many, G., F. Bourrin, X. Durrieu de Madron, I. Pairaud, A. Gangloff, D. Doxaran, A. Ody, R. Verney, C., Menniti, D. Le Berre and M. Jacquet. **2016**. « Particle assemblage characterization in the Rhone River ROFI. » *Journal of Marine systems* 157. 39-51. doi:10.1016/j.jmarsys.2015.12.010.

Marion, C., F. Dufois, M. Arnaud, and C. Vella. **2010**. « In situ record of sedimentary processes near the Rhône River mouth during winter events (Gulf of Lions, Mediterranean Sea). » *Continental Shelf Research* 30 (9): 1095‑1107. doi:10.1016/j.csr.2010.02.015.

Marsaleix, P., C. Estournel, V. Kondrachoff and R. Vehil. **1998**. « A numerical study of the formation of the Rhône River plume ». *Journal of Marine Systems* 14 (1–2): 99‑115. doi:10.1016/S0924-7963(97)00011-0.

Miles, T, S. Glenn and O. Schofield. **2013**. « Temporal and spatial variability in fall storm induced sediment resuspension on the Mid-Atlantic Bight ». *Continental Shelf Research* 63 (7): S36‑49. doi:10.1016/j.csr.2012.08.006.

Miles, T., G. Seroka, J. Kohut, O. Schofield and S. Glenn. **2015**. « Glider observations and modeling of sediment transport in Hurricane Sandy ». *Journal of Geophysical Research: Oceans* 120 (3): 1771‑91. doi:10.1002/2014JC010474.

Milligan, T. G., P. S. Hill and B. A. Law. **2007**. « Flocculation and the loss of sediment from the Po River plume ». *Continental Shelf Research*, Sediment Dynamics in the Western Adriatic Sea, 27 (3–4): 309-21. doi:10.1016/j.csr.2006.11.008.

Morel, A. **1973**. « The scattering of light by sea water: Experimental results and theoretical approach. » *Optics of the sea, interface and in-water transmission and imaging* AGARD Lecture Series (61): 3.1.1‑3.1.76.

Morel, A. **1974**. « Optical properties of pure water and pure sea water. » *Optical aspects of oceanography*, Acadamic Press, London, 1‑24.

Naudin, J.J., G. Cauwet, M.J. Chrétiennot-Dinet, B. Deniaux, J.L. Devenon and H. Pauc. **1997**. « River discharge and wind influence upon particulate transfer at the land–ocean interaction: case study of the Rhone River plume ». *Estuarine, Coastal and Shelf Science* 45 (3): 303‑16. doi:10.1006/ecss.1996.0190.

Naudin, J.J., G. Cauwet, C. Fajon, L. Oriol, S. Terzić, J.L. Devenon, et P. Broche. **2001**. « Effect of mixing on microbial communities in the Rhone River plume ». *Journal of Marine Systems* 28 (3–4): 203‑27. doi:10.1016/S0924-7963(01)00004-5.

Neumeier, U., C. Ferrain, C.L. Amos, G. Umgiesser and M. Z. Li. **2008**. « SedTrans05: An improved sediment-transport model for continental shelves and coastal waters with a new algorithm for cohesive sediments. » *Computer and Geosciences*. doi:10.1016/j.cageo.2008.02.007.

Niewiadomska, K., H. Claustre, L. Prieur and F. d'Ortenzio. **2008**. « Submesoscale physical-biogeochemical coupling across the Ligurian current (northwestern Mediterranean) using a bio-optical glider. » *Limnology and Oceanography* 53 (5): 2210.

Nittrouer, C. A, J. A Austin, M. E. Field, J. H Kravitz, J. Syvitski and P.L Wiberg. **2009**. « Continental margin sedimentation: From sediment transport to sequence stratigraphy. »

Ody, A., D. Doxaran, Q. Vanhellemont, B. Nechad, S. Novoa, G. Many, F. Bourrin, R. Verney and I. Pairaud. **2016**. « Potential of high spatial and temporal ocean color satellite data to study the dynamics of suspended particles in a non-tidal river plume. » *Remote Sensing* 8 (3): 245.

Pacanowski, R.C., and S.G.H. Philander. **1981**. « Parameterization of vertical mixing in numerical models of tropical oceans ». *Journal of Physical Oceanography* 11 (11): 1443‑51.

Palinkas, C.M., C.A. Nittrouer, R.A. Wheatcroft and L. Langone. **2005**. « The use of 7Be to identify event and seasonal sedimentation near the Po River delta, Adriatic Sea ». *Marine Geology* 222-223 (11): 95-112. doi:10.1016/j.margeo.2005.06.011.

Pairaud, I., Repecaud M., Ravel C., Fuchs R., Arnaud M., Champelovier A., Rabouille C., Bombled B., Toussaint F., Garcia F., Raimbault P., Verney R., Meule S., Gaufres P., Bonnat A., Cadiou J-F. **2016**. « MesuRho. Plateforme instrumentée de suivi des paramètres environnementaux à l'embouchure du Rhône. » In *Mesures à haute résolution dans l'environnement marin côtier*. 2016. Schmitt, F.G. et Lefebvre A. (Eds.). CNRS Alpha. ISBN : 978-2-271-08592-4. pp.73- 87.

Pont, D. **1996**. « Evaluation of water fluxes and sediment supply. » *Oral Communication, MEDDELT, Final Meeting*, Venezia, October 2–5.

Rogowski, P., E. Terrill and J. Chen. **2014**. « Observations of the Frontal Region of a Buoyant River Plume Using an Autonomous Underwater Vehicle ». *Journal of Geophysical Research: Oceans* 119 (11): 7549‑67. doi:10.1002/2014JC010392.

Rong, Z., R. Hetland, W. Zhang and X. Zhang. **2014**. « Current–wave interaction in the Mississippi–Atchafalaya river plume on the Texas–Louisiana shelf ». *Ocean Modelling* 84 (12): 67‑83. doi:10.1016/j.ocemod.2014.09.008.

Ruddick, K., F. Ovidio and M. Rijkeboer. **2000**. « Atmospheric correction of SeaWiFS imagery for turbid coastal and inland waters ». *Applied optics* 39 (6): 897‑912.

Sadaoui, M., W. Ludwig, F. Bourrin and P. Raimbault. **2016**. « Controls, budgets and variability of riverine sediment fluxes to the Gulf of Lions (NW Mediterranean Sea) ». *Journal of Hydrology* 540: 1002-15.

Sadaoui M, W. Ludwig, F. Bourrin, E. Romeroc. « The impact of reservoir construction on riverine sediment and carbon fluxes to the Mediterranean Sea». *Progress in Oceanography* (this issue).

Sahay, A., P. Chauhan, P. Nagamani, N. Sanwalani and R. Dwivedi. **2011**. « Backscattering of light by coastal waters using hyperspectral in-situ measurements: A case study off Veraval, Gujarat, India ».

Saldías, G. S., M. Sobarzo, J. Largier, C. Moffat and R. Letelier. **2012**. « Seasonal variability of turbid River plumes off central Chile based on high-resolution MODIS imagery ». *Remote Sensing of Environment* 123 (08): 220‑33. doi:10.1016/j.rse.2012.03.010.

Saldías, G. S., R.K. Shearman, J.A. Barth and N. Tufillaro. **2016**. « Optics of the offshore Columbia River plume from glider observations and satellite imagery ». *Journal of geophysical research: Oceans* (121). doi:10.1002/2015JC011431.

Simpson, J. H., and J. Sharples. **2012**. « Introduction to the physical and biological oceanography of shelf seas ». *Cambridge University Press*.

Slade, W. H., and E. Boss. **2015**. « Spectral attenuation and backscattering as indicators of average particle size. » *Applied Optics* 54, 7264-7277.

Sullivan, J. M., P. L Donaghay and J. E. B Rines, **2010**. Coastal thin layer dynamics: consequences to biology and optics. Continental Shelf Research 30, 50–65. http://dx.doi.org/10.1016/j.csr.2009.07.009.

Teledyne RD Instruments. **2007**. « Waves primer: Wave measurements and the RDI ADCP waves array technique. Available from RDInstruments.com. »

Thill, A., S. Moustier, J. M. Garnier, C. Estournel, J. J. Naudin and J. Y. Bottero. **2001**. « Evolution of particle size and concentration in the Rhône river mixing zone: influence of salt flocculation ». *Continental Shelf Research* 21 (18): 2127‑40.

Thomas, A., and R. Weatherbee. **2006**. « Satellite-measured temporal variability of the Columbia River plume ». *Remote Sensing of Environment* 100 (2): 167‑78. doi:10.1016/j.rse.2005.10.018.

Turner, J. S. **1973**. « Buoyancy effects in fluids ». *Cambridge University*.

Ulses, C., C. Estournel, J. Bonnin, X. Durrieu de Madron and P. Marsaleix, **2008**. « Impacts between storms and dense water cascading on shelf-slope exchange in the Gulf of Lions (NW Mediterranean) ». *Journal of Geophysical Research: Oceans* 113, C02010. http://dx.doi.org/10.1029/2006JC003795.

UNESCO. **1983**. « Algorithms for computation of fundamental properties of seawater ». *Technical papers in marine science* 44: 53.

Webb Research. **2005**. « Operations manual Slocum shallow battery glider ». Ver. 1.6

Chapter 6.

Glider monitoring of shelf suspended particle dynamics and transport during storm and flooding conditions

Chapter 6. Glider monitoring of shelf suspended particle dynamics and transport during storm and flooding conditions

François Bourrin[1, 2], **Gaël Many**[1, 2], Xavier Durrieu de Madron[1, 2], Jacobo Martín[3, 4], Pere Puig[3], Loic Houpert[2, 5], Pierre Testor[6], Stéphane Kunesch[1, 2], Karim Mahiouz[7], Laurent Béguery[7, 8]

[1] Univ. Perpignan Via Domitia, Centre de Recherche et de Formation sur les Environnements Méditerranéens, UMR 5110, 52 avenue Paul Alduy, F-66860, Perpignan France

[2] CNRS, Centre de Recherche et de Formation sur les Environnements Méditerranéens, UMR 5110, 52 avenue Paul Alduy, F-66860, Perpignan France

[3] ICM-CSIC, Passeig Marítim de la Barceloneta 37–49, 08003 Barcelona, Spain

[4] CADIC-CONICET, Bernardo Houssay 200, 9410, Ushuaia, Argentina

[5] SAMS-SMI, Oban, Argyll, PA37 1QA, UK

[6] LOCEAN, UPMC-CNRS-IRD-MNHN, 4 place Jussieu 75252 PARIS Cedex 05 France

[7] CNRS-DT INSU, Zone portuaire de Brégaillon, BP 330, 83507 La Seyne-sur-mer cedex

[8] ACSA, 9 Europarc, 13590 Meyreuil, FRANCE

Online version

List of Figures

Abstract

Transfers of particulate matter on continental margins primarily occur during energetic events. As part of the CASCADE (CAscading, Storm, Convection, Advection and Downwelling Events) experiment, a glider equipped with optical sensors was deployed in the coastal area of the Gulf of Lions, NW Mediterranean in March 2011 to assess the spatio-temporal variability of hydrology, suspended particles properties and fluxes during energetic conditions. This deployment complemented a larger observational effort, a part of the MOOSE (Mediterranean Ocean Observing System of the Environment) network, composed of a coastal benthic station, a surface buoy and moorings on the continental slope. This set of observations permitted to measure the impact of three consecutive storms and a flood event across the entire continental shelf. Glider data showed that the sediment resuspension and transport observed at the coastal station during the largest storm (Hs > 4m) was effective down to a water depth of 80m. The mid-shelf mud belt, located between 40 and 90 m depth, appears as the zone where the along-shelf flux of suspended sediment is maximum. Besides, the across-shelf flux of suspended sediment converges towards the outer limit of the mid-shelf mud belt, where deposition of suspended particles probably occurs and contributes to the nourishment of this area. Hydrological structures, suspended particles transport and properties changed drastically during stormy periods and the following flood event. Prior to the storms, the shelf waters were weakly stratified due in particular to the presence of cold dense water on the inner- and mid-shelf. The storms rapidly swept away this dense water, as well as the resuspended sediments, along the shelf and towards a downstream submarine canyon. The buoyant river plumes that spread along the shelf after the flooding period provoked a restratification of the water column on the inner- and mid-shelf. The analysis of glider's optical data at different wavelengths suggests that the coastal area and the bottom nepheloid layer during the largest storm are primarily composed of coarse particles, probably macroflocs, and that the size of particles decreases further offshore. A similar trend, albeit less contrasted, is observed after the flooding. This work provided a unique synoptic view across the entire shelf of the impact of a typical Mediterranean storm on bottom sediment erosion and particulate fluxes. Repeated glider transects across the south-western part of the Gulf of Lions shelf permitted for the first time to measure continuously the thermo-haline structures, the suspended particles concentrations and size, the current speed, and to estimate the particulate transport before, during and after typical Mediterranean storm events. Glider data complement and compare well with concomitant high frequency time series at fixed stations along the coast and in a downstream submarine canyon.

6.1 Introduction

6.1.1 Observations of the sediment transport during floods and storms

Sediment dynamics on continental margins is usually influenced by sediment inputs from rivers. Riverine fine-grained particles commonly accumulate on the mid-shelf and form a mud belt (Hill et al., 2007). Several authors (Cattaneo et al., 2007; Harris and Wiberg, 2002; McCave, 1972) proposed that fine-grained sediments are eventually advected by currents in the across-shelf pathway and that the location and thickness of the fine-grained deposits depends upon the balance between hydrodynamics and sedimentary inputs. In this balance, floods and storms appear as key processes (Moore, 1969; Wright and Coleman, 1974; Harris and Wiberg, 2002; Nittrouer et al., 2007), which are still challenging to witness and to explicitly assess the magnitude on the fine-grained sediment transport (Corbett et al., 2014).

Until recently, most in situ observations of suspended particle transport during flood and storm events were gathered at few fixed locations over one or some components of the shelf (inner-, mid-, outer-shelf, shelf break). Such observations provide precise information on the temporal variability of a narrow water column, but do not enable to describe the spatial gradients across the entire shelf and evaluate the overall suspended particle transport. Remote-sensing observations provide snapshots of the distribution of suspended particles, which are however restricted to the surface layer and to cloud-free days. Likewise, identification of suspended particles properties, especially their concentration, size distribution and composition (mineral or organic), that is central for the understanding of their origin and their fate (Boss et al., 2001b; Curran et al., 2007; Doxaran et al., 2009) suffer from the same gaps in terms of spatial and temporal variability throughout the shelf's water column.

Testor et al. (2010) recapitulated the new sampling capabilities offered by gliders during the last decade in various locations. Glenn et al. (2008) first evaluated the potential of autonomous gliders equipped with physical and optical sensors to study the spatial and temporal variability of sediment resuspension and transport across the Middle Atlantic Bight continental shelf. Lately, Miles et al. (2013) quantified in the same region the spatial variability of sediment resuspension and transport during a large fall storm using gliders as well as fixed platforms (high frequency radars and meteorological buoys). Both studies demonstrated that gliders satisfactorily documented vertical and horizontal gradients of the primary parameters (i.e. temperature, salinity, density, suspended particle concentration, depth-averaged currents).

Moreover, gliders with bio-optical multispectral sensors also efficiently yielded the concentration, size, and composition of suspended particulate matter together with physical properties of the water column (Niewiadomska et al., 2008). Hence, gliders appeared as valuable tools – together with traditional fixed platforms – to improve our understanding of the still poorly known sedimentary responses to stormy events and to provide validation data sets for models.

Here we present a study combining multiple platforms - including mooring, ship, satellite and glider data - to assess the shelf sediment dynamics and transport as well as the main properties of suspended particles during storm and flooding conditions in the Gulf of Lions (GoL) in the north-western Mediterranean.

6.1.2 Regional settings

During the last decades, the Gulf of Lions has been targeted by numerous observational programs dealing with the present-day particle flux dynamics (Weaver et al., 2006; Durrieu de Madron et al., 2008). Sediment dynamics on this continental shelf is essentially dependent upon sediment inputs from the Rhône River in the northeast and to a lesser extent to several small rivers along the central and western part of the gulf. River inputs, which are essentially active during violent and brief flood events, control the sedimentation rate on the inner-shelf and on prodeltas. These humid events are enhanced by the strong marine winds coming from the East and South-East (E-SE) sectors. Various observational (Bonnin et al., 2008; Bourrin et al., 2008a; Ferré et al., 2005; Guillén et al., 2006; Palanques et al., 2006 and 2008; Ogston et al., 2008; Martín et al., 2013) and modelling (Dufois et al., 2008; Ferré et al., 2008; Ulses et al., 2008a) studies emphasized the role of severe E–SE storms on the transport of sediment in suspension and redistribution of the shelf sediments. The E–SE storms have a marked seasonal impact with a maximum occurrence during autumn and winter, and are often concomitant with flooding of the small rivers. The major sedimentary units (sandy inner-shelf interspersed with muddy river prodeltas, mid-shelf mud belt, and silty-sandy outer-shelf; Fig. 6.1a) reflect the effect of wave and current activity. Observations clearly showed that the sandy inner-shelf primarily results from the impact of waves. Modelling suggested that the strong cyclonic shelf circulation during E-SE storms favors the south-westward dispersal and accumulation of the fine sediment inputs from rivers on the mid-shelf, while it leads to a significant winnowing of the fine sediment on the outer-shelf. This circulation converges towards the SW end of the gulf that is the main exit from the continental shelf (DeGeest et al., 2008).

Most of the observations obtained until now were collected at few fixed points using benthic tripods or mooring lines on the inner shelf and in canyon heads, while there is a lack of observations and knowledge about the continuity of particle transport and sediment dynamics across the mid and outer-shelf. Moreover, since this transport primarily occurs during storms, there is a specific need to collect data during energetic conditions to better document the variability of suspended particles properties and quantify the water and solid transports across the entire shelf to assess the estimations based on modelling.

6.1.3 Presentation of the experiment

A dedicated study was conducted in the south-western part of the GoL shelf (Fig. 6.1a), where it narrows and most of the suspended sediment transport converges during E-SE storms and river floods. The study area presents contrasted sedimentological features with: (i) a sandy inner-shelf interspersed with rocky outcrops and muddy prodeltas next to river mouths, and (ii) a mid-shelf mud belt between 40 and 90 m, and (iii) coarser sediment with sandy patches on the outer-shelf between 90 and 200 m water depth around the Cap de Creus and Lacaze-Duthiers canyon heads. The mid shelf mud belt is characterized by a fine sediment fraction > 50%, ranges between 4 and 26 km from the coast (Fig. 6.1b). The overall experiment lasted 2 months, from 25 February 2011 to 28 April 2011, and enabled to monitor the effect of strong E-SE storms that occurred during the first two weeks of March 2011, and the subsequent flooding of the small coastal rivers. While fixed platforms were used both on the inner shelf (buoy and benthic tripod next to the Têt River mouth) and in the southernmost canyon (mooring lines in the Cap de Creus Canyon head, see Fig. 6.1a), mobile platforms (research vessel, autonomous glider) were also used to sample the entire continental shelf between 15 m and 200 m water depth. Satellite images were used to depict when possible the large-scale distribution of suspended particulate matter in the surface layer.

Based on the datasets collected in the Cap de Creus Canyon by moored instruments, hydrographical profiling and vessel-mounted ADCP, Martín et al. (2013) described the sediment transport along the canyon, with a particular focus on the effect of the E-SE storm events. They showed that most of the along-canyon sediment transport took place along the southern canyon flank and during a relatively short episode (13–15 March) of dominant eastern winds comprising two consecutive storms. During this period, a tongue of cold, freshened and turbid water of shelf origin sank into the canyon along its southern flank to depths up to 350 m. The intruding water was less dense than ambient waters, being pushed beyond its equilibrium depth by the storm-induced downwelling. Sediment transport along the canyon flank associated with that water body was well distributed in a range of 200 m above the bottom. Martín et al. (2013) provided a rough estimation of 1×10^5 tons of suspended sediments being transported into the canyon within the downwelled coastal plume during the 3-day stormy period. Considering that the main contribution of river inputs which flooded during and after the largest storm took place after the major episode of along-canyon sediment transport, they suggested that the erosion of inner shelf sediments by the action of storm waves and currents was likely the primary source of sediments feeding the suspended particle pool of the coastal water plume intruding the canyon.

The present work is complementary to the aforementioned paper and describes a comprehensive set of observations collected on the shelf that aims at assessing (i) the variations of the suspended particle concentration, properties, and transport across the entire shelf width before, during and after stormy and flooding events, and (ii) the impact of the mid-shelf mud belt on the suspended sediment supply during the storm.
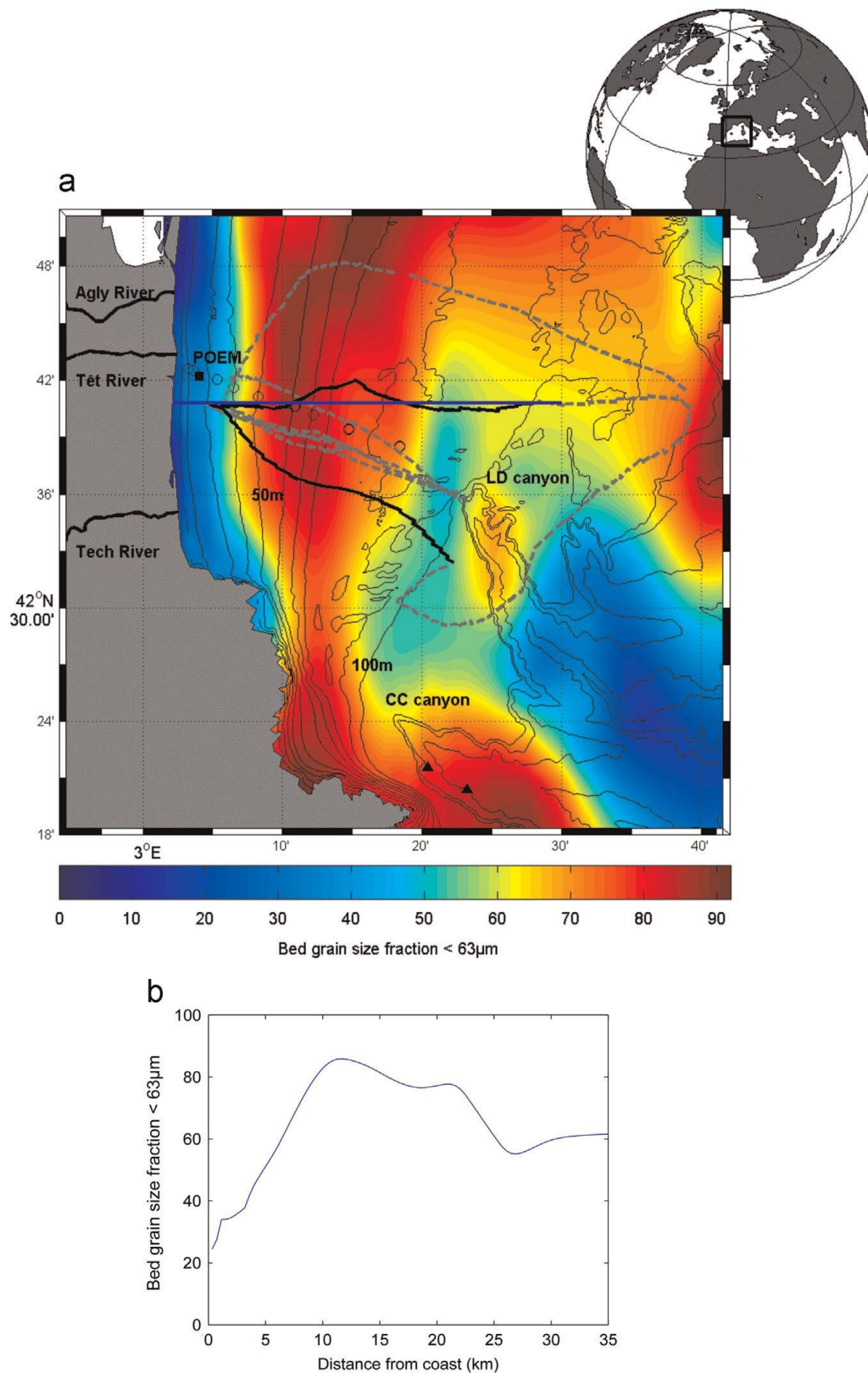
Figure 6.1: (a) Map of the shelf surface sediment characteristics of the southwestern Gulf of Lions around the glider track. The location of the coastal POEM buoy (solid square), the moorings deployed inside submarine canyons (triangles), and the glider track (solid black and dashed grey lines) are also indicated. The black solid lines indicates the part of the sections presented in Figs. 7 and 9 respectively. The E–W projection section is identified by the blue solid line. Isobaths are every 10 m depth. "LD Canyon" and "CC Canyon" labels shows the location of the head of the Lacaze-Duthiers and Cap de Creus canyons respectively. (b) Content of fine sediment (<63µm) in bottom sediment as a function of the distance from the coast along the E–W glider projection section. The mid-shelf mud belt, characterized by a fine sediment fraction >50%, ranges between 4 and 26 km from the coast and lays out between 40 m and 90 m water depths.

6.2 Materials and methods

6.2.1 Oceanographical observations

6.2.1.1 Coastal buoy data

Time series of meteorological parameters (air temperature, wind speed and direction), near-surface temperature-salinity-depth (CTD), turbidity and chlorophyll a (Chl-a), current profiles, waves characteristics, and seabed-level were collected at the POEM (Plateforme d'Observation de l'Environnement Méditerranéen) buoy located at 28 m water depth, 2.5 km off the Têt River mouth (Fig. 6.1a). This buoy has a three-point helicoidal anchoring tightly linked to mid-water depth flotation to prevent any sediment resuspension (Bourrin et al., 2008). It sheltered a seabed area allowing the deployment of benthic instruments and protecting them from trawling activities. Hydrological data were collected at 1 m below the surface using a YSI 6600-EDS CTD probe installed on the buoy. The probe has a CTD sensor and additional optical sensors that measure light backscattering at 880 nm, and fluorescence of Chl-a. Data were recorded every 15 min.

Current and wave data were collected using a 600 kHz Teledyne RDI upward-looking acoustic Doppler current profiler (ADCP) equipped with a wave gauge, deployed on a bottom frame. High-frequency measurements of near-surface wave orbital velocities, surface track, and pressure were used to compute significant wave height (H_s), peak period (T_p) and peak wave direction (D_p) according to the technical manual of Teledyne RD Instruments (2007). Waves were measured during 20 min bursts every 3 h. Currents were measured at 1 Hz in 1 m depth cells from 2 to 27 meters above the bottom (mab), between wave burst measurements and were averaged every 3 h. We used thereafter the following convention for current values: positive northward and negative southward for the along-shelf component, and positive westward and negative eastward for the cross-shelf component.

The maximum bottom shear stress (τ) was calculated using the wave-current combination model developed in Madsen and Wood (2002). Inputs for computation are the maximal wave orbital velocity (U_{mw}) measured during wave burst from the ADCP, wave period (T_p), current velocity (u_z) at 2 m above the bottom and the wave-current angle (ang_{wc}). The bottom was assumed to be flat and bottom roughness was estimated from mean grain-size at the POEM site.

Acoustic backscattered intensities were measured along the four beams of the ADCP. The acoustic pulse emitted from a single beam of the ADCP has a certain initial intensity, which progressively diminishes as it travels through the water column and is reflected from the suspended particles. Suspended particulate matter (SPM) concentrations were derived from acoustic backscattering signal using Sediview software HR Wallingford, based on an iterative method to solve a simplified version of the sonar equation (derived from Thorne and Campbell, 1992 and Hay, 1991):

$$\text{Log10Mr} = \frac{\{dB + 2r\,(\alpha_w + \alpha_s) - K_s\}}{S}$$

where M_r is the mass concentration per unit volume of range r, S the relative backscatter coefficient, α_w is the water attenuation coefficient and α_s the sediment attenuation coefficient, K_s the site and instrument constant and dB the measured relative backscatter intensity corrected for spherical spreading. The signal measured from the four beams were averaged and forced against in-situ gravimetric SPM concentration measurements. Sediment attenuation was estimated using relative effective particle size of 25 µm measured prior to the experiment with an in-situ Sequoia LISST-100 type B (data not shown). Calibration constant K_s and backscatter coefficient S used for the calibration were 35 and 20 respectively.

Seabed elevation data were collected using two NKE Altus 2MHz sonic altimeters deployed on both sides of the buoy's sheltered area. These instruments positioned at ~ 40cm above the bed, were mounted on light tripod frames, whose legs were tightly screwed into the sediment, hence preventing any sediment scouring under the transducer. They enabled to measure seabed level variation with a 0.6 mm resolution and maximum echo-amplitude intensities related to the quantity of suspended sediments.

6.2.1.2 Glider data

The glider-based time series consisted of lines of 25 to 50 km long (Fig. 6.1a) that run across the shelf from the POEM Buoy (28 m water depth) to the shelf edge (100 m water depth) in the vicinity of the Lacaze-Duthiers canyon head (Fig. 6.1a). The autonomous glider was a coastal (30-200 m) Teledyne Webb Research Slocum (Davis et al., 2002) that moved at an average speed of 20–30 cm s^{-1} in a sawtooth-shaped trajectory between 1 m below the surface and 1-2 m above the seabed. Glider diving parameters were adjusted during the mission to drive the glider as near as possible to the bottom without touching the seabed. Near surface (0-1 m) data were solely collected when the glider surfaced, once every 6 dives, for getting new position fix and data transmission. The glider compass measurements were provided by an on-board precision navigation TCM3 (PNI). The calibration of the compass was carried out before and after the deployment and the accuracy of the current estimates is the order of 1 cm s^{-1}. By dead reckoning using the glider compass bearing during the dive, estimates of depth-averaged current were calculated based on the difference between the glider's expected surfacing location and the actual new GPS position (Webb Research Slocum manual, 2005).Given the average horizontal speed, it usually took about 1.5 day to cross the shelf. The glider was equipped with an unpumped Seabird SBE-41CP CTD sensor, 1 WetLabs ECO-BB2FLS bio-optical sensor puck and 1 WetLabs ECO-FLNTU. Temperature and conductivity measurements were corrected for thermal lag effect to avoid salinity bias following the work of Morison (1994) extended by Garau et al. (2011). The ECO-BB2FLS provided light backscattering measured at 2 different wavelengths (532 and 880 nm) and fluorescence of the CDOM (Coloured Dissolved Organic Matter). The ECO-FLNTU provided light scattering at 700 nm calibrated in NTU (Normalized Turbidity Units) and the fluorescence of Chl-a.

The strong southward currents during the storms forced to adjust the trajectory by moving away from the initial straight route to cancel out the drift, thus yielding to curved paths (Fig. 6.1a). The cross-shelf section achieved after the flood period, following the stormy period, was oriented westward because the starting point was located NE of the head of the canyon in an area where lower currents allowed to better control the navigation of the glider. For the sake of consistency and clarity, CTD and optical data along the different glider paths were projected along a W-E section running across the shelf from the coastline, south of the Têt River mouth, to the 100 m isobaths on the outer-shelf (see blue line in Fig. 6.1a). The projection of the observations was carried out according to depth. The projected data were then linearly interpolated to obtain fields with a 1 m vertical resolution and 100 m horizontal resolution.

The glider provided an estimate of the surface to bottom vertically and horizontally averaged velocity (drift) between two surfacings, where its position was precisely determined by GPS. To further characterize the along-shelf current structure along this section, geostrophic velocities were estimated to determine how much the along-shelf flow was affected by the cross-shelf density field and describe the vertical shear in the water column (Pond and Pickard, 1983). The baroclinic component of the geostrophic velocities was first derived using the glider's interpolated density field, and using a zero bottom reference level. The absolute velocity field was subsequently derived by adjusting the depth-averaged geostrophic velocities to the corresponding glider's drift normal to the section interpolated on the same interval as for the geostrophic velocity profiles. The correction from the glider's drift includes the barotropic geostrophic component as well as ageostrophic terms, such as currents induced by surface wind stress and bottom friction.

6.2.1.3 Ship data

Vertical profiling of water column properties was conducted during the CASCADE (CAscading, Storm, Convection, Advection and Downwelling Events) cruise (1-23 March 2011), covering a wide set of coastal, shelf, slope, and basin stations. The casts used in this work are restricted to a section of 9 stations performed along the glider section between 10 and 90 m water depth on 17 March 2011 (see Fig. 6.1a for station locations). Casts were carried out using a Seabird 911Plus CTD probe equipped with a SBE 32 Carousel water sampler. The data included CTD, dissolved oxygen concentration, light attenuation at 660 nm (C-Star sensor), light backscattering at 880 nm (Seapoint sensor), Chl-a fluorescence. The casts were conducted from the surface to less than 1 m above the seafloor. Water samples were collected and filtered on board on 0.45 μm nuclepore filters. Dry weights were used to convert the turbidity signals (expressed in NTU) from POEM subsurface CTD backscattering sensor (Bb, 880 nm), shipboard CTD backscattering sensor (Bb, 880 nm) and glider ECO-FLNTU (Bb, 700 nm) sensor into SPM concentrations (Fig. 6.2). The glider FLNTU sensor directly gives turbidity output in NTU. We used a spatial objective analysis to match turbidity measurements from the glider with calibrated NTU signal from the subsurface CTD backscattering sensor calibrated versus gravimetric measurements each time the glider crossed nearby the buoy. We used a type-II linear regression analysis between SPM and turbidity units to

derive a model to predict SPM concentrations from FLNTU glider sensor. This analysis is implemented in the MATLAB program lscubic.m by E.T. Peltzer (for details, see http://www.mbari.org/staff/etp3/regress.htm). This model reduces the uncertainty for estimations of low turbidity values.
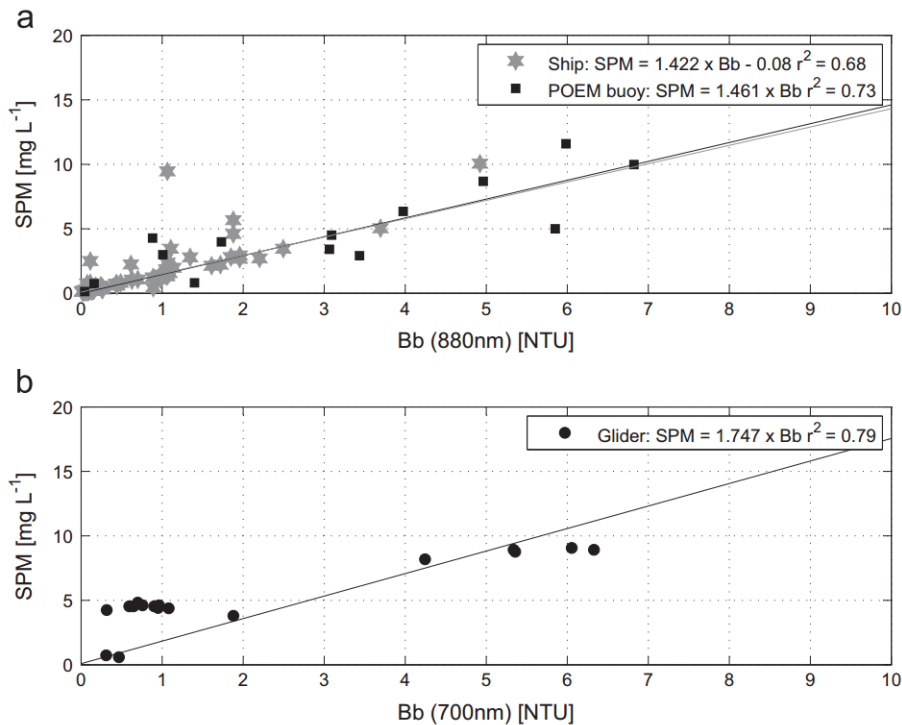
Figure 6.2 . Calibration of water turbidity data, recorded by optical backscattering sensors (OBS), versus suspended sediment concentrations. Top: backscattering sensor at 880 nm from subsurface POEM buoy (YSI OBS) and ship-board CTD (Seapoint OBS). Bottom: backscattering sensor at 700 nm from glider (Wet-Labs FLNTU)

6.2.1.4 Canyon mooring data

Two instrumented mooring lines were deployed during the CASCADE cruise (3-21 March 2011) along the western flank of the Cap de Creus Canyon at depths of 290 m and 365 m respectively (Fig. 6.1a). Both lines were equipped with a downward-looking 300 kHz RDI ADCP at 160 mab), three Seapoint backscattering sensors (OBS at 880 nm) at 10, 75 and 115 mab respectively, and a Seabird SBE 37-SMP CTD probe at 8 mab. Results from these moorings are described in detail in Martin et al. (2013). The OBS sensor at 10 mab was calibrated using the generic equation from Guillén et al. (2000), which is based on statistical analysis of different sets of turbidity data from the same region.

6.2.2 Ancillary data

6.2.2.1 River data

Hourly water discharges of rivers opening to the Gulf of Lions (Rhône, Hérault, Orb, Aude, Agly, Têt, Tech, Fig. 6.3b) were measured by gauging stations located near river mouths and provided by the Compagnie Nationale du Rhône and the French national data bank ''HYDRO'' (http://www.hydro.eaufrance.fr/accueil.html). Solid discharges were estimated using updated calibrations for each river based on the work of Bourrin et al. (2006) (Sadaoui M., personal communication). Sources of Hérault, Orb and Aude rivers are located in the Massif Central and sources of Agly, Têt and Tech in the Pyrenees. When pooled, they are thereafter referred in the text as "Central", "Pyrenean" and Rhône rivers (Fig. 6.3b).

6.2.2.2 Satellite data

Spatial maps of daily SPM concentrations (Fig. 6.3a), with a 1 km resolution, were obtained by merging products from Moderate Resolution Imaging Spectroradiometer (MODIS) on Aqua satellite and Medium-spectral resolution, imaging spectrometer (MERIS) on Envisat satellite. Products, analysis and calibrations used were provided by IFREMER Nausicaa services and OC5 IFREMER algorithms for SPM and Chl-a concentrations estimations from Gohin and Stanev (2011).
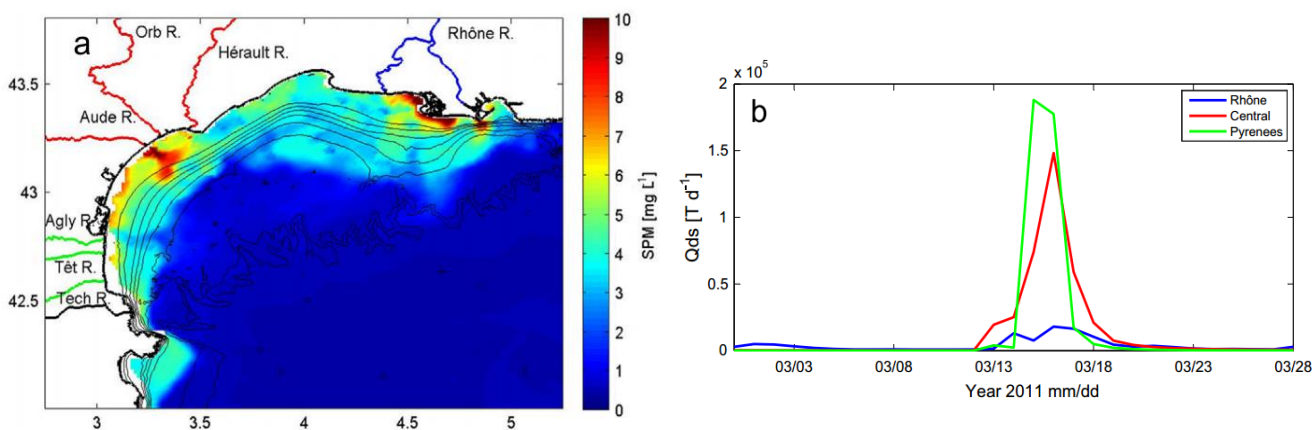
Figure 6.3 . Left: Satellite picture of suspended particulate matter in the Gulf of Lions during 19 March 2011 showing the river turbid plumes along the Gulf of Lions coast. The picture is a merge product from MODIS and MERIS provided by IFREMER Nausicaa. Right: Daily solid discharges from rivers. The central cluster combines the Hérault, Orb and Aude rivers, and the Pyrenean cluster combines Agly, Têt and Tech rivers.

6.2.3 Derivation of particle properties

Glider based WET-Labs ECO sensors FLNTU (λ=700nm) and BB2FLS (λ= 532 and 880 nm) where used to derive the particulate backscattering coefficients (b_{bp}), and to approximate the mean particle size. WET-Labs ECO sensors gave the scattering [$\beta(\theta)$] at one angle (117 and 140 deg for BB2FLS and FLNTU sensors respectively from Sullivan et al., 2010) in the backward direction. While the BB2FLS sensor directly gave the total scattering [$b_b(\lambda)$] for each wavelength, the FLNTU sensor was factory calibrated in NTU output. The total scattering was then extracted from the raw NTU signal by multiplying by the Beta Scale Factor. This factor was obtained by multiplying the NTU Scale Factor by a coefficient (0.0025 for this FLNTU unit). The particulate backscattering coefficients at each wavelength [$b_{bp}(\lambda)$] was then calculated from the particulate scattering [$b_p(\lambda)$] by subtracting the scattering due to pure water from the relation described in Morel (1974).

In marine waters, the spectral slope of the particulate scattering in visible and near infra-red decreases monotonically with increasing wavelength and is approximated by a hyperbolic model: $b_{bp}(\lambda) \sim Ac \times \lambda^{-\gamma}$, where γ is the spectral slope and Ac is the corresponding amplitude (Boss et al., 2001a, 2001b). The size dependence of the number of particles, N(D), can be described by a the power-law function $N(D) = N_0 (D/D_0)^{-\xi}$, and has a mean particle size $\approx D_{min} \times (1-\xi)/(2-\xi)$ with D_{min} being the minimum observable particle size. Boss et al. (2001a) reported a relationship between the exponent ξ and the spectral slope γ, namely $\xi = \gamma + 3 - 0.5 \exp(-6\gamma)$. The mean particle size thus increases with decreasing ξ, and hence the spectral slope γ (the lower the γ, the higher the contribution of large particles to the total number of particles, and reciprocally). Loisel et al. (2006) exemplified the use of γ from satellite remote sensing of the global ocean as an index characterizing the contribution of small versus large particles size to the total particulate assemblage. In the present study, we applied this method to derive an index of the overall particle size repartition in the coastal area from glider-based measurements. The spectral slope, , γ is calculated as the slope of the linear regression between $\log_e(b_{bp}(\lambda))$ and $\log_e(\lambda)$ [i.e. $\log_e(b_{bp}(\lambda)) = \log_e(Ac) - \gamma \times \log_e(\lambda)$] and using λ = 532, 700 and 880 nm (Fig. 6.4). In the present study, we applied this method to derive an index of the overall particle size repartition in the coastal area from glider based measurements.
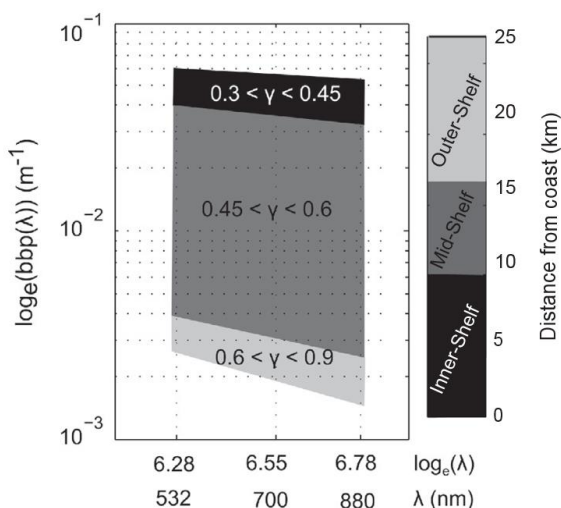
Figure 6.4 . Example of spectral slopes of backscattering coefficient (γ), for the inner, mid and outer-shelf. This coefficient is calculated as the slope of the linear relationship between $\log_e(b_{bp}(\lambda))$ and $\log_e(\lambda)$ [i.e., $\log_e(b_{bp}(\lambda)) = \log_e(Ac) - \gamma \times \log_e(\lambda)$], estimated for λ = 550, 700 and 880 nm.

6.3 Results

6.3.1 Meteorological and hydrodynamical conditions

Wind, waves, and currents – Time series of meteorological and wave data recorded by the POEM coastal buoy during winter 2010–2011 are shown in Fig. 6.5. A period of sustained NW winds (Tramontane) with speeds up to 15 m s^{-1} occurred in late February 2011 prior to the start of the experiment (Fig. 6.5a). During the first 2 weeks of March, winds veered from the northwest to the southeast (marine winds). Three successive south-eastern storms occurred during March, peaking on 8, 13 and 15 March 2011 with maximum significant wave heights (H$_s$) of 3.2, 4.6 and 3.7 m (Fig. 6.5b) and maximum wave peak periods (T$_p$) of 9.4, 9.7 and 10.1 s respectively (Martín et al., 2013). These wave conditions correspond to typical winter storms in the region (Guizien, 2009). The 13 March storm was the most remarkable of the three in terms of wave energy, particularly in the central part of the GoL, its effects being comparatively milder in its south-western sector (DREAL, 2011). On the inner-shelf, strong southward along-shore currents with maximum speed of 55 cm s^{-1} prevailed during the stormy period (Fig. 6.5c).

Rivers discharges and plumes – River solid discharge for the different rivers of the Gulf of Lions during winter 2010–2011 are shown in Fig. 6.3b. The sustained SE winds from 12 to 16 March pulled a Mediterranean humid air mass towards southern France, forcing precipitation by orographic control on the Massif Central and above all on the Pyrenees. In contrast, precipitations were abnormally weak on the Rhône watershed (Eau France, 2011). As a consequence, the contribution of western rivers to the total solid discharge in the GoL was unusually high, accounting for up to 85 % during this event, contrasting with a usual annual contribution of only 10 % (the rest corresponding to the Rhône River alone). The highest solid discharges of coastal rivers were measured on 16 March with a maximum of 1.9 and 1.5 x 10^5 t d^{-1} respectively for Pyrenean and Central Rivers compared to a maximum of 0.2 x 10^5 t d^{-1} for the Rhône River (Fig. 6.3b). The river plumes were clearly seen on satellite picture (Fig. 6.3a), and their coalescence due to the apparent cyclonic along-shore flow formed a large turbid ribbon covering the inner and middle shelf.

In the study area, the Têt River water and solid discharges peaked at 728 m^3 s^{-1} and 4 t d^{-1}, respectively (Fig. 6.5f). While subsurface temperature did not show any significant change (Fig. 6.5d), the arrival of fresh and turbid water shortly after the peak of the flood was measured at the POEM buoy with subsurface salinity down to 20 (Fig. 6.5e). A first significant peak of SPM concentration (up to 15 mg L^{-1}) was observed the 13 March associated to a small increase of the river discharge but the maximum of SPM concentration was observed immediately after the flood peak with values up to 50 mg L^{-1}. No significant change in the subsurface Chl-a content was observed during and after the flood except the 28 March probably due to biofouling effect on the probe.
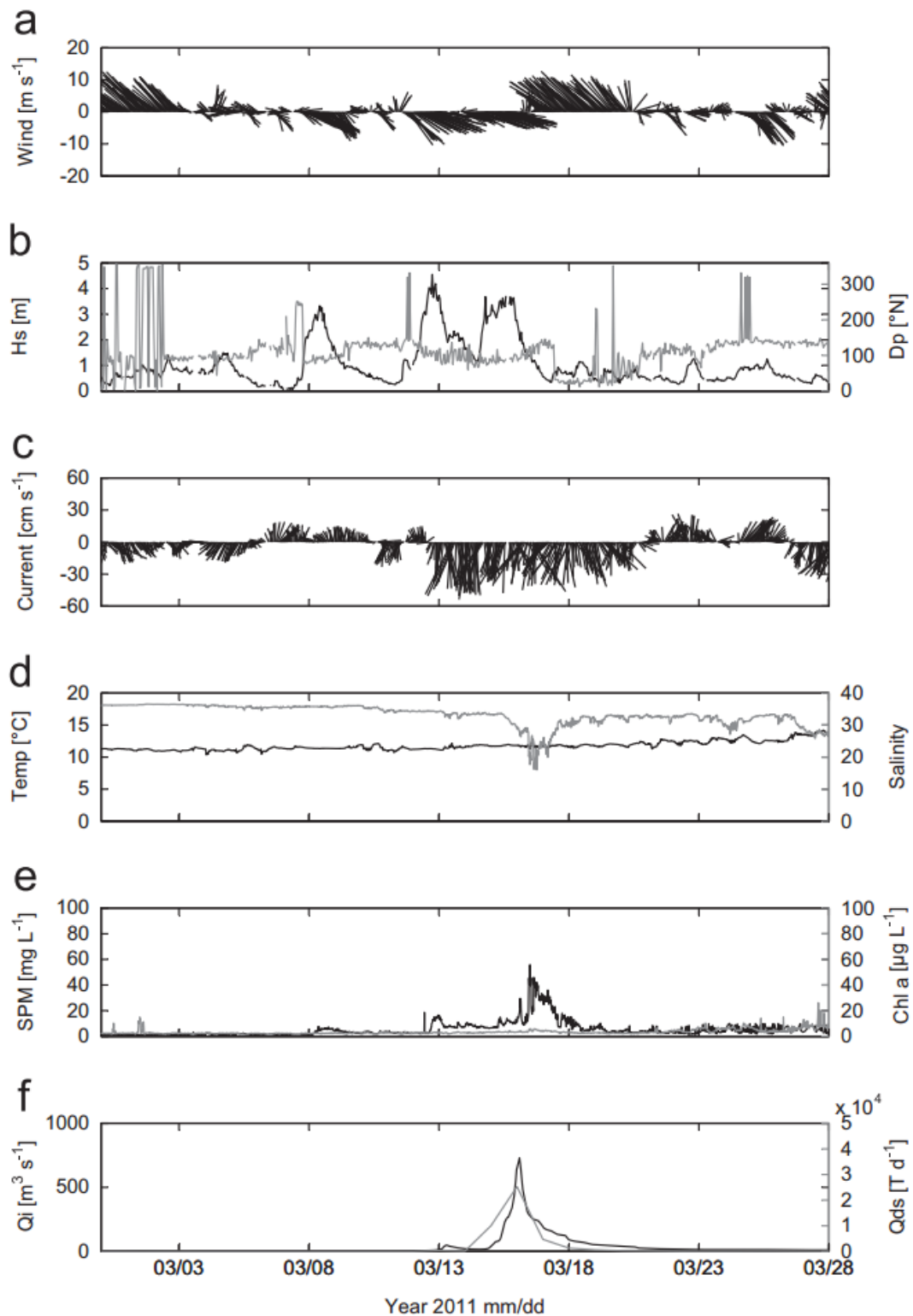
Figure 6.5 : Time-series of atmospheric and oceanographic conditions at the POEM station and discharges from the Têt River between late February and late March 2011. (a) wind, (b) significant wave height (Hs; black) and peak wave direction (Dp; grey), (c) depth-averaged current, (d) subsurface temperature (black) and salinity (grey), (e) subsurface SPM (black) and Chlorophyll-a concentration (gray), (f) daily Têt river liquid (Qi; black) and solid (Qds; gray) discharges. By convention wind direction indicates its origin, while current direction points at its destination.

6.3.2 Shelf hydrodynamics and suspended particulate matter transport during the storm and the subsequent flood

6.3.2.1 Fixed observations at the coastal station

ADCP-derived profiles of current and SPM concentrations at the POEM buoy are presented in Fig. 6.6. Current speed is generally relatively homogenous all over the water column with average speed of about 10-20 cm s^{-1} (Fig. 6.6a, b), except during the E-SE storm period where current peaked at 55 cm s^{-1} (Fig. 6.6a, b). Current direction alternately veered from northward to southward during the measurement period and was straight southward during the stormy period (12-16 March). Total (combined wave and current-induced) bottom shear stress showed the occurrence of three stormy events with strong stress values. The last two storms on the 12-13 March and 14-15 March peak at 6.8 and 7.9 Pa respectively (Fig. 6.6c).

Prior to the storms, SPM concentration profiles showed a bottom turbid layer of about 10 m thick with concentration varying from 5 mg L^{-1} at the upper limit of the turbid layer to 13 mg L^{-1} at 2 mab. During the storms, SPM concentrations increased up to 40 mg L^{-1} close to the seabed, and the bottom turbid layer sometimes extend up to 20 mab (Fig. 6.6d). The along- and cross-shore particle transport remained low during the first storm on the 8-9 March, due to moderate stress associated to this event, but strongly increased up to – 20 kg m^{-2} h^{-1} in the along-shore direction (toward the south) for the following storms (Fig. 6.6e). Seabed elevation measurements and near-bottom echo amplitude from the ALTUS altimeters indicated a significant erosion of the seabed between 25 and 40 mm (Fig. 6.6f), and a significant increase of the backscattering intensity (Fig. 6.6g) during the E-SE stormy period (12-16 March). It seems that the seabed level rose back to its original level immediately after the storm.

6.3.2.2 Cross-shelf observations

The glider permitted to characterize the hydrological and hydrodynamical conditions across the shelf during the two strongest storms (12-13 March and 14-15 March). These two sections showed comparable structures, and the results from the latter section are presented in Figure 6.7. The inner and mid-shelf were occupied by a core of colder, fresher but slightly denser water, forming in its distal part a thick bottom wedge reaching depth up to 90 m, underneath a lens of lighter water spanning over the outer-shelf. A density front thus separated the denser water on the inner and mid-shelf from the warmer, saltier, and lighter water on the outer-shelf. Further off-shore appeared typical warmer, saltier slope water getting onto the shelf. A bottom nepheloid layer 20-30 m thick with particulate concentrations up to 40 mg L^{-1} near the coast, and < 5 mg L^{-1} on the outer-shelf was associated to the coastal plume of denser water. Moderate Chl-a concentrations (up to 2 μg L^{-1}) appeared in both the surface layer and the bottom layer close to the inner shelf (up to 50 m deep). The current profiles at the POEM buoy (Fig. 6.6a, b) and along the cross-shelf section (Fig. 6.7c) indicated a relative vertical homogeneity of the velocity of currents during the storm.
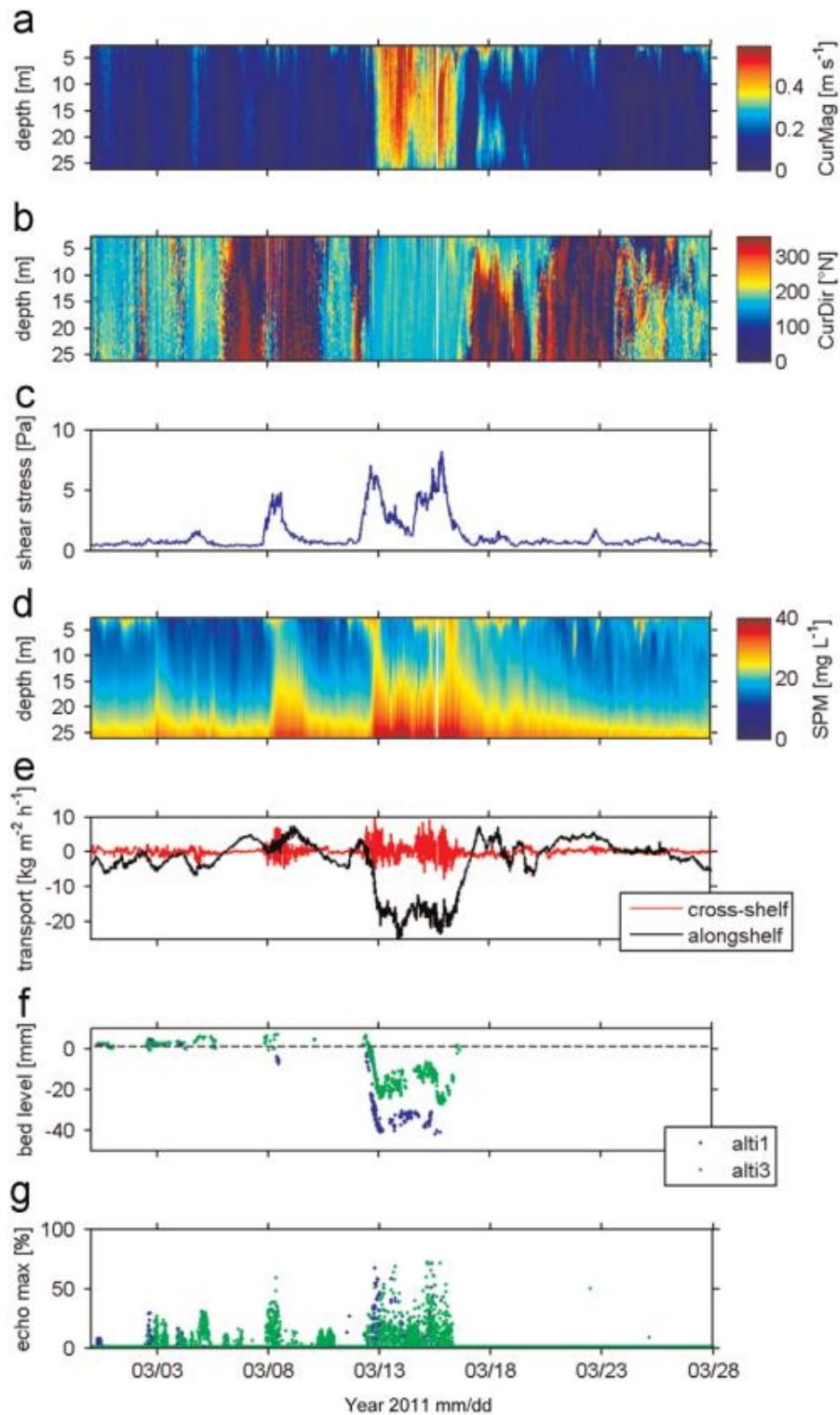
Figure 6.6 : Bottom-mounted ADCP and altimeters measurements at the POEM station between late February and late March 2011. (a) Current magnitude, (b) current direction, (c) bottom shear stress, (d) suspended sediment concentration derived from ADCP backscattered intensity (e) particulate transport in the cross-shelf (red, + eastward and - westward) and along-shelf (blue, + northward and - southward) directions, (f) seabed elevation, and (g) altimeter backscattered intensity (maximum echo amplitude).

Based solely on the depth-averaged currents estimated from the glider drifts, the cross-shelf and along-shelf vertically averaged components of the currents, water and particle transports across the shelf during the storm are presented in Figure 6.8.

The cross-shelf current and transport components, which were low at the POEM buoy at a water depth of 28 m (Fig. 6.6e), were oriented off-shore with a maximum on the mid-shelf (water depths between 30 m and 80 m), and vanished again on the outer-shelf. The instantaneous cumulated northward cross-shelf transport of water and particles on the inner and mid-shelf during the storm amounted to 6 x 10^5 m^3 s^{-1} and 0.5 t s^{-1} respectively (Fig. 6.8 b,c). The along-shelf current component was always southward with maximum speeds near the coast, and minimum speeds for water depths between 70 and 80 m depth at the level of the core of lighter water (Fig. 6.7c).

The along-shelf transport of water increased with the water depth and was maximum on the outer-shelf. However, the along-shelf transport of particle was maximum on the inner and mid-shelf, and the instantaneous cumulated along-shelf transport of water and particle throughout the section amounted to − 95 x 10^5 m^3 s^{-1} and − 3.9 t s^{-1} respectively.

Values of depth-averaged current, water transport and particle transport at the POEM site based on ADCP measurements at 28 m depth are reported in Figure 6.8 and are of the same order than glider estimated values at the coast. Considering an area of about 3.75 x 10^4 m^2 between the coast and the glider covered area, southward depth-averaged current, water and particulate transport are estimated to − 0.41 m s^{-1}, − 1.5 x 10^4 m^3 s^{-1}, and − 0.21 t s^{-1} respectively.
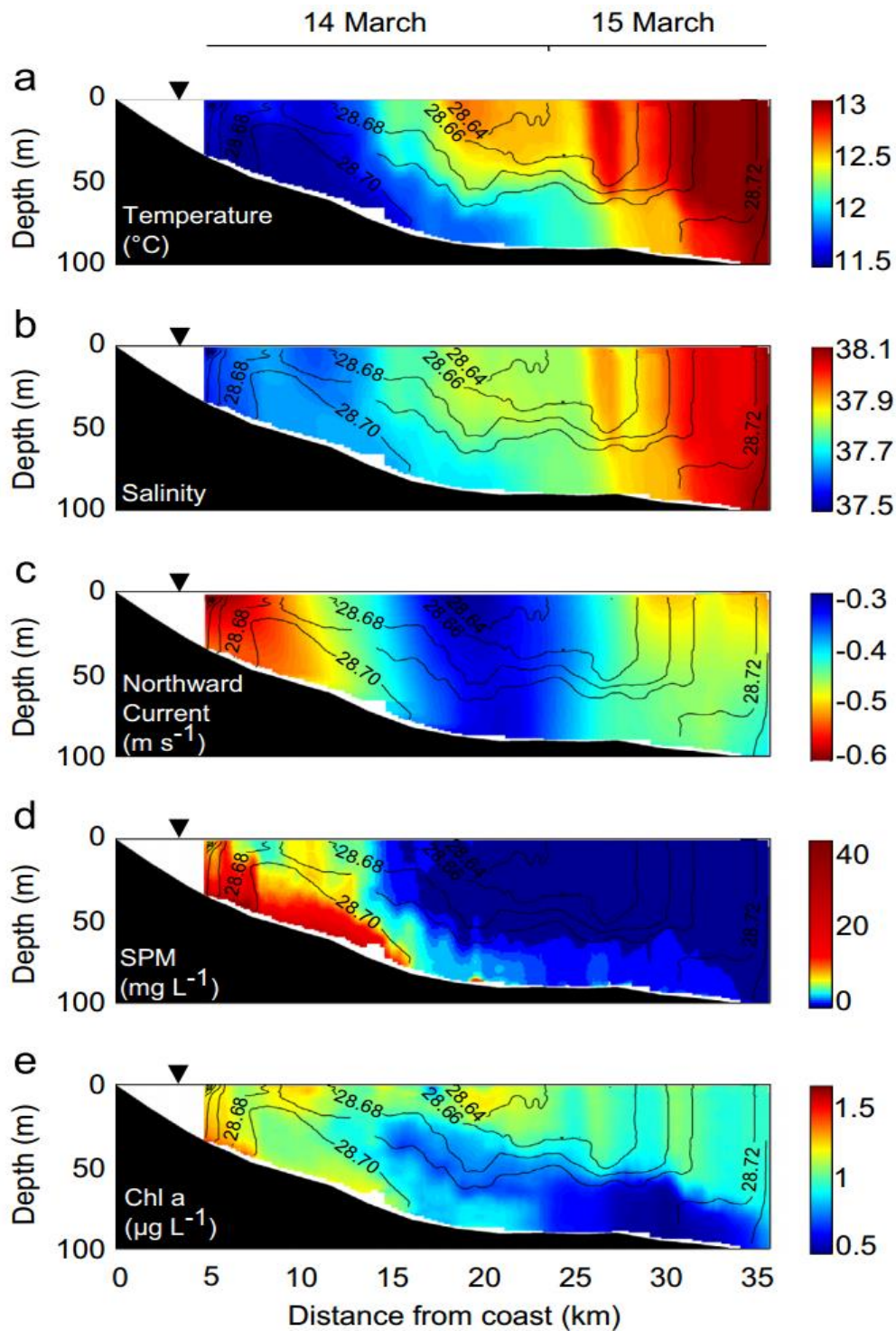
Figure 6.7 : Cross-shelf hydrography between the POEM coastal buoy (triangle on top of each panel) and offshore along the projected transect (blue line in Fig. 1) based on glider measurements during a E-SE storm (14–15 March 2011). (a) Temperature, (b) salinity, (c) along-shelf current velocity (+ northward, - southward), (d) suspended particulate matter concentration, and (e) Chlorophyll-a concentration. The contour-lines on each figure represent isovalues of the density anomaly sigma-theta.
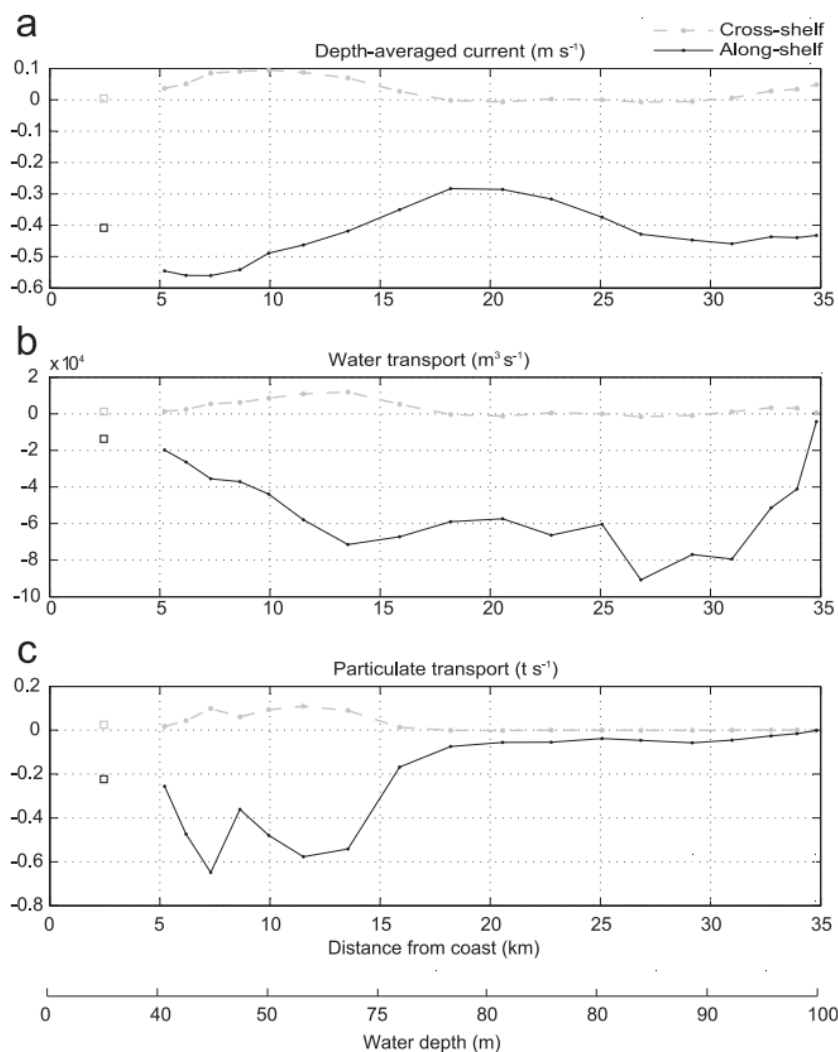
Figure 6.8 : Cross-shelf and along-shelf components of (a) depth-averaged current, (b) water transport, (c) suspended particles transport derived from glider measurements during the storm (14–15 March 2011). The values at a distance of 2.5 km off the coast are derived from the bottom-mounted ADCP measurement at the POEM station (squares).

A four-day flood (15 - 18 March) followed the stormy period (Fig. 6.5f). A glider section was performed at the end of the flooding period (19 - 20 March), and the observed hydrographical conditions are presented in Figure 6.9. Significant changes were observed with respect to the stormy conditions. The offshore end of the Têt River freshwater surface plume was clearly visible 4 to 7 km off the coast, and corroborated the observations at the POEM buoy (Fig. 6.5d, e and f). The influence of freshwater inputs from river upstream of the study area was detected at the surface as far as 20 km off the coast (taking the isohaline 37.5 or isopycnal 28.6 kg m^{-3} as upper limits). A sharp density front separating the main region of freshwater influence and offshore water appeared around 10 km off the coast. Suspended particle concentrations were drastically lower than during the stormy period, and the highest concentrations (up to 5 mg L^{-1}) were confined to the Têt River plume. A diffuse bottom nepheloid layer about 10 m thick extended over the inner and mid-shelf. Chl-a concentrations showed highest values (up to 2 µg L^{-1}) close to the coast in a subsurface layer extending across the region of freshwater influence.
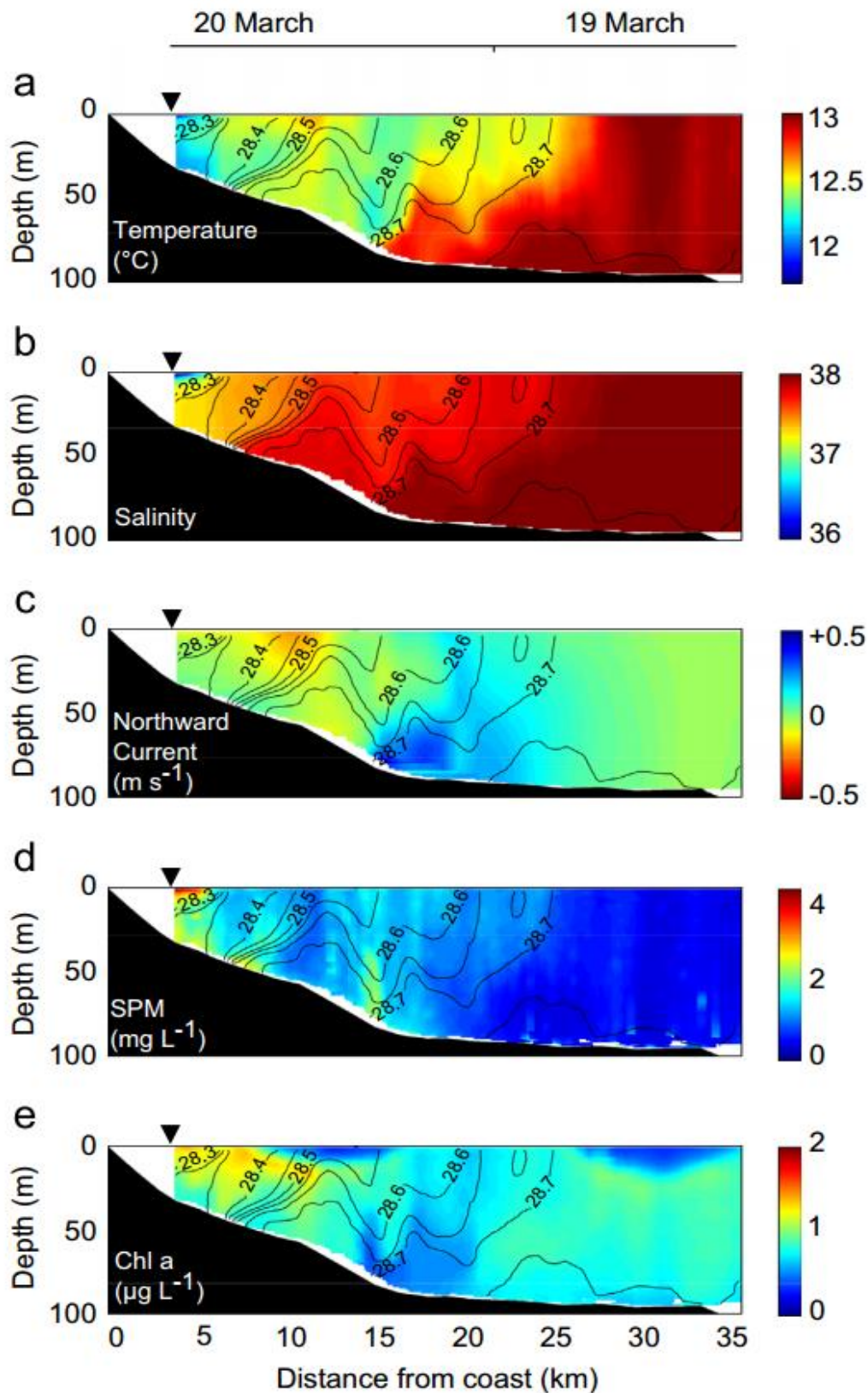
Figure 6.9 : Cross-shelf hydrography between the POEM coastal buoy and offshore along the projected transect (blue line in Fig. 1) based on glider measurements during and after the flood (19–20 March 2011). (a) temperature, (b) salinity, (c) along-shelf current velocity, (d) suspended particulate matter concentration, and (e) Chlorophyll-a concentration.

The cross-shelf and along-shelf vertically averaged components of the currents, water and particle transports across the shelf after the flood are presented in Figure 6.10. Cross-shelf current, as well as water and particulate transports increased seaward from the coast. The instantaneous cumulative cross-shelf transport of water and particles on the inner and mid-shelf amounted to 1.7 x 10^5 m³ s^{-1} and 0.2 t.s^{-1} respectively. The along-shelf component of the current and transports were close to zero on the inner shelf. They increased and were oriented southwards on the mid-shelf, due to strong geostrophic currents at the level of the density front, and reversed farther seaward. Hence, the instantaneous cumulated along-shelf water and particulate transport across the section nearly cancelled out and amounted to 1.0 x 10^5 m³ s^{-1} and 0.1 t s^{-1} respectively. Values of depth-averaged current, water transport and particulate transport at the POEM site based on ADCP measurements at 28 m depth are reported in Figure 6.10 and are of the same order but significantly bigger than glider estimated values at the coast: − 0.12 m s^{-1}, − 0.4 x 10^4 m³ s^{-1}, and − 0.02 t s^{-1} respectively.
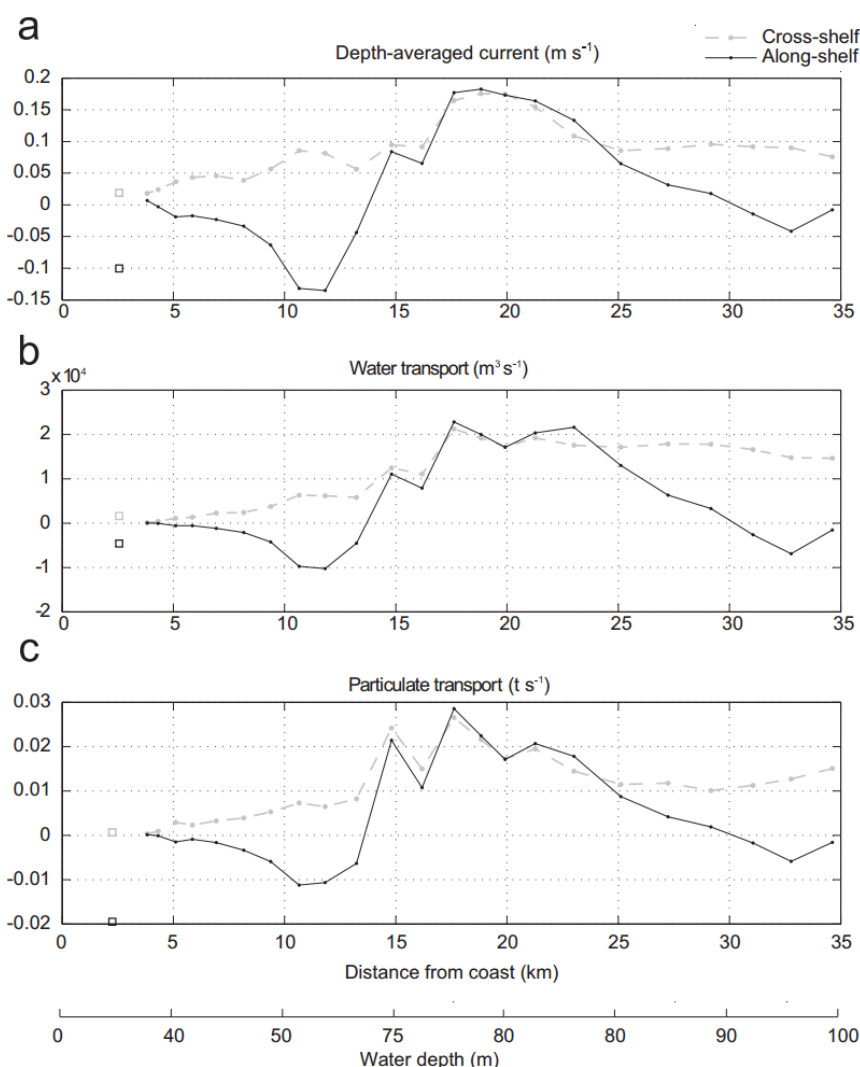
Figure 6.10 : Cross-shelf and along-shelf components of (a) depth-averaged current, (b) water transport, (c) suspended particle transport derived from glider measurements made during and after the flood (19–20 March 2011). The values at a distance of 2.5 km off the coast are derived from the bottom-mounted ADCP measurement at the POEM station (squares).

Time series of cumulative water and particulate cross-shelf and along-shelf transports for the different glider sections performed between early March to late March are presented in Figure 6.11 a, b. Strong southward along-shelf transports prevailed during the stormy period with maximum cross-shelf and along-shelf transport ($+ 0.5$ and $- 3.9$ t s^{-1} respectively) during the 14-15 March storm. Both transport components dropped markedly afterwards, while exhibiting a weak northward along-shelf transport. Cumulative particle transport was normalized by the surface of the glider section to compare with ADCP transport measurements of Fig. 6.6e and is shown in Fig. 6.11c. ADCP-derived cumulative transport was also maximum during the storm with peak values of $+ 5$ and $- 25$ kg m^2 h^{-1} in the cross-shelf and along-shelf directions, while glider derived cumulative transport show values of $+ 1$ and $- 6$ kg m^2 h^{-1} respectively
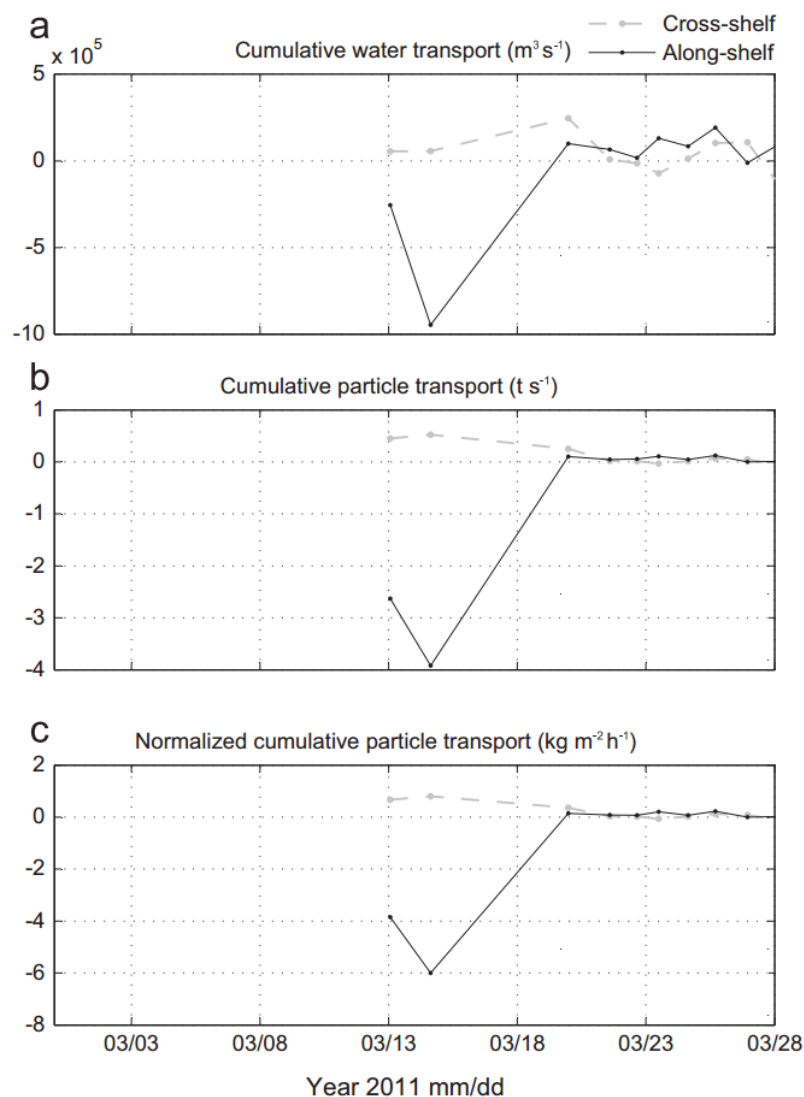
Figure 6.11 : Cumulated water (a) and particle (b) transports along the glider's cross shelf section between mid-March to late March 2011 (see Fig. 6.1 for the transects location). (c) Cumulative along and cross-shelf particle transport estimated from bottom-mounted ADCP measures at the POEM station.

6.3.2.3 Canyon observations

The impact of the storms was simultaneously observed at the coastal POEM site and the Cap de Creus Canyon head (Fig. 6.12). During the stormy period (13 - 15 March) the potential temperature at 8 mab within the canyon head rapidly decreased from 12.8 °C to 11.5 °C, which was approximately the same temperature observed on the shelf (Fig. 6.12c). After the storms, the canyon head potential temperature increased to its pre-storm value. The impact of the storms was also shown by the salinity signal within the canyon head, which slightly decreased during the stormy period from 38.2 to 37.8 and returned to previous values after the storms (Fig. 6.12d). Subsurface salinity at the coast decreased rapidly from 35.5 to 16 during the flooding period but no corresponding change was observed inside the canyon during the same period. Current magnitude (Fig. 6.12e) both at the coast and in the canyon head increased rapidly during the storms and reached maximum values of 50 and 90 cm s^{-1} respectively. Currents were southward at both sites during the consecutive stormy events (Fig. 6.12f). The near-bottom SPM concentrations at the coast increased to 20 mg L^{-1} during the first storm (8 March), but no change was observed in the canyon head (Fig. 6.12g). The SPM concentrations increased again at the coast during the following storm (13 March) and remained at values between 15 and 35 mg L^{-1} until the 21 March. In the canyon head, a first increase of SPM concentrations up to 25 mg L^{-1} was observed about 12 h after the storm peak of the 13 March, and the second increase up to 50 mg L^{-1} was reached concomitantly during the third storm peak on the 15 March.

6.3.3 Suspended particle properties

Optical properties of suspended particles during the last storm (14-15 March 2011) and after the flood (18-21 March) are presented in Figures 6.13 and 6.14 respectively. During the stormy period (Fig. 6.13), suspended particles on the inner shelf displayed the largest total backscattering signal (b_{bp} at 700 nm) with values between 0.05 and 0.45 m^{-1}. These coastal particles were also characterized by high Chl-a concentrations with values between 1 and 1.2 µg L^{-1}. Contrarily, particles further offshore presented a weaker total backscattering signal (< 0.03 m^{-1}) and lower Chl-a concentrations (< 0.8 µg L^{-1}) (Fig. 6.13a). Coastal particles presented lower values of γ index (< 0.5) than the offshore particles (> 0.7) (Fig. 6.13b).

After the flooding period (Fig. 6.14), the total backscattering signal was relatively low (< 0.05 m^{-1}), with respect to the stormy period. Coastal particles exhibited the highest backscattering signal (∼ 0.05 m^{-1}) and Chl-a concentrations (up to 1.6 µg L^{-1}) (Fig. 6.14a). Coastal particles also presented slightly lower values of γ index (< 0.6) than the offshore particles (0.7 - 0.8) (Fig. 6.14b).
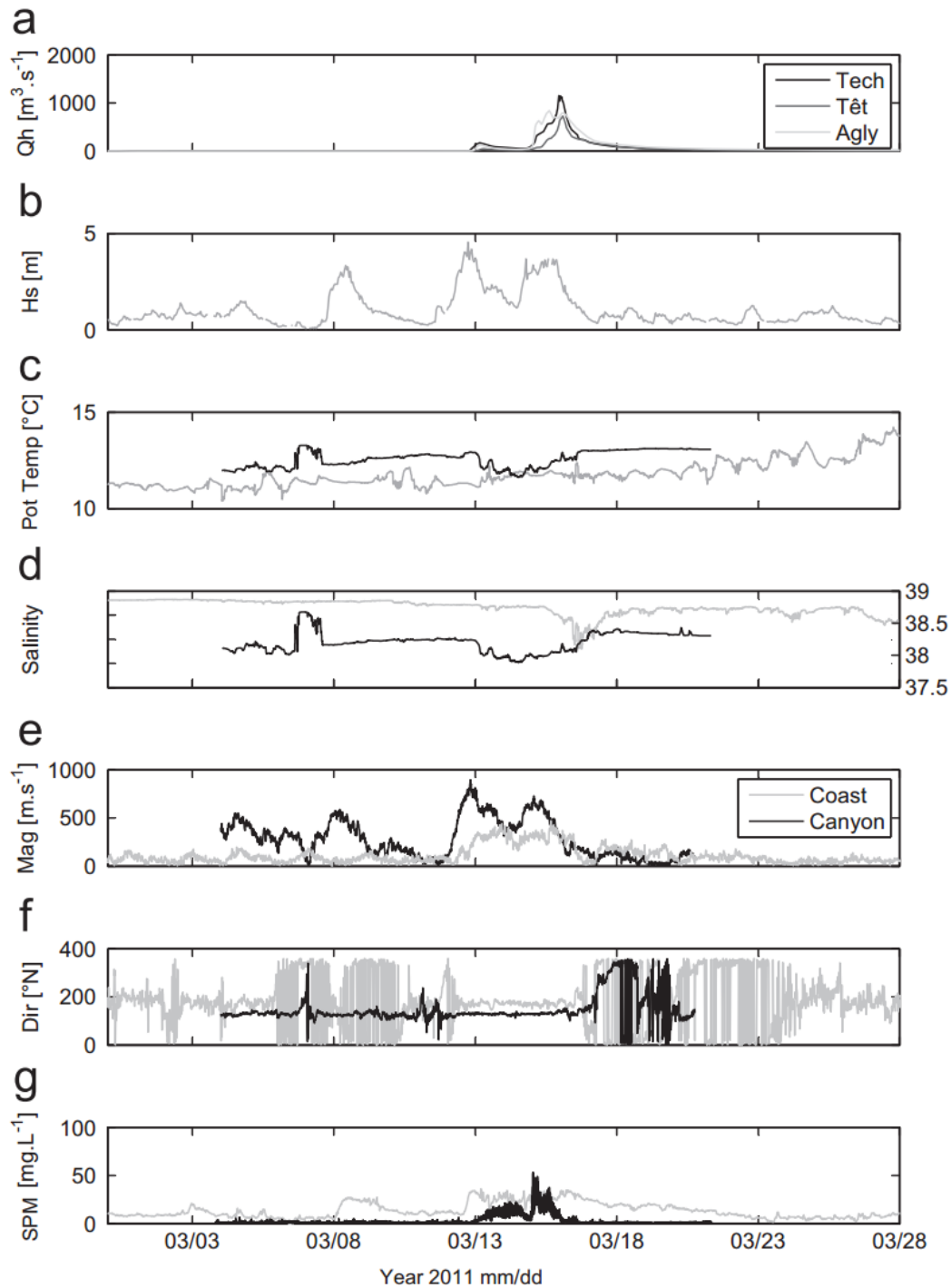
Figure 6.12 : Simultaneous data time-series from the POEM site at 28 m depth and the Cap de Creus Canyon head at 265 m depth: (a) hourly river discharge of Pyrenean coastal rivers, (b) significant wave height at the coastal site, (c) potential temperature at the coast (black, sub-surface CTD) and in the canyon (grey, CTD 8 mab at 265 m depth), (d) salinity at the coast (black, sub-surface CTD) and in the canyon (grey, CTD 8 mab at 265 m depth) (e, f) current magnitude and direction from ADCPs (black, 2 mab at 28 m depth; grey, 160 mab at 265 m depth), (g) SPM concentrations (black, ADCP-derived at the coast and grey, OBS-derived, 10 mab at 265 m).
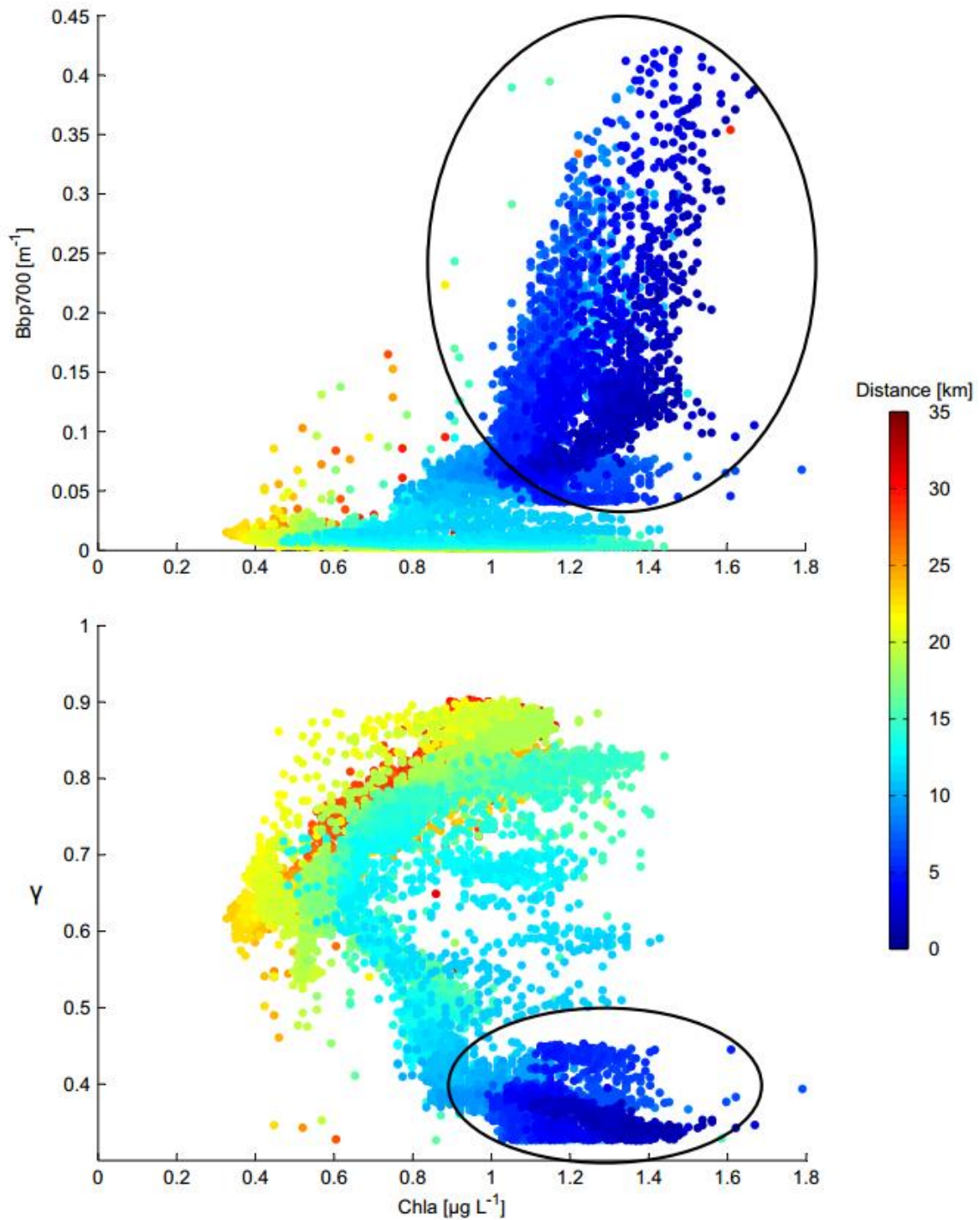
Figure 6.13 : Optical properties of suspended particles during the storm (14–15 March 2011). Top: scatter plot of Chl-a concentrations versus particulate backscattering (bbp) at 700 nm as a function of distance from the coast. Bottom: scatter plot of Chl-a concentrations versus γ index as a function of distance from the coast. The black circles show the characteristics of particles inside the storm bottom nepheloid layer.
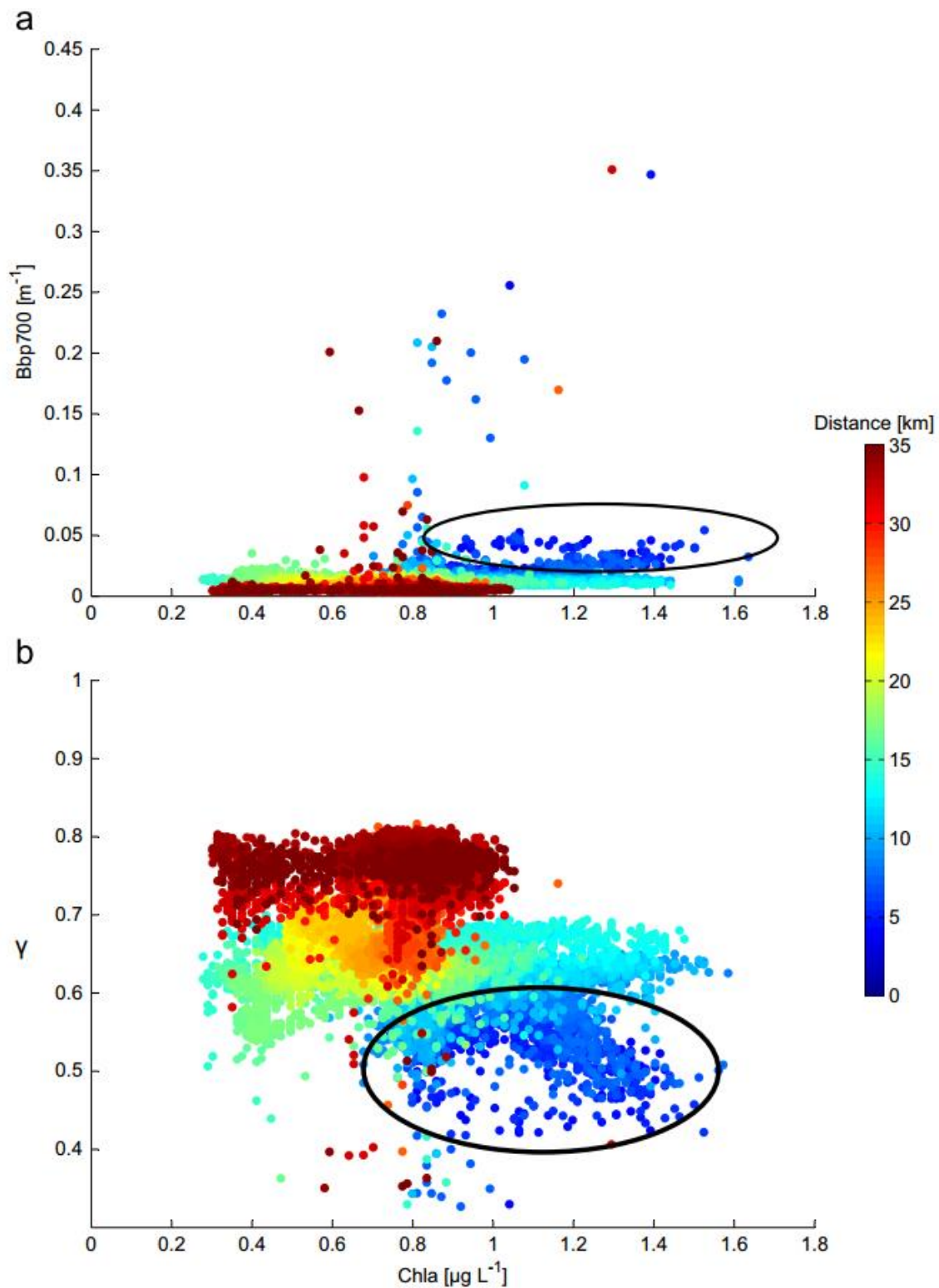
Figure 6.14 : Optical properties of suspended particles after the flood (19–20 March 2011). Top: scatter plot of Chl-a concentrations versus particulate backscattering at 700 nm as a function of distance from the coast. Bottom: scatter plot of Chl-a concentrations versus γ index as a function of distance from the coast. The black circles show the characteristics of particles inside the flood bottom nepheloid layer and the surface river plume.

6.4 Discussion

6.4.1 Variability of hydrological structures and suspended particulate matter transport

Back-to-back storm and flood events are a typical feature in the Gulf of Lions, and are designated as "wet storms" (Guillén et al., 2006). However their impact on the shelf hydrology, hydrodynamics and particle transport have been barely documented because weather conditions are usually too energetic for seagoing missions. The few studies that described sediment transport during such events were carried out from bottom-mounted instruments deployed on the inner shelf close to the Têt (Guillén et al., 2006; Bourrin et al., 2008a, b) or the Rhône (Marion et al., 2010) river mouths.

The present measurements at the POEM buoy and across the shelf during the storms and after the flood show a very rapid change, within a few days, of hydrological structures on the inner and middle shelf. The core of dense coastal water present at the end of February / early March is typical of winter conditions during which cold and dense water is formed along the coast of the GoL under the influence of strong northerly winds. These dense waters spread towards the south-eastern end of the GoL and are mainly exported to the northern Catalan shelf or the continental slope in the vicinity of the Cap de Creus Canyon (Ulses et al., 2008c).

The dynamics of dense shelf water is sensitive to the wind intensity. In a modelling work on the same area during the winter of 2005, during which very dense water was formed, Bourrin et al. (2008a) showed that the dense water core is confined to the coast when northerly winds are strong and that a bottom layer, similar to that observed on the glider section (Fig. 6.7), detached from the main core and extended towards the mid-shelf when the wind subsides. As seen on the cross-shelf section, and also shown by Martín et al. (2013) from observations gathered in the Cap de Creus Canyon, the density of nearshore waters observed during March 2011, however, is barely larger than the outer-shelf waters and weaker than the slope water, which suggests that the volume of dense water present on the shelf in early March was probably small.

Moreover, E-SE storms strongly influence the dynamics of water masses on the continental shelf. The observations clearly show an important southward along-shelf flow on the inner and middle shelf, which is characteristic of the intense cyclonic circulation that takes place during E-SE storms (Ulses et al., 2008b). These currents induce a rapid transport and massive flushing of dense water off the shelf into the Cap de Creus Canyon (Palanques et al., 2006, 2008) or towards the Catalan shelf, south of the Cape de Creus peninsula (Ribó et al., 2011). Bourrin et al. (2008b) showed that during a storm and flood event in the same area, both SPM eroded on the inner-shelf by waves and SPM introduced by freshwater inputs were rapidly advected by along-shelf currents southward towards the canyons but did not evidence the presence of cold waters on the shelf. In the present study, the large inputs of fresher water during the river floods ensuing the stormy period produce a large buoyant plume that takes the place of the dense coastal water.

Thus, observations at the coast and across the shelf reveal extremely rapid and drastic changes in water masses, stratification and flow on the entire shelf by consecutive storm and flood events in wintertime (Figs. 6.7 and 6.9).

Surface sediment responds quickly to increasing shear stress. Significant sediment erosion and transport take place within hours of the onset of the storms. Observations of bottom shear stress and seabed elevation (Fig. 6.6), which show erosion over several centimetres during the storm, corroborate the observations made by Guillén et al. (2006) at the same point during the winter 2003-2004 under the impact of E-SE storms with significant wave heights between 3 and 8 m. Compared to these aforementioned studies, the new observations gathered with the glider across the shelf provide essential information on the evolution of the SPM distribution and transport in the water column. The observed structures show a strong horizontal concentration gradient across the shelf with significant decrease beyond the mid shelf (Fig. 6.7d).

During the storms, the cumulative along-shelf transport is an order of magnitude higher than the cross-shelf transport, and remains confined to the inner shelf where velocities and resuspension due to waves are strongest (Fig. 6.8). Significant transport, both in the along- and cross-shelf directions, is associated to the bottom plume of dense water that spreads on the mid and outer-shelf. The observations collected concomitantly in the Cap de Creus Canyon (Martín et al., 2013) clearly indicated that the water and SPM transported along the shelf during the storm rapidly reach (in less than half a day) the southern exit of the GoL.

Considering a range of southward SPM transport along the glider's cross-shelf section of 2-4 $t.s^{-1}$ during the 12-16 March storm period (Fig. 6.11b), the total SPM transport during this 5-day long period amounts between 0.9 and 2.1 x 10^6 tons, knowing that this quantity does not take into account the transport within the coastal band shallower than 30 m due to the glider limitation. The transport on the inner-shelf is approximated to 0.09 x 10^6 tons considering a triangular section for the inner shelf below 30 m water depth (3.75 10^4 m^2) and the average transport measured at the POEM station during the stormy period ($\sim$20 $kg.m^{-2}.h^{-1}$).

The total transport through the cross shelf section ($\sim$1 and 2.2 x 10^6 tons) is about one order of magnitude larger than the SPM transport estimated by Martín et al. (2013) as being transferred along the southern canyon flank of the Cap de Creus during the storm-induced downwelling ($\sim$1 x 10^5 tons). Hence, due to the weak density contrast of coastal waters with the slope waters, it appears that most of the transport bypassed the Cap de Creus Canyon towards the northern Catalan shelf, while only a limited fraction (around 5 – 10 %) was exported to the upper canyon. Furthermore the SPM transport through the cross shelf section during the storm is comparable to the total solid river discharge to the GoL during the subsequent flooding period (13-18 March) that was estimated as 0.9 x 10^6 tons.

The seaward variation of the cross-shelf particulate transport generates a divergence between 30 and 50 m depth, and a convergence between 60 and 80 m depth. The divergence on the inner shelf can be related to the high bottom shear stress combined with off-shelf current during storm, which are effective at removing fine sediments and transport them seaward. Conversely, the convergence on the mid-shelf can lead to a deposition of the coarsest particles in suspension. There is a fairly clear correspondence between the outer limit of the mid-shelf mud belt and the

limit at which the cross-shelf transport vanishes. The presence of fine sediment on the mud belt, that can be easily resuspended, nonetheless probably contributes to the supply of the bottom nepheloid layer, which extends on the distal part of the mid-shelf (between roughly 15 and 25 km off the coast).

These results conform well to expectations from the academic modelling study of Harris and Wiberg (2002), which concluded that on narrow, steep shelf (seabed slope ∼0.05%), such as the study area (mean slope ∼0.045% between 0 and 90 m water depths), the cross-shelf flux convergence of fine grained sediment enhances the storm beds formed at mid-shelf depths. Further, our observations indicate that despite the decrease of wave-induced shear stress with increasing depth, strong storm currents (between 30 and 50 cm.s^{-1}) taking place on the mid and outer-shelf likely produce a winnowing of fine sediment. This is also consistent with the modelling studies of Ulses et al. (2008a) and Dufois et al. (2008), which indicated significant erosion on the outer-shelf by strong bottom currents during storm events.

6.4.2 Variability of suspended particles properties

The abrupt change of the hydrological structures on the shelf between the stormy and flooding periods is also visible on the suspended particles properties. The spectral slope of backscattering signal at 3 different wavelengths measured from the glider is used to estimate the spatio-temporal variability of particles. The overall seaward increase of γ both for stormy (Fig. 6.13b) and flooding (Fig. 6.14b) conditions would imply that coastal particles assemblage is composed by a higher percentage of large particles than the offshore particles assemblage.

This seaward decrease of particles size was also suggested by Niewiadomska et al. (2008) in a coastal front system off the Riviera coast in the NW Mediterranean using the same method. The use of an optically derived γ index was first used for the global ocean to estimate from satellite data the contribution of small versus large suspended particles (Loisel et al., 2006). The present study is one the first study describing the characteristics and size of the suspended particles assemblage from glider based measurements in the coastal area. Futures studies need more investigations in order to compare this index with in-situ grain-size analysis and calibrate measurements form autonomous platforms.

As is shown in greater detail in Figure 6.15a, the turbid bottom nepheloid layer that developed between 5 and 10 km from the shoreline during the storm is primarily composed of coarse particles. Both suspended sediment concentration (Fig. 6.7d) and particle size (Fig. 6.15b) decrease with increasing distance from the seabed. Such changes are consistent with particle resuspension and settling in the bottom layer, two processes that are dependent on particle size and density. The resuspension also appears to be effective above the mid-shelf mud belt where the percentage of fine sediments is maximum (Fig. 6.1). This maximum also corresponds to the current convergence where the coarsest particles are likely to be deposited. It is believed that coarse

particles present in the bottom nepheloid layer can be flocs formed by the stirring and aggregation of single fine particles that are resuspended from the inner-shelf sediment. As a matter of fact, Durrieu de Madron et al. (2005) and Curran et al. (2007) show that clayey and fine silty resuspended particles tends to form flocs populations (from microflocs around 30 µm to macroflocs > 100 µm). Besides, the high Chl-a concentrations suggest that particles of biological origin (Fig. 6.13a, b) probably also contribute to the large particles pool.
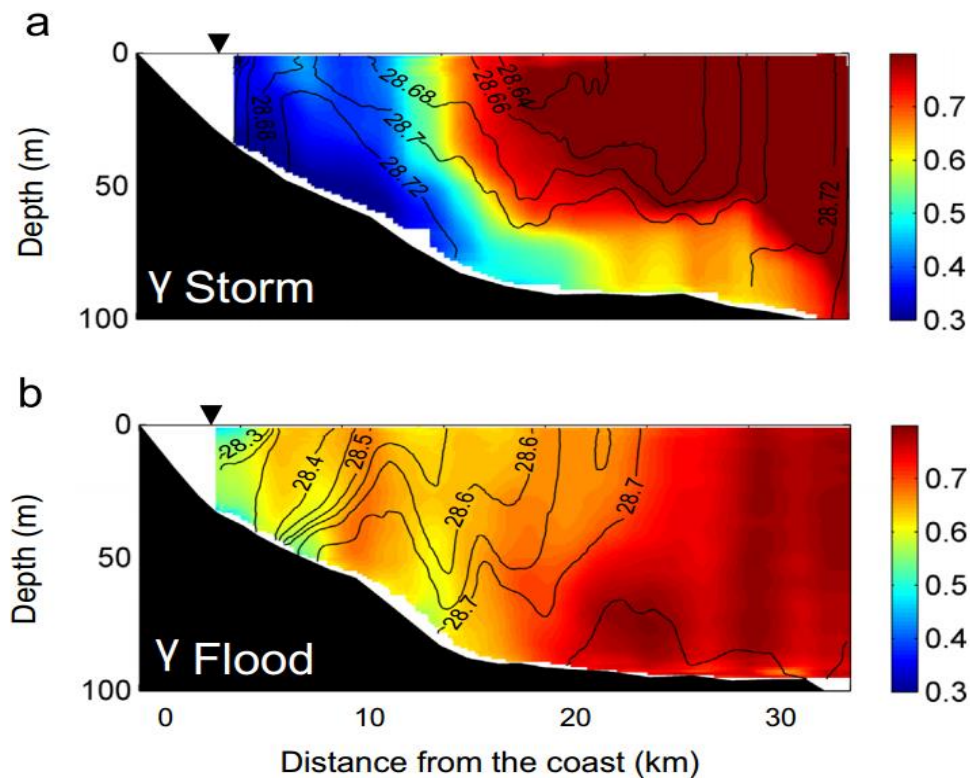
Figure 6.15 : Cross-shelf glider section of gamma index during the storm (a) and after the flood (b)

After the storm, the bottom nepheloid layer mostly constituted of coarse particles was rapidly swept away and advected towards the Cap de Creus Canyon and the northern Catalan shelf. During the flooding period, only a thin and diffuse bottom nepheloid layer persists on the shelf (Fig. 6.9d). This layer is less turbid, has a weaker Chl-a content, and is composed of finer particles than during the stormy period (Fig. 6.15b). This kind of bottom nepheloid layer has been often observed on the continental shelf of the Gulf of Lions and is considered to be permanent. The decrease of the concentration of mineral and biological particles in suspension, and the lower turbulence during this period could explain the diminution of particle size. The surface turbid plume associated to the flooding of the coastal rivers has the same characteristics in terms of backscattering spectral dependency than the flood bottom nepheloid layer. This layer appears to have the same relative grain-size as the bottom nepheloid layer, but is probably composed by different particles because of the higher Chl-a content. However, this statement must be considered carefully since we have relatively few measurements inside the river plumes because of the extension of the surface plume and the low capacity of the glider to go very close to the coast.

6.5 Conclusions

This work provided a unique synoptic view across the entire shelf of the impact of a typical Mediterranean storm on bottom sediment erosion and particulate fluxes. Repeated glider transects across the south-western part of the Gulf of Lions shelf permitted for the first time to measure continuously the thermo-haline structures, the suspended particles concentrations, the current speed, and to estimate the particulate transport before, during and after typical Mediterranean storm events. Glider data complement and compare well with concomitant high frequency time series at fixed stations along the coast and in a downstream submarine canyon.

Particulate matter transport was primary along-shelf, and higher above the mid-shelf mud belt, which is composed of more easily erodible fine sediment. A seaward cross-shelf transport occurs on the inner-shelf and part of the mid-shelf and vanishes further offshore, evidencing a convergence flux likely implying a deposition of particles on the distal part of the mid-shelf. Most of the transport of shelf water during the E-SE storm exits rapidly the Gulf of Lions shelf, a small part downwelled towards the Cap de Creus Canyon head, while the rest was exported towards the northern Catalan shelf.

We used the spectral relationship between the particulate backscattering coefficient and the wavelength of the backscattering sensors to estimate the gamma index, which is a proxy of the particle size in the coastal zone. This index shows that the largest particles were confined at the coast, and in the bottom nepheloid layer, where the SPM concentrations are the largest, whereas the smallest particles are located offshore. Further investigations with in-situ grain size measurements have to be done to confirm the effectiveness of this index.

Acknowledgements

References

Babin, M., Morel, A., Fournier-Sicre, V., Fell, F., Stramski, D., **2003**. Light scattering properties of marine particles in coastal and open ocean waters as related to the particle mass concentration. Limnology and Oceanography 48, 843–859.

Bonnin, J., Heussner, S., Calafat, A., Fabres, J., Palanques, A., Durrieu de Madron, X., Canals, M., Puig, P., Avril, J., Delsaut, N., **2008**. Comparison of horizontal and downward particle fluxes across canyons of the Gulf of Lions (NW Mediterranean): Meteorological and hydrodynamical forcing. Continental Shelf Research 28, 1957–1970. doi:10.1016/j.csr.2008.06.004

Boss, E., Pegau, W.S., Gardner, W.D., Zaneveld, J.R.V., Barnard, A.H., Twardowski, M.S., Chang, G., Dickey, T., **2001a**. Spectral particulate attenuation and particle size distribution in the bottom boundary layer of a continental shelf. Journal of Geophysical Research: Oceans (1978–2012) 106, 9509–9516.

Boss, E., Twardowski, M.S., Herring, S., **2001b**. Shape of the particulate beam attenuation spectrum and its inversion to obtain the shape of the particulate size distribution. Applied Optics 40, 4885–4893.

Bourrin, F., Durrieu de Madron, X., Ludwig, W. **2006**. Contribution to the study of coastal rivers and associated prodeltas to sediment supply in the Gulf of Lions (NW Mediterranean Sea). Vie et Milieu, 56(4), 307-314.

Bourrin, F., Durrieu de Madron, X., Heussner, S., Estournel, C., **2008a**. Impact of winter dense water formation on shelf sediment erosion (evidence from the Gulf of Lions, NW Mediterranean). Continental Shelf Research 28, 1984–1999. doi:10.1016/j.csr.2008.06.006.

Bourrin, F., Friend, P.L., Amos, C.L., Manca, E., Ulses, C., Palanques, A., Durrieu de Madron, X., Thompson, C.E.L., **2008b**. Sediment dispersal from a typical Mediterranean flood: The Têt River, Gulf of Lions. Continental Shelf Research 28, 1895–1910. doi:10.1016/j.csr.2008.06.005.

Cattaneo, A., Trincardi, F., Asioli, A., Correggiari, A., **2007**. The Western Adriatic shelf clinoform: energy-limited bottomset. Continental Shelf Research 27, 506–525. doi:10.1016/j.csr.2006.11.013

Corbett, D.R., Walsh J.P., Harris C.K., Ogston A.S., Orpin A.R., **2014**. Formation and preservation of sedimentary strata from coastal events: Insights from measurements and modeling. Continental Shelf Research, 86, 1-5.

Curran, K., Hill, P., Milligan, T., Mikkelsen, O., Law, B., Durrieu de Madron, X., Bourrin, F., **2007**. Settling velocity, effective density, and mass composition of suspended sediment in a coastal bottom boundary layer, Gulf of Lions, France. Continental Shelf Research 27, 1408–1421.

Davis, R.E., Eriksen, C.C., Jones, C.P., **2002**. Autonomous buoyancy-driven underwater gliders. The technology and applications of autonomous underwater vehicles 37–58.

DeGeest, A.L., Mullenbach, B.L., Puig, P., Nittrouer, C.A., Drexler, T.M., Durrieu de Madron, X., Orange, D.L., **2008**. Sediment accumulation in the western Gulf of Lions, France: The role of Cap de Creus Canyon in linking shelf and slope sediment dispersal systems. Continental Shelf Research 28, 2031–2047. doi:10.1016/j.csr.2008.02.008.

Doxaran, D., Ruddick, K., McKee, D., Gentili, B., Tailliez, D., Chami, M., Babin, M., **2009**. Spectral variations of light scattering by marine particles in coastal waters, from visible to near infrared. Limnology and Oceanography 54, 1257.OS

DREAL, **2011**. DREAL_LR-rapport_coup_de_mer_12-16_mars_2011.

Dufois, F., Garreau, P., Le Hir, P., Forget, P., **2008**. Wave- and current-induced bottom shear stress distribution in the Gulf of Lions. Continental Shelf Research 28, 1920–1934. doi:10.1016/j.csr.2008.03.028.

Durrieu de Madron, X., Ferré, B., Le Corre, G., Grenz, C., Conan, P., Pujo-Pay, M., Buscail, R., Bodiot, O., **2005**. Trawling-induced resuspension and dispersal of muddy sediments and dissolved elements in the Gulf of Lion (NW Mediterranean). Continental Shelf Research 25, 2387–2409. doi:10.1016/j.csr.2005.08.002.

Durrieu de Madron, X., Wiberg, P.L., Puig, P., **2008**. Sediment dynamics in the Gulf of Lions: The impact of extreme events. Continental Shelf Research 28, 1867–1876. doi:10.1016/j.csr.2008.08.001

Eau France, **2011**. Bulletin National de Situation Hydrologique [WWW Document]. URL http://www.eaufrance.fr/docs/bsh/2011/04/precipitations.php (accessed 7.10.14).

Ferré, B., Durrieu de Madron, X., Estournel, C., Ulses, C., Le Corre, G., **2008**. Impact of natural (waves and currents) and anthropogenic (trawl) resuspension on the export of particulate matter to the open ocean: Application to the Gulf of Lion (NW Mediterranean). Continental Shelf Research 28, 2071–2091. doi:10.1016/j.csr.2008.02.002

Ferré, B., Guizien, K., Durrieu de Madron, X., Palanques, A., Guillén, J., Grémare, A., **2005**. Fine-grained sediment dynamics during a strong storm event in the inner-shelf of the Gulf of Lion (NW

Mediterranean). Continental Shelf Research 25, 2410–2427. doi:10.1016/j.csr.2005.08.017

Garau, B., Ruiz, S., Zhang, W.G., Pascual, A., Heslop, E., Kerfoot, J., Tintoré, J., 2011. Thermal Lag Correction on Slocum CTD Glider Data. Journal of Atmospheric and Oceanic Technology 28, 1065–1071. doi:10.1175/JTECH-D-10-05030.1

Glenn, S., Jones, C., Twardowski, M., Bowers, L., Kerfoot, J., Kohut, J., Webb, D., Schofield, O., 2008. Glider observations of sediment resuspension in a Middle Atlantic Bight fall transition storm. Limnology and Oceanography 53, 2180–2196.

Gohin, F., Stanev, E., 2011. Annual cycles of chlorophyll-a, non-algal suspended particulate matter, and turbidity observed from space and in-situ in coastal waters. Ocean Science 7.

Guillén, J., Bourrin, F., Palanques, A., Durrieu de Madron, X., Puig, P., Buscail, R., 2006. Sediment dynamics during wet and dry storm events on the Têt inner shelf (SW Gulf of Lions). Marine Geology 234, 129–142. doi:10.1016/j.margeo.2006.09.018.

Guillén, J., Palanques, A., Puig, P., Durrieu de Madron, X., Nyffeler, F. 2000. Field calibration of optical sensors for measuring suspended sediment concentration in the western Mediterranean. Scientia Marina, 64(4), 427-435.

Guizien, K., 2009. Spatial variability of wave conditions in the Gulf of Lions (NW Mediterranean sea). Vie et Milieu 59, 261.

Harris, C.K., Wiberg, P., 2002. Across-shelf sediment transport: Interactions between suspended sediment and bed sediment. Journal of Geophysical Research: Oceans, 107, 8–1. Doi : 10.1029/2000JC000634.

Hay, A.E., 1991. Sound scattering from a particle-laden, turbulent jet. The Journal of the Acoustical Society of America 90, 2055–2074.

Hill, P.S., Fox, J.M., Crockett, J.S., Curran, K.J., Friedrichs, C.T., Geyer, W.R., Milligan, T.G., Ogston, A.S., Puig, P., Scully, M.E., 2007. Sediment delivery to the seabed on continental margins. Continental-Margin Sedimentation: From Sediment Transport to Sequence Stratigraphy, IAP Special Publication 37, 49–100.

HR Wallingford, 2003. The Sediview Method, Sediview Procedure Manual, 88p., V3, July 2003.

Loisel, H., Nicolas, J.-M., Sciandra, A., Stramski, D., Poteau, A., 2006. Spectral dependency of optical backscattering by marine particles from satellite remote sensing of the global ocean. Journal of Geophysical Research 111. doi: 10.1029/2005JC003367.

Madsen, O.S., Wood, W., 2002. Sediment transport outside the surf zone. Coastal Engineering Manual, Part III Coastal Processes, Engineer Manual 1110–2.

Marion, C., Dufois, F., Arnaud, M., Vella, C., 2010. In situ record of sedimentary processes near the Rhône River mouth during winter events (Gulf of Lions, Mediterranean Sea), Continental Shelf Research, 30, 9, 1095-1107.

Martín, J., Durrieu de Madron, X., Puig, P., Bourrin, F., Palanques, A., Houpert, L., Higueras, M., Sanchez-Vidal, A., Calafat, A.M., Canals, M., Heussner, S., Delsaut, N., Sotin, C., 2013. Sediment transport along the Cap de Creus Canyon flank during a mild, wet winter. Biogeosciences 10, 3221–3239. doi:10.5194/bg-10-3221-2013

McCave, I.N., 1972. Transport and escape of fine-grained sediment from shelf areas, in: Shelf Sediment Transport: Process and Pattern. Dowden, Hutchinson, and Ross, Stroudsburg, Pennsylvania, pp. 225–248.

Miles, T., Glenn, S.M., Schofield, O., 2013. Temporal and spatial variability in fall storm induced sediment resuspension on the Mid-Atlantic Bight. Continental Shelf Research 63, Supplement, S36–S49. doi:10.1016/j.csr.2012.08.006

Moore, D.G., 1969. Reflection profiling studies of the California continental borderland: structure and Quaternary turbidite basins. Geological Society of America.

Morel, A., 1974. Optical properties of pure water and pure sea water. Optical aspects of oceanography 1.

Morison, J., Andersen, R., Larson, N., Dasaro, E., Boyd, T., 1994. The correction for thermal-lag effects in Sea-Bird CTD data. J. Atmos. Ocean. Tech.11:1151–1164.

Niewiadomska, K., Claustre, H., Prieur, L., d' Ortenzio, F., 2008. Submesoscale physical-biogeochemical coupling across the Ligurian current (northwestern Mediterranean) using a bio-optical glider. Limnology and Oceanography 53, 2210.

Nittrouer, C.A., Austin Jr, J.A., Field, M.E., Kravitz, J.H., Syvitski, J.P.M., Wiberg, P.L., 2007. Writing a Rosetta stone: insight into continental margin sedimentary processes and strata. In Continental margin sedimentation: from sediment transport to sequence stratigraphy, edited by C.A. Nittrouer, J.A. Austin Jr, M.E. Field, J.H. Kravitz, J.P.M. Syvitski, P.L. Wiberg, Special publication number 37 of the International Association of Sedimentologists, 1-48

Ogston, A.S., Drexler, T.M., Puig, P., 2008. Sediment delivery, resuspension, and transport in two contrasting canyon environments in the southwest Gulf of Lions. Continental Shelf Research 28, 2000–2016. doi:10.1016/j.csr.2008.02.012.

Palanques, A., Durrieu de Madron, X., Puig, P., Fabres, J., Guillén, J., Calafat, A., Canals, M., Heussner, S.,

Bonnin, J., **2006**. Suspended sediment fluxes and transport processes in the Gulf of Lions submarine canyons. The role of storms and dense water cascading. Marine Geology 234, 43–61. doi:10.1016/j.margeo.2006.09.002.

Palanques, A., Guillén, J., Puig, P., Durrieu de Madron, X., **2008**. Storm-driven shelf-to-canyon suspended sediment transport at the southwestern Gulf of Lions. Continental Shelf Research 28, 1947–1956. doi:10.1016/j.csr.2008.03.020.

Pond, S., Pickard, G.L. **1983**. Introductory dynamical oceanography (2nd edition) Pergamon Press, New York (1983), p. 329

Ribó, M., Puig, P., Palanques, A., Lo Iacono, C., **2011**. Dense shelf water cascades in the Cap de Creus and Palamós submarine canyons during winters 2007 and 2008. Marine Geology 284, 175–188. doi:10.1016/j.margeo.2011.04.001

Sullivan, J.M., Donaghay, P.L., Rines, J.E.B., **2010**. Coastal thin layer dynamics: Consequences to biology and optics. Continental Shelf Research 30, 50–65. doi:10.1016/j.csr.2009.07.009

Teledyne RD Instruments, **2007**. WAVES PRIMER: Wave Measurements and the RDI ADCP Waves Array technique. Available from RDInstruments.com.

Testor, P., Meyers, G., Pattiaratchi, C., Bachmayer, R., Hayes, D., Pouliquen, S., Petit de la Villeon, L., Carval, T., Ganachaud, A., Gourdeau, L., **2010**. Gliders as a component of future observing systems. Proceedings of OceanObs' 09: Sustained Ocean Observations and Information for Society 2.

Thorne, P.D., Campbell, S.C., **1992**. Backscattering by a suspension of spheres. The Journal of the Acoustical Society of America 92, 978–986.

Ulses, C., Estournel, C., Durrieu de Madron, X., Palanques, A., **2008a**. Suspended sediment transport in the Gulf of Lions (NW Mediterranean): Impact of extreme storms and floods. Continental Shelf Research 28, 2048–2070. doi:10.1016/j.csr.2008.01.015

Ulses, C., Estournel, C., Bonnin, J., Durrieu de Madron, X., Marsaleix, P., **2008b**. Impacts between storms and dense water cascading on shelf-slope exchange in the Gulf of Lions (NW Mediterranean). Journal of Geophysical Research. 113, C02010, doi: 10.1029/2006JC003795.

Ulses C., Estournel C., Puig P., Durrieu de Madron X., Marsaleix P., **2008c**. Dense water cascading in the northwestern Mediterranean during the cold winter 2005. Quantification of the export through the Gulf of Lion and the Catalan margin. Geophysical Research Letters, 35, L07610, doi: 10.1029/2008GL033257.

Weaver, P.P.E., Canals, M., Trincardi, F., **2006**. EUROSTRATAFORM Special Issue of Marine Geology. Marine Geology 234, 1–2. doi:10.1016/j.margeo.2006.09.001

Webb Research, Operations Manual Slocum Shallow Battery Glider Ver 1.6 1/11/2005.

Wright, L., Coleman, J.M., **1974**. Mississippi River mouth processes: effluent dynamics and morphologic development. The Journal of Geology 751–778.

Chapter 7.

Conclusions and outlooks

Chapter 7. Conclusions and outlooks

List of Figures

7.1 Summary results

This work highlighted the different mechanisms that enable the sedimentation of SPM delivered from the Rhône River during flooding conditions as well as the impacts of marine storms on the SPM export off the Gulf of Lions shelf. While these events were considered as episodic, they occurred over large areas and appeared as key processes in the regulation of sediment dynamics over the shelf.

7.1.1 The impact of a flood in the Rhône River ROFI

7.1.1.1 The role of fine-sediments flocculation

We highlighted the variability of the particle assemblage in the Rhône River ROFI during a flood event of the Rhône River (see Chapter 4; Fig. 7.1). An instrument package composed of a CTD, a LISST-100 type B (1.25–250μm), and a LISST-HOLO (20–2000μm) was used to characterize the hydrological parameters and suspended particles properties (concentration, size, composition, shape, and effective density). Results emphasized the necessity of combining both LASER and holography measurements to determine 1) the largest particle size distribution, 2) the nature of SPM and 3) the shape of biggest flocs. The diversity of flocs shape highlighted their non-sphericity aspect, which implied the need of a "randomly-shape" algorithm to properly invert the PSD from the light scattering in seawater. Besides, a coastal *slocum* glider was deployed to detail the spatial description of the hydrological parameters and particles properties. We verified the ability of glider, equipped with backscattering sensors at several wavelengths, to describe the fine-scale variability of the SPM, and to provide an index (γ) of their size distribution. This index was finally compared and validate against in situ LISST measurements.

Observations can be summarized as follows:

- During the 2014 flood event, large river discharge (> 5000 m^3 s^{-1}) and continental wind, favored the dispersal of the Rhône River plume (> 30 km) over the shelf. Surface SPM concentrations decreased seaward from 20 mg L^{-1} close to the river mouth to 1.5 mg L^{-1} at the shelf break. A bottom nepheloid layer was observed across the entire shelf with concentrations decreasing seaward from 8 to less than 1 mg L^{-1}. The link existing between both river plume and BNL on the inner-shelf, induced by the Rhône discharge and episodic sediment resuspension, was shown.
- Observations showed that most of suspended particles were mainly flocculated in micro and macro-flocs (30 – 400 μm) in inner-shelf waters. The role of SPM concentrations and salinity gradient in the control of the fine-sediments (~10 μm) flocculation was emphasized. The particle assemblage in the Rhône River plume and in the BNL became progressively finer seaward due to the micro- and macro-flocs settling and dilution. The

related effective density increased from 370 to 1600 kg m^{-3} with maximum values above the mid-shelf mud-belt.
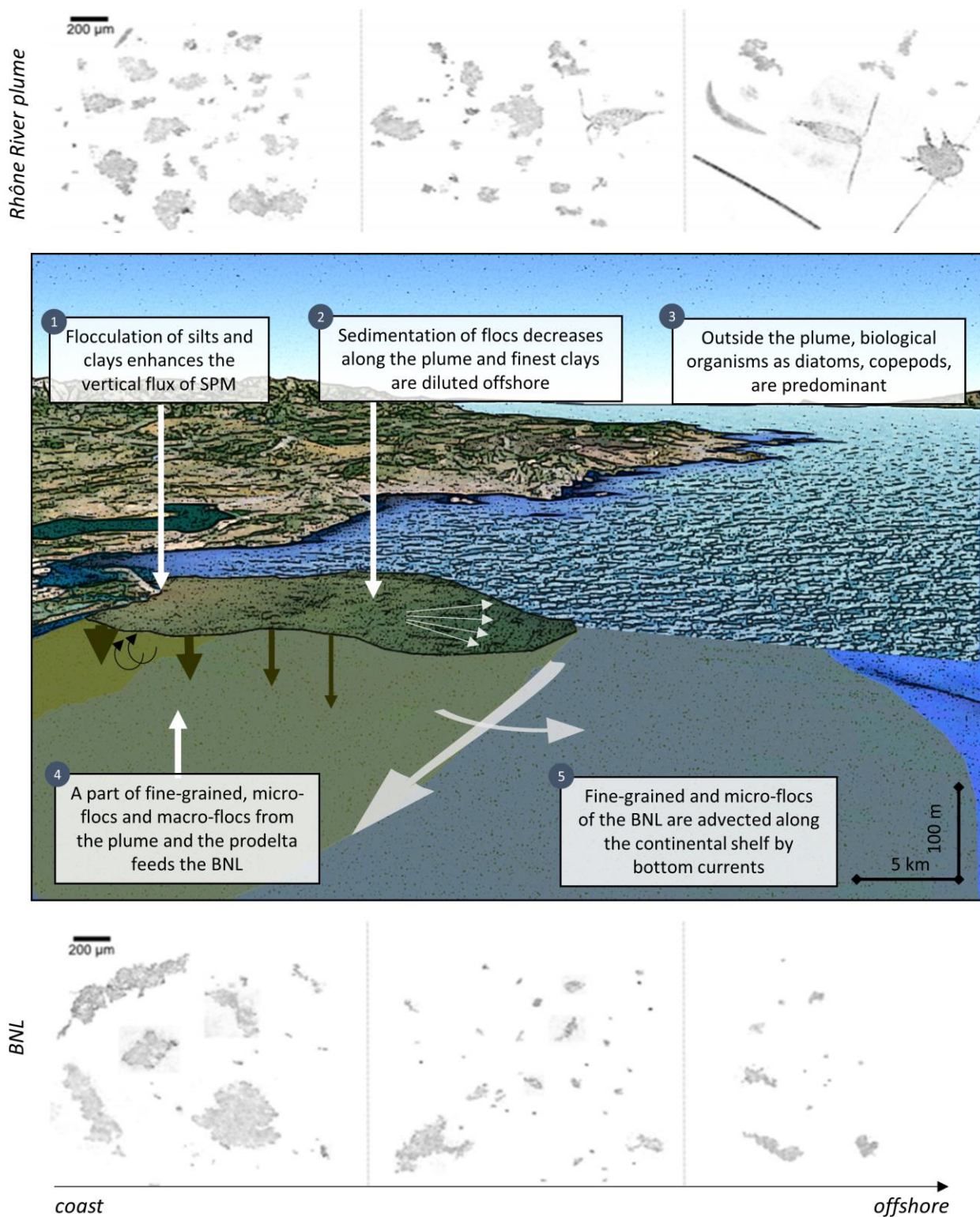
Figure 7.1 : Graphical abstract of the particle assemblage variability in the Rhône River ROFI. Images of micro- (20-125 µm) and macro-flocs (>125 µm) composing the River plume and the BNL are shown. View is from the SW.

7.1.1.2 Nepheloid layers dynamics

We highlighted the high-variability of Rhône ROFI nepheloid layers during a flood event (see Chapter 5; Fig. 7.2). Large scale satellite and glider observations were combined with coastal buoy measurements to get a unique view of the impact of different wind regimes on SPM dynamics in the Rhône River ROFI. The spectral slope of glider and MODIS backscattering measurements, γ, was used to characterize the large-scale spatial and temporal variability of the particle assemblage.

Observations can be summarized as follows:

- The development of the Rhône River plume (5-50 mg L^{-1}) as well as the presence of a persistent bottom nepheloid layer over the entire shelf (1-2 mg L^{-1}) were observed. The Rhône River plume was highly stratified and presented maximum SPM concentration in a thin surface layer (<1 m, MODIS data). The particle assemblage was 1) finer in the surface than in the subsurface layer and 2) variable along a cross-shelf transect within the River plume and the BNL, which became finer seaward.

- Continental wind enhanced the export of the SPM over the entire shelf through the surface plume (25 km offshore) whereas marine winds fostered the plume against the coast. Due to an increase of SPM concentrations (>35 mg.L^{-1}) that seemed to enhance the fine-sediments flocculation, marine wind seemed to favor the sedimentation of particles through the whole water column that alimented the BNL (5 mg L^{-1}) down to 60 m depth as well as episodic INL (1 mg L^{-1}). This alimentation could be accentuated by the SPM resuspended from the local prodelta (< 20 m depth).

- The glider backscattering measurements combined with the estimation of stratification and mixing parameters highlighted the role of a storm event on the creation of a cyclonic current close to the coast, which favored the break of the plume stratification and the along-shelf transport of Rhône River particles. This transport could be accentuated by particles resuspension down to 60 m depth and occurred in the whole water column.
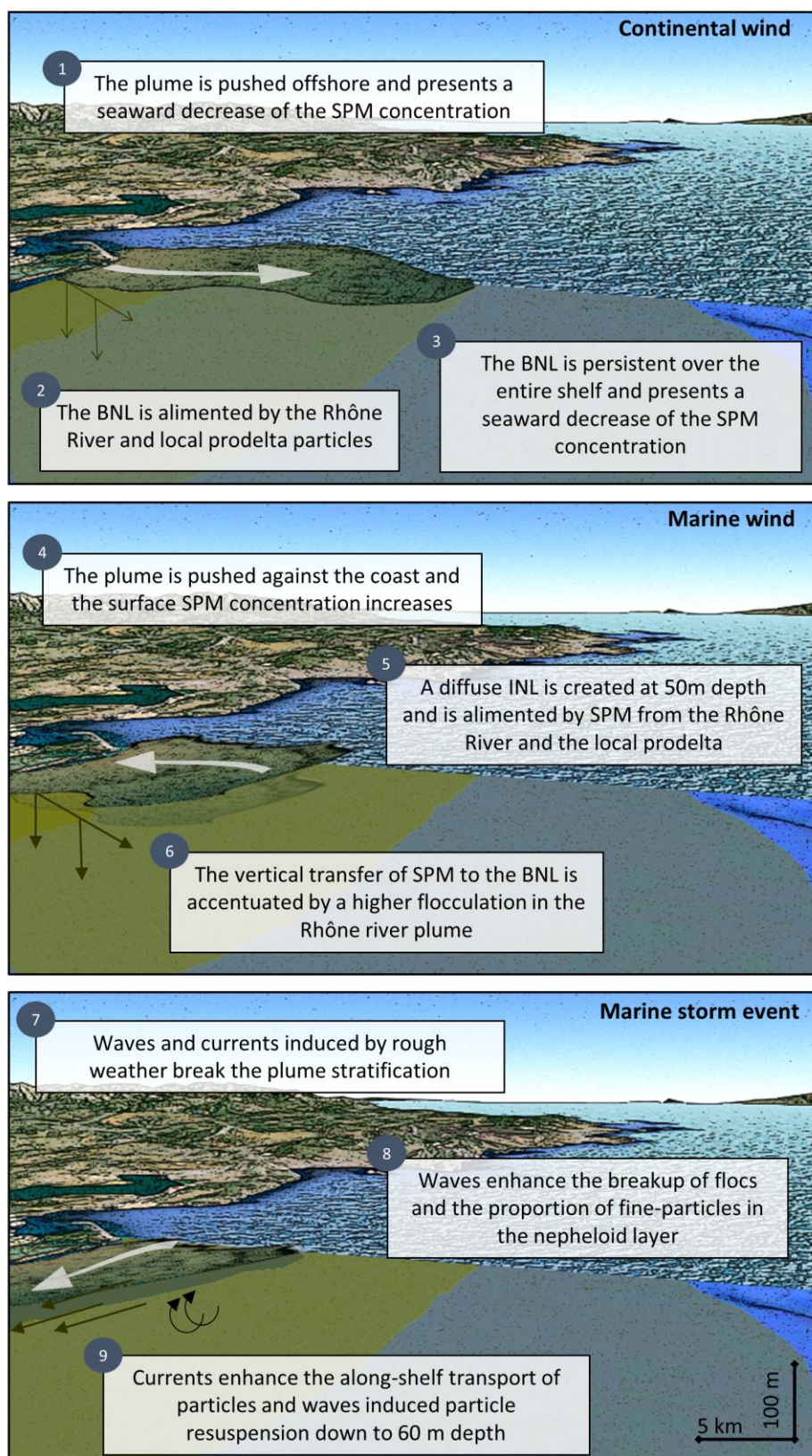
Figure 7.2 : Graphical abstract of meteorological forcings on SPM dynamics in the Rhône River ROFI during flooding conditions. a-b) Continental and marine wind events (no wave / current). Impacts of a marine storm event (i.e. marine wind, current > 0.5 m s^{-1} and waves > 4 m high) are shown. View is from the SW.

7.1.2 The impact of a storm in the export of SPM offshelf

The role of a marine "wet" storm in the particulate transport in the southwest part of the GoL shelf was presented (see Chapter 6; Fig. 7.3). A glider was deployed to assess the spatial and temporal variability of hydrology, suspended particles properties and fluxes. Results were completed with satellite, coastal buoy, and submarine canyon mooring measurements. Glider observations were decisive to determine how the particulate along- and cross-shelf transport was affected by the marine storm. High-resolution (i.e. approx. 1 profile / 200 m and 1 section per day) observations permitted to understand the resuspension and transport processes with a high accuracy. While the estimation of the particulate transport was in line with the coastal buoy observation, the canyon mooring lines clearly helped in the determination of the preferential export mechanism. At last, the derivation of the spectral slope of backscattering measurements, γ, enabled to highlight the cross-shelf variability of the particle assemblage during storm and subsequent flooding conditions.

Observations can be summarized as follows:

- The sediment resuspension (erosion of 4 cm at 23 m depth) observed at the coastal station during the storm (wave > 4 m) was effective over the shelf for depth down to 80 m (maximum SPM of 45 mg L^{-1}). The increase of SPM concentrations observed close to the seabed seemed to enhance the fine-sediments flocculation.
- Due to the strong cyclonic circulation, the along-shelf flow (southward max. ∼0.6 m.s^{-1}) was stronger than cross-shelf flux (eastward max. ∼0.1 m.s^{-1}). The mid-shelf mud belt, located between 40 and 90 m depth, appeared as the area where the southward along-shelf flux of suspended sediments is maximum (0.6 t s^{-1}). Besides, the weak cross-shelf flux of suspended sediments converged towards the outer limit of the mid-shelf mud belt, where deposition of SPM probably occurred and contributed to the nourishment of this area.
- During the 5 days storm, the southward particulate transport was estimated to 1-2 Mt. Most of this transport exited rapidly the Gulf of Lions shelf, a small part (∼10 %) downwelled towards the Cap de Creus Canyon head, while the rest was probably exported towards the northern Catalan shelf.
- The SPM delivery by the subsequent coastal rivers flood rapidly compensated the sediment erosion induced by the storm. The buoyant river plumes (max. SPM ∼5 mg L^{-1}) that spread along the shelf after the flooding period provoked a restratification of the water column on the inner- and mid-shelf.
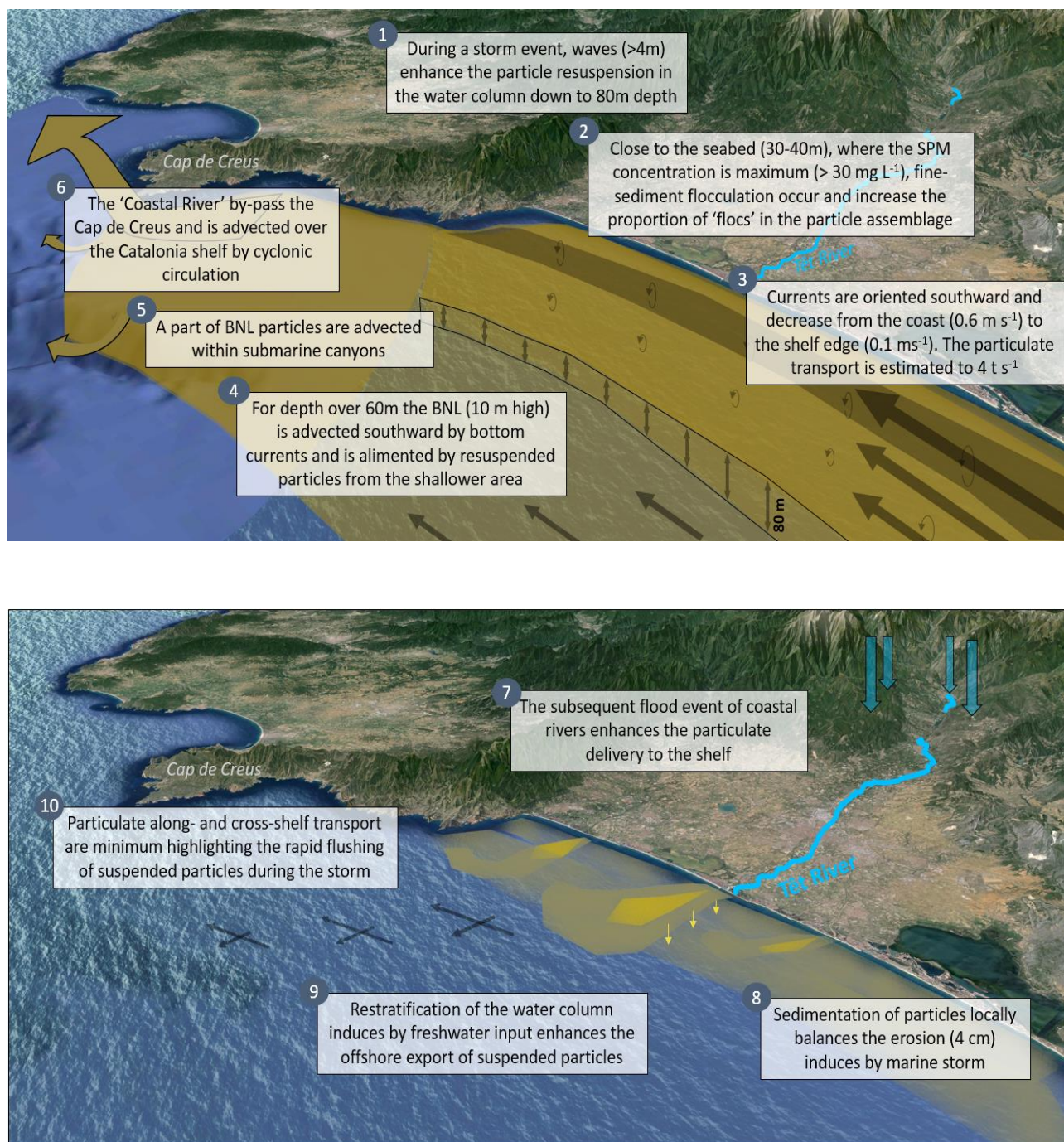
Figure 7.3 : Graphical abstract of the impact of a "back-to-back" storm and flood event on SPM dynamics over the SW part of the shelf of the GoL. View is from the NE.

7.2 Synthesis

7.2.1 Impacts of events on nepheloid layers dynamics

This PhD highlighted the importance of meteorological events in SPM dynamics at both the entrance and exit of the Gulf of Lions shelf. While a Rhône flood enhanced the particulate delivery in the adjacent ROFI and generated various nepheloid layers, marine storms induced an important resuspension of coastal sediments and enhanced the particulate transport offshelf. These events emphasized the high-dynamical character of SPM dynamics over the Gulf of Lions shelf that played a major role in coastal turbidity, sedimentary budget of the shelf and expansion of mud areas.

Rhône River flood - The different mechanisms permitting the vertical transfer of particles from the Rhône River plume to the BNL as well as the possible advection of SPM off the Rhône River ROFI were identified. While continental winds favored the export of the Rhône River plume offshore, weak marine winds favored the alimentation of the INL and the BNL and thus enhanced the vertical transfer of particles from the Rhône River plume to local prodelta and related BNL (Fig. 7.4 - Annex 2). This observation was poorly documented due to the episodic character of such structures and the sampling difficulties. While Aloisi et al. (1982) predicted the presence of these nepheloid layers close to the Rhône River mouth during fall conditions, we clearly emphasized the role of marine winds as a key factor permitting the creation and alimentation of such structures during flooding conditions of the Rhône River.
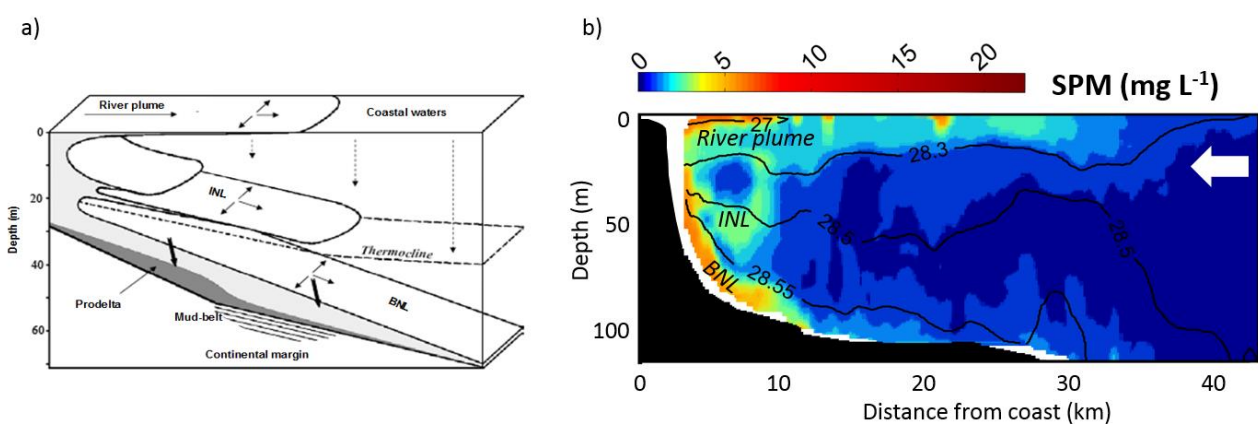
Figure 7.4 : Comparison between a) conceptual view of the different nepheloid layers (river plume, INL and BNL) that can be observed in the Rhône River ROFI (Aloisi et al., 1982) and b) cross-shelf section of the SPM concentration determined by the glider during the TUCPA 2014 experiment. Density contour lines are shown in black. River plume, INL and BNL are shown. Marine wind that favored the alimentation of such structures is shown by a white arrow.

Besides, we highlighted that rough weather induced by strong marine winds broke the river plume stratification, enhanced the break-up of in situ flocculated particles and favored the resuspension down to 60 m depth and the along-shelf advection of suspended particles. These observations

were in line with the recent modeling work of Dufois et al. (2014), which highlighted the role of storms in the particulate redistribution from the prodelta to the shelf. Marine storms thus participate to the sediment dynamics over the Rhône prodelta at the annual scale and, depending on their intensities and frequencies could highly participate to the non-preservation of the recent flood layers produced by the Rhône floods in sedimentary records.

Marine storm – Based on glider observations, the impact of a storm on the particulate transport over the entire SW part of the shelf was estimated to 4 t s^{-1} in the southward direction with a cross-shelf component of 0.5 t s^{-1} in the eastward direction (see Chapter 6; Table 7.1). This transport was about 25-30 times higher than during fall conditions estimated during the TUCPA2013 experiment based on glider measurements in the same area during April and May 2013 (data not presented in this work). Besides, we have shown that directly after the storm period the particulate transport drastically decreased and reached minimum values, 4-5 times lower than during fall conditions. This observation highlighted the rapid flushing of all the suspended particles during the storm as well as the non-negligible particulate transport that occurred during fall and stratified conditions.

	Storm conditions	Post-storm conditions	Fall conditions
Survey	CASCADE2011	CASCADE2011	TUCPA2013
Along-shelf	3.92 / Southward	0.03 / Northward	0.13 / Southward
Cross-shelf	0.52 / Eastward	0.03 / Eastward	0.02 / Eastward

Table 7.1 : Summary of cumulative particulate transport (expressed in t s^{-1}) estimated during storm and post-storm conditions (CASCADE 2011) and during fall conditions (TUCPA 2013 – data not presented in this work) over the SW part of the GoL.

Storms appeared as key factors in the regulation of the sedimentary budget of the shelf (Fig. 7.6). We highlighted that a total of ~1-2 Mt of sediment have been exported offshelf during a typical annual Mediterranean storm, contrasting with the 0.5 Mt estimated during the 45 days of fall conditions. These results were in the same order of magnitude of the annual particulate delivery from the Rhône River (approx. 8 Mt, Sadaoui et al., 2016) as well as the particulate delivery that occurred during major Rhône River flood events, as during the 2003 flood event (11 000 m^3 s^{-1}), which loaded approx. 3-5 Mt of sediments to the Gulf of Lions (Maillet et al., 2006; see also modeling of Kettner et al. (2004)). These amounts were also superior to the total of the annual particulate inputs from small coastal rivers (~1 Mt y^{-1}, from Bourrin (2007)). These estimations clearly highlighted the role of storms in the particulate transport occurring over the shelf. The succession of such events could highly participate to the erosion of deposited sediments that could limit the sediment accumulation over this part of the shelf and could confirm that the southwest part of the Gulf of Lions act as a bypass area.

Based on the estimation of the particulate transport that occurred in the SW part of the shelf ($\sim$1-2 Mt) and that one in the Cap de Creus submarine canyon by Martin et al. (2013) (0.1 Mt), we emphasized that only a small part of the SPM (i.e. $\sim$10%) seemed to be exported through the canyon. It thus appeared that most of the particulate transport bypassed the Cap de Creus toward the northern Catalan shelf during this event. This observation, in line with the hydrodynamical study of Degeest et al. (2008), highlighted the role of the Cap de Creus and the cyclonic circulation in the particulate export off the shelf. While the work of Degeest et al. (2008) have been carried out during different conditions (i.e. cascading) both results showed the predominant role of particulate bypassing in the extension of the area impacted by the particulate transport from the Gulf of Lions. While the Cap de Creus canyon is the main canyon on the Gulf of Lions transferring suspended material to the deep sea, the major exit of particulate material seemed to be the small part of the shelf between the canyon head and the promontory of the Cap de Creus.
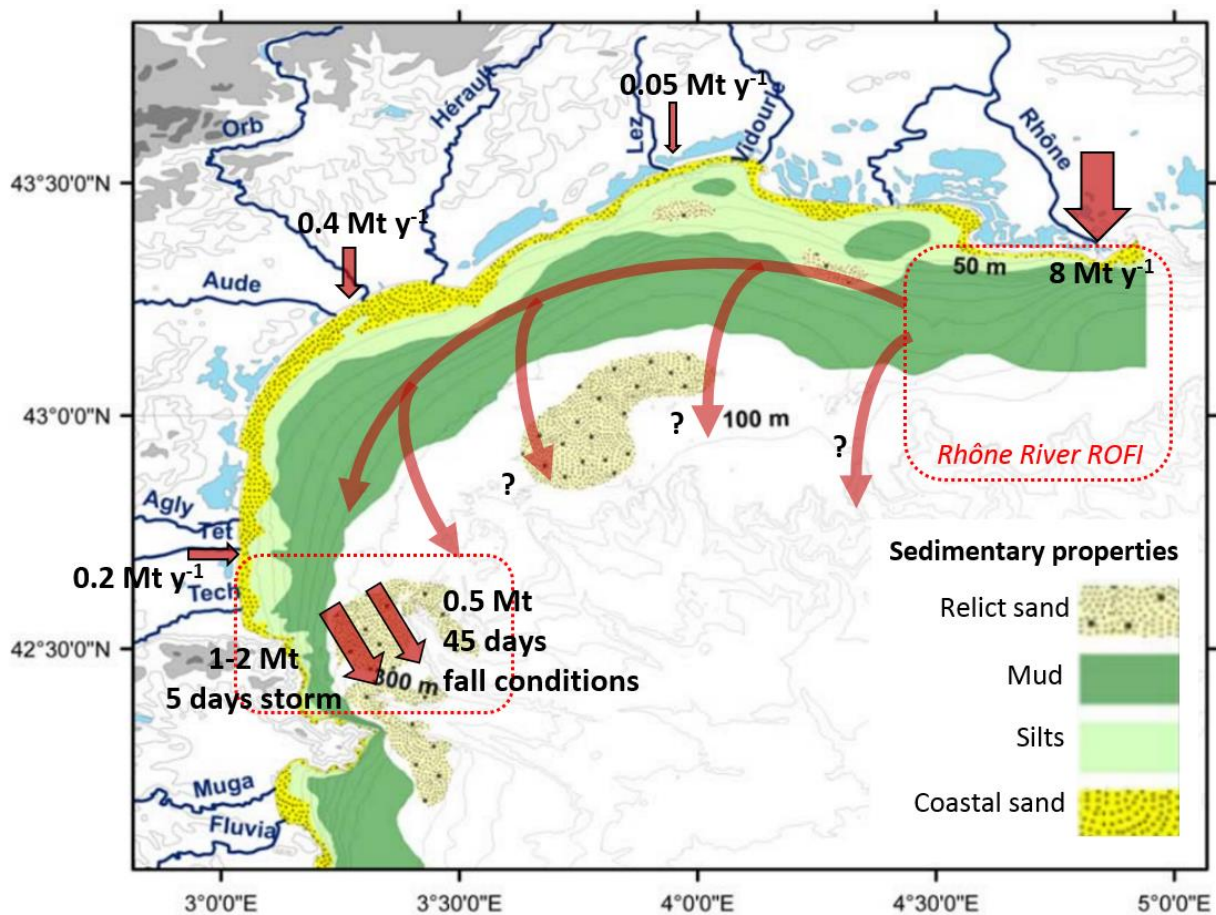
Figure 7.5 : Sedimentary budget of the shelf of the Gulf of Lions. Morphological map adapted from Monaco and Aloisi (2000). Rhône River data is from Sadaoui et al. (2016). Small coastal rivers data are from Bourrin (2007). Red rectangles show the study areas of this work.

7.2.2 Particle assemblage characterization

In addition to the quantification of fluxes of suspended material over the shelf, we put forward our knowledge on the characteristics of suspended particles in the Gulf of Lions. We established for the first time a characterization of the particle assemblage variability in the Rhône River ROFI. This study highlighted the role of the flocculation in the growth of fine-sediment flocs, enhancing their size (> 300 μm) while decreasing their effective density (< 500 kg m^{-3}). We estimated that micro- and macro-flocs could present settling velocities of 2 to 17 mm s^{-1} (i.e. 7 to 60 m h^{-1}). While these estimations could be improved with the estimation of the effective density per size class and the estimation of the fractal dimension of flocs, they were in line with the work of Manning and Schoellhamer (2013).

These results highlighted the fast vertical transfer of large flocs within the Rhône ROFI and confirmed hypothesis made by Naudin et al. (1997) and Thill et al. (2001), which emphasized the role of the flocculation in the sedimentation of a part of fine sediments close to the river mouth. The Rhône River prodelta thus trapped a large part of fine sediments delivered by the Rhône River and acted as a sediment, carbon and related contaminant sink during this flood event. These observations contrast with the bypassing character of the SW part of the shelf described previously. Several authors have highlighted this character of the Rhône River prodelta (Radakovitch et al., 1999; Durrieu de Madron et al., 2000; Lansard, 2004; Bourrin, 2007). Authors quantified to 50% (~ 4 Mt y^{-1}) the part of sediments delivered by the Rhône River that is trapped in the prodelta.

Besides, this PhD permitted to estimate for the first time an index of the size of suspended particles from moving platforms and satellites both equipped with similar optical sensors. We highlighted the response of this index, γ, with the variability of the particle assemblage during both flooding and storm conditions (see Chapter 4, 5 and 6). We nevertheless highlighted a possible overestimation of the particulate backscattering coefficient from MODIS measurements through the QAA approach (see Chapter 5) that could lead to uncertainties on the determination of γ. Results were in line with the recent study of Slade and Boss (2015) and emphasized the link existing between γ and the SPM concentration, i.e. the more the SPM concentration the more the proportion of large flocs in the particle assemblage (low γ).

Additionally, we verified the correlation between γ and the Junge parameter, *j*, estimated from particle number distributions measured by laser diffraction and holography (see Chapter 4), which was in line with studies of Boss et al. (2001) and Buonassissi and Dierssen (2010). This was crucial in the verification of the good response of γ to the variability of the particle assemblage in the Rhône ROFI during flooding conditions.

The use of this index permitted to describe the impact of various wind conditions on the high-temporal and spatial variability of the particle assemblage composing nepheloid layers within the Rhône ROFI (see Chapter 5). At last, the derivation of γ enabled to emphasize the flocculation occurring within the BNL during resuspension events induced by storm conditions over the SW part of the shelf as well as the fine particle assemblage that spread at the sea surface after the coastal rivers flood (Chapter 6). These observations clearly highlighted the need of the use of

backscattering sensors at several wavelengths on board on glider to derive an index of the particle size especially to observe the impact of events in the coastal area.

To go further in the analysis of the response of γ to the variability of the suspended particles size, all the data presented in this work were computed and compared (Figure 7.6). It highlighted the similar trend occurring between the SPM concentration and the proportion of flocs in the particle assemblage during these situations. While the estimation of γ from satellite observations highlighted the high proportion of fine-sediments (i.e. γ ~0.6-1.4) in the thin surface layer of the Rhône River plume, the estimation of γ from glider measurements during various conditions shows that "submarine" particle assemblages were more dominated by flocs (i.e. γ ~0.3-0.9).

Differences observed between glider measurements during the CASCADE and TUCPA experiment could be explained by a more important proportion of finest particles in the Rhône River plume due to a limited flocculation by the vertical density gradient. Uncertainties concerning the backscattering sensors sensibility to the differences in the particle properties (as nature and shape) could also explained such differences.

While the use of this index was decisive in the following of the particle assemblage variability during these events with a high temporal and spatial resolutions, in situ particle size measurements remain necessary to properly estimate the largest range of particle size distribution (i.e. 1-2000 µm) as well as to provide visual information of the nature of suspended particles (organic vs inorganic, "flocs" vs unique particles) and shape parameters. While these parameters are increasingly used in modelling works, their in situ characterizations remains poorly known and the diversity of flocs shape could cause uncertainties concerning the estimation of their settling velocities.

Figure 7.6 : Spectral slope of glider backscattering measurements, γ, as a function of the SPM concentrations (mg L⁻¹) during storm (blue) and flooding (green) conditions (Chapter 6 − CASCADE 2011 − λ = 532, 700 and 880 nm) and flooding conditions of the Rhône River (red dots, Chapter 4 & 5 − TUCPA 2014 − λ = 532, 660 and 700nm). Spectral slope estimated from MODIS measurements of the Rhône River plume are shown in black (see Chapter 5).

7.3 Future Challenges

7.3.1 Future research in the Gulf of Lions

Rhône ROFI – Future research in the Rhône River ROFI should focus on the flocculation process itself. Mechanisms involved in the formation of flocs are still poorly known. We do not know among SPM concentration, salinity, or organic matter content which parameter is the most important in the control of this process. A future work focusing on the interface between the Rhône River water and the Rhône River plume in the ROFI should be done to characterize this flocculation. The strategy could be improved with the long-term monitoring of Rhône River particles properties upstream, within and downstream the Rhône River mouth as well as with in situ monitoring of particles properties and salinity conditions over the prodelta (< 20 m depth).

The transition zone between the thin surface layer (<1 m) and the subsurface layer (1 – 5 m) should be studied with more details. A need still exists to improve the vertical description of the flocs nature and proportion along the dilution of Rhône River waters in a non-intrusive way. This remains a challenge especially with research vessels, which can block the flow and disturb the stratification of the surface plume during measurements. Concerning the use of the glider, more development should also be done to provide good description of the thin surface layer. For instance, the glider could surface after each profile instead of "licking" the thin surface layer before diving. Another option would be to switch on glider sensors while transmitting data and receiving mission order at the sea surface.

A future work should be done concerning the seasonal and inter-annual variability of the Rhône River ROFI particle assemblage properties (nature, size, shape and effective density). During this thesis, 3 consecutive winters have been sampled (2014, 2015, and 2016). Different flooding and meteorological conditions have been encountered and could have an impact on the particle assemblage variability. This dataset has not been discussed in this work due to a lack of time but could provide additional information to improve our knowledge on the inter-annual variability of particles within the ROFI as well as to decrease uncertainties of our estimations of the effective densities measured during the TUCPA experiment and presented in Chapter 4.

The modelling of particles settling velocities remains decisive. Future works may improve the measurements of the particle assemblage properties, especially the measurement of the settling velocity, the effective density and several shape parameters per size class. This could be achieved with the deployment of an IN situ Size and Settling Column Tripod (INSSECT; see Mikkelsen et al. (2004) and Manning and Schoellhamer (2013)) as well as with a Particle Imaging Camera System (PICS, see Smith and Friedrichs (2011; 2015)) over the Rhône River prodelta that enable the in situ measurements of these parameters with precision.

Besides, we have shown that marine wind could favor the sedimentation of suspended particles through a more important flocculation in the surface river plume close to the coast during flooding conditions of the Rhône River. Several Rhône River floods occurred during the duration of this PhD (Fig. 7.7). During these events, the surface of the river plume highly responded to wind regimes and followed the dynamic presented in Chapter 5. Following our observations, the BNL and INL

could be alimented during each marine wind events. The vertical transfer of flocs might be enhanced favoring the deposition of fine-sediments over the Rhône River prodelta. This have to be identified studying statistical occurrences of marine wind events related to Rhône River flood events and plume structures as well as with a high-resolution modelling work based on both glider and satellite observations.
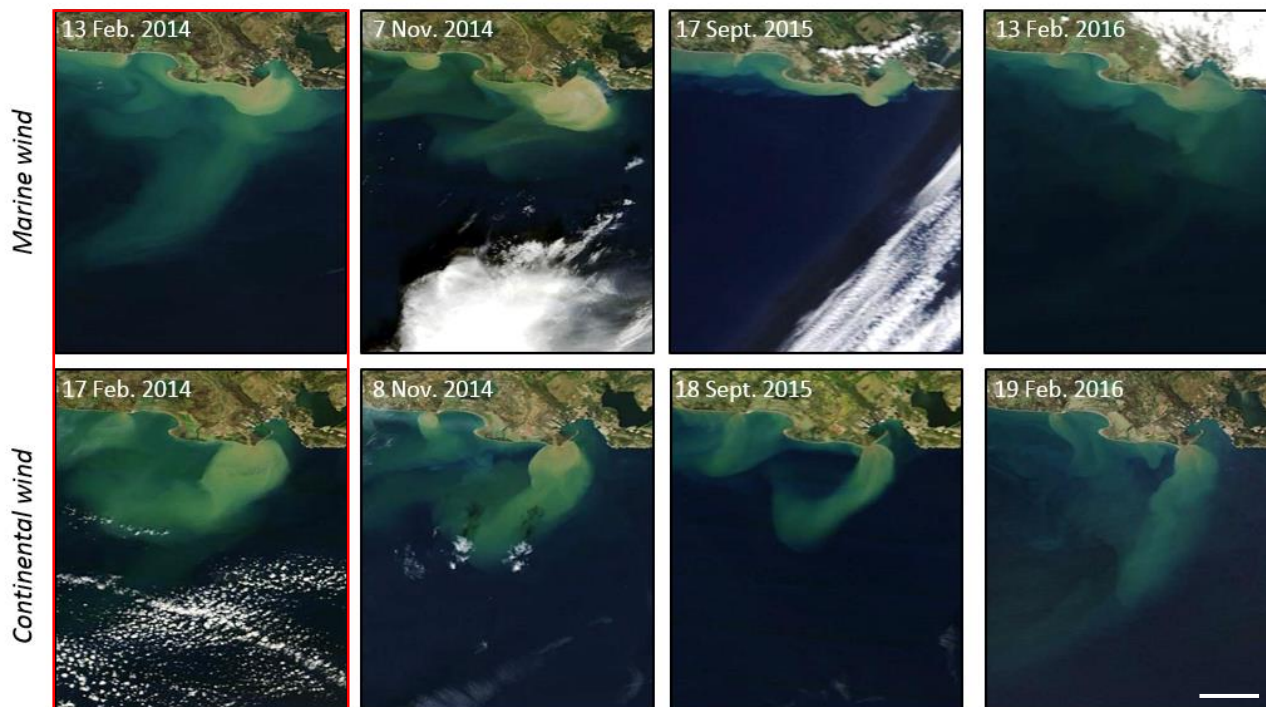
Figure 7.7 : RGB images (MODIS-Aqua/-Terra) combination showing the recurrence of the impact of marine (top) and continental (bottom) winds on the structure of the Rhône River plume during flooding conditions. The red rectangle highlights the flood detailed in Chapter 4 and 5. The white bar shows the 10 km scale.

Southwestern Gulf of Lions – Over the southwest part of the gulf, future research should focus on the variability of storm events in the particulate export offshelf to assess the multi-annual impact of such events in the sedimentary budget of the shelf. More glider deployments should be carried out during winter time to determine this variability in accordance with a long-term modelling work based on fixed and autonomous platforms measurements.

While the mechanisms of the particulate export offshelf during marine storms have been identified, a need still exists in the determination of the particulate transport over the entire shelf. Following the modelling work of Ulses (2005) and the morphological map of Monaco and Aloisi (2000) it is obvious that a large part of sediments delivered by the Rhône River is transported along-shelf and aliment the mid-shelf mud-belt (see Fig. 7.5). Cross-shelf particulate transport during storm events could nevertheless participate to the alimentation of this mud-belt as well as export sediment offshelf and have to be estimated. Besides, there is still a lack of knowledge on the role of the central part of the shelf in the variability of the suspended particles properties of the Gulf of Lions (~80 m depth).

These gaps have to be fill in future works by 1) the estimation of the particulate transport over the entire shelf during a long-period (i.e. approx. 1 year) and 2) the long-term monitoring of SPM dynamics and properties close to the seabed down to 80 m depth. Both observations could be carried out with glider(s) cross-shelf deployment(s) (equipped with optical and acoustic sensors, see 7.3.2, see also possible deployments in Fig. 7.8) and benthic moorings (equipped with LISSTs and ADCP instruments) over the mid-shelf mud-belt (Fig. 7.8). This dataset, combined with the observations of existing coastal buoys and submarine canyons moorings could then be important to constrain modelling work and finally improve the sedimentary budget at the scale of the whole shelf.
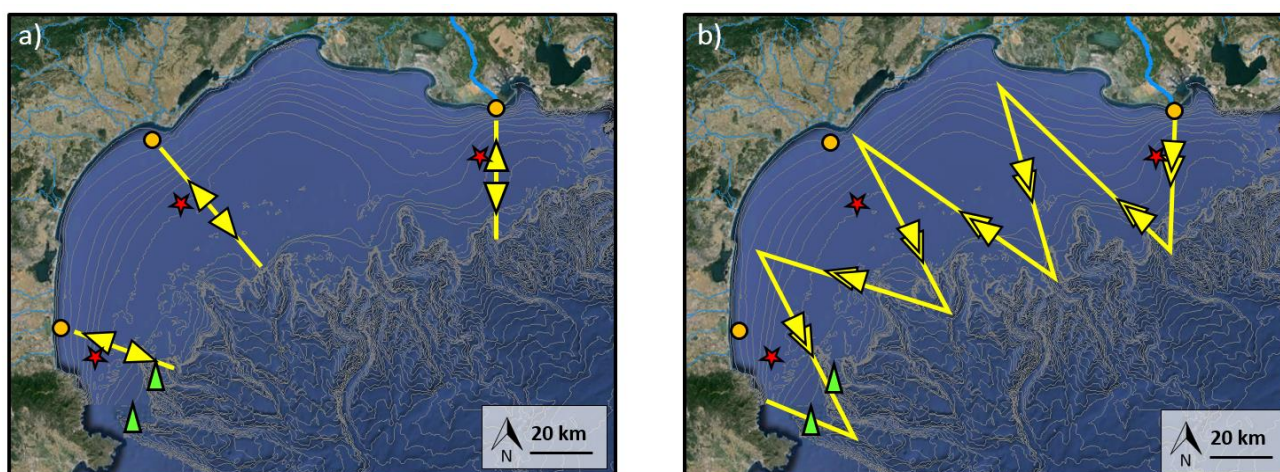
Figure 7.8 : Possible future deployments of gliders over the shelf of the Gulf of Lions (yellow lines). a) Three gliders deployed over the shelf along cross-shelf transects. The objective is to quantify during a long-period the particulate bottom transport over the entire shelf, b) One glider deployment from Marseille to Port-Vendres. Eight cross-shelf sections. The objective is to provide a "snapchot" of the particulate transport during a short-period (<2 weeks) over the whole shelf and within submarine canyons. Red stars show the possible positions of benthic tripods over the mid-shelf mud-belt. Orange circles and green triangles show respectively the position of existing coastal buoys and canyons mooring lines.

7.3.2 Towards a generalization of gliders in SPM dynamics studies and coastal observations

Gliders have shown their ability in the monitoring of SPM dynamics and properties over continental margins during flooding and storm conditions (see the dataset acquired in the Gulf of Lions and presented in this work in Annexes 2 and 3). Due to the miniaturization of recent optical sensors and their "*middle cost for high efficiency*" character, these autonomous platforms are nowadays a unique and challenging way to monitor SPM dynamics within coastal seas. While their low-energy consumption allows long-period and large-scale deployments, they provide a high density of information that is decisive to study sub meso-scale phenomena as coastal resuspension, particulate transport, river plume dispersal and particulate assemblage variability. Besides, they have shown their complementarity with remote sensing observations and also fill the gap of measurements between coastal buoys and submarine canyons moorings.

Figure 7.9 : Nortek Aquadopp current profiler fixed on a slocum glider. From Baumgartner and Fratantoni (2008).

Among the parameters derived in this work, the estimation of currents and related particulate transports (Chapter 6) could be improved by the implementation of acoustic sensors on gliders. An example of such implementation (a Nortek Aquadopp in this case) is visible in Fig. 7.9 (Baumgartner and Fratantoni, 2008). The use of such sensors could greatly improve the measurements of coastal currents and turbidity in the whole water column. It could also improve the detection of largest suspended particles (as flocs) and could thus complete the optical measurements, which are more sensible to fine sediments. The MATUGLI Programme (Mesures Autonomes de la TUrbidité par GLIder, 2016-2020), which succeeds to the TUCPA framework presented in this work, will test such system with the implementation of a RDI ADCP DVL Explorer (600 kHz) on a *slocum* coastal glider (G2).

Besides, the future miniaturization of particle properties sensors (as LASER diffraction, holography, see the new LISST-200X from Sequoia Inc. - 2016) could permit their fixation on gliders. This will be decisive in the determination of high-resolution variability of particle size, nature and shape within shelf seas during flooding and storm conditions and could highly complete the observations made during this work in the Rhône ROFI (Chapter 4 - 5) and over the southwest part of the Gulf of Lions shelf (Chapter 6).

Such outcomes call into questions the future of gliders in coastal observations. While gliders are now commonly used in in situ offshore ocean observing systems, there is still a lack of data in coastal seas and in the transition regions between offshore waters and coastal seas (see details in Liblik et al. (2016)). They are now gradually integrating several coastal observing systems such as the United States Integrated Ocean Observing Systems (US IOOS; Willis, 2013) or the Coastal Observing SYstem for Northern and Arctic seas (COSYNA; Stanev et al., 2011), which favor their deployments along "endurance lines".

In the Mediterranean, especially in the Gulf of Lions, it now seems crucial to integrate gliders as sustained platforms in the coastal zone to complete the Mediterranean Ocean Observing System for the Environment (MOOSE) to assess the long-term variability of hydrological, hydrodynamical and biogeochemical processes controlling shelf particulate transport, SPM dynamics and properties and related contaminant transports as well as shelf-slope exchanges.

References

Aloisi, J. C., J. P. Cambon, J. Carbonne, G. Cauwet, C. Millot, A. Monaco, and H. Pauc. **1982**. « Origine et rôle du néphéloïde profond dans le transfert des particules au milieu marin. Application au Golfe du Lion ». *Oceanologica Acta* 5 (4): 481–491.

Baumgartner, M. F., and D. M. Fratantoni. **2008**. « Diel periodicity in both sea whale vocalization rates and the vertical migration of their copepod prey observed from ocean gliders ». *Limnology and Oceanography* 53 (5part2): 2197–2209.

Boss, E., M. S. Twardowski, and S. Herring. **2001**. « Shape of the particulate beam attenuation spectrum and its inversion to obtain the shape of the particulate size distribution ». *Applied Optics* 40 (27): 4885‑93.

Buonassissi, C. J., and H. M. Dierssen. **2010**. « A regional comparison of particle size distributions and the power law approximation in oceanic and estuarine surface waters. » *Journal of Geophysical Research* 115 (C10). doi:10.1029/2010JC006256.

Bourrin, F. 2007. « Variabilité des apports sédimentaires par les fleuves côtiers: Cas du systeme Têt: Littoral Roussillonnais dans les Golfe du Lion ». *Thèse de Doctorat, Université de Perpignan*. 305 p.

Durrieu de Madron, X., A. Abassi, S. Heussner, A. Monaco, J.C. Aloisi, O. Radakovitch, P. Giresse, R. Buscail, and P. Kerherve. **2000**. « Particulate matter and organic carbon budgets for the Gulf of Lions (NW Mediterranean) ». *Oceanologica acta* 23 (6): 717‑30.

Dufois, F., R. Verney, P. Le Hir, F. Dumas, and S. Charmasson. **2014**. « Impact of winter storms on sediment erosion in the Rhone River prodelta and fate of sediment in the Gulf of Lions (North Western Mediterranean Sea) ». *Continental Shelf Research* 72: 57-72. doi:10.1016/j.csr.2013.11.004.

Kettner, A. J., E. W. Hutton, and J. P. Syvitski. **2004**. « Simulating the Impact of Sediment Flux of the 2003 Flood Event of the Rhone River on the Golf of Lions, France ». *AGU Fall Meeting Abstracts* 23 (décembre). http://adsabs.harvard.edu/abs/2004AGUFMOS23C1321K.

Lansard, B. **2004**. « Distribution et remobilisation du plutonium dans les sédiments du prodelta du Rhône ». Université de la Méditerranée-Aix-Marseille II. http://tel.archives-ouvertes.fr/tel-00007417/.

Liblik, T., J. Karstensen, P. Testor, P. Alenius, D. Hayes, S. Ruiz, K. J. Heywood, S. Pouliquen, L. Mortier, and E. Mauri. **2016**. « Potential for an underwater glider component as part of the Global Ocean Observing System ». *Methods in Oceanography* 17 (12): 50‑82. doi:10.1016/j.mio.2016.05.001.

Maillet, G. M., C. Vella, S. Berné, P. L. Friend, C. L. Amos, T. J. Fleury, and A. Normand. **2006**.

« Morphological Changes and Sedimentary Processes Induced by the December 2003 Flood Event at the Present Mouth of the Grand Rhône River (Southern France) ». *Marine Geology* 234 (1-4): 159-77. doi:10.1016/j.margeo.2006.09.025.

Manning, A. J., and D. H. Schoellhamer. **2013**. « Factors controlling floc settling velocity along a longitudinal estuarine transect. » *Marine Geology* 345 (10): 266‑80. doi:10.1016/j.margeo.2013.06.018.

Mikkelsen, O., T. Milligan, P. Hill and D. Moffatt. **2004**. « INSSECT - an instrumented platform for investigating floc properties close to the seabed ». *Limnology and Oceanography: Methods* 2, 2226-236.

Monaco, A., and J.C. Aloisi. **2000**. « Carte de la nature des fonds du Golfe du Lion. » Perpignan. site ORME : http://medias.obs-mip.fr/orme/.

Naudin, J. J., G. Cauwet, M. J. Chrétiennot-Dinet, B. Deniaux, J. L. Devenon, and H. Pauc. **1997**. « River Discharge and Wind Influence Upon Particulate Transfer at the Land–Ocean Interaction: Case Study of the Rhone River Plume ». *Estuarine, Coastal and Shelf Science* 45 (3): 303‑16. doi:10.1006/ecss.1996.0190.

Radakovitch, O., S. Charmasson, M. Arnaud, and P. Bouisset. **1999**. « ^{210}Pb and Caesium Accumulation in the Rhône Delta Sediments ». *Estuarine, Coastal and Shelf Science* 48 (1): 77–92.

Sadaoui, M., W. Ludwig, F. Bourrin, and P. Raimbault. **2016**. « Controls, budgets and variability of riverine sediment fluxes to the Gulf of Lions (NW Mediterranean Sea). » Journal of Hydrology, in press

Slade, W. H., and E. Boss. **2015**. « Spectral attenuation and backscattering as indicators of average particle size ». *Applied Optics* 54 (24): 7264. doi:10.1364/AO.54.007264.

Smith, S. J., and C. T. Friedrichs. **2011**. « Size and settling velocities of cohesive flocs and suspended sediment aggregates in a trailing suction hopper dredge plume. » *Continental Shelf Research* 31 (10): S50‑63. doi:10.1016/j.csr.2010.04.002.

Smith, S. J., and C. T. Friedrichs. **2015**. « Image processing methods for in situ estimation of cohesive sediment floc size, settling velocity and density » *Limnology and Oceanography: Methods* 13. 250-264. doi:10.1002/lom3.10022.

Stanev, E., J. Stellenfleth, J. Staneva, S. Grayek, J. Seemann, and W. Petersen. **2011**. « Coastal observing and forecasting system for the German Bight – estimates of hydrophysical states ». *Ocean Science* 7 (5): 569‑83. doi:10.5194/os-7-569-2011.

Thill, A., S. Moustier, J. M. Garnier, C. Estournel, J. J. Naudin, and J. Y. Bottero. **2001**. « Evolution of particle size and concentration in the Rhône river mixing zone:

influence of salt flocculation. » *Continental Shelf Research* 21 (18): 2127‑40.

Ulses, C. **2005**. « Dynamique océanique et transport de la matière particulaire dans le Golfe du Lion: crue, tempête et période hivernale. » *Thèse de Doctorat,*

Université de Toulouse. 262 p.

Willis, Z. **2013**. « US Integrated Ocean Observing System (IOOS) delivering benefits and the Global HF Radar and Glider Initiative ». 2013 MTS/IEEE OCEANS—Bergen, JUN 10–14 2013.

General conclusion

This PhD provided a unique view of the impacts of storm and flood events on suspended particulate matter dynamics and properties in the Gulf of Lions. While episodic, these events induced a high variability in the turbidity of the coastal zone. They play a major role in the regulation of the sedimentary budgets of the shelf. The monitoring of such events appeared as decisive to understand factors impacting benthic habitats, sequestration of carbon and transport of contaminants in the water column.

Based on a multi-platform approach, composed of fixed platforms, glider, satellite and ship observations, we described in details the spatial and temporal variability of nepheloids across the shelf during such events. We demonstrated the need of gliders, equipped with several sensors, to provide useful information with high temporal and spatial resolutions, which greatly completed the existing observational strategy. Additionally, we verified the ability of glider and satellite to provide an index of the suspended particles size, which was decisive to understand coastal SPM properties variability within the gulf.

We highlighted the role of the flocculation phenomena in the regulation of the vertical transfer of fine sediments from the Rhône River to the local prodelta. Besides, we emphasized the role of wind in the highly dynamical character of nepheloids in the same area. These observations highlighted the role of the Rhône River prodelta, which trapped a large part of flocculated fine sediments delivered by the Rhône River and acted as a sediment, carbon and related contaminant sink. Furthermore, the role of a marine storm in the export of sediments offshelf was identified. We highlighted the role of such event in the resuspension of deposited sediments and in the particulate transport over the whole shelf. Results enabled to improve our knowledge on the sedimentary budget of the shelf as well as to describe the bypassing character of the southwest part of the shelf in the land-derived material continuum.

At last, outlooks of this work were discussed, especially the need of the determination of the inter-annual variability of these events, which could play a main role in sedimentary budgets of the shelf. We also emphasized the need to integrate gliders as sustained platforms within shelf seas to complete existing observation system to assess long-term variability of hydrological, hydrodynamical and biogeochemical processes that occur in the Gulf of Lions.

remote sensing

MDPI

Potential of High Spatial and Temporal Ocean Color Satellite Data to Study the Dynamics of Suspended Particles in a Micro-Tidal River Plume

Anouck Ody [1],*, David Doxaran [1], Quinten Vanhellemont [2], Bouchra Nechad [2], Stefani Novoa [1], Gaël Many [3], François Bourrin [3], Romaric Verney [4], Ivane Pairaud [5] and Bernard Gentili [1]

[1] Laboratoire d'Océanographie de Villefranche sur Mer (LOV), UMR 7093, CNRS/UPMC, F-06230 Villefranche Sur Mer Cedex, France; david.doxaran@obs-vlfr.fr (D.D.); stefani.novoa@obs-vlfr.fr (S.N.); bernard.gentili@obs-vlfr.fr (B.G.)

[2] Royal Belgian Institute of Natural Sciences (RBINS), Operational Directorate Natural Environment, B-1200 Brussels, Belgium; qvanhellemont@naturalsciences.be (Q.V.); bnechad@naturalsciences.be (B.N.)

[3] Centre de Formation et de Recherche sur les Environnements Méditerranéens (CEFREM), UMR 5110, CNRS/UPVD, F-66100 Perpignan, France; gael.many@univ-perp.fr (G.M.); fbourrin@univ-perp.fr (F.B.)

[4] IFREMER, Centre Bretagne, Laboratoire de Dynamique Hydro-Sédimentaire, F-29280 Brest, France; Romaric.Verney@ifremer.fr

[5] IFREMER, Centre Méditerranée, Laboratoire Environnement Ressources Provence Azur Corse, F-83507 La Seyne sur Mer, France; Ivane.Pairaud@ifremer.fr

* Correspondance: anouck.ody@obs-vlfr.fr; Tel.: +33-493-763-738

Abstract: Ocean color satellite sensors are powerful tools to study and monitor the dynamics of suspended particulate matter (SPM) discharged by rivers in coastal waters. In this study, we test the capabilities of Landsat-8/Operational Land Imager (OLI), AQUA&TERRA/Moderate Resolution Imaging Spectroradiometer (MODIS) and MSG-3/Spinning Enhanced Visible and Infrared Imager (SEVIRI) sensors in terms of spectral, spatial and temporal resolutions to (i) estimate the seawater reflectance signal and then SPM concentrations and (ii) monitor the dynamics of SPM in the Rhône River plume characterized by moderately turbid surface waters in a micro-tidal sea. Consistent remote-sensing reflectance (Rrs) values are retrieved in the red spectral bands of these four satellite sensors (median relative difference less than ~16% in turbid waters). By applying a regional algorithm developed from *in situ* data, these Rrs are used to estimate SPM concentrations in the Rhône river plume. The spatial resolution of OLI provides a detailed mapping of the SPM concentration from the downstream part of the river itself to the plume offshore limits with well defined small-scale turbidity features. Despite the low temporal resolution of OLI, this should allow to better understand the transport of terrestrial particles from rivers to the coastal ocean. These details are partly lost using MODIS coarser resolutions data but SPM concentration estimations are consistent, with an accuracy of about 1 to 3 $g \cdot m^{-3}$ in the river mouth and plume for spatial resolutions from 250 m to 1 km. The MODIS temporal resolution (2 images per day) allows to capture the daily to monthly dynamics of the river plume. However, despite its micro-tidal environment, the Rhône River plume shows significant short-term (hourly) variations, mainly controlled by wind and regional circulation, that MODIS temporal resolution failed to capture. On the contrary, the high temporal resolution of SEVIRI makes it a powerful tool to study this hourly river plume dynamics. However, its coarse resolution prevents the monitoring of SPM concentration variations in the river mouth where SPM concentration variability can reach 20 $g \cdot m^{-3}$ inside the SEVIRI pixel. Its spatial resolution is nevertheless sufficient to reproduce the plume shape and retrieve SPM concentrations in a valid range, taking into account an underestimation of about 15%–20% based on comparisons with other sensors and *in situ* data. Finally, the capabilities, advantages and limits of these satellite sensors are discussed in the light of the spatial and temporal resolution improvements provided by the new and future generation of ocean color sensors onboard the Sentinel-2, Sentinel-3 and Meteosat Third Generation (MTG) satellite platforms.

Keywords: remote sensing; high resolution; suspended particulate matter; coastal waters; river plumes

Annex 2. Glider data (Rhône ROFI - TUCPA 2014)
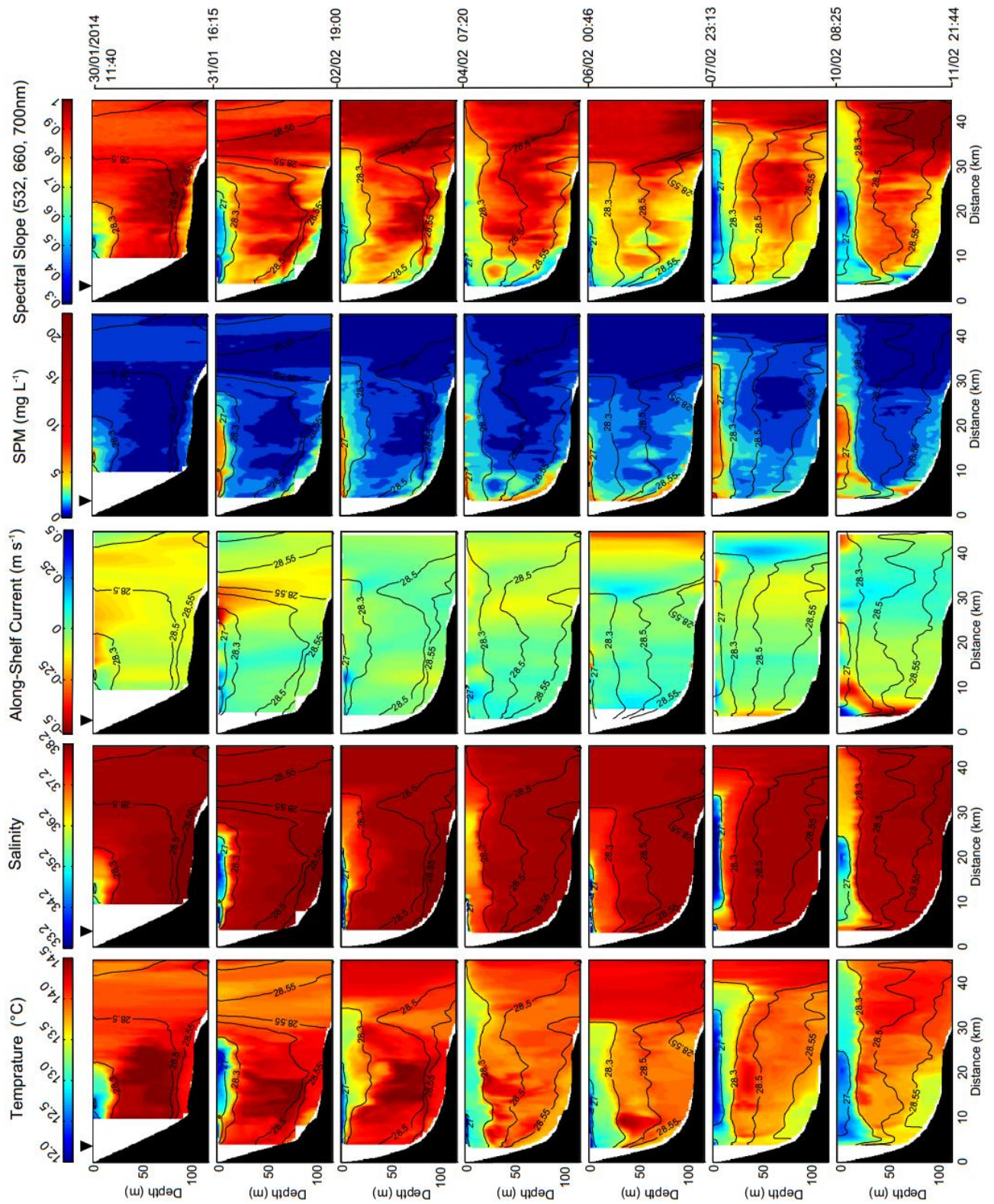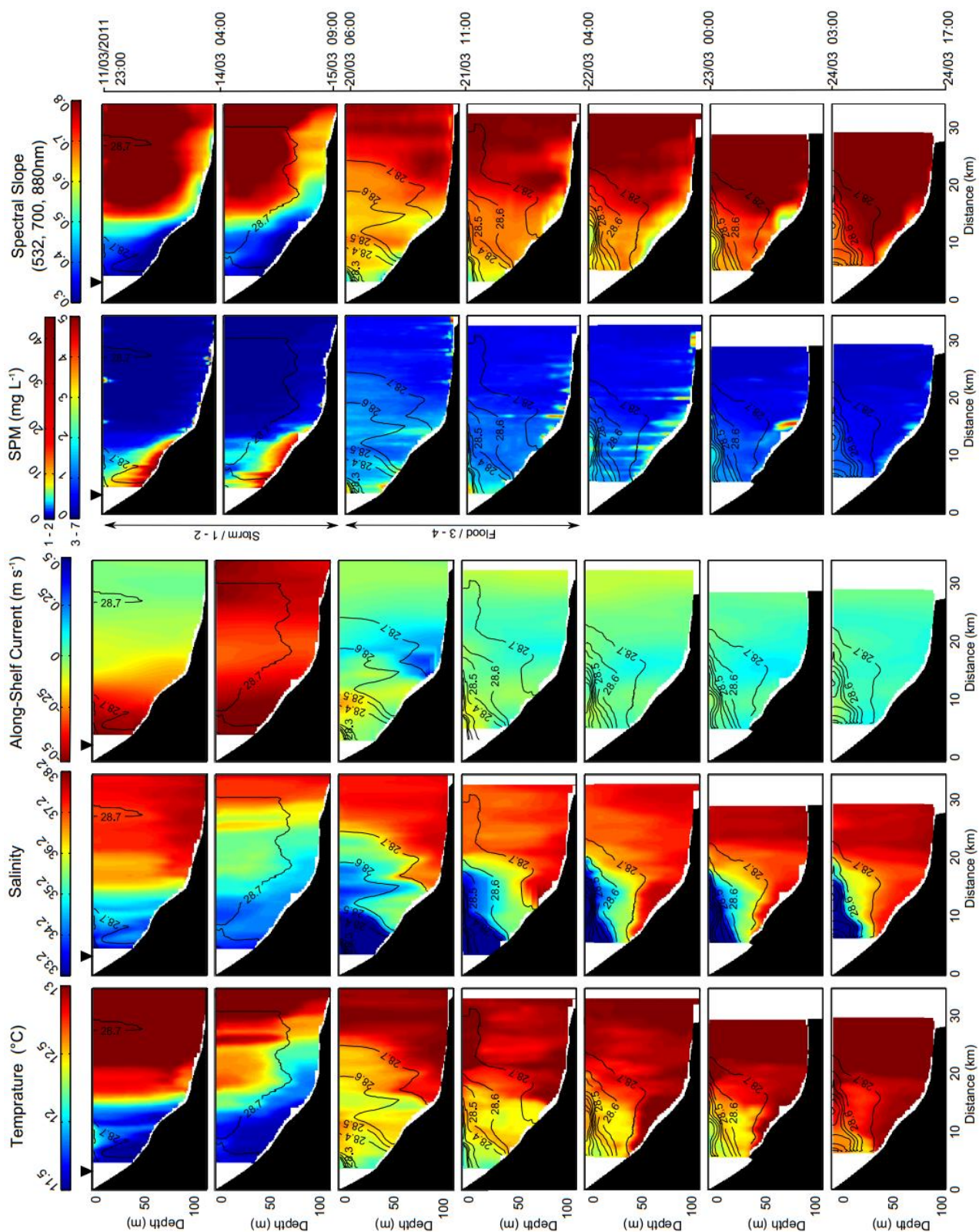
Résumé (Français)

1. Introduction

La zone côtière représente un compartiment de l'océan global, où la terre, la mer et l'atmosphère interagissent fortement. Elle rassemble de nombreux compartiments comme les deltas, les régions sous influences d'eau douce (aussi appelée ROFIs pour « Regions Of Freshwater Influence ») et les marges continentales. Cette zone, aussi appelée épipélagique en océanographie, est généralement caractérisée par des profondeurs maximales de 200 m. Elle est délimitée dans sa zone interne par la côte et par les pentes continentales à l'autre extrémité.

Bien que sa surface soit faible (approx. 7% de la surface totale des océans) cette zone rassemble de nombreux enjeux et risques. Elle représente ainsi une zone de concentration préférentielle pour les apports de matières provenant des continents (comme les sédiments, les nutriments et les contaminants) qui jouent un rôle primordial dans la séquestration des éléments chimiques (comme le carbone), les budgets sédimentaires des plateaux continentaux et le bon état écologique des habitats benthiques. En chiffre, la zone côtière représente à elle seule près de 15% de la production biologique mondiale et près de 75-90% du piégeage des apports par les rivières. Economiquement, la zone côtière représente près de 90% des efforts de pêches.

Dans un tel contexte, les pays européens ont mis en place la Directive Cadre sur l'Eau (DCE – 2000) et la Directive Cadre Sur le Milieu Marin (DCSMM – 2008). Ces directives définissent plusieurs paramètres clés afin de mesurer et d'évaluer l'état initial et l'évolution de la qualité de la zone côtière. Parmi ces paramètres, la turbidité (i.e. la clarté de l'eau) apparaît comme un paramètre décisif contrôlant la qualité de l'eau et régulant les processus biogéochimiques. La réponse des différentes communautés scientifiques s'organise sur les bases de la Gestion Intégrée de la Zone Côtière (GIZC). Ce programme international tente de fédérer les orientations scientifiques nationales autour d'objectifs communs concernant les aspects fondamentaux de la réponse de l'océan côtier aux forçages climatiques et anthropiques.

Les études scientifiques précédentes se sont ainsi intéressées à la turbidité (provenant de sources naturelles et anthropiques) au sein de la zone côtière, avec, pour principaux objectifs, la caractérisation in situ de la variabilité spatiale et temporelle de la dynamique des matières en suspension (MES) jouant un rôle majeur dans le continuum terre-mer du matériel particulaire. Les mesures, réalisées à partir de plateformes variées (bateau, bouée côtière, mouillage benthique, satellite ou robot sous-marin autonome ou « glider »), ont permis de mettre en évidence la diversité des structures turbides, appelées néphéloïdes, observable au sein de la zone côtière, ainsi que l'importance des évènements extrêmes (tempêtes, crues) et

des propriétés particulaires (nature, taille et vitesse de chute) dans les processus régulant la dynamique des MES. Les auteurs ont décrit la turbidité au sein de la zone côtière comme un paramètre clé impliqué dans le transport de contaminants dans la colonne d'eau, l'extension des zones benthiques polluées et l'impact négatif sur la productivité biologique en réduisant la pénétration de la lumière dans les eaux de surface et la photosynthèse associée.

Le travail présenté dans cette thèse est relié aux projets CASCADE (CAscading, Storm, Convection, Advection and Downwelling Events) et TUCPA (Turbidité Côtière et Plateformes Autonomes). Il fait suite aux recherches effectuées dans le cadre du projet européen EUROSTRATAFORM (EUROpean margin STRATAs FORMation) qui a permis de mettre en évidence la complexité de la dynamique des MES ainsi que le rôle des propriétés particulaires au sein de la zone côtière du Golfe du Lion (Méditerranée) dans le devenir des apports continentaux depuis les sources (rivières) aux puits (plateau continental, canyons sous-marins, océan profond) (Syvitski et al., 2004; Weaver et al., 2006; Durrieu de Madron et al., 2008).

Les principaux objectifs de cette thèse, réalisée au "Centre de Formation et de Recherche sur les Environnements Méditerranéens" (CEFREM – UMR5110 CNRS/UPVD) de l'Université de Perpignan (France) sont de développer nos connaissances concernant le rôle des évènements de crue et de tempête, dans les échanges de matière particulaire au sein du continuum terre-mer du Golfe du Lion. Tandis que les tempêtes participent activement à la resuspension des sédiments déposés sur le plateau du golfe et accentuent le transport particulaire; les crues des fleuves côtiers, majoritairement celles du Rhône, jouent un rôle décisif dans la propagation, la chute et la sédimentation du matériel particulaire en suspension.

Les questions clés développées en amont de cette thèse peuvent être résumées comme :

- Quelle est la variabilité spatiale de l'assemblage particulaire au sein de la ROFI du Rhône lors d'un évènement de crue ?
- Quelle est la dynamique des différents néphéloïdes au sein de la ROFI du Rhône pendant un évènement de crue ?
- Quel est l'impact d'une tempête sur le transport particulaire du Golfe du Lion ?

Ce travail est basé sur des observations côtières in situ de la dynamique des MES et des propriétés optiques des particules en suspension au sein du Golfe du Lion. Il a permis de réaliser plusieurs mesures novatrices afin de caractériser l'hydrologie, l'hydrodynamisme, la turbidité et les propriétés particulaires à partir de plateformes variées (satellite, bouées côtières, mouillages, gliders et bateaux océanographiques).

Cette thèse est organisée autour de 7 chapitres. Le premier présente le contexte de ce travail et est suivi des paramètres régionaux de la zone d'étude. Ces chapitres sont construits autour des précédentes observations réalisées au sein des marges continentales au niveau mondial et du plateau du Golfe du Lion. La stratégie multiplateforme adoptée en amont de ce travail est présentée dans le Chapitre 3.

Trois articles composent les chapitres suivants de cette thèse (Chapitre 4, 5 et 6). Le Chapitre 4 présente l'étude de la variabilité spatiale des propriétés de l'assemblage particulaire (nature, taille, densité effective) au sein de la ROFI du Rhône pendant un évènement de crue (Many et al., 2016). Le Chapitre 5 décrit la dynamique haute-fréquence des néphéloïdes au sein de cette même zone combinant les observations réalisées à partir de bouée côtière, glider et satellite (Many et al., *in prep*.). Le Chapitre 6 détaille l'impact d'une tempête marine sur l'hydrologie, l'hydrodynamisme et le transport de MES au-dessus du plateau du Golfe du Lion (Bourrin et al., 2015). Enfin, les conclusions générales de cette étude et les prospectives sont abordées dans le Chapitre 7.

Ce travail a été réalisé en partenariat avec de nombreux collaborateurs. La Figure 1 présente le rôle de chacun dans la réalisation de cette étude.
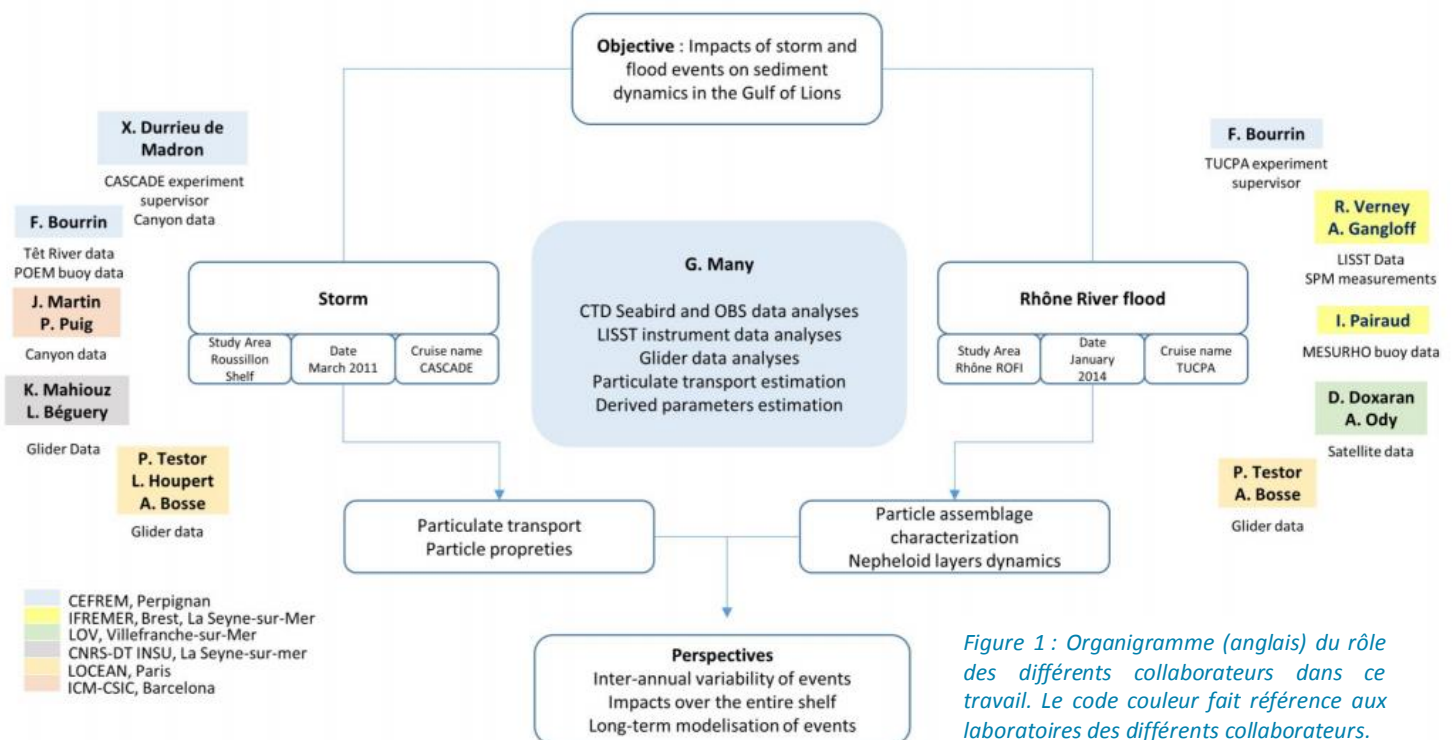
Figure 1 : Organigramme (anglais) du rôle des différents collaborateurs dans ce travail. Le code couleur fait référence aux laboratoires des différents collaborateurs.

Cette étude se place dans la continuité des observations réalisées dans les dernières décennies. En effet les implications du Rhône et du transport particulaire de fond ont été largement étudiées par le passé, à travers différents projets nationaux ou européens et basées sur des plateformes d'observation variées. L'infographie page suivante présente l'évolution de ces observations et permet de situer cette thèse dans la continuité de ces travaux. En

Précédentes études sur la dynamique des MES au sein du Golfe du Lion

Programme

Années

Français   Européen

1980

Observations

?

Rôle du Rhône et du transport benthique

Rhône   fond

ECOMARGE

Première description des néphéloïdes dans la ROFI du Rhône

Première description du néphéloïde benthique (BNL)

1990

PNOC   EuroMARGE

MATER   INTERPOL

Processus de sédimentation

Variabilité spatiale et temporelle

Rôle de la flocculation dans la chute et la sedimentation des particules fines

Variabilité saisonnière et description spatiale sur l'ensemble du plateau

PNEC   EuroSTRATAFORM

Variabilité spatiale et temporelle

Le role de la flocculation dans le transport des MES

2000

Modélisation de la dynamique du panache

Tempêtes

HERMIONE   MERMEX   TUCPA   MATUGLI

Crue

Le role des tempêtes dans le transport de MES proche de la côte

2010

Thèse

Observations satellite de l'extension spatiale du panache

Le role des tempêtes dans l'export de MES au sein des canyons

Dynamique et propriétés des MES délivrées au sein du plateau

Le rôle des tempêtes dans la dynamique, les propriétés et le transport des MES sur l'ensemble du plateau

2020

Techniques

campagne en mer   mouillage   modélisation   bouée côtière   satellite   glider

Approche multiplateforme

	Extension*					
Temps	-	++	++	++	++	+
Espace	+	-	++	-	++	+

	Résolution*					
Temps	+	++	+	++	+	+
Espace	-	::	-	::	+	+

Créé par **G.Many** (2016)

2. Principaux résultats

Ce travail a mis en évidence les différents mécanismes permettant la sédimentation des matières en suspension (MES) délivrées par le Rhône en période de crue et a permis de déterminer le rôle d'une tempête sur l'export de matière particulaire en dehors du Golfe du Lion. Tandis que ces évènements sont considérés comme épisodiques, ils se produisent sur de larges échelles et apparaissent comme des processus clés dans la régulation de la dynamique sédimentaire de la marge continentale.

2.1. L'impact d'une crue dans la dynamique des MES au sein de la région sous influence d'eau douce du Rhône

2.1.1 Le rôle de la floculation dans la sédimentation des particules fines

Nous avons montré la variabilité de l'assemblage particulaire au sein de la ROFI du Rhône pendant un évènement de crue du fleuve (Figure 2). Un package instrumental, composé d'une sonde CTD, un LISST-100 (diffraction LASER) et un LISST-HOLO (caméra holographique) a été utilisé afin de caractériser les paramètres hydrologiques et les propriétés particulaires des particules en suspension (concentration, taille, nature, forme et densité effective). Les résultats ont mis en évidence la nécessité de combiner les mesures de diffraction LASER avec les mesures holographiques afin de déterminer 1) le plus large spectre de la distribution en taille des particules, 2) la nature des MES et 3) la forme des plus grosses particules en suspension. La diversité de la forme des particules en suspension a montré la non-sphéricité des particules d'une manière globale. Cette observation a permis de confirmer la nécessité d'utiliser un algorithme basé sur des particules non-sphériques afin d'inverser la distribution en taille des particules à partir de la diffusion de la lumière dans l'eau de mer.

En parallèle, un glider « slocum » a été déployé afin de décrire la variabilité spatiale des paramètres hydrologiques et particulaires. Nous avons vérifié l'habilité du glider, muni de capteurs de turbidité à plusieurs longueurs d'onde, à fournir un index de la distribution en taille des MES. Cet index a finalement été comparé et validé contre des mesures in situ (instruments LISST).

Les observations réalisées peuvent être résumées comme suit :

- Pendant un évènement de crue du Rhône en 2014, le fort débit (> 5000 m^3/s) lié aux vents continentaux ont favorisé la dispersion du panache du Rhône vers le large (> 30km). La concentration de surface en MES a montré une diminution drastique

le long du transect côte-large de 20 mg/L proche de l'embouchure à 1.5 mg/L proche de la pente continentale. Un néphéloïde benthique (BNL pour « bottom nepheloid layer ») a été observé au-dessus de l'ensemble du plateau présentant une diminution en MES de 8 mg/L à moins de 1 mg/L en allant vers le large. Un lien existant entre le panache du Rhône et le BNL a été mis en évidence, possiblement accentué par les évènements de resuspension proche de la côte.

- Les observations ont mis en évidence un phénomène de floculation des particules fines (1-10 μm, argiles et silts fins) en micro- et macro-flocs (30-400μm) proche de la côte. La concentration en MES et le fort gradient de salinité semblent réguler ce phénomène. L'assemblage particulaire au sein du panache du Rhône et du BNL s'affine en allant vers le large, traduisant la chute et la dilution des flocs au sein des eaux côtières. La densité effective de l'assemblage particulaire a ainsi montré une nette augmentation le long du transect côte-large avec des valeurs allant de 370 à 1600 kg/m^3, et présentant des valeurs maximales au-dessus de la vasière médiane.
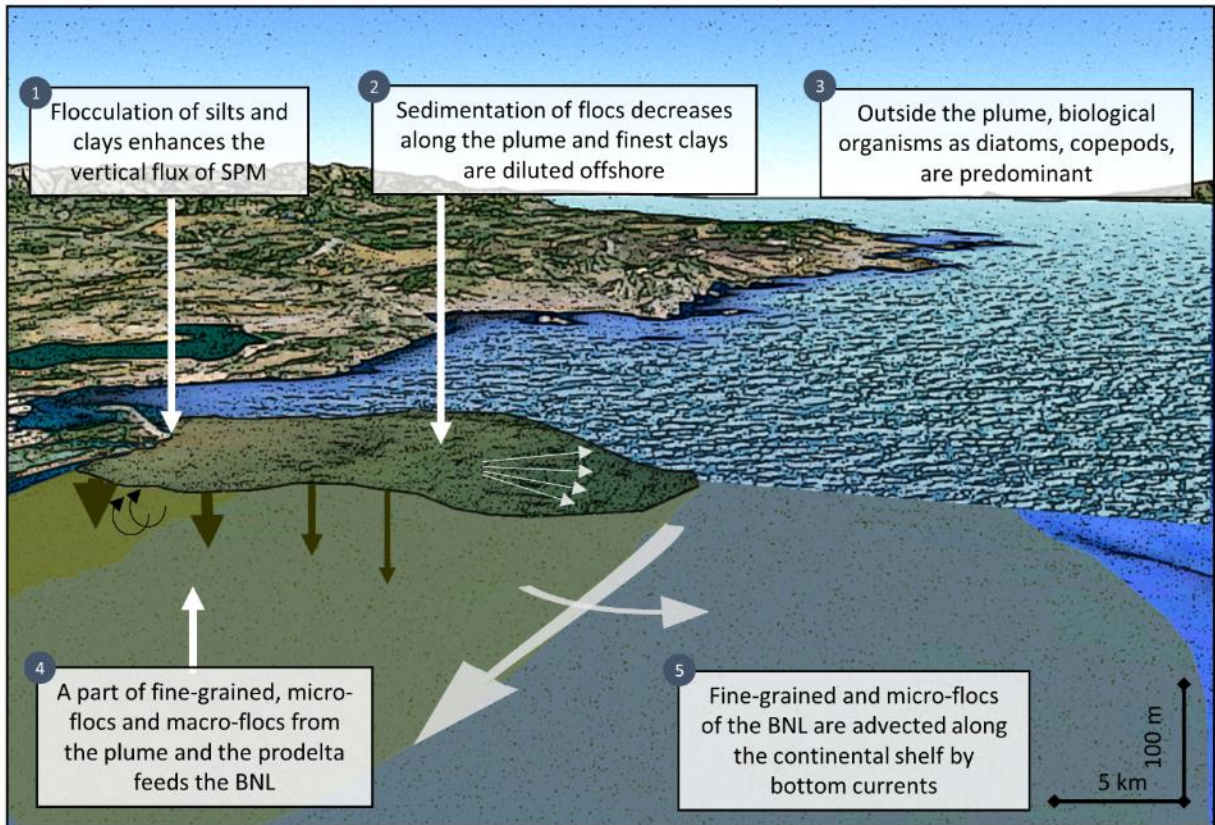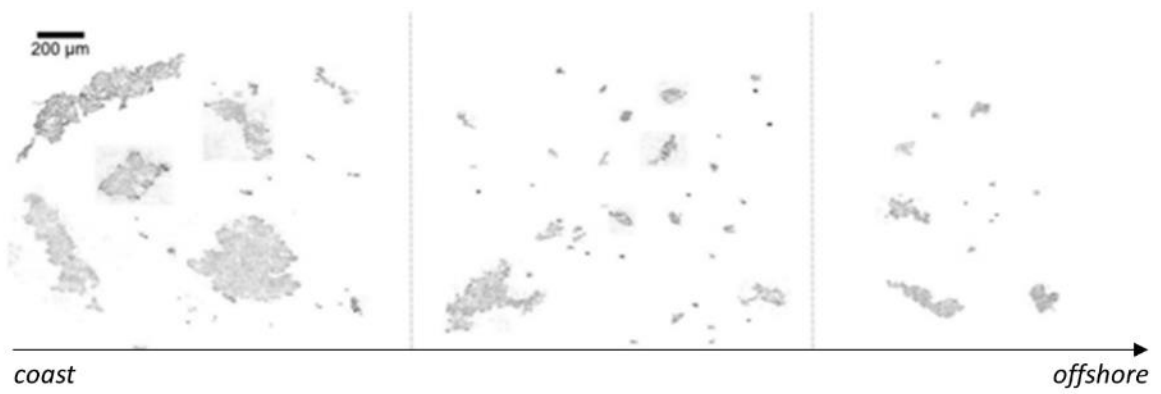
Figure 2 : Résumé graphique (anglais) de la variabilité de l'assemblage particulaire dans la ROFI du Rhône. Les images des micro- (20-125 µm) et macro-flocs (>125 µm) qui composent le panache du Rhône et le néphéloïde benthique sont mis en évidence. La vue est du sud-ouest.

2.1.2 La dynamique des néphéloïdes

Nous avons montré la forte variabilité des néphéloïdes existante au sein de la ROFI du Rhône pendant un évènement de crue (Figure 3). Les observations grandes échelles réalisées à partir de satellite et glider ont été combinées aux données d'une bouée côtière afin d'obtenir une vue unique de l'impact de différents régimes de vent sur la dynamique des MES. La pente spectrale dérivées à partir des mesures glider et satellite de rétrodiffusion particulaires à plusieurs longueurs d'onde a été utilisée afin de caractériser la variabilité spatiale et temporelle haute-fréquence de l'assemblage particulaire.

Les observations réalisées peuvent être résumées comme suit :

- Le développement du panache du Rhône (5-50 mg/L) ainsi que du néphéloïde benthique (1-2 mg/L) au-dessus de l'ensemble du plateau a été observé. Le panache du Rhône était fortement stratifié et a montré des valeurs de concentration en MES maximales (> 35 mg/L) au sein d'une fine couche de surface (< 1m, données satellitaires). L'assemblage particulaire était 1) plus fin dans la fine couche de surface que dans la couche de subsurface et 2) variable le long du transect en travers du plateau au sein du panache et du BNL, s'affinant en allant vers le large.
- Les vents continentaux ont augmenté l'export de MES au-dessus du plateau du Golfe du Lion alors que les vents marins ont plaqué le panache du Rhône le long de la côte. Durant ces mêmes vents marins, la concentration en MES a augmenté fortement en surface, ce qui semble avoir favorisé une plus grande floculation des particules fines et, de ce fait, un transfert vertical des particules en suspension du panache du Rhône vers le BNL plus important. Ce transfert pourrait être accentué par des phénomènes épisodiques de resuspension induits par les vagues au-dessus du prodelta Rhodanien (< 20m de profondeur).
- Les mesures de rétrodiffusion particulaire réalisées grâce au glider, combinées avec les estimations des paramètres de stratification ont permis de mettre en évidence le rôle d'une tempête modérée dans la rupture de stratification du panache du Rhône et dans le transport le long de la côte des particules en suspension. Ce transport pourrait être localement accentué par de la remise en suspension des sédiments pour des profondeurs maximales de 60 m venant augmenter la concentration en MES dans l'ensemble de la colonne d'eau.
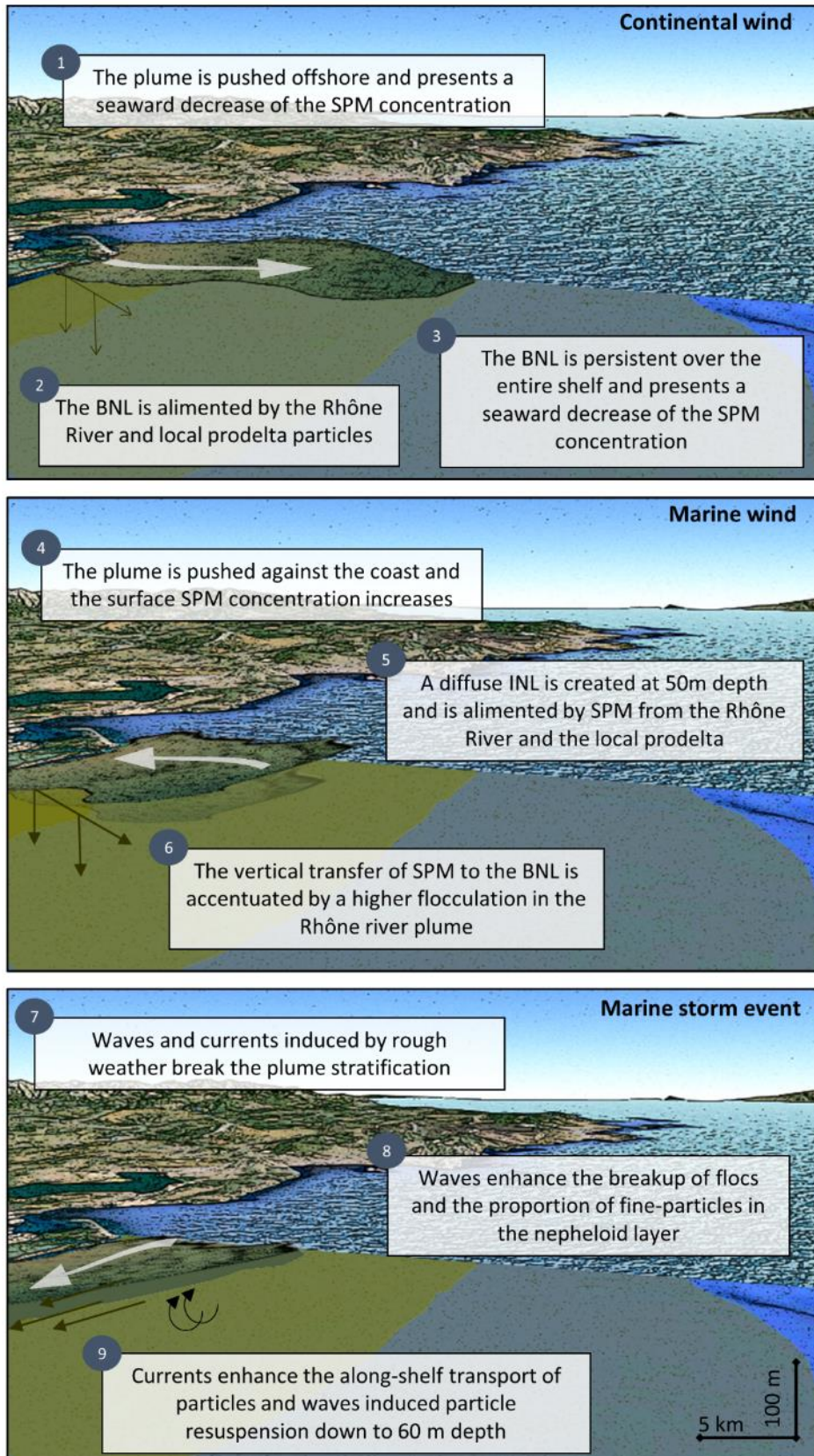
Figure 3 : Résumé graphique (anglais) des forçages météorologiques sur la dynamique des MES dans la ROFI du Rhône pendant un évènement de crue. Haut et milieu - Evènements de vents continentaux et marins sans fortes vagues. Bas – Impacts d'un évènement de tempête (vent marin, vagues > 3m et courant > 0.5 m/s). La vue est du sud-ouest.

2.2 L'impact d'une tempête dans l'export de MES en dehors du plateau.

Le rôle d'une tempête et d'une crue concomitante sur la dynamique des MES et le transport particulaire au-dessus de la partie sud-ouest du Golfe du Lion a été identifié (Figure 4). Un glider a été déployé durant 2 mois, afin de déterminer la variabilité haute-fréquence de l'hydrologie, l'hydrodynamisme et les flux et propriétés des MES. Ces résultats ont été combinés aux données acquises par satellite, bouée côtière et lignes de mouillages au sein de canyons sous-marins. Les observations gliders ont été décisives afin de déterminer comment les transferts particulaires le long de la côte et en travers du plateau étaient affectés durant la tempête. Ces observations haute-résolutions, (i.e. un profil tous les 200 m) ont permis de mettre en évidence les phénomènes de resuspension et de transport particulaire avec une forte précision. Enfin, la dérivation de la pente spectrale des mesures glider de rétrodiffusion particulaire à plusieurs longueurs d'onde a permis de décrire la variabilité spatiale de l'assemblage particulaire pendant les évènements successifs de tempête et de crue.

Les observations réalisées peuvent être résumées comme suit :

- La resuspension des sédiments (érosion de 4 cm à 23 m de profondeur) observée grâce à la bouée côtière pendant la tempête (vagues > 4 m) était effective sur l'ensemble du plateau pour des profondeurs maximales de 80 m (max. concentration MES de 45 mg/L). L'augmentation de la concentration en MES proche du fond semble augmenter la floculation des sédiments fins et pourrait limiter le transport particulaire.
- Pendant la tempête, les courants le long de la côte ont été estimés à plus de 0.6 m/s contre 0.1 m/s en travers du plateau, démontrant le rôle de la tempête dans l'accentuation de la circulation cyclonique générale au sein du Golfe du Lion. Cette circulation entraina un fort transport de particules en suspension vers l'extrémité sud du plateau, maximum au-dessus de la vasière médiane (flux de 0.5 t/s). En parallèle, le flux particulaire en travers du plateau semble favoriser l'alimentation de la vasière médiane par l'advection des sédiments resuspendus par les vagues proche de la côte.
- Le transport particulaire cumulé sur la période de la tempête a été estimé à 1-2 Mt. La plupart des particules transportées semble avoir « by-passé » le Cap de Creus vers le nord du plateau Catalan. La comparaison entre les flux estimés à partir du glider et ceux au sein du canyon sous-marin du Cap de Creus a ainsi pu permettre d'estimer à 10% la part des particules transportées par la tempête expulsée à travers ce canyon.
- Les MES délivrées lors de la crue des fleuves concomitante à la tempête ont localement compensé l'érosion induite par la resuspension des sédiments. Les panaches fluviaux induits par l'augmentation du débit des fleuves ont entrainé une restratification rapide des eaux côtières.

During a storm event, waves (>4m) enhance the particle resuspension in the water column down to 80m depth

Close to the seabed (30-40m), where the SPM concentration is maximum (> 30 mg L^{-1}), fine-sediment flocculation occur and increase the proportion of 'flocs' in the particle assemblage

Cap de Creus

The 'Coastal River' by-pass the Cap de Creus and is advected over the Catalonia shelf by cyclonic circulation

A part of BNL particles are advected within submarine canyons

Currents are oriented southward and decrease from the coast (0.6 m s^{-1}) to the shelf edge (0.1 ms^{-1}). The particulate transport is estimated to 4 t s^{-1}

For depth over 60m the BNL (10 m high) is advected southward by bottom currents and is alimented by resuspended particles from the shallower area

80 m

The subsequent flood event of coastal rivers enhances the particulate delivery to the shelf

Cap de Creus

Particulate along- and cross-shelf transport are minimum highlighting the rapid flushing of suspended particles during the storm

Restratification of the water column induces by freshwater input enhances the offshore export of suspended particles

Sedimentation of particles locally balances the erosion (4 cm) induces by marine storm
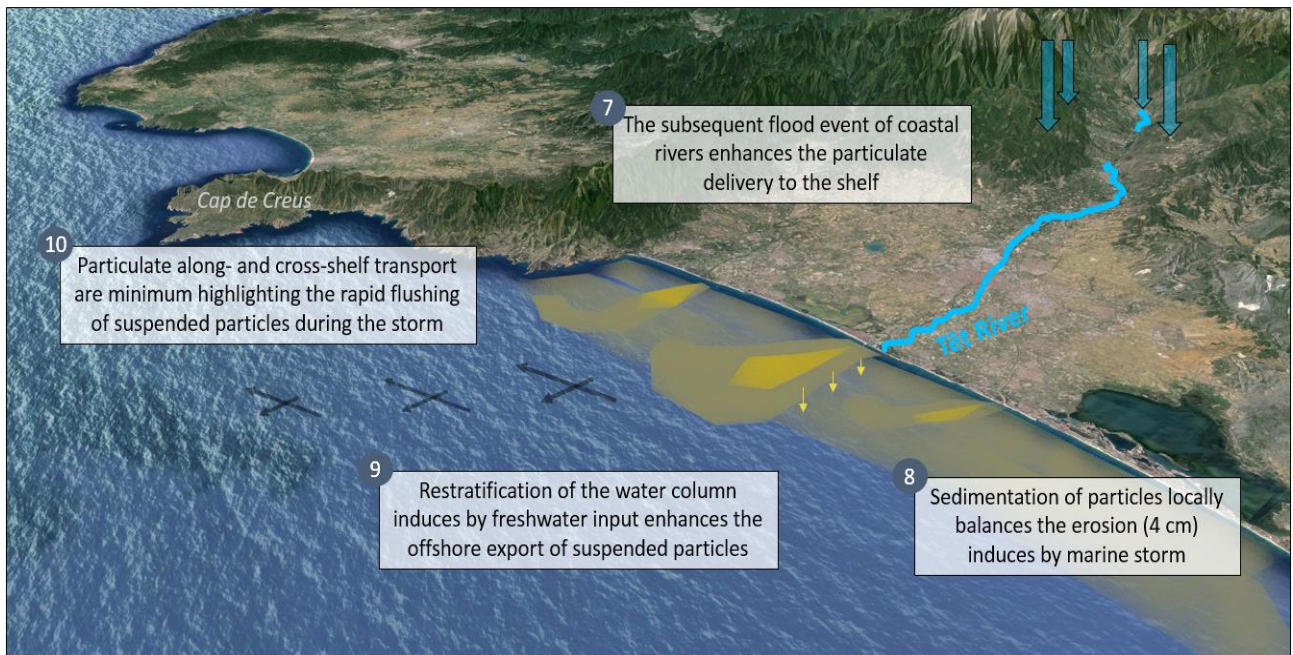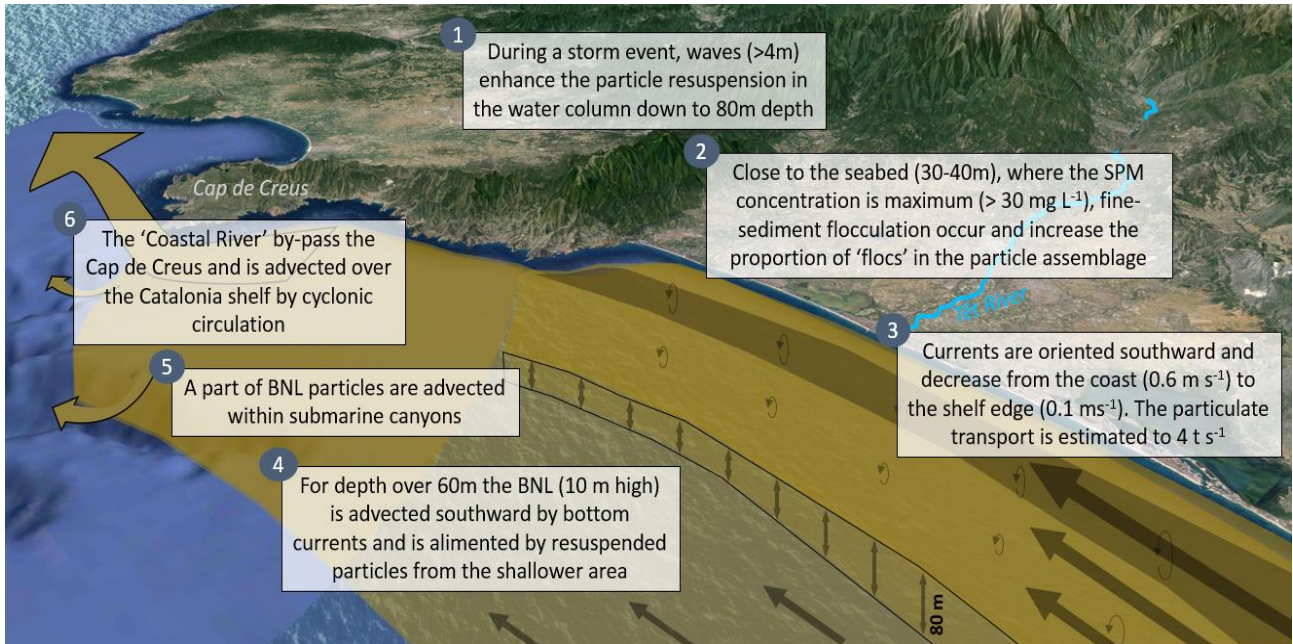
Figure 4 : Résumé graphique (anglais) de l'impact d'une tempête et d'une crue concomitante sur la dynamique des MES dans la partie sud-ouest du Golfe du Lion. La vue est du Nord-Est.

Synthèse des observations

Cette thèse a mis en évidence l'importance des évènements météorologiques sur la dynamique des matières en suspension (MES) aux extrémités du plateau du Golfe du Lion. Alors qu'une crue du Rhône augmente les apports de matière au sein de la ROFI et génère plusieurs néphéloïdes, une tempête induit une importante remise en suspension des sédiments déposés proche de la côte et augmente le transport particulaire en dehors du plateau. Ces évènements ont souligné le fort dynamisme des MES au dessus du plateau du golfe, entrainant une forte variabilité dans la turbidité côtière et jouant un rôle particulier dans le budget sédimentaire de la marge continentale et l'expansion des zones sous influences des particules fines.

Crue du Rhône – Les différents mécanismes permettant le transfert vertical des particules depuis le panache du Rhône vers le néphéloïde benthique et l'advection des MES en dehors de la ROFI ont été mis en évidence. Alors que les vents continentaux favorisent l'export de matériel vers le large, les faibles vents marins entrainent l'alimentation des néphéloïdes intermédiaire et benthiques en face de l'embouchure, augmentant le transfert vertical des particules et leur sédimentation. Cette observation, pauvrement documentée dans la littérature due aux difficultés d'échantillonnage et au caractère épisodique de tels évènements, pourrait jouer un rôle primordial dans le piégeage de sédiments au sein du prodelta du Rhône.

En parallèle, nous avons souligné le rôle d'une tempête, induite par de forts vents marins, dans la rupture de la stratification du panache du Rhône, augmentant le cassage des agrégats de particules fines et favorisant le transport le long de la côte des particules en suspension. Ces observations, en accord avec les récents travaux de modélisation, ont permis de mettre en évidence le rôle des tempêtes dans la redistribution des particules délivrées par le Rhône sur l'ensemble du plateau. Les tempêtes jouent ainsi un rôle particulier dans la dynamique sédimentaire du prodelta du Rhône à l'échelle annuelle et, en fonction de leurs fréquences et de leurs intensités, pourraient fortement contribuées à la non-préservation des évènements de crue du Rhône dans les enregistrements sédimentaires du prodelta.

Tempête marine – Basé sur des observations gliders de la dynamique des MES au sein de la partie sud-ouest du plateau du golfe, l'impact d'une tempête marine sur le transport particulaire a été estimé à 4 t/s vers le sud. Ce transport semble être 20-30 fois supérieur à celui observé en période calme et met clairement en évidence le rôle des tempêtes dans l'export de particules en dehors du plateau. Ces évènements apparaissent donc comme les principaux facteurs régulant le budget sédimentaire du plateau (Figure 5). Nous avons mis en évidence qu'un total de 1-2 Mt de sédiment avait été exporté en dehors du plateau pendant la période de la tempête. Malgré les incertitudes existantes sur cette estimation, ce transport est du même ordre de grandeur que la totalité des sédiments apportés par le Rhône en une

année. Il est aussi équivalent à la totalité des sédiments apportés par l'ensemble des fleuves côtiers autre que le Rhône pendant une année (Tech, Têt, Aude, Agly, Vidourle). Ces estimations montrent clairement le rôle des tempêtes dans le transport particulaire. La succession de tels évènements pourrait fortement contribuée à l'érosion des sédiments déposés sur cette partie de la marge continentale et confirment le caractère de « by-pass » sédimentaire de la partie sud-ouest du Golfe du Lion.
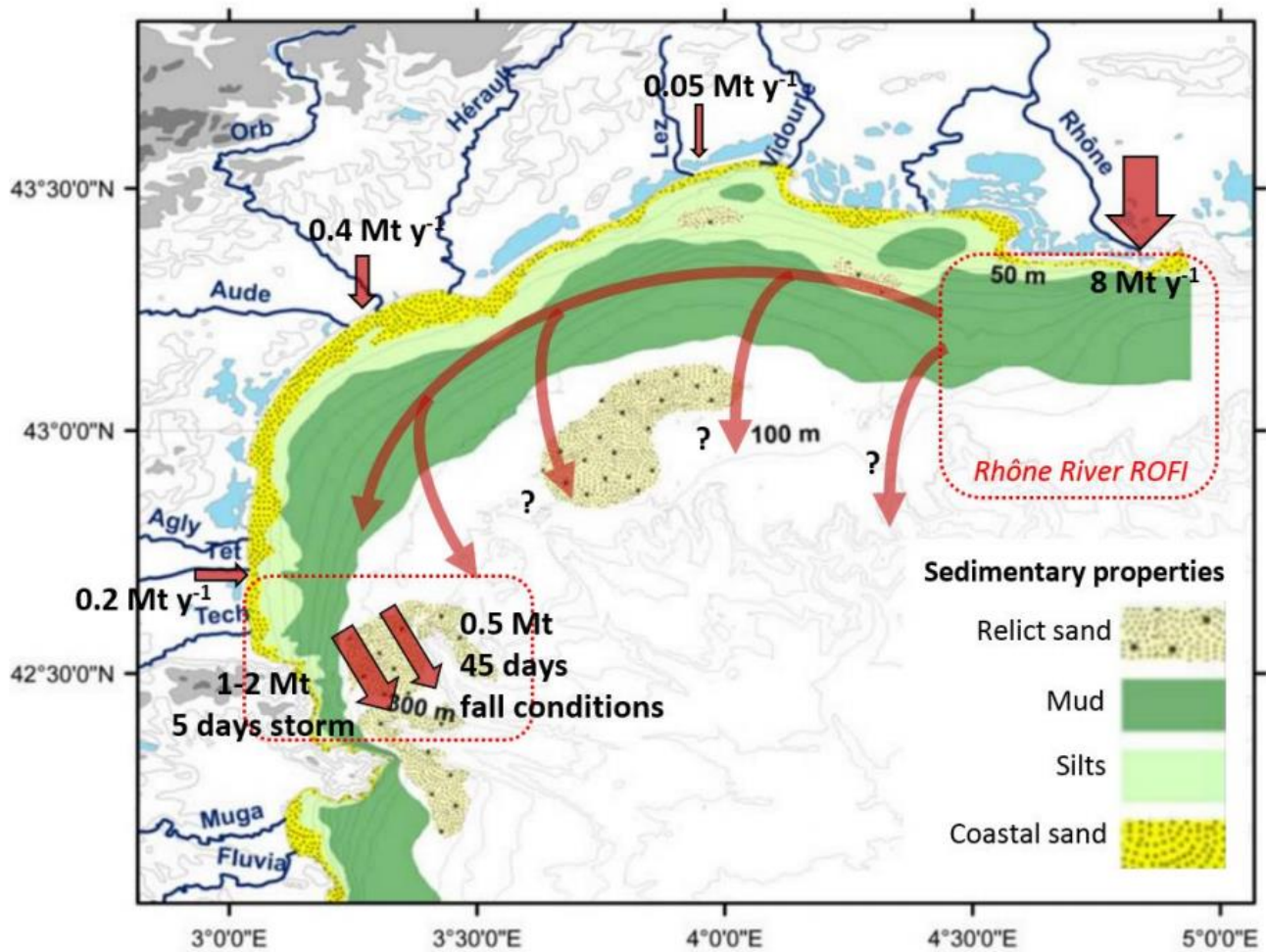

Figure 5 : Budget sédimentaire du plateau du Golfe du Lion. La morphologie des sédiments est spécifiée. Les rectangles rouges mettent en évidence les zones étudiées dans ce travail. Notez le fort transport particulaire estimé pendant la tempête du même ordre de grandeur que les apports annuels du Rhône et 20-30 fois supérieur à celui estimé pendant la période calme et stratifiée.

En plus de la quantification des flux sédimentaires au-dessus du plateau du Golfe du Lion, nous avons développé nos connaissances sur la caractéristique des MES pendant des évènements de crue et de tempête. Nous avons établi pour la première fois une caractérisation in situ de la variabilité de l'assemblage particulaire au sein de la ROFI du Rhône pendant un évènement de crue du fleuve. Cette étude a permis de mettre en évidence le rôle de la floculation des sédiments fins dans le transfert vertical des particules en suspension, augmentant leurs tailles et diminuant leurs densités effectives. Nous avons estimé que les micro- et macroflocs

pourraient chuter au travers de la colonne d'eau à des vitesses de 2 à 17 mm/s (i.e. 7 à 60 m/h). Alors que ces estimations pourraient être améliorées par la détermination de la densité des particules en suspension par classe de taille et par une détermination de la vitesse de chute par une approche fractale, elles montrent bien le rôle de cette floculation dans la sédimentation rapide des particules fines du panache du Rhône vers le prodelta. Le prodelta du Rhône semble donc jouer le rôle de puit sédimentaire (de carbone et de contaminants associés). Cette observation contraste avec le caractère de by-pass de la partie sud-ouest du golfe décrite précédemment.

En parallèle, cette thèse a permis de montrer pour la première fois, la possibilité de dériver un indice de la taille des particules depuis les mesures de rétrodiffusion particulaire établies à partir des plateformes autonomes (gliders) et satellitaires. Nous avons souligné la réponse de cet index avec la variabilité de l'assemblage particulaire pendant les évènements de crue et de tempête. De manière générale, les résultats ont été en lien avec les estimations réalisées dans les études précédentes en laboratoire ou in situ à partir de capteurs optiques déployés depuis des bateaux océanographiques. Ils ont montré le lien existant entre l'augmentation de la concentration en MES et l'augmentation de la proportion d'agrégat dans l'assemblage particulaire. L'utilisation de cet index a permis de décrire l'impact de différents régimes de vents sur la variabilité de l'assemblage particulaire au sein des néphéloïdes en face de l'embouchure du Rhône (voir le Chapitre 5). Enfin, la dérivation de cet index nous a permis de mettre en évidence la possible floculation s'effectuant au sein du BNL pendant un évènement de remise en suspension induite par une tempête (Chapitre 6). Ces observations ont clairement mis en évidence le besoin d'un tel index dans la compréhension des phénomènes régulant la dynamique des MES au sein de la zone côtière. Techniquement, il semble crucial de continuer à utiliser un tel index et donc à utiliser des capteurs de rétrodiffusion particulaire a plusieurs longueurs d'onde embarqués sur les gliders et les satellites.

Conclusion

Cette thèse a fourni une vue unique des impacts des évènements du type crue et tempête marine sur la dynamique des matières en suspension au sein du Golfe du Lion. Bien qu'épisodiques, ces évènements tiennent une place importante dans la variabilité de la turbidité au sein de la zone côtière. Le suivi de ces évènements apparaît décisif afin de comprendre les facteurs impactant le budget sédimentaire de la marge continentale et le transport de contaminant dans la colonne d'eau.

L'approche multiplateforme adoptée, rassemblant les observations réalisées à partir de plateformes fixes, glider, satellite et bateaux, a permis de décrire en détail la variabilité spatiale et temporelle des néphéloïdes au sein du golfe. L'utilisation des gliders a permis de

compléter la stratégie d'observation existante en fournissant d'importantes informations avec de hautes résolutions spatiale et temporelle.

Nous avons montré le rôle du phénomène de floculation dans la régulation du transfert vertical de sédiments fins depuis la surface vers le prodelta lors d'un évènement de crue du Rhône. Parallèlement, nous avons souligné l'importance des différents régimes de vent dans la forte dynamique des néphéloïdes au sein de cette même zone. Ces observations ont permis de mettre en évidence le rôle du prodelta du Rhône dans le piégeage d'une grande partie des sédiments fins délivrés par le Rhône lors d'une période de crue. Cette zone apparaît donc comme un puit de sédiments, de carbone et de contaminants associés.

En parallèle, le rôle d'une tempête marine dans l'export de sédiments en dehors du plateau a été identifié. Nous avons mis en évidence le rôle d'un tel évènement dans la remise en suspension des sédiments déposés ainsi que dans leur transport au-dessus du plateau. Ces résultats ont permis d'augmenter nos connaissances sur le budget sédimentaire du plateau mais aussi de décrire le caractère de « by-pass » que joue la partie sud-ouest du plateau dans les échanges de matière particulaire au sein du continuum terre-mer du Golfe du Lion.

Enfin, les perspectives de ce travail ont été abordées. Il semble primordial d'étudier la variabilité interannuelle de ces évènements afin de perfectionner nos connaissances sur le budget sédimentaire du Golfe du Lion. Nous avons montré le besoin d'intégrer les gliders comme des plateformes de mesures durables au sein des eaux côtières afin de compléter le système d'observation existant et de déterminer sur le long terme la variabilité des processus hydrologiques, hydrodynamiques et biogéochimiques ayant lieu au sein du Golfe du Lion.

Références des articles constituant cette thèse (dans l'ordre d'apparition dans le texte principal) :

Many, G., F. Bourrin, X. Durrieu de Madron, I. Pairaud, A. Gangloff, D. Doxaran, A. Ody, R. Verney, C., Menniti, D. Le Berre et M. Jacquet. **2016**. « Particle assemblage characterization in the Rhone River ROFI. » *Journal of Marine Systems* 157 (05): 39-51. DOI: 10.1016/j.jmarsys.2015.12.010

Many, G., F. Bourrin, D. Doxaran, X. Durrieu de Madron, A. Ody, I. Pairaud. 2016 « Glider and satellite monitoring of suspended particle dynamics during flooding conditions in the Rhône ROFI » (***in prep.***)

Bourrin, F., G. Many, X. Durrieu de Madron, J. Martín, P. Puig, L. Houpert, P. Testor, S. Kunesch, K. Mahiouz, et L. Béguery. **2015**. « Glider monitoring of shelf suspended particle dynamics and transport during storm and flooding conditions ». *Continental Shelf Research* 109 (10): 135-49. doi:10.1016/j.csr.2015.08.031

Abstract (French)

La dynamique des matières en suspension joue un rôle primordial au sein de la zone côtière en étant le principal vecteur de matière particulaire depuis les sources (rivières) vers les puits (marges continentales, canyons sous-marins, océan profond). Le suivi de cette dynamique, notamment pendant les évènements de crues des fleuves et des tempêtes, est primordial afin d'estimer les budgets sédimentaires des marges continentales, de suivre l'évolution des habitats benthiques et de déterminer le rôle de cette dynamique dans le transport de contaminants. Cette thèse a pour objet l'étude des impacts de tels évènements sur la dynamique des particules en suspension au sein du Golfe du Lion (Méditerranée). Une approche multiplateforme, couplant les différentes plateformes de mesures existantes (campagne en mer, glider, satellite, mouillage, bouée côtière) et basée sur la mesure de la turbidité en terme quantitatif et qualitatif a été adoptée. Les résultats ont permis de décrire 1) la dynamique des néphéloïdes en fonction des forçages (vents, vagues, courants) durant des évènements de crue du Rhône et de tempête marine, 2) la variabilité spatiale et temporelle de l'assemblage particulaire lors de ces mêmes évènements par une caractérisation in situ et 3) de montrer le rôle des plateformes autonomes du type gliders dans le suivi de la dynamique des particules en suspension en zone côtière.

Abstract (English)

Coastal suspended particulate matter dynamics play a main role in the fate of land-derived material from the source (rivers) to sink (continental margins, submarine canyons, deep sea). The monitoring of this dynamic, especially during flooding and storm conditions, is decisive to understand factors impacting sedimentary budgets of continental margins, health of benthic habitats and spread of contaminants. The aim of this PhD is to study the impacts of such events on the suspended particles dynamics over the shelf of the Gulf of Lions (NW Mediteranean). A multi-platform approach, combining existing observation platforms (survey, glider, satellite, mooring and coastal buoy) and based on the measurement of the turbidity was adopted. Results enabled to describe 1) the impacts of forcings (winds, waves, currents) on the dynamics of nepheloid layers during flooding and storm conditions, 2) the variability of the particle assemblage during such events through an in situ characterization and 3) the role of gliders in the monitoring of suspended particles dynamics within the coastal zone.